DESIGN, SYNTHESIS AND EVALUATION OF CJ-15,801 AND PANTOTHENIC ACID ANALOGUES AS DRUG CARRIERS

Thesis submitted in accordance with the requirements of the University of Liverpool for the degree of Doctor in Philosophy

by

Ricardo Lopez-Gonzalez

JUNE 2018

Abstract

Since the discovery of antibiotics in the 20th century, the quality of life and life expectancy have improved significantly for humanity. However, these benefits are at risk due to negative therapeutic side effects, and the emergence of drug resistance strains of bacteria.

Active drug delivery systems are new approaches to improve the performance of the drugs. Unlike passive targeting approaches, active approaches take advantage of specific interactions between the delivery system and the cell's receptor, to reach the desired target and deliver the ligand.

CJ-15,801 is a natural antibiotic produced by the fungus *Sematosporium sp.*, which acts as antimetabolite in the coenzyme A pathway. CJ-15,801 shares a large degree of structural similarity with pantothenic acid (vitamin B_5), the key difference being the presence of the enamide unit.

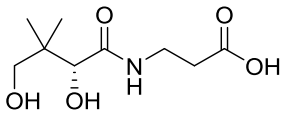

pantothenic acid

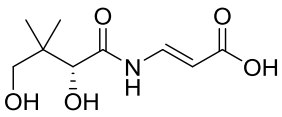

CJ-15,801

In this project, pantothenate and CJ-15,801 derived analogues were coupled to small molecular weight fluorescent probes, and fluorescent proteins, in order to follow the uptake in different organisms, including worms, bacteria and apicomplexan parasites.

New BODIPY-pantothenate derivatives **42**, **43** were synthesized and their uptake was tested, together with BODIPY-CJ-15,801 derivatives **121**-**128**, revealing promising results in the nematode *C. elegans*, the apicomplexan *B. bovis*, the trypanosomatida *L. passim* and *Mycobacterium* strains. Additionally, new phiLOV complexes **90**-**104** were synthesized and studied in biological models. Significant uptake was observed with complex **90** in *C. elegans*, and complexes **102** and **104** in *B. bovis*, thus strengthening the argument that a selective uptake mechanism is taking place.

As further evidence of the usefulness of this approach, a CJ-BODIPY analogue attached to the drug praziquantel **129**, also revealed selective uptake in *C. elegans*.

In conclusion, we have developed a new drug delivery system, which is able to deliver small organic and large bio-molecules in a wide range of organisms, and can be generated from commercially available starting materials.

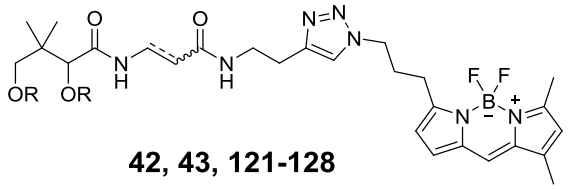

42, 43, 121-128

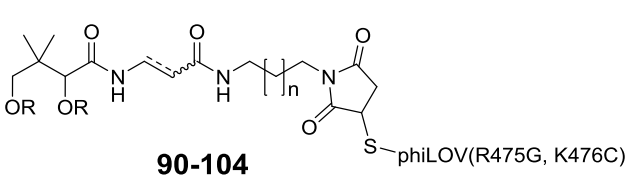

90-104

R = H, $C(CH_3)_2$

Contents

PGR Policy on Plagiarism and Dishonest Use of Data
PGR CoP Appendix 4 Annexe 1

PGR DECLARATION OF ACADEMIC INTEGRITY

NAME (Print)	Ricardo Lopez Gonzalez
STUDENT NUMBER	201172099
SCHOOL/INSTITUTE	Department of Chemistry/XJTLU
TITLE OF WORK	'DESIGN, SYNTHESIS AND EVALUATION OF CJ-15,801 AND PANTOTHENIC ACID ANALOGUES AS DRUG CARRIERS'

This form should be completed by the student and appended to any piece of work that is submitted for examination. Submission by the student of the form by electronic means constitutes their confirmation of the terms of the declaration.

Students should familiarise themselves with Appendix 4 of the PGR Code of Practice: PGR Policy on Plagiarism and Dishonest Use of Data, which provides the definitions of academic malpractice and the policies and procedures that apply to the investigation of alleged incidents.

Students found to have committed academic malpractice will receive penalties in accordance with the Policy, which in the most severe cases might include termination of studies.

STUDENT DECLARATION
I confirm that:

- I have read and understood the University's PGR Policy on Plagiarism and Dishonest Use of Data.
- I have acted honestly, ethically and professionally in conduct leading to assessment for the programme of study.
- I have not copied material from another source nor committed plagiarism nor fabricated, falsified or embellished data when completing the attached material.
- I have not copied material from another source, nor colluded with any other student in the preparation and production of this material.
- If an allegation of suspected academic malpractice is made, I give permission to the University to use source-matching software to ensure that the submitted material is all my own work.

SIGNATURE..... Ricardo Lopez Gonzalez .....

DATE..... 01/Jun/2018 .....

Acknowledgements

I would like to thank Dr. Rudy Marquez for all the support during this research, and to let me take care and raise his 'baby'. For being a proactive advisor throughout all my PhD process. I appreciate the opportunities to learn Chemistry and Biology in his group, but also with different groups around the world.

The most special thanks to my family, Yadira and Ximena, thank you for tolerating my mood and the time that I employed in the lab throughout all the PhD, and finally it's over!!

Thanks also goes to all our collaborators, because I complemented my project with your expertise: UoG: Dr. Christie, Dr. Petersen and all his group, Dr. Mullen and Dr. Carrick, Dr. Briton and Dr. Flachbartova. XJTLU: Dr. Kadowaki and Qiushi Liu, Dr. Tefsen, Abhipsa Sahu and Xinyue Wang. UoN: Dr. Kaneko, Dr. Asada and all his group.

I would also like to thank all the members of the Marquez group, from UoG: Alan and Mhairi, Sean, Ezequiel, Riccardo, Alejandro, Tom, Collins, Liam and Joanne. XJTLU: Zach, Lilly, Nerissa, Xing Xing.

Thanks to the staff members of the Department of Chemistry at XJTLU, they always offered support to do my research better, special thanks to Dr. Amigues and Dr. Lau, Jianfang Wu, Ruba, Tong Ji and Pei pei.

I would like to thank my sponsor, CONACYT, for the financial support during my PhD.

To my parents Ydalia and Ricardo, my brother Zeus and Alicia, and now, Leia and Perseo, that always wish the best to me.

To Emilio, I hope our experience help you to try new things in your life.

“ One never leaves entirely,
an invisible thread joins the butterfly to its mother tree,
the imaginary wet nurse who, in place of milk, provides nostalgia
and strength
and courage.”
XOLO, Mardonio Carballo, 2012

Dedicated to Yadira and Ximena,
you are walking this long way too,
and never have said no,
thank you for your support.

Abbreviations

Boc	*tert*-butyloxycarbonyl
Boc_2O	di-*tert*-butyl dicarbonate
BODIPY	4,4-difluoro-4-bora-3a,4a-diaza-*s*-indacene
BTFFH	bis(tetramethylene)fluoroformamidinium hexafluorophosphate
CFU	colony-forming unit
CoA	coenzyme A
MeOH	methanol
DEAD	diethyl azodicarboxylate
DIAD	diisopropyl azodicarboxylate
DIPEA	*N,N*,*N*-diisopropylethylamine
DMAP	4-(dimethylamino)pyridine
DMF	dimethylformamide
DCC	*N,N′*-dicyclohexylcarbodiimide
EDC	*N*-(3-dimethylaminopropyl)-*N′*-ethylcarbodiimide
Et_3N	triethylamine
EtOAc	ethyl acetate
FR	folic acid receptor
GE	glycol ether
GFP	green fluorescent protein
HBTU	*N,N,N′,N′*-tetramethyl-O-(1*H*-benzotriazol-1-yl)uronium hexafluorophosphate
LOV	light-oxygen-voltage-sensing protein
MALDI	matrix-assisted laser desorption/ionization
mW	microwave
n-BuLi	*n*-butyllithium
p-TsOH	*p*-toluenesulfonic acid
p-TsCl	*p*-toluenesulfonyl chloride
PPh_3	triphenylphosphine

PE	petroleum ether
PVM	parasitic vacuole membrane
RBC	red blood cell
RFB	rifabutin
Rf	retardation factor
rt	room temperature
SDS-PAGE	sodium dodecyl sulphate-polyacrylamide gel electrophoresis
TASF	tris(dimethylamino)sulfonium difluorotrimethylsilicate
TBTU	*N,N,N′,N′*-tetramethyl-O-(benzotriazol-1-yl)uronium tetrafluoroborate
TBAF	tetrabutylammonium fluoride
TFA	trifluoroacetic acid
TFFH	tetramethylfluoroformamidinium hexafluorophosphate
TLC	thin layer chromatography
THF	tetrahydrofuran
TMSE	trimethylsilylether
WHO	World Health Organization
Φ	quantum yield
ε	molar extinction coefficient or molar absorptivity

1. Introduction.

"The time may come when penicillin can be bought by anyone in the shops. Then there is the danger that the ignorant man may easily underdose himself and by exposing his microbes to non-lethal quantities of the drug make them resistant." Nobel Lecture, Dec 1945, Alexander Fleming.

1.1 Host *versus* guest: "the battle for survival"

Throughout history, humanity has been in a relentless conflict with pathogenic organisms. Evidence of this long struggle has been documented extensively by ancient cultures. The Code of Hammurabi described in 2250 B.C. a chronic illness affecting a couple, which bears all the hallmarks of tuberculosis.[1] In 1545 A.D, an outbreak of "cocoliztli", killed between 5-15 million Aztecs, causing the fall of Tenochtitlan. The agent responsible for "cocoliztli" is still unknown today.[2] These stories however, have started to change in 1928, when Alexander Fleming first realized that the mould *Penicillium* had antibacterial properties against staphylococcal colonies (Figure 1).[3]

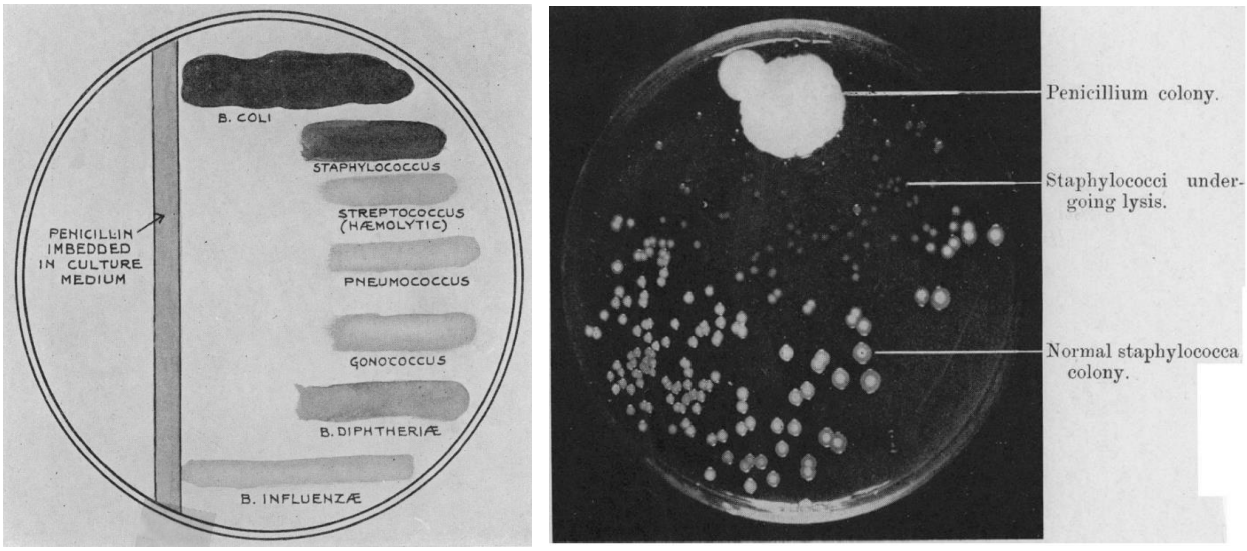

Figure 1. Descriptions of *Penicillium* antibacterial activity by Alexander Fleming.[3]

Penicillin was then subsequently isolated, and played a key role in the treatment of infections by allies forces in World War II. After 1945, the life expectancy increased 30 years, due to use and development of new antibiotics, vaccination programs, sanitization and nutrition. However, before the wide-spread distribution and commercialisation of penicillin was fully implemented, there was evidence of penicillin resistance from *Staphylococcus* strains isolated *in-vitro*.[4]

According to WHO reports, infectious diseases represent a serious problem to human health worldwide. In 2016, 10 million people were infected with, and more than 1.5 million died as a consequence of tuberculosis (TB). In the same year, malaria infected 200 million people worldwide and resulted in over 400 thousand deaths. Even though, health programs around the world have resulted in a remarkable reduction in the number of deaths due to neglected diseases, the emergence of multi-drug resistance strains present a new challenge. Indeed, over 600,000 new

cases of multi-drug resistant TB (MDR-TB) were reported worldwide in 2016.[5] The great adaptability of microorganisms to survive hostile environments, means that there is a need to develop new approaches to tackle new drug-resistant strains. However, there is also a need to reduce the toxicity of treatments, in order to offer effective therapies with reduced side effects and successful compliance rates.

1.2 Drug delivery systems

In 1982, Neumann and co-workers reported the successful transfer of the *thymidine kinase* (*TK*) gene to mouse L cells lacking the gene. This ground breaking result was accomplished through the use of the electroporation.[6] It was proposed that when the cells are exposed to external fields (i.e. electric pulses), the cell membrane is perturbed and disrupted, producing hydrophilic pores allowing water molecules to enter the cell (Fig. 2, A). This effect is largely observed in the area next to the anode, due to the negative transmembrane potential inside the cell respective to the outside (Figure 2, B). The new pores formed then allow compounds that normally can not permeate, such as hydrophilic molecules (DNA), to enter the cell. This transport occurs less than a second after the applied pulse takes place; as shown by Gabriel, using Chinese hamster ovary (CHO) cells. As part of Gabriel's experiment, CHO cells were incubated with the impermeable nuclear dye propidium iodide, and then exposed to a 20 ms pulse of 60 $V.cm^{-1}$. After 40 ms, the fluorescence dye was clearly visible inside the cell area next to the anode (Figure 2, C,D).[7]

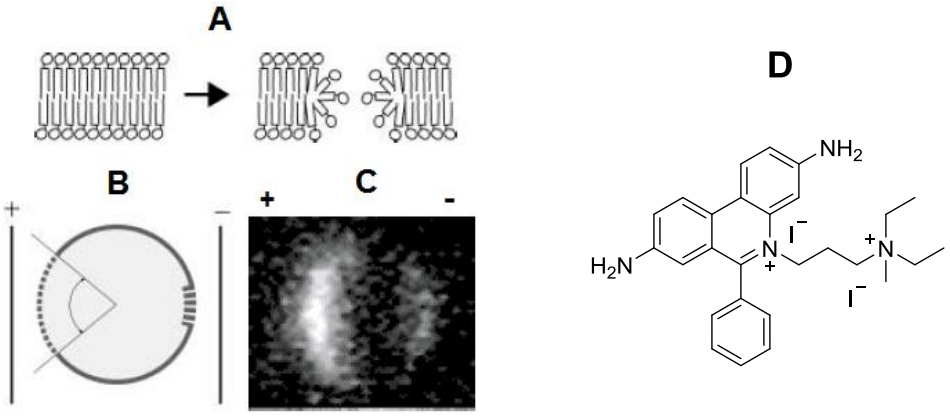

Figure 2. Electroporation process. **A**) Cartoon showing pore formation. **B**) Proposed distribution of permeation areas respect to electrodes. **C**) Image recorded less than 40 ms after electrical pulse in CHO cell exposed to propidium iodide (1μM) (anode (+), cathode (-)).[8] **D**) Propidium iodide.

Even though the viability of the cells is affected significantly, this method has been used to deliver drugs both *in-vitro* and *in-vivo*. Electroporation has also been used in the clinic to deliver drugs directly into malignant tumours in patients.[8-9] A group of patients with colorectal liver metastases, received electric pulses in and around the tumour before injection of bleomycin during open surgery

with good results, however, the lack of accuracy for the placement of the electrodes is still an issue yet to be resolved (Figure 3).[10]

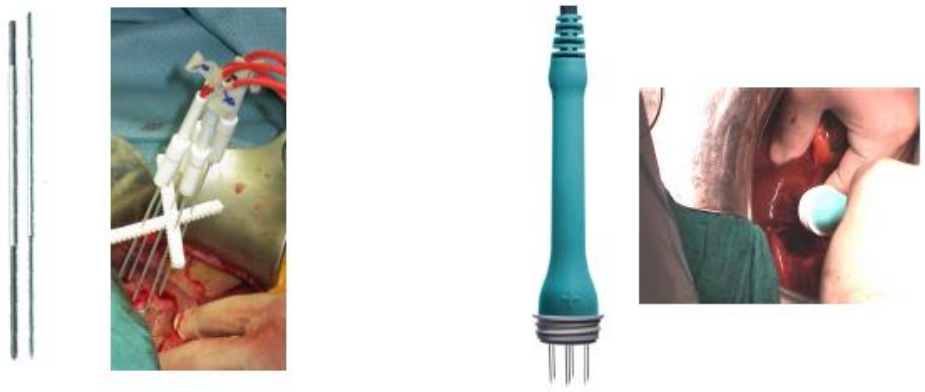

Left: Long needle electrodes with variable geometry. Right: electrodes with fixed geometry.

Figure 3. Medical electroporation during open surgery.[10]

Whilst the research to extend the applications of electroporation is still growing, nanoparticles and liposomes have emerged as new alternative approaches. Nanoparticles and liposomes range in size from 1 to 100 nm (at least in one dimension) and have found a niche in drug delivery, due to their optimized physicochemical and biological properties. Indeed, these carriers are more suitable to cross cell membranes than large molecules.[11]

To reach effective concentrations in *M. tuberculosis* bacilli inside host macrophages represents one of the most important challenges for antimycobacterial agents, due to low levels of drug permeation.[12]

Based on previous reports of liposomes uptake by infected macrophages after systemic administration, Pedrosa studied the therapeutic activity of the anti-mycobacterial rifabutin (RFB), encapsulated in liposomes in a murine model. As the lungs, liver and spleen are the main targets for *M. tuberculosis* in this biological model, the number of CFU for each organ was determined after the treatment.

Practically, after intravenous infection with *M. tuberculosis* H37Rv and 3 weeks post infection, no significant difference was found between the lungs of mice treated for two weeks with rifabutin and liposome-RFB. However, the liver and spleen of mice treated with liposomes-RFB exhibited a significant reduction in the number of bacilli comparing with only rifabutin. Thus, this passive targeting strategy represents a new approach for the treatment of non pulmonary TB infections (Figure 4).[13]

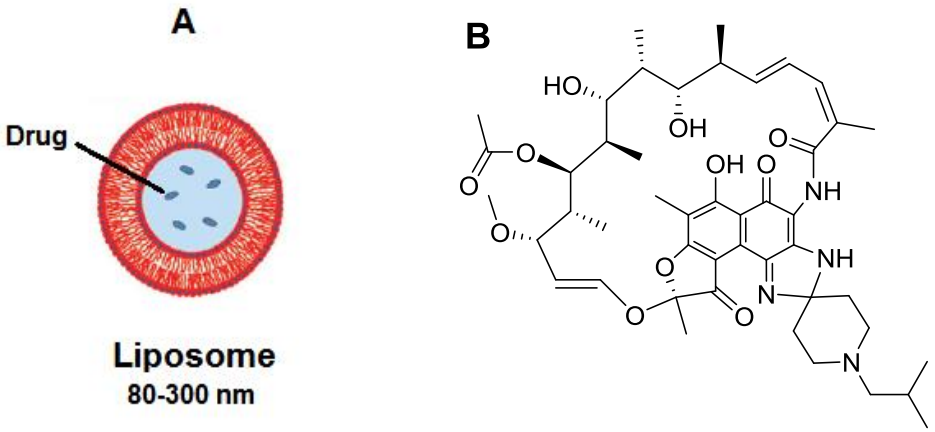

Figure 4. Liposomes as drug carrier. **A**) General structure of liposomes.[14] **B**) Rifabutin.

Instead of using passive targeting, Gabizon developed an active targeting approach, which hinged on attaching the drug to liposomes which have affinity for the specific cell or tissue. Using this approach, folate derived liposomes were designed to target the folic acid receptors (FR) that are overexpressed in human cancer cells. Results showed a 26-fold increment in binding for the modified liposomes compared to the non-functionalised liposomes in cancer cell lines (Figure 5).[15]

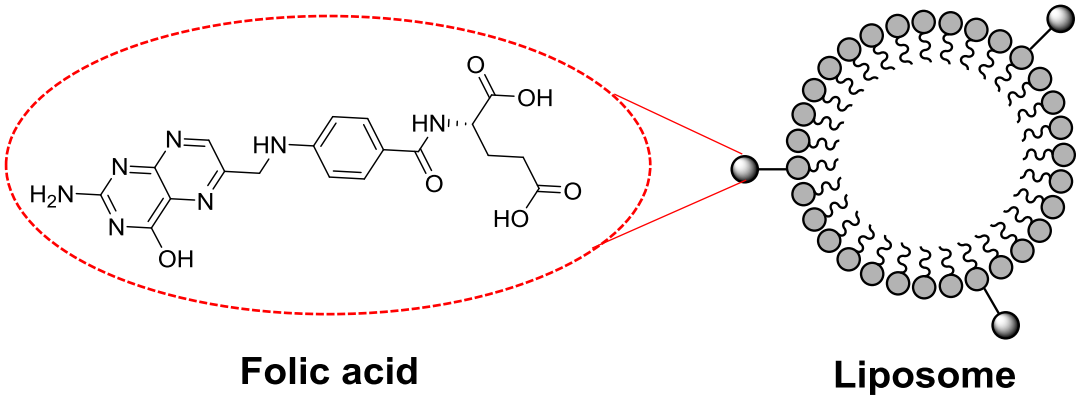

Figure 5. Folic acid used for active targeting.

Apart from liposomes, other delivery based nanosystems recently developed range from magnetic nanoparticles to nanoemulsions, polymeric nanoparticles, dendrimers and carbon nanoparticles. Unfortunately, issues like potential toxicity (nanotoxicology), troubles scaling up (reproducibility), economic and financial barriers, and unknown mechanisms of action, are crucial obstacles that are yet to be resolved (Figure 6).[16]

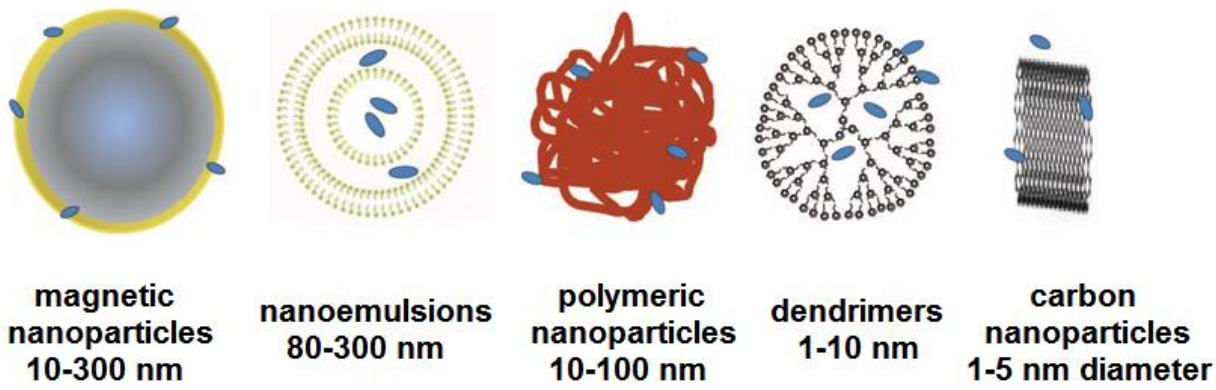

Figure 6. Nanoparticles systems.

Taking advantage of vitamin receptors on cells, the company Endocyte claimed to have developed a new targeted drug delivery system, using vitamins derivatives to reach specific receptors on tumour cells, bacteria, viruses, and their infected host cells.[17] Reddy subsequently reported antitumor activity of a folate derivative linked to mitomycin C **EC72** on FR-expressing M109 tumours. Reddy concluded that folate-targeted drug therapy was a viable clinical approach for the treatment of FR-positive cancers (Figure 7).[18]

Thus, targeting specific receptors or transporters on cells has proven to be a viable approach to deliver drugs. This approach provides a potentially selective delivery method with low side effects.[13b,19]

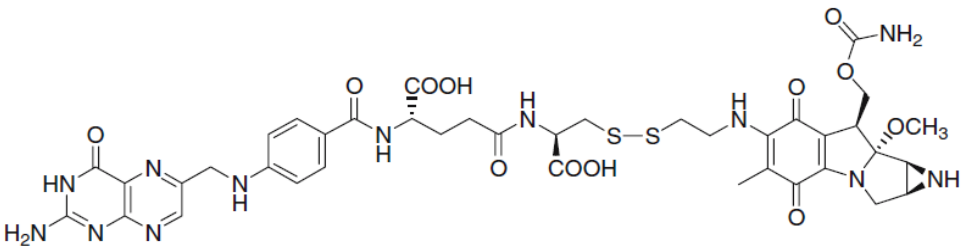

Figure 7. Folate derivative attached to mitomycin, **EC72**

1.3 Pantothenic acid and coenzyme A.

Pantothenic acid (vitamin B_5) is a precursor of coenzyme A (CoA). CoA is a cofactor present in all living cells as an acyl group carrier. It is involved in fatty acid synthesis, the tricarboxylic acid cycle (TCA) and secondary metabolism.[20] All live cells use the same enzyme-catalyzed steps from pantothenic acid to synthesize coenzyme A (except *Archaea*).[21]

Firstly, pantothenic acid **1** is phosphorylated by pantothenate kinase (PanK) to generate 4'-phosphopantothenate (PPAN), before the addition of a cysteine residue by phosphopantothenoyl-cysteine synthetase (PPCS) to give 4'-phosphopantothenoyl-cysteine (PPC). Decarboxylation of PPC by phosphopantothenoylcysteine decarboxylase (PPCDC) then produces 4'-

phosphopantetheine (PPantSH). Phosphopantetheine is subsequently adenylylated by phosphopantetheine adenylyl transferase (PPAT) to generate dephospho-CoA (dPCoA), which is finally converted to CoA by dephospho-CoA kinase (DPCK) (Scheme 1).[22]

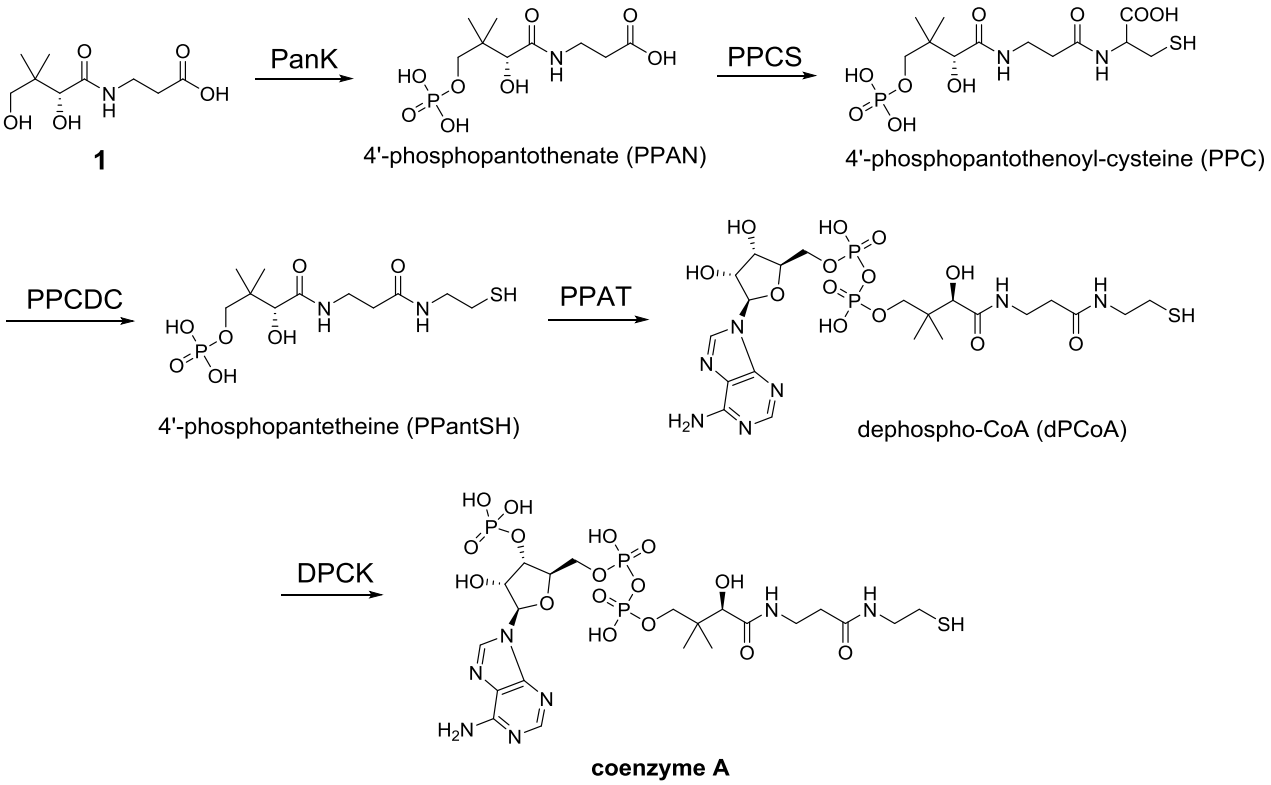

Scheme 1. Coenzyme A biosynthetic pathway.[22]

1.4 *Plasmodium*

Plasmodium is a protozoan parasite which belongs to the apicomplexan phylum. There are more than 100 *Plasmodium* species, but only five species infect humans: *vivax*, *falciparum*, *ovale*, *malariae* and *knowlesi*.[23] *P. vivax* is a key species in Asia and Latin America; and can also be found in some parts of Africa. *P. vivax* is unique as it has a a dormant liver stage called “hypnozoites” that can be activated and invade the host months or years after the mosquito bite.[23] *P. falciparum* on the other hand, represents almost 95% of cases in Africa and South East Asia. The cerebral form of malaria caused by this specie is particular lethal and leads to high mortality rates in children below 5 years of age.[24] Unfortunately, the drugs initially developed for treating malaria (i.e., chloroquine) have lost their effectiveness due to the emergence of resistance strains. Resistance has also developed to artemisinin and its derivatives, which makes the need to develop new therapies a pressing need. A significant amount of research is currently focused on understanding more about the metabolism of *Plasmodium* in order to develope new therapies.

Reproduction of *Plasmodium* follows an asexual replication in the human host, and sexual differentiation in the *Anopheles* mosquito.[25] Biologically, the sporozoites are transmitted into the

human host by a mosquito bite, and then travel through the bloodstream to the liver. Inside the infected liver cells, the sporozites grow and develop into merozoite (hepatic stage).

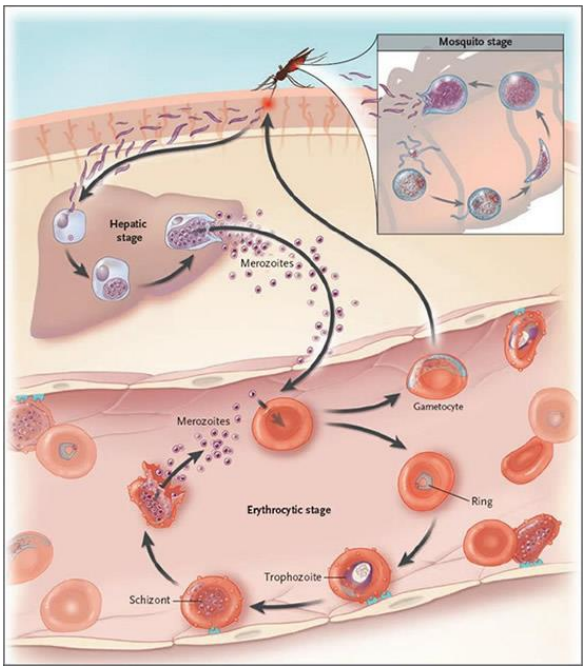

Figure 8. Lifecycle of *Plasmodium.*[26]

After the hepatic stage, the merozoites are released into the bloodstream, and infect the circulating erythrocytes, initiating the erythrocytic stage. At this stage, asexual replication takes place and the parasite goes from a ring stage to a trophozoite, and then matures into a schizont (containing new merozoites). When the schizont ruptures the erythrocyte, merozoites are released into the bloodstream and infect new erythrocytes. A small proportion of the parasites then differentiate to generate gametocytes (sexual form).

Upon feeding, the mosquito takes the gametocytes into the gut where they begin sexual differentiation.[27] Practically, the gametocytes in the gut of the mosquito become active, and transform into fertile gametes. Mechanistically, in order to start the gamete forming process, the gametocytes need to break free from the erythrocyte by breaking the erythrocytic membrane and the parasitic vacuole membrane (PVM) (Figure 8).[28]

1.5 *Plasmodium*: Discovering the transporters.

In 2000, Krishna's group identified the first transporter in *P. falciparum*, PfHT1. This protein carries hexoses (glucose and fructose) inside the parasite, and is located in the parasite's plasma membrane.

Later, PfNT1 and PfNT2 were discovered by Mamoun's group. PfNT1 is responsible for carring purine nucleosides and nucleo-bases across the parasite's membrane in *P. falciparum*. On the other hand, PfNT2, an intracellular purines permease, was found to be involved in the transport of purines

to the parasite's endoplasmic reticulum during malaria infection. Recently, Mamoun reported the identification of PfPAT, the first pantothenic acid transporter, located in the parasite's plasma membrane (Figure 9).[29]

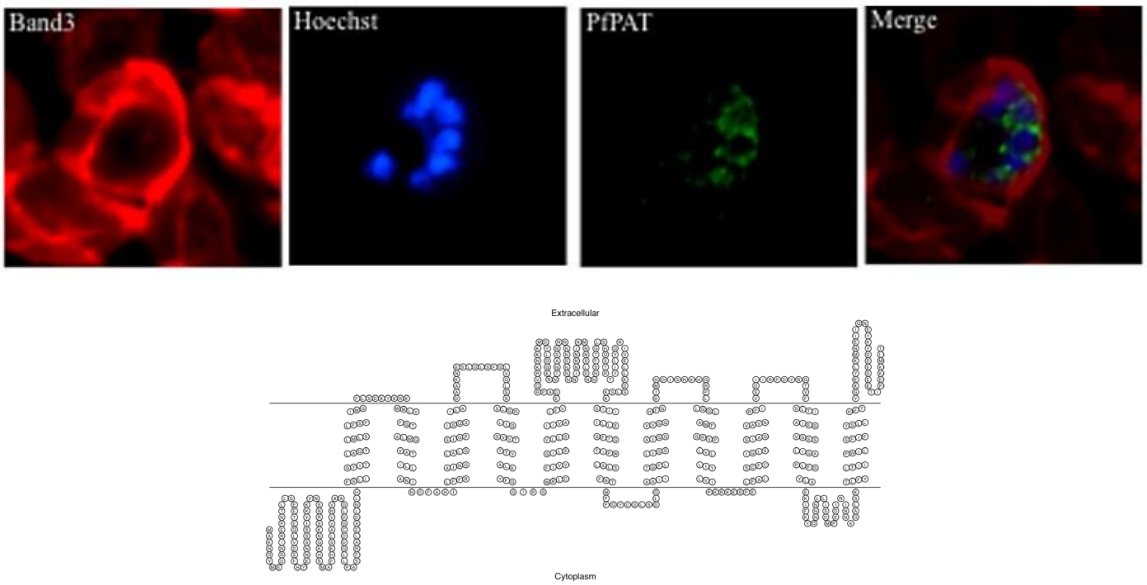

Figure 9. Pantothenic acid transporter PfPAT in *P. falciparum.*

Top: Localization of PfPAT in *P. falciparum* 3D7 parasites at the schizont stage using anti-band3 antibodies to mark RBC membrane in red. Hoescht 33258 dye visualized the parasite nucleus in blue. Anti-PfPAT antibodies revealed the PfPAT transporter in green, and merge photo.

Bottom: Topology of PfPMT. Transmembrane segments were predicted using the TNHMM program and the topology designed using the TOPO2 program.[29e]

1.6 Pantothenamides

Pantothenamides are secondary or tertiary pantothenic acid derived amides developed after decades of efforts. Pantothenamides work by inhibiting the growth of *P. falciparum* in the erythrocytic stage. Interestingly, amongst the pantothenamide based inhibitors developed, only α-pantothenamides (α-PanAm) and homopantothenamides (HoPanAm) have shown to be stable. Indeed, *n*-pantothenamides (*n*-PanAm) are rapidly hydrolysed by pantetheinase (vanin proteins) into pantothenic acid. Encourangly however, α-PanAm and HoPanAm derived inhibitors show high affinity for the parasite's enzymes, making them promising starting points for drug development (Scheme 2).[30]

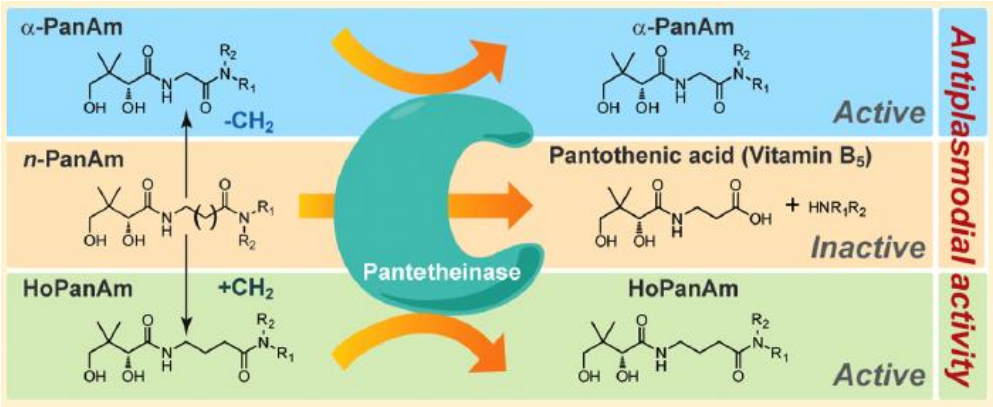

Scheme 2. Pantothenamides and antiplasmodial activity.[30]

1.7 Synthesis of CJ-15,801.

1.7.1 Pantothenic acid and CJ-15,801.

In 2001, Yutaka Sugie's research group screened compounds from soil samples whilst searching for new antibiotics. One of the samples exhibited antibacterial activity against multi-drug resistant strains of *Staphylococcus aureus*. Sugie then went to discover that the fungus *Sematosporium sp.* CL28611 was responsible for the activity through the production of a novel antibiotic compound. The antibiotic isolated, CJ-15,801 **2**, bears a high level of structural similarity with pantothenic acid. The only difference between pantothenic acid and CJ-15,801 is the presence of the enamide unit (Figure 10).[31]

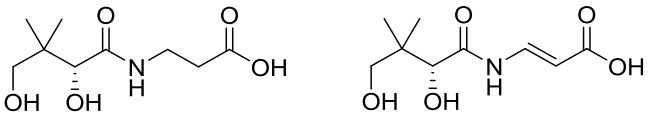

1 **2**

Figure 10. Pantothenic acid **1** and (*R*)-CJ-15,801 **2**.

1.7.2 CJ-15,801 and *Plasmodium.*

Plasmodium in the intraerythrocytic stage feeds on, and degrades much of the host cell´s hemoglobin and aminoacids in order to synthesize its own proteins. *P. falciparum* also ingests extra nutrients from the host cell including glucose, purines, isoleucine, thiamine (vitamin B_1)[21] and pantothenic acid (vitamin B_5).[32] The erythrocyte's membrane is largely impermeable to pantothenic acid, thus the parasite needs to generate profound structural and morphological changes in the host's cell membrane. *Plasmodium* induces the generation of New Permeation Pathways (NPPs) in the host's cells, thus increasing the permeability of a wide range of solutes (including pantothenic acid). It is believed that through this mechanism, the parasite adapts the host's electrolyte

composition to suit the parasite´s needs for nutrition and waste removal. *P. falciparum* has the machinery to convert pantothenic acid into CoA; but for other *Plasmodium* species, CoA is generated in the host cell cytosol, and then absorbed by the parasite.[33]

Inhibition studies by Kirk showed that CJ-15,801 inhibits *in vitro* proliferation of *P. falciparum*'s intraerythrocytic stage, with an IC_{50}= 39 ± 3 µM, and shows complete inhibition at ~250 µM. Kirk and co-workers also found that CJ-15,801 had no-effect on mammalian cell proliferation (rat hepatoma) at these concentrations. Increased concentrations of pantothenic acid concentrations reversed the inhibitory effect of CJ-15,801. Unfourtunately, Kirk did not have enough material to elucidate the mechanism of action.[34]

1.7.3 Mechanism of action of CJ-15,801.

Dr. Strauss's group in collaboration with two groups from UC San Diego found that CJ-15,801 is phosphorylated by pantothenate kinase (PanK) to generate 4'-phospho-CJ-15,801 (P-CJ).

Phosporylated CJ-15,801 (P-CJ) then reacts with cytidine triphosphate (CTP) in the presence of phosphopantothenoylcysteine synthetase (PPCS), to afford P-CJ-CMP which has high affinity for PPCS. Thus, P-CJ-CMP effectively blocks the active site, with results in inhibition of the enzyme. As consequence, cell growth is affected due to the reduction in CoA levels (Figure 11). Further studies indicate that PanK enzymes from *S. aureus*, are able to convert CJ-15,801 to P-CJ, with similar efficiency to the conversion of pantothenic acid to phosphopantothenate.

In summary, CJ-15,801 acts as antimetabolite in the CoA biosynthetic pathway revealing a potential approach to develop new antimicrobial drugs.[35]

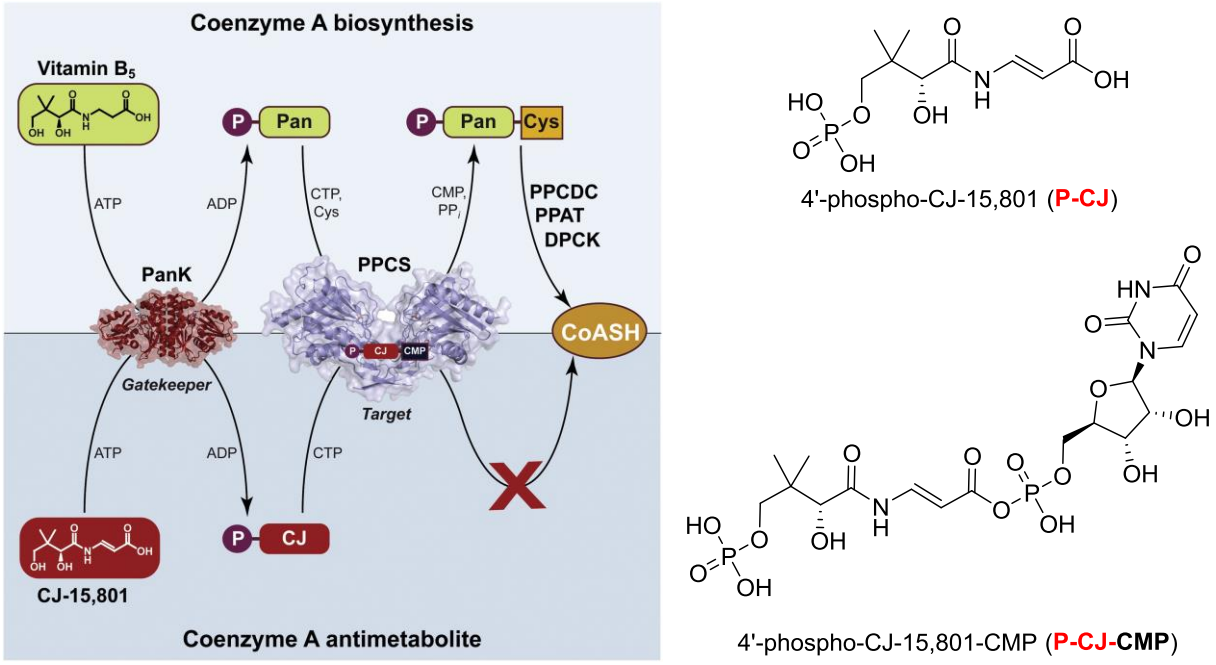

Figure 11. Mechanism of action of CJ-15,801.[35]

1.7.4 Porco's total synthesis of CJ-15,801.

The promising biological activity of CJ-15,801, combined with its interesting enamide unit aroused the interest of the synthetic community. Porco completed the first synthesis of CJ-15,801 through the Cu^{+1} catalysed coupling of amide **3** with iodo acrylate **4**. Mechanistically, the reaction proceeds through the formation of intermediate **5** (Scheme 3), in which the [Cu] chelates to the ketal oxygen (Figure 12). This coordination seems to be critical in order to achieve acceptable yields. Reductive elimination then proceded to generate the desired enamide unit **5**.[36]

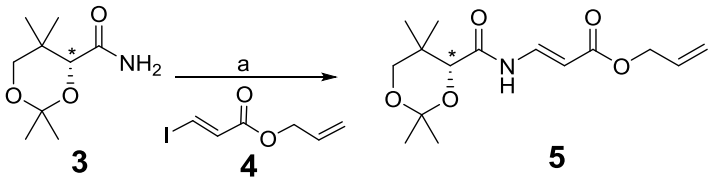

Reagents and conditions: a) 10 mol% $Cu(MeCN)_4PF_6$, 20 mol% 1,10-phenanthroline, Rb_2CO_3, dimethylacetamide, 45 °C, 19 h, 90%. ***** stereocenter.

Scheme 3. Synthesis of *N*-acyl vinilogous carbamate **5**

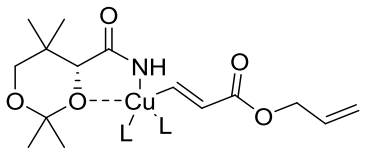

Figure 12. Proposed oxygen chelation.

Completion of the synthesis of CJ-15,801 **2** was then achieved by deprotection of the diol unit with $BiCl_3$, followed by cleavage of the allyl ester using polymer-supported (PS) *N*-hydroxy-phthalimide (Scheme 4).

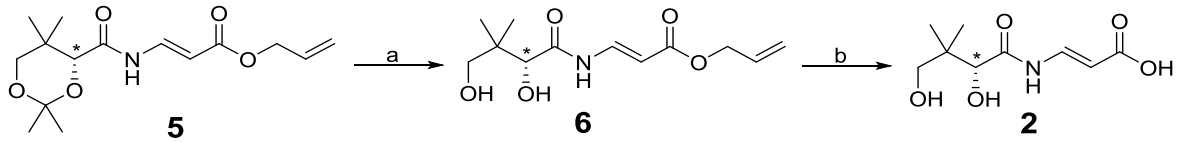

Reagents and conditions: a) $BiCl_3$, aq. CH_3CN, rt, 5 h, 75%; b) PS-*N*-hydroxy-phthalimide, $Pd(PPh_3)_4$, THF, 35 °C, 12 h, 80%. ***** stereocenter.

Scheme 4. Final steps to yield CJ-15,801 **2.**

1.7.5 Nicolaou's synthesis of CJ-15,801.

Nicolaou published the formal synthesis of CJ-15,801 in 2005.[37] Nicolaou's synthesis began with β-alanine **7** which was treated with allyl alcohol **8** to yield aminoester **9**. Opening of *D*-(-)-pantolactone **10** with aminoester **9** then proceeded to generate diol **11** (Scheme 5).

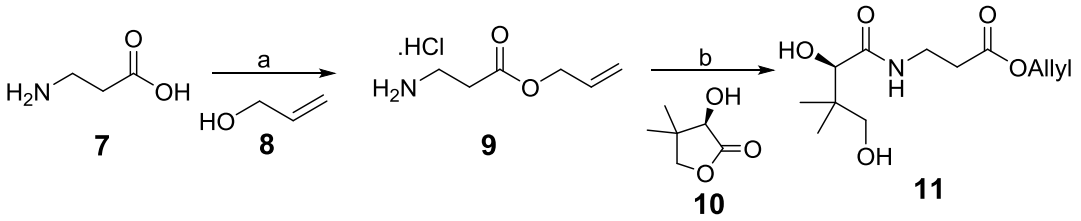

Reagents and conditions: a) HCl, 100%; b) *D*-(-)-pantolactone **10**, $NaHCO_3$, toluene, reflux, 20 h, 59%.

Scheme 5. Synthesis of diol **11.**

Diol **11** was then protected as acetonide **12**, which was then oxidised using Dess-Martin Periodinane to yield a mixture of *cis* **13** and *trans* **14** *N*-acyl vinylogous carbamates (**13**:**14** = 8:1, 93% combined yield). In order to obtain CJ-15,801 **2**, Porco's method was used to deprotect the *trans* isomer **14**. Removal of the ketal unit from enamide **13** followed by treatment with $Pd(PPh_3)_4$ completed the synthesis of *cis*-CJ-15,801 **15** (Scheme 6).

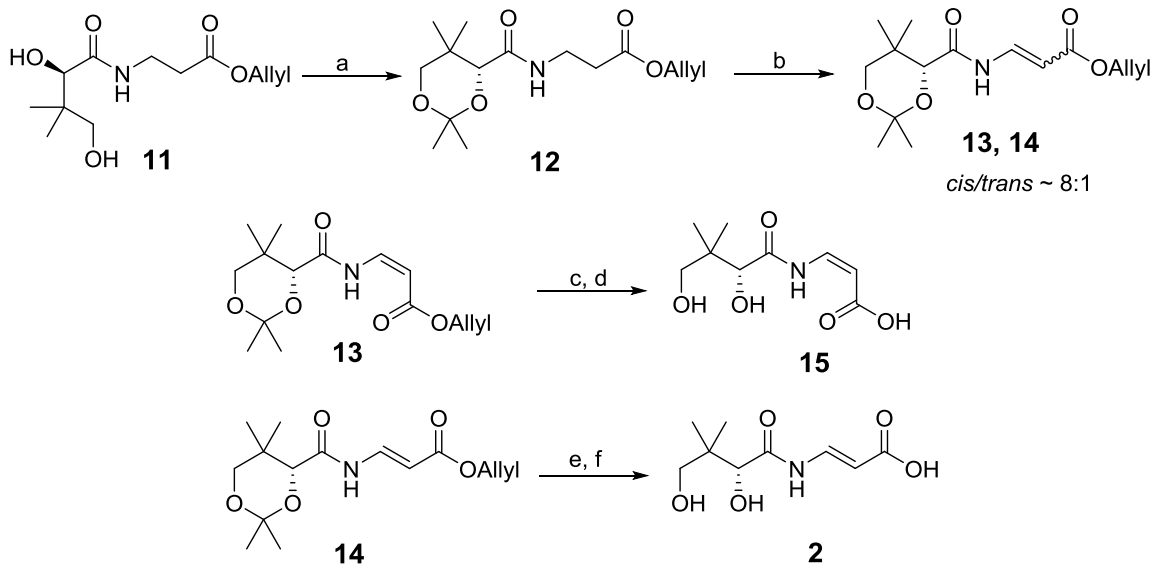

Reagents and conditions: a) 2-methoxypropene, *p*-TsOH, acetone, rt, 1 h, 78%; b) Dess-Martin periodinane, fluorobenzene, 85 °C, 2 h, 93% (based on 39% starting material recovery); c) $BiCl_3$ (0.2 eq.), aq. CH_3CN, 25 °C, 14 h, 98%; d) [$Pd(PPh_3)_4$] (0.2 eq.), dioxane/H_2O (4:1), 25 °C, 14 h, 87%; e) $BiCl_3$ (0.2 eq.), aq. CH_3CN, rt, 5 h, 75%; f) PS-*N*-hydroxy-phthalimide, $Pd(PPh_3)_4$, THF, 35 °C, 12 h, 80%.

Scheme 6. Synthesis of CJ-15,801 **2** and *cis*-CJ-15,801 **15**.

1.7.6 Reddy's synthesis.

Reddy's synthesis of CJ-15,801 and its *cis*-isomer[38] began with bicyclic amino acid **16** which was converted into allyl ester **17**. Treatment of *D*-(-)-pantolactone **10** with allyl ester **17** then afforded

vinylogous amide **18** (d.r. ~ 3:2). Treatment of amide **18** under thermal retro Diels-Alder conditions, then proceeded to generate *cis*-CJ-15,801 allyl ester **19** (Scheme 7).

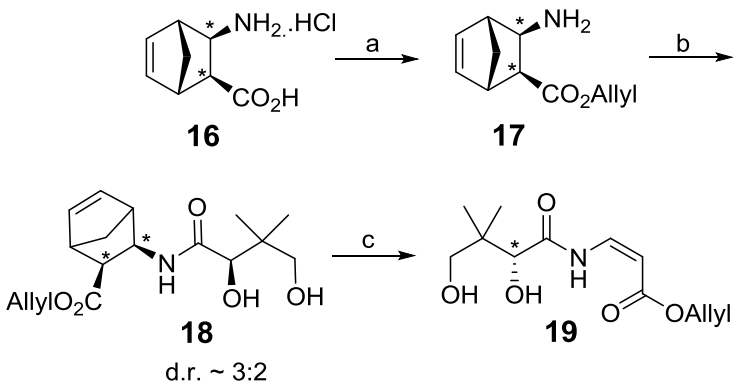

Reagents and conditions: a) allyl alcohol **8**, dioxane, reflux, 80%; b) *D*-(-)-pantolactone **10**, toluene, reflux, 60%; c) diphenyl ether, ~230 °C, 20 min., 77%. *****stereocenter.

Scheme 7. Reddy's synthesis of the *cis*-allyl ester of CJ-15,801 **19**.

In order to afford the required *E*-allyl ester **6** for the synthesis of CJ-15,801, Reddy used 1,1-cyclopropylcyclopentadiene **20** which underwent a Diels-Alder reaction with nitro ester **21** to afford the tricyclic intermediates **22a** and **22b** (d.r.~ 5:1). Treatment of intermediates **22a** and **22b** with *D*-(-)-pantolactone **10** under thermal retro-Diels Alder conditions, then generated CJ-15,801 allyl ester **6** (Scheme 8).

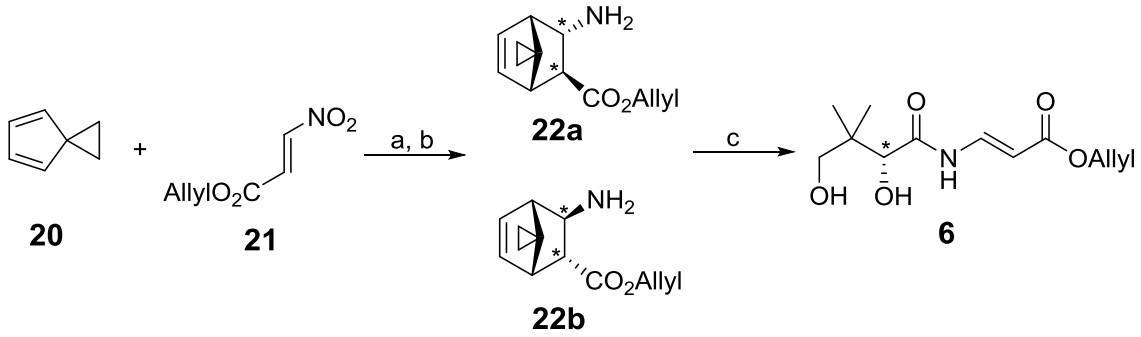

Reagents and conditions: a) benzene, 0 °C-room temperature, 3 h ; b) Zn/HCl, EtOH, 0 °C-room temperature, 3 h, 80%; c) *D*-(-)-pantolactone **10**, diphenyl ether, ~100 °C, 24 h; ~200 °C, 20 min, 50-55%. ***** stereocenter.

Scheme 8. Synthesis of CJ-15,801 allyl ester **6**.

1.7.7 Marquez's total synthesis of CJ-15,801.

Based on previous experience with olefination of *N*-formylmides, the Marquez group published the total synthesis of CJ-15,801 in 2011.[39] To access the *N*-formylimide **24**, *D*-(-)-pantolactone **10** was

opened using neat ammonia to afford amide **23**. Through diol protection and then formylation over amide **23**, the desired *N*-formylimide **24** was obtained in good yield (Scheme 9).

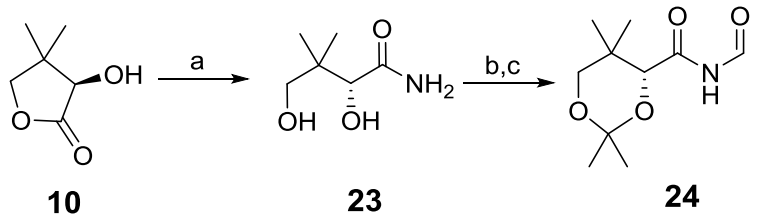

Reagents and conditions: a) NH_3, -33 °C, 16 h, 99%. b) 2-methoxypropene, *p*-TsOH, acetone, CH_2Cl_2, 0 °C to rt, 1 h. c) *n*-BuLi, *N*-formylbenzotriazole, THF, 0 °C to rt, 2 h, 63%.

Scheme 9. Synthesis of *N*-formylimide **24**.

Olefination of *N*-formylimide **24** with commercially available ylides afforded the expected vinilogous esters, however attempts to generate the acrylic acid after deprotection of silyl ethers gave unreacted materials or low yields.

In order to generate a route with potential applications, *N*-formylimide **24** was olefinated with ylide **25** to give a separable mixture of *E*/*Z* TMSE acrylates **26** and **27**. Sequential deprotection of silyl ether **27** using TBAF as a fluoride source, and removal of ketal from acrylic acid **28** by careful addition of $BiCl_3$, afforded in moderate yields the expected CJ-15,801 **2** (Scheme 10).

This fast and flexible route generates CJ-15,801 and interesting analogues. Benefits over previous approaches in term of cost and efficiency, and the ease for further functionalization of derivatives, make this approach a suitable tool for CJ-15,801 framework research.

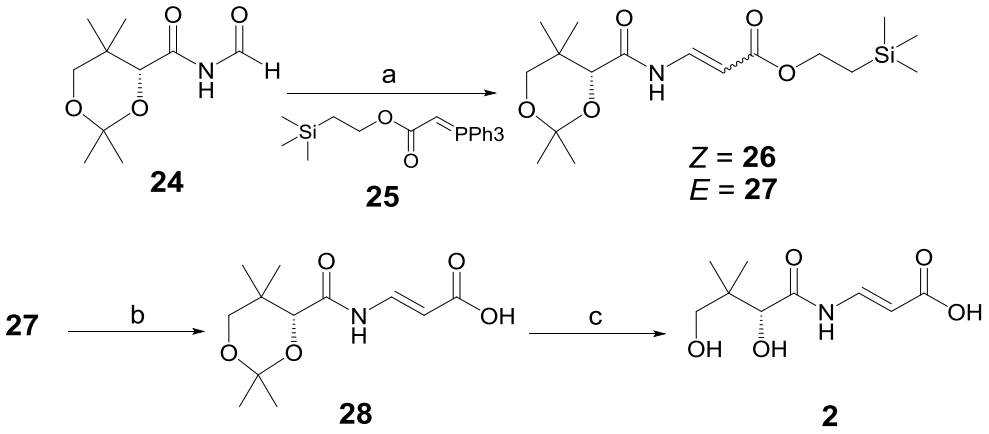

Reagents and conditions: a) **25**, benzene, 80 °C, 19 h, 76% (*E:Z*, 1.5:1.0). b) TBAF, THF, rt, 16 h, 79%. c) $BiCl_3$, CH_3CN, H_2O, rt, 19 h, 56%.

Scheme 10. Synthesis of CJ-15,801 **2.**

2. Results and discussion

2.1 Design and synthesis of new pantothenic acid analogues coupled to BODIPY FL.

Since Triebs and Kreuzer reported the first synthesis of the BODIPY core (4,4-difluoro-4-bora-3a,4a-diaza-*s*-indacene), many patents and articles have been published describing its wide range of applications. Due to their high fluorescence quantum yield (Φ), good solubility, as well as their photochemical and thermal stability, BODIPYs have been used extensively in biological labelling. BODIPYs are perfectly suited for use in biological studies due to their neutral core, which minimises the number of potential interactions with the bound ligand. BODIPYs are also stable at different pHs and have low photobleaching,[40] thus BODIPYs have become a key tool in fluorescence microscopy. BODIPYs are also cell permeable, which has further allowed them to be used as labelling agents on a wide variety of ligands.[41] Thus, it is not surprising that a number of BODIPY derivatives have been generated through the years.

A significant number of conjugated BODIPYs are commercially available for cellular labeling and detection, such as BODIPY ® FL NHS (succinimidyl ester), which is used to label primary amines of proteins, amine-modified oligonucleotides, and other amine-containing molecules; and BODIPY ® FL maleimide, suitable for labeling cysteine residues in proteins and thiolated oligonucleotides (Figure 13).[42]

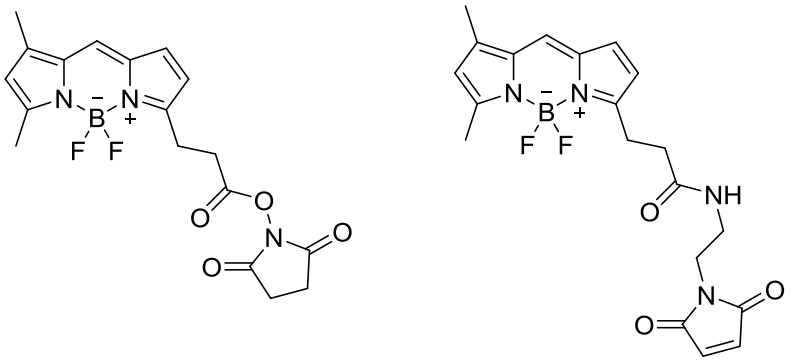

Figure 13. Commercial conjugated BODIPYs ® FL.[42]

Since its introduction in 2001 by Sharpless, ‘click’ reactions have proven to be versatile tools to produce libraries of compounds due to its ability to tolerate a wide range of functionalities.[43] In order to generate suitable functionalized BODIPYs for ‘click’ chemistry, Huo synthesized a new BODIPY **29**, bearing the required azido group on the 8 position of the BODIPY core. Cell viability test in human HepG-2 cells displayed minimal cytotoxicity, but fluorescent intensities for this dye are dependent of solvent viscosity (Figure 14).[44] Frequently, low performance has been reported for 8-azido and 8-amino BODIPY derivatives as imaging dyes, due to significant wavelength shifts.

The Marquez group reported the synthesis of newly functionalised 3-azido **30** and 3-amido **31** BODIPY-FL derivatives, starting from commercially available starting materials and presenting excitation/emission curves similar to commercial BODIPY FL ®. The derivatives were then successfully used in peptide and 'click' reactions with different ligands (Figure 14).[45]

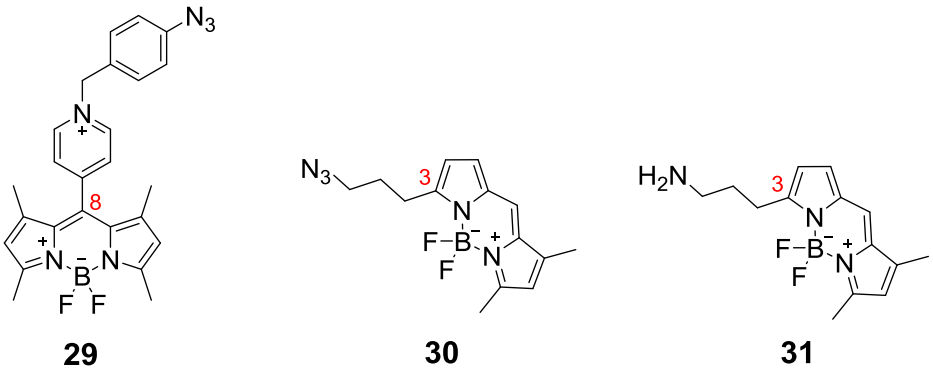

Figure 14. Functionalized BODIPYs for 'click' (**29**, **30**) and peptide (**31**) chemistry.

A very efficient route for the synthesis of CJ-15,801 and its diol-protected analogues was published previously by the Marquez group.[39a] A number of different CJ-15,801 derivatives coupled with BODIPY-FL were then generated, and their uptake tested in *P. falciparum* cultures. Excitingly, preliminary results showed significant uptake in the intraerythrocytic stages of the parasite's life cycle, without any apparent uptake into non-infected erythrocytes (Figure 15).[46]

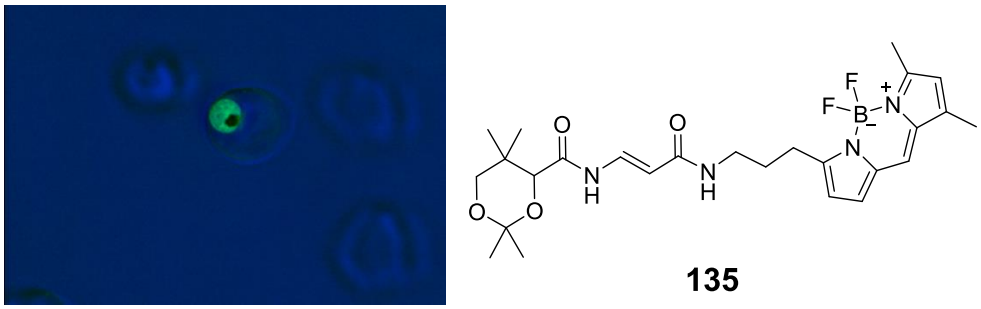

Figure 15. Uptake test of BODIPY-CJ-15,1801 analogue **135** in *P. falciparum*.[46]
Photo was taken through FITC filter, from experiments performed in RBCs infected with *P. falciparum* 3D7 at 25 µM and 37 °C after 45 min incubation.

AIMS.

The initial aims of the project, were to generate a new set of pantothenic acid derived fluorescent probes and to compare their uptake and selectivity to that of the CJ-15,801 derivatives in different biological systems.

Thus, the initial synthetic targets were the ketal and diol pantothenic acid-BODIPY complexes **42** and **43** (Scheme 11).

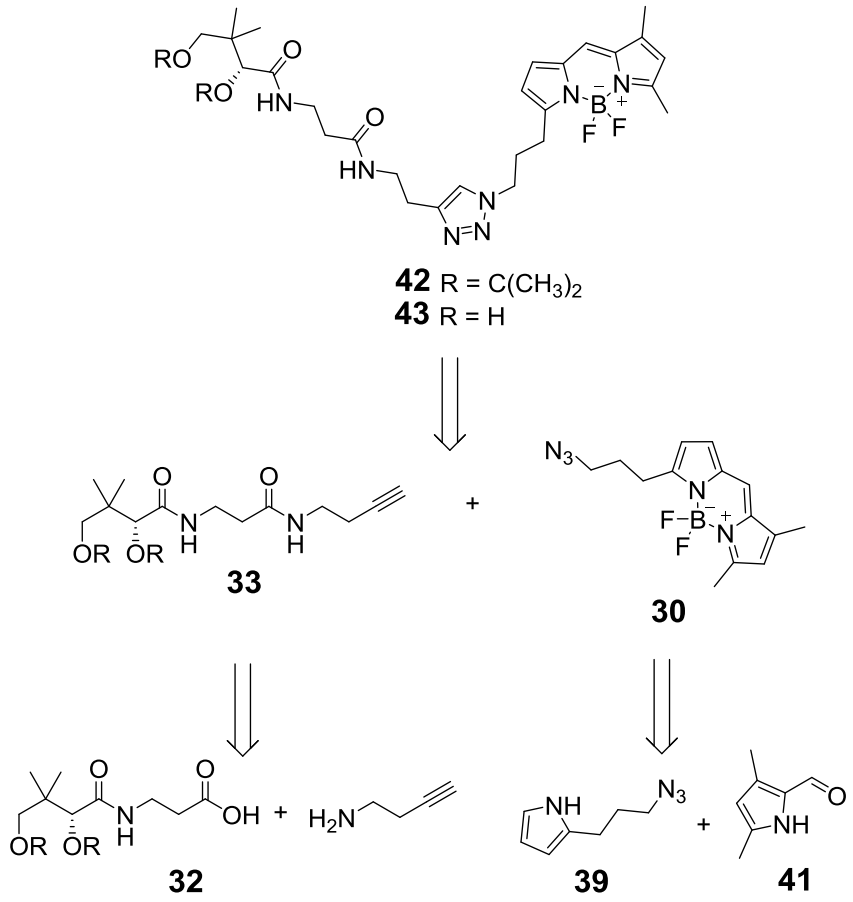

Scheme 11. Retrosynthesis of pantothenate derived analogues.

Retrosynthetically, BODIPY-pantothenic acid analogue **42** and BODIPY-pantothenic acid **43** were envisioned as originating from a 'click' reaction between alkyne **33** and azide **30**. While treatment of derived pantothenate **32** with amino-butyne could generate the desired alkyne unit **33**. On the other hand, the required azido-BODIPY **30** could be obtained from azide **39** and aldehyde **41**, following previous results within the group.[45]

The synthesis of alkyne **33,** began with the ketal protection of *D*-pantothenic acid hemicalcium salt **1** using Gaudelli's procedure to produce the expected acetonide **32**, in moderate yield.[47] Coupling of acid **32** with 1-amino-3-butyne, using HBTU as a coupling agent under microwave assisted reaction conditions then afforded the key alkyne intermediate **33** in good yield (Scheme 12).

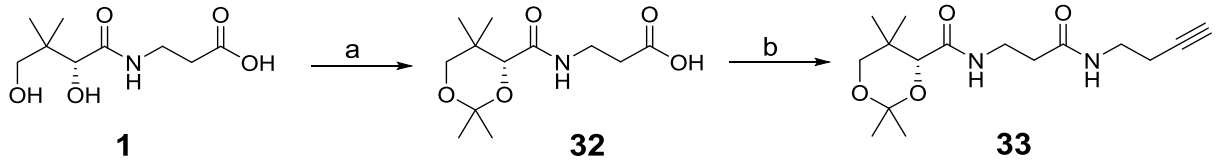

Reagents and conditions: a) acetone, *p*-TsOH, 4 Å ms, rt, 18 h, 55%, b) 1-amino-3-butyne, HBTU, DIPEA, CH_2Cl_2, mW, 80 °C, 3.5 h, 90%.

Scheme 12. Synthesis of alkyne **33.**

The synthesis of the BODIPY-azide coupling partner **39** began with the Wittig olefination of 1*H*-pyrrole-2-carboxaldehyde **34** with methyl(triphenylphosphoranylidene)acetate to afford the desired conjugated ester **35** as a single *E*-isomer in good yield. Hydrogenation of enoate ester **35** generated the corresponding ester **36**, which upon reduction of the ester group gave the desired primary alcohol **37** in high yield over two steps. Activation of the primary alcohol **37** using *p*-TsCl then produced tosylate **38** in moderate yield. Finally, reaction of tosylate **38** with NaN_3, afforded the desired azide **39** in good yield (Scheme 13).[45]

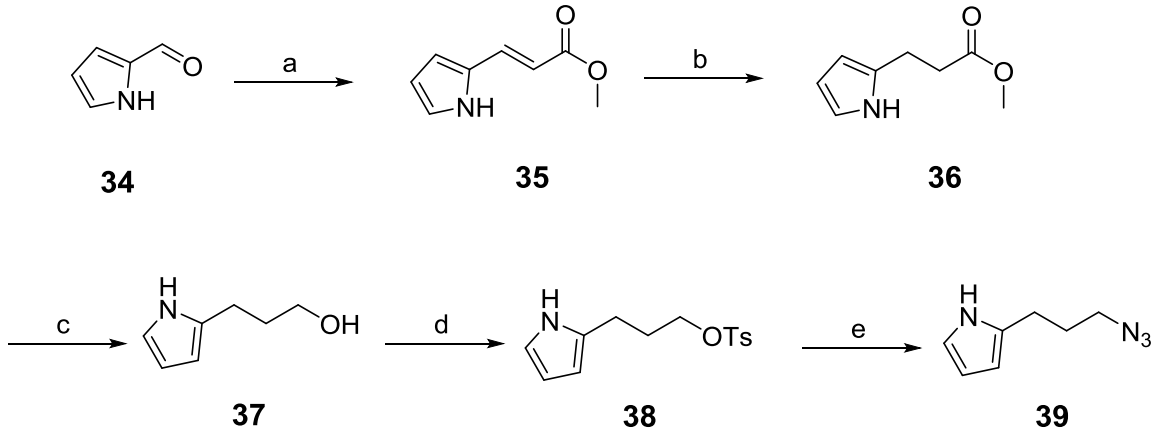

Reagents and conditions: a) methyl(triphenylphosphoranylidene)acetate, benzene, 80 °C, 18 h, 73%. b) H_2, Pd/C 10%, rt, 18 h, 93%. c) Et_2O, $LiAlH_4$, 0 °C to rt, 16 h, quantitative. d) *p*-TsCl, CH_2Cl_2, Et_3N, 0 °C to rt, 2 h, 60 %. e) NaN_3, DMF, 70 °C, 16 h, 68%.

Scheme 13. Synthesis of azide building block **39**.

Having the azide **39** unit in hand, attention was focused on the completion of the BODIPY unit. Acylation of dimethylpyrrole **40** using Vilsmeier–Haack conditions, afforded the expected aldehyde **41** in moderate yield. Azide **39** was then coupled with aldehyde **41** using $POCl_3$ and $BF_3.Et_2O$ to generate the expected BODIPY-FL analogue **30** in good yield (Scheme 14).[45]

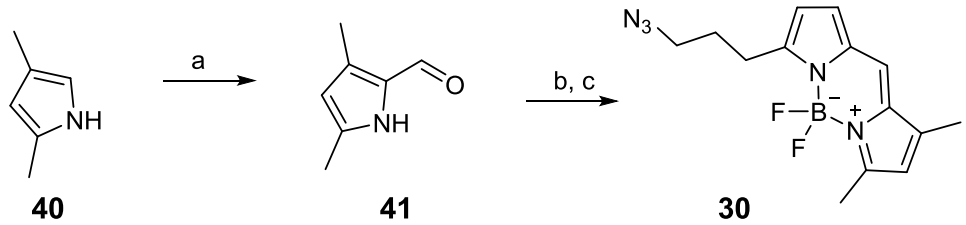

Reagents and conditions: a) DMF, $POCl_3$, 0 °C to 40 °C, 18 h, 45%. b) **39**, CH_2Cl_2, $POCl_3$, 0 °C to rt, 6.5 h. c) $BF_3.Et_2O$, DIPEA, 0 °C to rt, 18 h, 59% after two steps.

Scheme 14. Synthesis of azido-BODIPY **30**.

Practically, it was decided to attempt the coupling between azido-BODIPY **30** and alkyne **33** using DIPEA and CuI, as the copper source, thus avoiding the addition of reducing agents which had the

potential to interfere with the BODIPY core. Gratifyingly, the 'click' reaction afforded the desired triazole **42** in good yield and a single regio-isomer, thus completing the synthesis of the new BODIPY-ketal pantothenic acid analogue **42** (Scheme 15).[45]

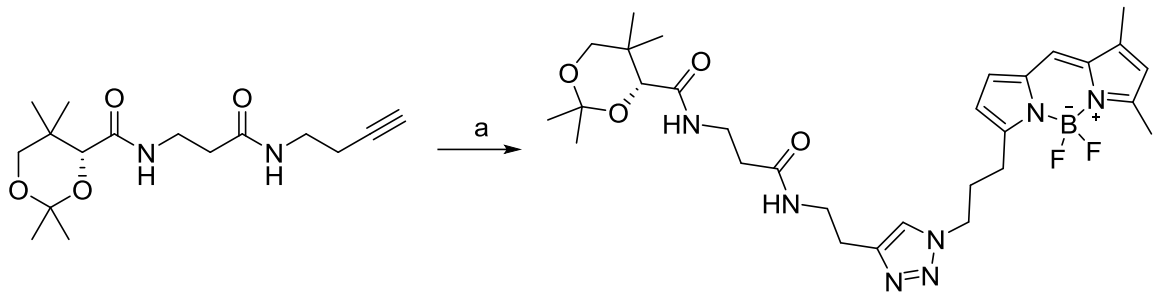

33 **42**

Reagents and conditions: a) azido-BODIPY **30,** CuI, DIPEA, THF, 70 °C, 18 h, 87%.

Scheme 15. Synthesis of pantothenic acid analogue **42**.

With the ketal protected pantothenic acid derivative **42** available, the removal of the ketal unit was attempted. Excitingly, treatment of ketal **42** under $BiCl_3$ promoted conditions, generated the desired new pantothenic acid derived analogue **43**. Although the reduction proceeded in low yield due to the formation of a large number of byproducts, this approach provided enough material for our biological testing needs (Scheme 16).

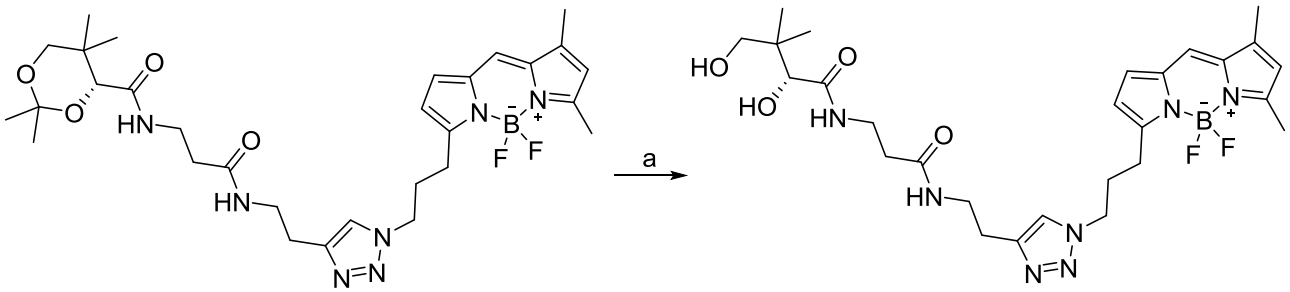

42 **43**

Reagents and conditions: a) $BiCl_3$, CH_3CN, H_2O, rt, 17 h, 28%.

Scheme 16. Synthesis of pantothenic acid-BODIPY complex **43**.

2.2 Evaluation of CJ-15, 801 and pantothenic acid analogues coupled to BODIPY FL in *C. elegans*.

Uptake tests were performed in *C. elegans* in collaboration with Dr. Collette Briton and her group from the Institute of Biodiversity, Animal Health & Comparative Medicine (UoG). The BODIPY-CJ-15,801 analogues **121**-**128** provided by Dr. S. O'Byrne and the newly synthesized BODIPY-pantothenate analogues **42** and **43** (synthesis previously described in section 2.1) were considered to study the uptake in this multicellular model.

The nematode *C. elegans* is a free-living worm, with a short and simple life cycle, making it an ideal biological model. Anthelmintic and nematocidal development programs often take advantage of its similarities with other species in the phylum *Nematoda* to carry out *in-vitro* studies.[48]

The actual uptake tests were performed using a wild-type strain Bristol N2 mixture stage *C. elegans* culture. All the compounds were tested at 50 μM concentrations following the procedure described in section 5.

In the case of the pantothenate derivatives, diol **43** showed a slight amount of fluorescence in the gut lumen and gut cells of larvae after 3 h. No increase was observed after 20 h incubation. In the case of the ketal protected pantothenate derivative **42**, the best results were obtained after 20 h incubation.

Larvae treated with BODIPY **30**, as control, showed slight fluorescence in the gut lumen and the gut cells, similar than individuals treated with diol **43**. It seems that the uptake for both BODIPY **30** and diol **43** is reduced even after 20 h incubation (Figure 16).

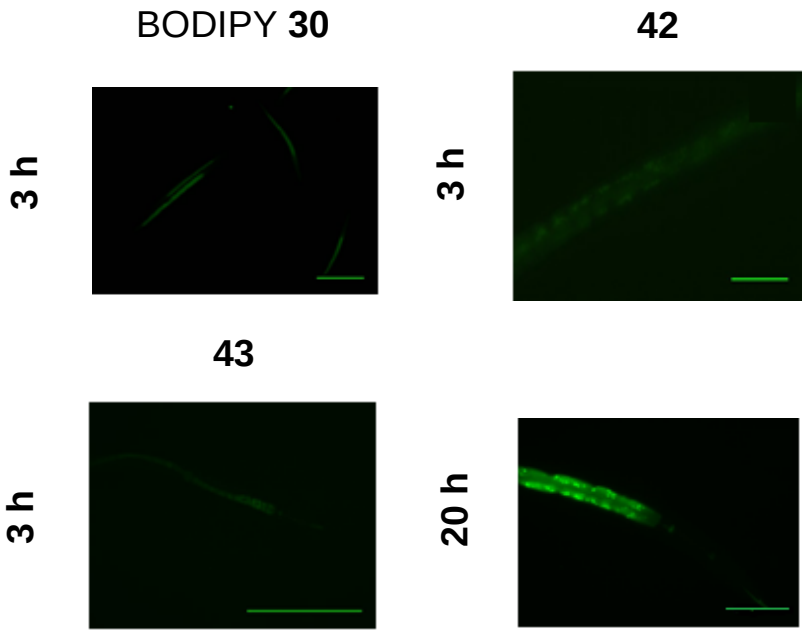

Figure 16. Uptake test of BODIPY-pantothenic acid derivatives **42, 43** and BODIPY **30** in *C. elegans*. Photos were taken through FITC filter, from experiments performed at 50 μM and 20 °C; samples were taken after 3 and 20 h incubation. BODIPY **30** and **43** size bar: 500 μm. **42** size bar: 100 μm.

Interestingly, the results from the CJ-15,801 derived probes showed that the best uptake was obtained with the *trans*-ketal CJ-15,801 derivative (*R*)-**121**. Indeed compound (*R*)-**121** showed significant uptake even after a 3h incubation. Fluorescence was localised in the gut lumen, gut cells and in the pharynx (Figure 16).

In order to measure the fluorescence intensities and compare the uptake of CJ-15,801 derivatives, the images were analysed by ImageJ 1.50b software following the procedure reported by Miller.[49] Gratifyingly, the microscope findings are consistent with the calculated intensities. After a 3 h incubation, derivative (*R*)-**121** exhibited the highest value compared with the rest of tested derivatives, whilst (*S*)-**122** derivative showed much lower value (6 times less) compared with its enantiomer. When the incubation was prolonged to 20 h, uptake of CJ-15,801 derivatives (*R*)-**124** and (*S*)-**123** could be reliably detected (Figure 17).

Ketal pantothenic derivative **42** showed minimal and slight fluorescence intensities after 3h and 20 h incubation. On the other hand, pantothenic acid derivative **43** exhibited consistently minimal fluorescence at 3 h and 20 h incubation (Figure 17).

Notably, for both groups (CJ-15,801 and pantothenic acid derivatives), the ketal compounds exhibited more uptake compared with its diol counterparts. It seems that lipophilicity plays an important role for the uptake process of our fluorescent derivatives (clogP ~ 3.6 for ketal derivatives *vs.* clogP ~1.1 for diols, calculated by ChemDrawPro 15.0). However, the absolute configuration and geometry on the CJ-15,801 core clearly played a key role in the selective uptake mechanism. Only (*R*)-**121** derivative exhibited an outstanding uptake, confirmed by microscopy and quantitative analysis, over its enantiomer (*S*)-**122** and regioisomer (*R*)-**123**.

According to several reports, pantothenic acid is one of the required vitamins for successful cultivation of *C. elegans.*[50] Based on this information, it seems that the low fluorescent intensities from pantothenic acid derivatives **42** and **43** after incubation, could be caused by degradation of the derivatives by the *C. elegans* machinery.

After the uptake of derivatives **42** and **43**, the organism started to metabolize rapidly the complexes. The slightly increased fluorescence after 20 h for ketal derivative **43** could be accumulation of derivative due to its lipophilic properties. Additionally, worms were visible alive and without apparent detriment of mobility throughout these short-term tests.

Due to its tough cuticle, toxicity and drug discovery researchers consider *C. elegans* not to be a good absortion model. Thus, to solve this issue, chemical removal of the cuticle, *C. elegans* collagen-deficiency mutated strains or higher initial compound concentrations (25–100 μM) are typically used in *C. elegans*-based drug screens.[51] Excitingly, the cuticle of the worms in these experiments was intact, adding a valuable characteristic to our drug delivery system as a drug carrier.

Based on our results, we believe that CJ-15,801 and pantothenic acid derivatives exhibit a selective uptake mechanism in *C. elegans*.

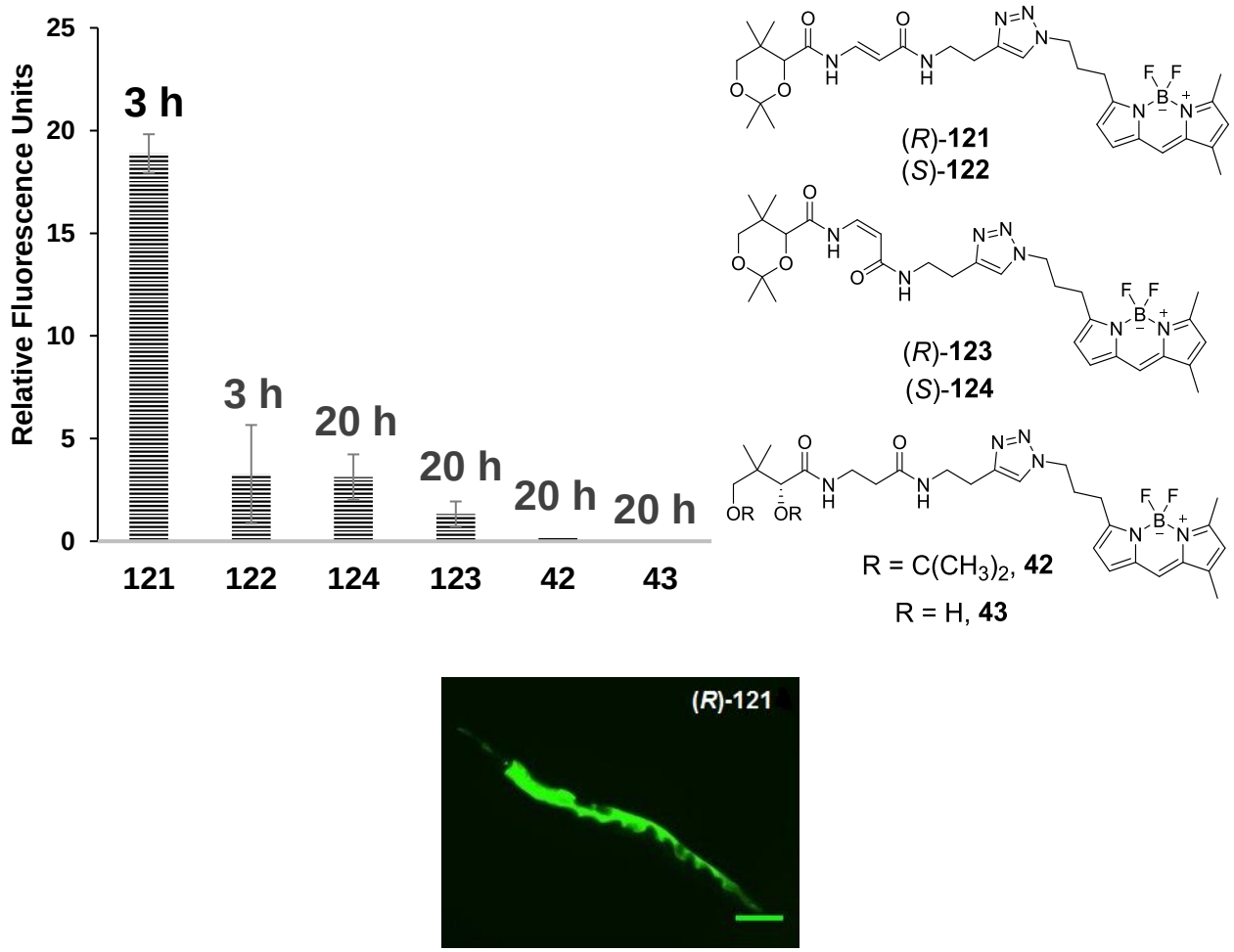

Figure 17. Uptake test of BODIPY-CJ-15,801 derivatives **42**, **43** and **121-124** in *C. elegans*. Bar chart represents Relative Fluorescence Units (RFU) from experiment performed at 50 μM and 20 °C, samples were taken after 3 and 20 h incubation. RFU's were calculated from images using ImageJ software. (Units x10^6).

Photo was taken from sample treated with BODIPY-CJ-15,801 derivative (*R*)-**121** through FITC filter, from experiment performed at 50 μM and 20 °C after 3 h incubation, size bar: 100 μm.

In collaboration with Dr. Jonathan Ewbank, from the Centre d'Immunologie de Marseille-Luminy, long-term studies were performed with the *C. elegans* strain *fer-15(b26ts)*, to test the persistence of fluorescence post-uptake. The worms were incubated with either DMSO, BODIPY **30** or CJ-15,801 derivative (*R*)-**121** at 50 μM for either 3 or 20 h. After the initial incubation the compounds were removed, and the worms cultivated under standard conditions.

The worms were then analysed under the fluorescence microscope at different time points post incubation. The worms incubated for 20 h with BODIPY **30** and derivative (*R*)-**121** after 2 h post-incubation presented consistency with our previous results. The worms treated with BODIPY **30** showed slight fluorescence in the gut lumen and gut cells, and the group treated with derivative (*R*)-**121** exhibited high fluorescence in the gut lumen, gut cells and the pharynx.

Interestingly, 78 h post-incubation worms treated with CJ-15,801 derivative (*R*)-**121** still exhibited fluorescence in the gut cells and the pharynx. The worms were viable and fully motile. The worms treated with BODIPY **30** only showed residual autofluorescence (Figure 18).

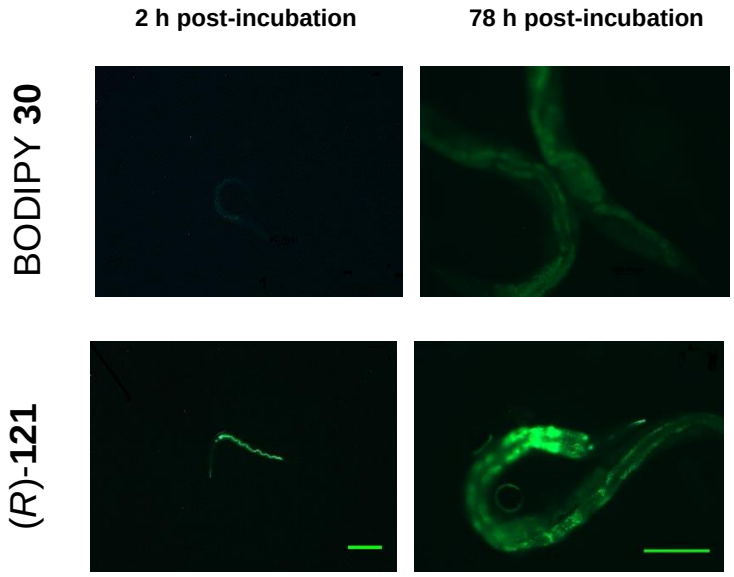

Figure 18. Long-term fluorescence evaluation of BODIPY-CJ-15, 801 derivative (*R*)-**121** and BODIPY **30** in *C. elegans*.

Photos were taken through FITC filter, from experiments performed at 50 µM and 25 °C and 20 h initial incubation; samples were taken after 2 and 78 h post-incubation. Size bars: 2 h post-incubation, 200 µm. 78 h post-incubation, 100 µm.

After the 3 and 20 h incubation periods, the worms were also analised using a COPAS Biosort system. In the COPAS Biosort an emission measurement is obtained for each single worm, and a G/TOF value generated.

After 66 h and 73 h post incubation, as expected, the fluorescence readings decreased over time. However, in the case of compound (*R*)-**121**, fluorescence was still present, observed under the microscope and measured by the biosorter. In contrast, worms treated with BODIPY **30** showed fluorescence levels similar to those of the DMSO control (Figure 19).

Crucially, as well as in short-term results, the viability and motility of the worms were not affected by CJ-15,801 derivative (*R*)-**121**. These results suggest that (*R*)-**121** derivative, at tested concentrations, exhibited low toxicity in *C. elegans* and can be used for long term studies.

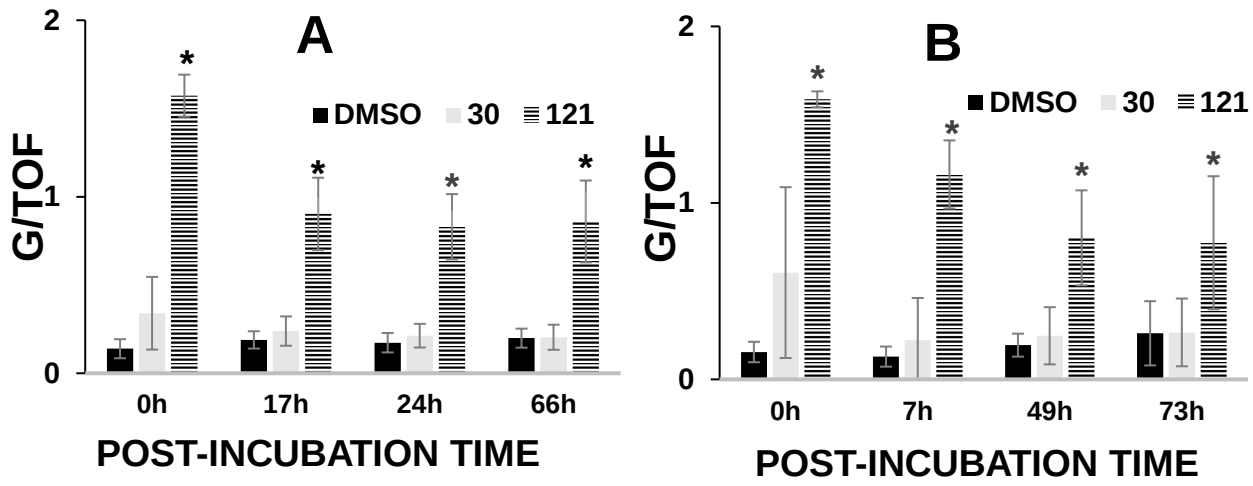

Figure 19. Long-term fluorescence evaluation of BODIPY-CJ-15,801 derivative (*R*)-**121** and BODIPY **30.**

Bar charts represents G/TOF (G: green fluorescence intensity *vs.* TOF: time of flight, represents the axial length of worm) from experiments performed at 50 µM and 25 °C, worms were treated with compounds for 3 and 20 h initial incubation. Then, the compounds were removed and the samples were taken after different time post-incubation points. **A**) 3 h initial incubation, **B**) 20 h initial incubation. (Units $x10^3$).The asterisks indicate significant differences ($*P < 0.05$) between derivative (*R*)-**121** and BODIPY **30** control- analysed using an independent Student's t-test. The figure represents a single experiment.

In drug development research it has been reported that when drugs are tested in *C. elegans,* they access the organism by two ways: either ingestion or diffusion across the cuticle.[48,51] Our results suggest that BODIPY **30** goes into the worms by a simple diffusion processes, and reach maximum uptake during the first three hours. At this point, it is either excreted or it suffers photobleaching, caused by physiological conditions.

In contrast the pantothenic acid and CJ-15,801 analogues exhibited different uptake processes. Our results suggest that pantothenic acid and CJ-15,801 derivatives are transported selectively, with the transporter being able to discriminate enantiomers. Interestingly, *C. elegans* accumulates the derivatives, and they have no apparent impact on its mobility and morphology. This opens the possibility that CJ-derivatives could be used as non-toxic carriers in nematode research.[50]

2.3 Design and synthesis of new CJ-15,801 and pantothenic acid derived analogues for bioconjugation with phiLOV.

The encouraging results obtained during the biological testing of the CJ-15,801-BODIPY analogues in *C. elegans*, revealed different uptake levels depending on the nature of the analogue. The fact that the CJ-15,801 analogues were able to differentially deliver BODIPY units (ca. 220 Da.) prompted us to consider the use of CJ-15,801 derivatives as delivery vehicles for larger molecules. Of particular interest was derivative (*R*)-**121**, which showed significant uptake even after a 3 h incubation in *C. elegans* tests.

It is worth reiterating that whilst the (*R*)-*trans*-ketal derivative **121** showed the highest uptake of all the derivatives, the (*S*)-*trans*-enantiomer **122** (6 times less) and the (*R*)-*cis*-isomer **123** (17 times less) showed the least amount of uptake. These remarkable differences in uptake strongly suggest that selective transport is taking place.

The fact that the uptake is not diffusion controlled, opened up the tantalising opportunity to explore its use for the delivery of molecules not easily delivered by other methods (i.e. diffusion). Thus, we became interested in exploring its ability to deliver a much larger biomolecule (i.e. a protein).

In an analogous way to the BODIPY dyes, fluorescent proteins (FP) have been used widely in fluorescence microscopy. The fusion of green fluorescent protein (GFP) with other proteins, represents one of the most widely used strategies for monitoring protein expression and localization. However, limitations have emerged over time. In particular, GFP performance can be reduced under low-oxygen conditions (i.e. when used in tumour growth assays) or by temperature and pH changes. The fusion itself can also affect the functionality of the target protein due to GFP's large size (27 kDa) (Figure 20, A).[52]

In 2007, Jaeger and co-workers reported the discovery of the LOV family of proteins. LOV proteins, are small proteins (12~19 kDa), and perform efficiently both in aerobic and anaerobic environments with fluorescence being regulated by Light, Oxygen or Voltage.[53] Further research then lead to the isolation of improved LOV proteins (iLOV) from *Arabidopsis thaliana*. iLOV and its photostable derivative (phiLOV) are monomeric proteins (~12 kDa) suitable for confocal imaging (Figure 20, B, D). Structurally, both iLOV and phiLOV contain a flavin mononucleotide (FMN), which under UV light, promotes the excision of a covalent bond between cysteine from the LOV domain and the FMN chromophore, which results in green fluorescence (Figure 20, C).[52b, 54]

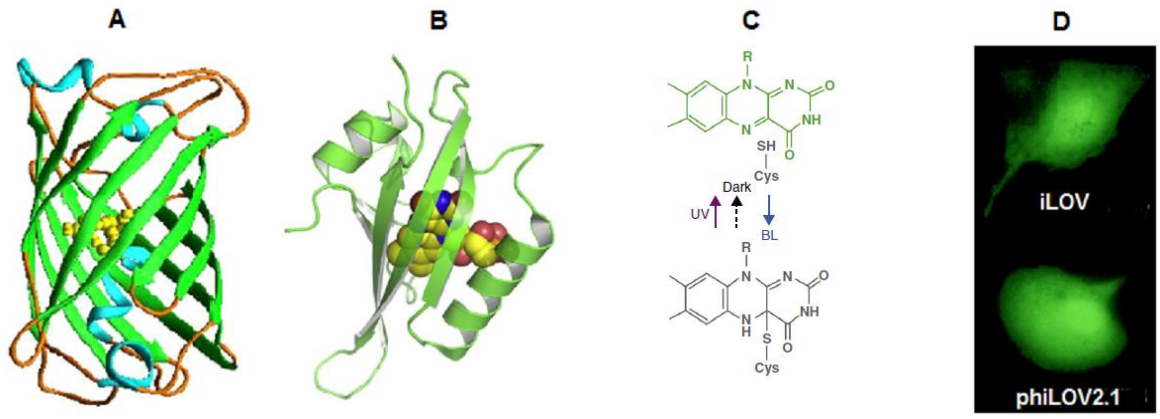

Figure 20. Green fluorescent protein (GFP) and LOV proteins.[52b, 55]
A) GFP (PDB entry 1GFL) visualized using PyMOL (chromophore is shown as spheres). B) iLOV (PDB entry 4EES) visualized using PyMOL. (FMN fluorophore is shown as spheres). C) Proposed natural photocycle in LOV domain. D) LOV proteins expressed in BSC1 monkey kidney cells.

Based on its fluorescence and stability at physiological conditions, phiLOV was an ideal model for our uptake studies. Maleimide derivitization of a protein is a common tool for conjugation with fluorescent probes, taking advantage of a free sulfhydryl group in the protein. In order to provide selectivity in proteins that contain more than one cysteine residue, site-directed mutagenesis is used to change those cysteines to serines or alanines.[56] Thus, it was decided to use a maleimide coupling approach, in which the protein would be coupled to the CJ-15,801 derivative through a cysteine residue (Scheme 17). The logic behind this approach being that it would provide a convergent approach for the generation of the construct, whilst reducing the risk of protein denaturing. The maleimide unit, could also potentially be accessed from some of the late intermediates generated during the synthesis of CJ-15,801.

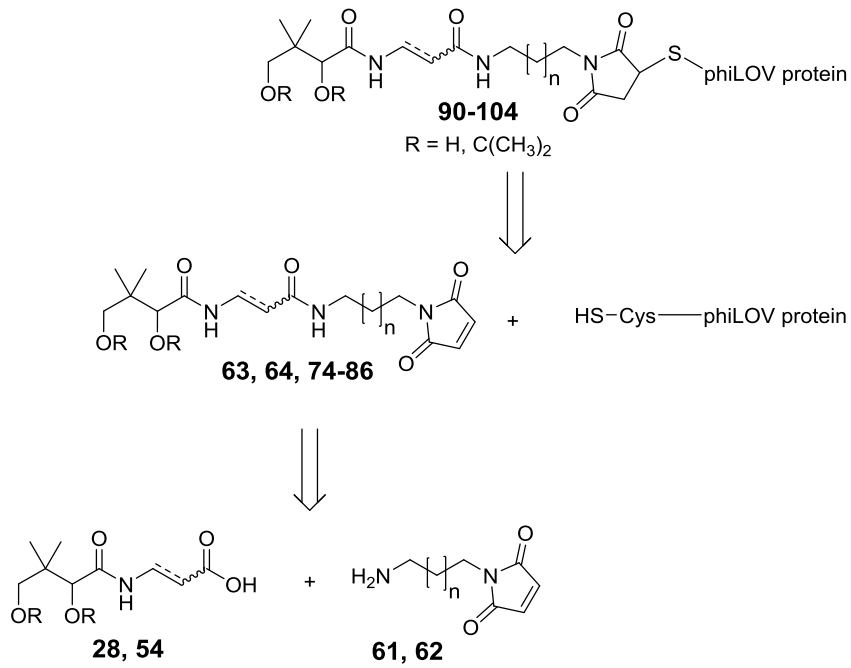

Scheme 17. Retrosynthetic analysis for the synthesis of phiLOV coupled to CJ-15,801 and pantothenic acid derived analogues.

The synthesis of the maleimide functionalised CJ-15,801 unit began with the opening of *D*-(-)-pantolactone **10** with neat ammonia, to afford the desired diol **23** in quantitative yield. Protection of the diol unit using 2-methoxypropene and *p*-TsOH, as proton source, generated the expected ketal **44** in working yields (Scheme 18).

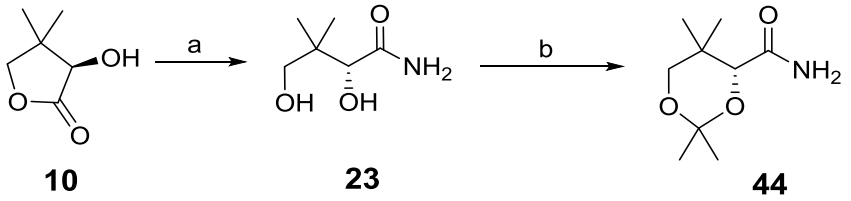

Reagents and conditions: a) NH_3, MeOH, -78 °C to rt, 16 h, 99%. b) 2-methoxypropene, *p*-TsOH, acetone, CH_2Cl_2, 0 °C to rt, 16 h, 55%.

Scheme 18. Synthesis of carboxamide **44**.

With the desired protected amide **44** in hand, formation of the *N*-formyl imide was attempted. The synthesis began with the quantitative generation of the formylating agent, *N*-formylbenzotriazole **49,** using formic acid **45** and acetic anhydride **46** following protocols developed previously in the group (Scheme 19).[57]

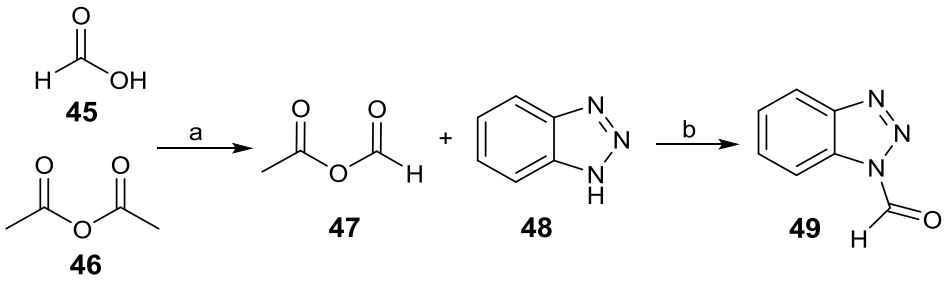

Reagents and conditions: a) 55 °C, 3 h, 74%. b) THF, 0 °C, 2 h, 97%.

Scheme 19. Synthesis of *N*-formylbenzotriazole **49**.

With a fresh batch of *N*-formylbenzotriazole **49** in hand, the desired formylation reaction was attempted following the procedure of Villa, M.[39b] Initially however, a test reaction using benzamide **50** was attempted. Gratifyingly, the expected imide unit was obtained in acceptable yield (Scheme 20).

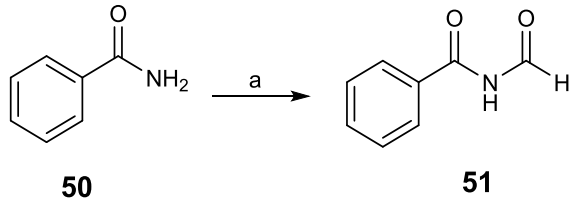

50 **51**

Reagents and conditions: a) *n*-BuLi, *N*-formylbenzotrizole **49**, THF, 0 °C to rt, 16 h, 36%.

Scheme 20. Synthesis of *N*-formylbenzamide **51.**

The same procedure was then used to attempt the formylation of the pantolactone derived amide **44**. As expected, the desired *N*-formyl imide **24** was obtained in good yield (Scheme 21).[39]

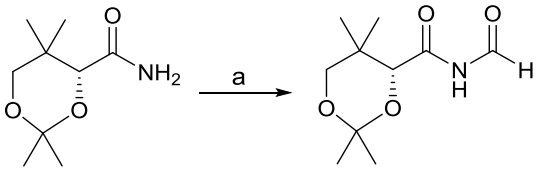

44 **24**

Reagents and conditions: a) *n*-BuLi, *N*-formylbenzotriazole **49**, THF, 0 °C to rt, 16 h, 87%.

Scheme 21. Synthesis of *N*-formyl imide **24**.

Having successfully generated the required *N*-formyl imide **24**, we focused our attention on the formation of the ylide reagent required for the olefination of the *N*-formyl group. The synthesis of the Wittig ylide **25** began by the esterification of bromoacetyl bromide with 2-(trimethylsilyl)ethanol **47**, to generate the desired bromoacetate **48** in good yield. Reaction of the crude bromoacetate **48** with triphenylphosphine, proceeded over four days to afford the required key phosphonium salt **25** in moderate yield (Scheme 22).[39a]

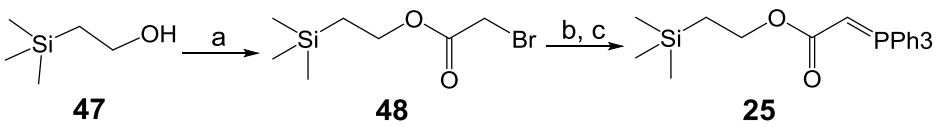

47 **48** **25**

Reagents and conditions: a) bromoacetyl bromide, Et_3N, CH_2Cl_2, 0 °C to rt, 16 h, 88%. b) PPh_3, toluene, rt, 96 h. c) sat. aq. $NaHCO_3$, 2 h, 50% after two steps.

Scheme 22. Synthesis of ylide **25.**

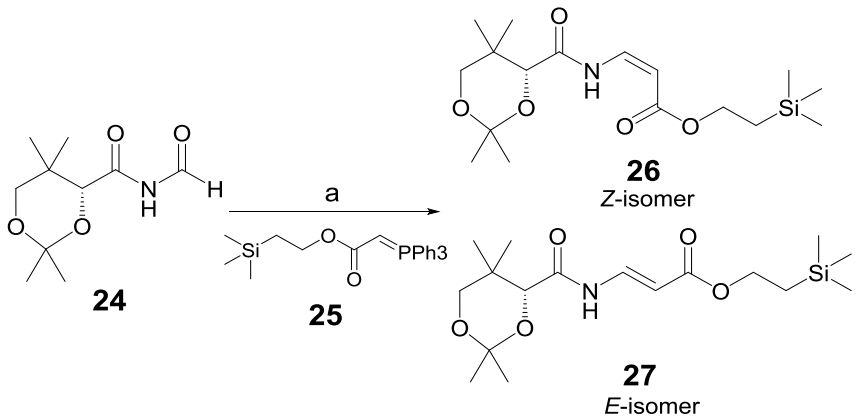

Reagents and conditions: a) **25**, benzene, 80 °C, 16 h, 95% (*E:Z*, 2.1:1.0).

Scheme 23. Wittig reaction.

The subsequent Wittig reaction between *N*-formyl imide **24** and stabilized ylide **25** proceeded in an optimized yield of 95% to afford the *E* and *Z* acrylates **26** and **27** in a 2.1:1.0 ratio (Scheme 23). Interestingly, a high percentage of the product ratio comprised the *cis* isomer even though a stabilized ylide was used. Stabilised ylides tend to preferentially yield the *E* products when reacted with simple aldehydes through the following transition state (Figure 21).[46, 58]

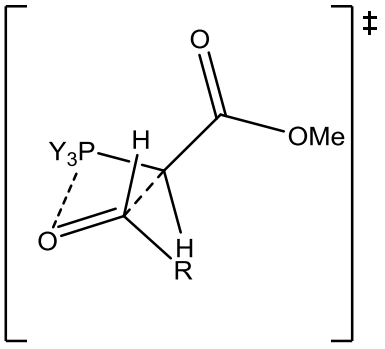

Figure 21. Proposed favorable transition state of stabilized ylides and simple aldehydes.[58]

The formation of the *cis* acrylate can be explained through the formation of a hydrogen bond between the *N*-formyl imide (N-H) and the stabilized ylide (C=O) which favours the *syn* transition state (Figure 22, a). In the case of simple aldehydes, the same stabilizing hydrogen bonding interaction is not

present which significantly increases the energy of the *syn* transition state, relatively to that the *trans* transition state (Figure 22, b).

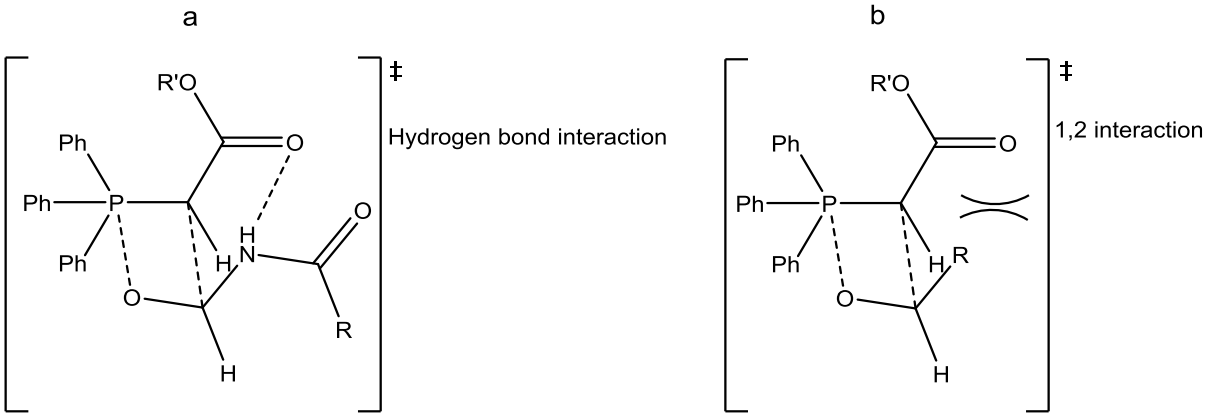

Figure 22. a) Proposed transition state for *cis* olefination products using *N*-formyl imides showing the stabilising hydrogen bond interaction. b) Proposed unfavourable *syn*-transition state during the Wittig olefination of aldehydes using stabilized ylides.[46]

With the complete CJ-15,801 framework in place, we switched our attention to the removal of the trimethylsilylethyl ester group, to generate the free carboxylic acid functionality. It is worth recalling that the trimethylsilylethyl group had been chosen due to its ability to be removed under conditions in which the enamide unit would not be affected.

Initial attempts to unmask the free acid using TBAF proved to be unsuccessful, which was consistent with results obtained by other members of the group. This was in mark contrast to results obtained during the initial studies towards the synthesis of CJ-15,801, in which TBAF was extremely efficient in removing the trimethylsilyl ethyl group. The reasons behind this change in behaviour are not yet clear, but it is likely to be related to the TBAF manufacturing and supply process.

In any event, switching from TBAF to TASF as the fluoride source proved successful, and provided us with the *cis* and *trans* ketal protected CJ-15,801 analogues **28** and **54** isomers in good to excellent yields[39a-46] (Scheme 24). No further efforts were conducted to identify the causes behind the issues with TBAF.

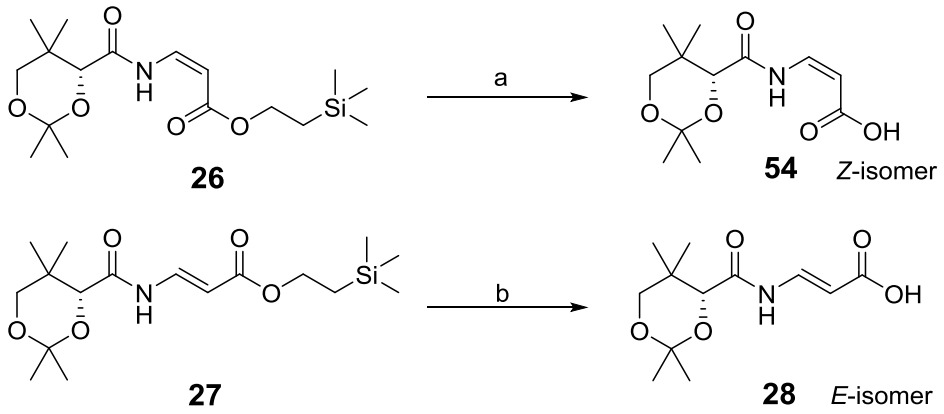

Reagents and conditions: a) TASF, DMF, 0 °C to rt, 20 h, 78%. b) TASF, DMF, 0 °C to rt, 20 h, 97%.

Scheme 24. Synthesis of *trans* and *cis* ketal protected CJ-15,801 analogues **28** and **54**.

Having completed the synthesis of the CJ-15,801 ketal analogues **28** and **54**, our efforts focused on the introduction of the maleimide unit, which would be used to link the CJ-15,801 analogues to the phiLOV mutants as previously described. Two linkers of different lengths were chosen initially (three-carbon and a five-carbon units) as we strived to determine the optimal distance between the protein and the delivery unit.

Different linker lengths would allow us to determine the ideal distance required to preserve the affinity of the carrier unit for its putative cell membrane transporter, and thus facilitate the protein transport. The 3-carbon alkyl spacer has been used successfully with probes such as BODIPY FL. Because it potentially reduces the interaction of the fluorophore with the biomolecule of interest. On the other hand, the use of the 5-carbon spacer would provide more information for further optimization of the tether length.[42,59]

The generation of the maleimide functionalised linkers was envisioned as being achieved through the selective derivatisation of differentially functionalized carbon linkers. Thus, the synthesis began with the Boc protection of the amino group of 5-aminopentanol **55**, to afford the corresponding carbamate **56** in good yield (Scheme 25).[60]

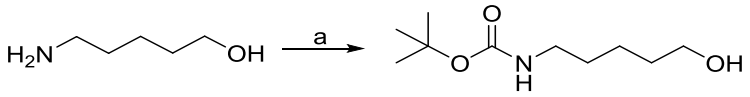

Reagents and conditions: a) Boc_2O, Et_3N, CH_2Cl_2, rt, 16 h, 74%.

Scheme 25. Synthesis of *N*-Boc-5-aminopentanol **56**.

Introduction of the maleimide unit was envisioned as taking place via a Mitsunobu reaction. Unfortunately, all attempts to couple alcohol **56** with maleimide **57** proved unsuccessful under standard Mitsunobu conditions.

Concerned that the lack of reactivity observed could be due to the purity of alcohol **56**, the same coupling was attempted using commercially available Boc-protected propanol **58**. Interestingly, coupling of maleimide **57** with commercially available Boc-protected propanol **58** in the presence of DEAD (Figure 23), also resulted in no product formation (Scheme 26).

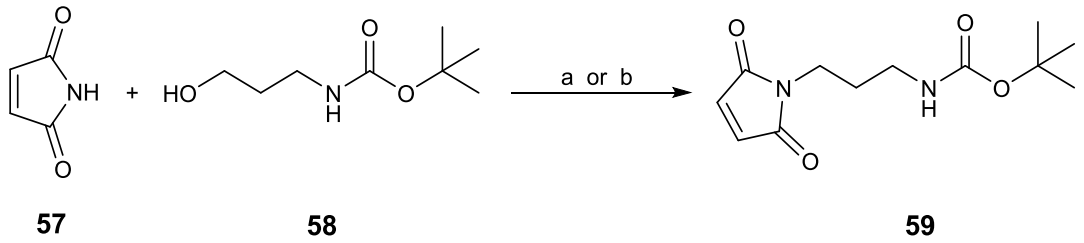

57 **58** **59**

Reagents and conditions: a) Ph_3P, DEAD, THF, rt, 16 h, 0%. b) Ph_3P, DIAD, THF, rt, 16 h, 69%.

Scheme 26. Mitsunobu reactions using DEAD and DIAD.

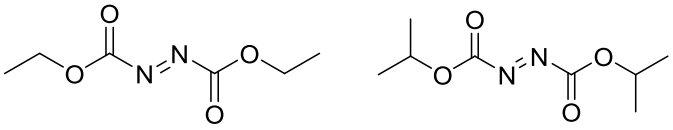

DEAD DIAD

Figure 23. Mitsunobu reagents.

Sen and co-workers[61] had previously reported the synthesis of phthalimide derived allylic amines, starting from allylic alcohols and phthalimide using DIAD (Figure 23) as a Mitsunobu reagent in good yields. Following Sen's precedence, the reaction of *N*-Boc protected amino propanol **58** was attempted in the presence of DIAD. Excitingly, under the modified conditions, the desired maleimide **59** was generated in good yield (Scheme 26).

Following the same successful DIAD promoted procedure, the five-carbon carbamate unit **56** was cleanly coupled with maleimide **57**, to generate the desired five-carbon substituted maleimide **60** in moderate yield (Scheme 27).

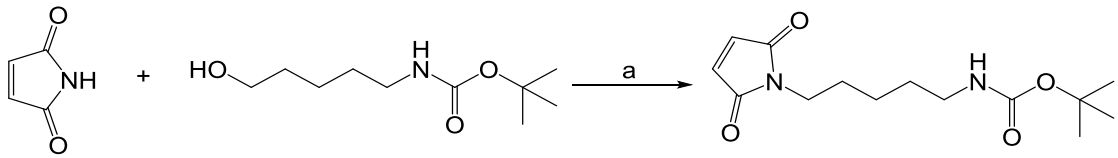

57 **56** **60**

Reagents and conditions: a) Ph_3P, DIAD, THF, rt, 16 h, 40%.

Scheme 27. Synthesis of 5-carbon maleimide derivative **60**.

With the maleimide unit in place, removal of the Boc protecting group was then undertaken. Gratifyingly, treatment of both the three and five carbon with trifluoroacetic acid underwent Boc removal cleanly to afford the desired substituted maleimides **61** and **62**, as TFA salts (Scheme 28).

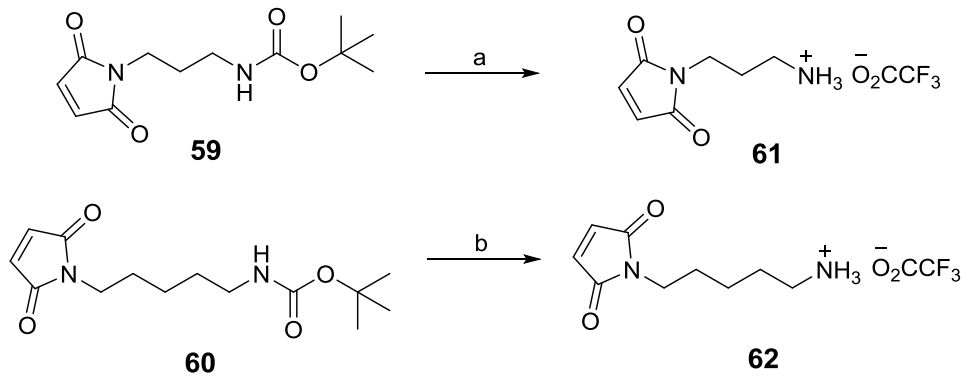

59 **61**

60 **62**

Reagents and conditions: a) TFA, CH_2Cl_2, rt, 3 h, 95%. b) TFA, CH_2Cl_2, rt, 2.5 h, 73%.

Scheme 28. Synthesis of maleimide three and five carbon linkers **61** and **62**.

With the amino functionalised linkers readily accessible, we decided to focus on their coupling with the different CJ-15,801 derivatives via amide linkages. Amide bonds are presented in biological systems, and have been widely used in medicinal chemistry. Their widespread use and versatility has resulted in a significant number of procedures and reagents being developed for their formation. DCC, belongs to the carbodiimides group of reagents, and has proven to be very reliable; however, it has the serious drawback that dicyclohexylurea is formed as a side product. EDC on the other hand, was developed as an improved carbodiimide coupling agent, with water soluble side products, thus facilitating the purification process (Figure 24).[62]

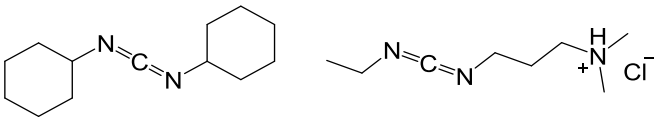

DCC EDC.HCl

Figure 24. Carbodiimides.

A different class of coupling agents, the aminium reagents (i.e. HBTU and TBTU), require a base to initiate the coupling process, but are more reactive than carbodiimides. In very difficult cases where both carbodiimides and aminium reagents fail, halouronium salts (i.e. BTFFH and TFFH) provide a way forward (Figure 25). These reagents work through the generation of an acyl fluoride intermediate *in-situ*, which then undergoes to the desired coupling.[62]

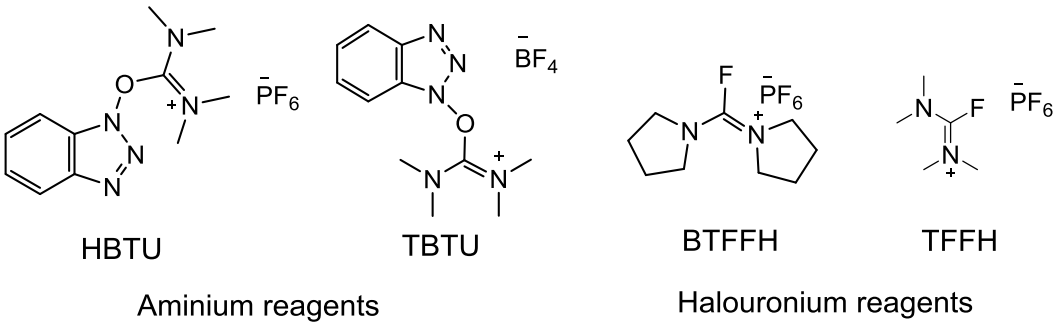

Figure 25. Coupling reagents.

Taking advantage of previous experience within the Marquez group for the coupling of primary amines with ketal-protected CJ-15,801 **28**, the coupling of maleimide **61** with carboxylic acid **28** was attempted under microwave conditions in the presence of BTFFH.[46] Although the reaction proceeded to afford the expected derivative **63**, the low yield obtained made this approach impractical (Scheme 29).

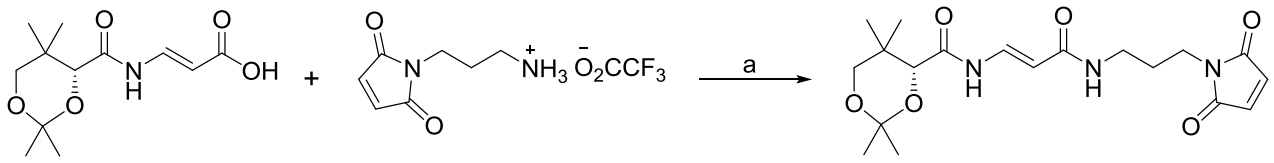

28 **61** **63**

Reagents and conditions: a) BTFFH (1.5 eq.), DIPEA, CH_2Cl_2, mW, 80 ^oC, 2.5 h, 33%.

Scheme 29. Coupling of CJ analogue **28** and the three-carbon linked maleimide derivative **61**.

The poor results with BTFFH prompted us to use HBTU as an alternative coupling agent for the reaction of the *cis*-CJ-15,801 isomer analogue **54** and the 3-carbon linked substituted maleimide **61**. Gratifyingly, the reaction gave the expected derivative **64**, albeit in low yield (Scheme 30).

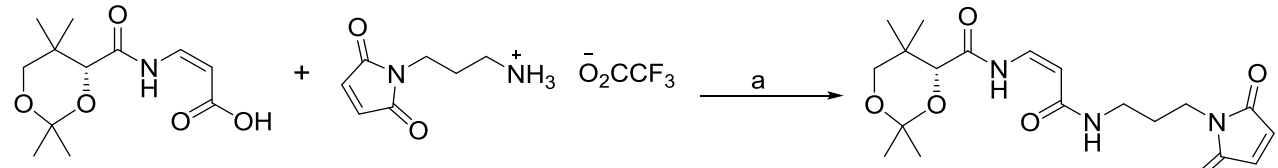

54 **61** **64**

Reagents and conditions: a) HBTU (1.5 eq.), DIPEA, CH_2Cl_2, mW, 80 ^oC, 2.5 h, 26%.

Scheme 30. Coupling of *cis*-CJ analogue **54** and the three-carbon maleimide derived linker **61**.

Although both BTFFH and HBTU gave the desired products, the yields were too low to be practical. Additionally, the Rf of the byproducts was very similar to that of the desired products. Indeed, even after purification by flash column chromatography, ^1H NMR analysis showed traces of impurities

which impacted the yield. Consequently, an alternative route was needed in order to generate the derivatives efficiently and without impurities.

Pentafluorophenyl trifluoroacetate[63] and pentafluorophenol[64] have been showed to be effective reagents to activate carboxylic acids as the corresponding pentafluorophenyl esters. Pentafluorophenyl esters are reactive intermediates which are easily purified, and more importantly, can be coupled with different nucleophiles without the need for further activation (Scheme 31).

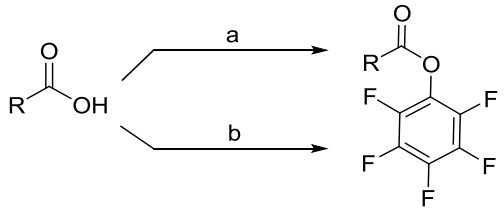

Reagents and conditions: a) Pentafluorophenyl trifluoroacetate, pyridine. b) pentafluorophenol, EDC or DCC.

Scheme 31. General approach for the synthesis of pentafluorophenyl esters.

Thus, the new approach for the synthesis of the maleimide derivatives began with the generation of the pentafluorophenyl ester of ketal protected CJ-15,801 **28**. Practically, ketal **28** and pentafluorophenol **65** were coupled using EDC and DMAP, to afford the desired pentafluorophenyl ester **66** as well as the unexpected *cis*-isomer **67** in a 1:1 ratio, in good overall yield (Scheme 32).

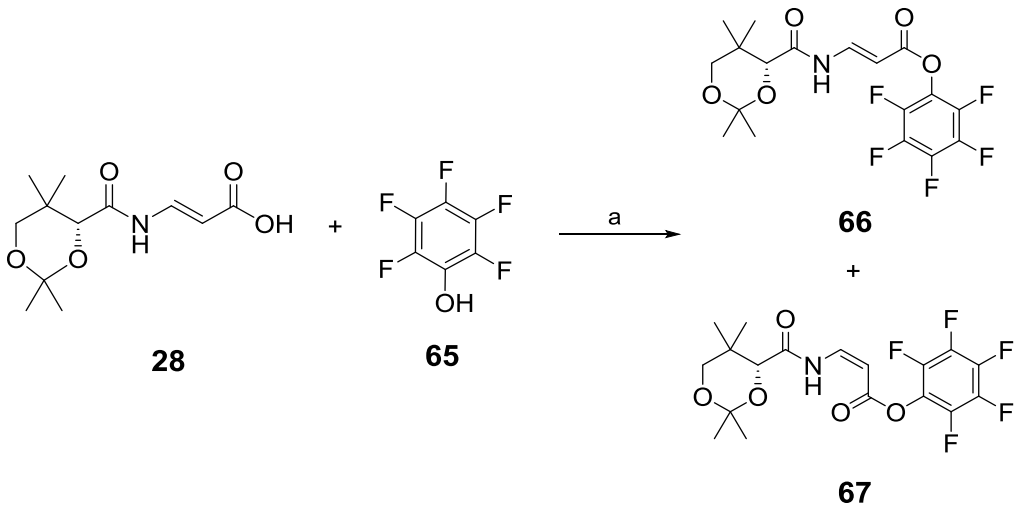

Reagents and conditions: a) EDC.HCl, DMAP, CH_2Cl_2, rt, 24 h, 82%, *E/Z* (1:1).

Scheme 32. Synthesis of pentafluorophenyl esters **66** and **67**.

Treatment of *cis*-ketal **54** with pentafluorophenol **65** proceeded to generate the *trans*-ester **66** and *cis*-ester **67** in quantitative yield as a mixture of double bond isomers *E/Z* ratio (1.0:1.8)(Scheme 33).

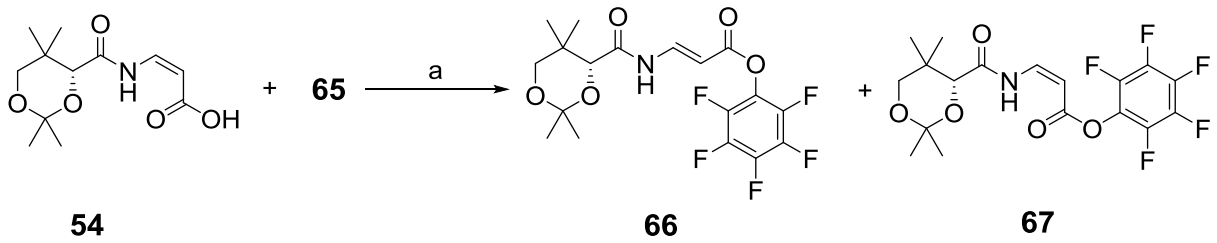

Reagents and conditions: a) EDC.HCl, DMAP, CH_2Cl_2, rt, 24 h, 99%, *E/Z* (1.0:1.8).

Scheme 33. Synthesis of pentafluorophenyl esters from **54**.

It is interesting to note that whilst simple *E*-double bonds are thermodynamically favoured, in both cases, the *E*/*Z* ratio is roughly 1:1. The product ratio can be explained by the conjugation of the ester products, which then equilibrate before being quenched. The significant amount of *Z* isomer observed can be explained by the extra stabilisation provided by the putative hydrogen bonding between the proton of the amide unit and the ester's carbonyl unit (Figure 26).

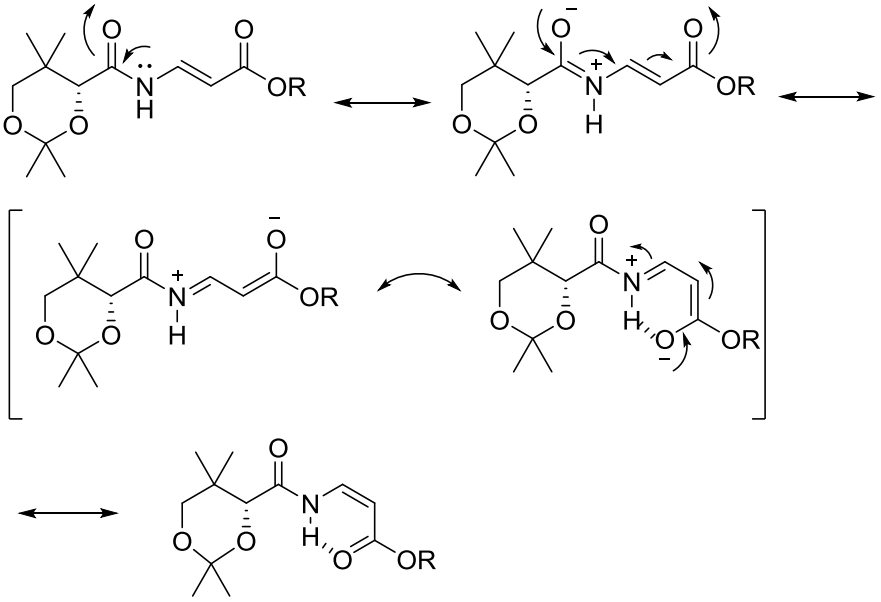

Figure 26. Proposed mechanism of ester products.

Having successfully generated the pentafluoro- substituted (*R*)-*cis*- and (*R*)-*trans*- enamides from *D*-(-)-pantolactone **10**, the route was reproduced on (*S*)-enamides **69** and **70** (compounds **69** and **70** were provided by Dr. S. O'Byrne, who completed their syntheses starting from (*L*)-(+)-pantolactone **68** (Figure 27). Activation of the (*S*)-acrylic acids **69** and **70** using pentafluorophenol **65** proceeded to afford the desired (*S*)-*trans*-ester **71** and (*S*)-*cis*-ester **72,** in low yields (Scheme 34). The yields were not optimised at this point.

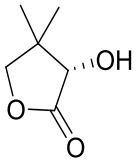

68

Figure 27. (*L*)-(+)-pantolactone

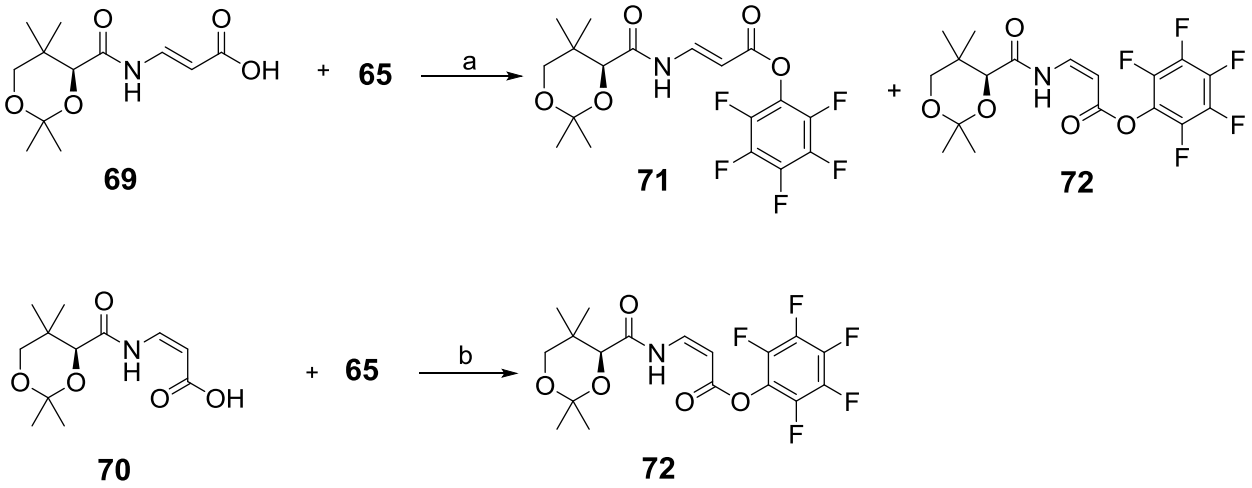

Reagents and conditions: a) EDC.HCl, DMAP, CH_2Cl_2, rt, 18 h, 26%, *E/Z* (3:1). b) EDC.HCl, DMAP, CH_2Cl_2, rt, 18 h, 40%.

Scheme 34. Synthesis of (*S*)-pentafluorophenyl esters **71** and **72**.

The ketal protected pantothenic acid analogue **32** was also coupled with pentafluorophenol **65,** using the same activation conditions described previously to give the desired ester **73** in good yield (Scheme 35).

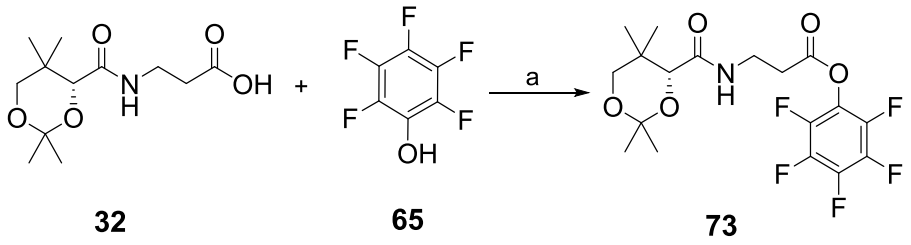

Reagents and conditions: a) EDC.HCl, DMAP, CH_2Cl_2, rt, 18 h, 81%.

Scheme 35. Synthesis of pantothenic acid derived analogue **73**.

Polyfluorinated esters have been coupled efficiently with amines in the absence of any coupling agents,[64c] thus providing a possible pathway for the synthesis of the desired maleimide functionalised derivatives. Gratifyingly, coupling of *E*-ester **66** with the three carbon maleimide unit

61 in the presence of DIPEA afforded the desired ketal-protected CJ derivative **63** in good yield as a single isomer (Scheme 36).

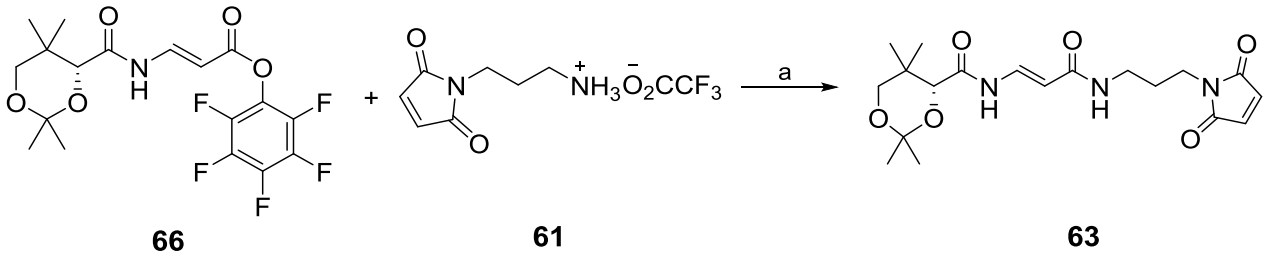

66 **61** **63**

Reagents and conditions: a) DIPEA, CH_2Cl_2, rt, 72 h, 90%.

Scheme 36. Coupling of (*R*)-*trans*-CJ ketal **66** with the three-carbon linker amino-maleimide **61.**

The same reaction protocol was then successfully used to couple the aminopropane derived maleimide with the (*R*)-*cis*-ketal protected unit **67**, the (*S*)-derivatives **71** and **72**, and the pantothenic acid derivative **73** to afford the corresponding maleimide derivatives **64**, **74-76** respectively (Table 1). The yields are not optimised, but the reactions yielded enough material to carry on to the next part of the project.

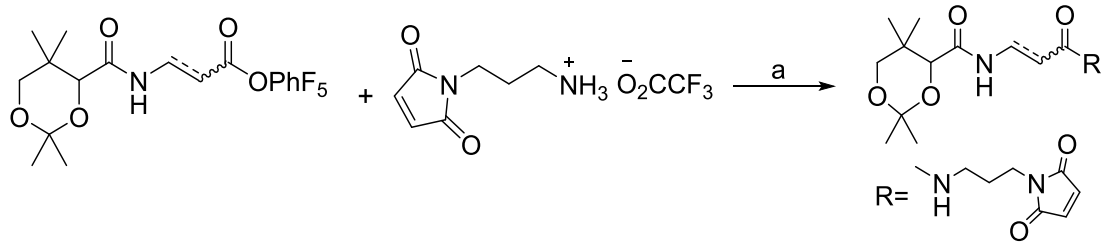

Starting material	***Product***	***Yield***	***Starting material***	***Product***	***Yield***
67	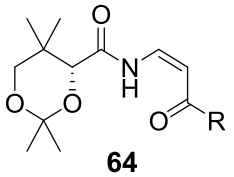 **64**	40%	**71**	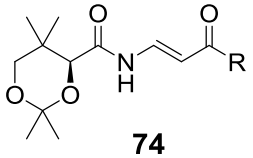 **74**	76%
73	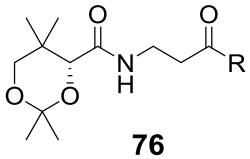 **76**	59%	**72**	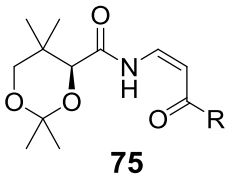 **75**	96%

Reagents and conditions: a) DIPEA, CH_2Cl_2, rt, 72 h.

Table 1. Synthesis of three-carbon linker amino maleimides **64**, **74-76**.

With the complete set of derivatives incorporating the 3-carbon linker in hand, the same coupling conditions were applied for the generation of the 5-carbon linker analogues. Gratifyingly, treatment of activated ester **66** with substituted maleimide **62**, under basic conditions, generated the desired derivative **77** in good yield (Scheme 37).

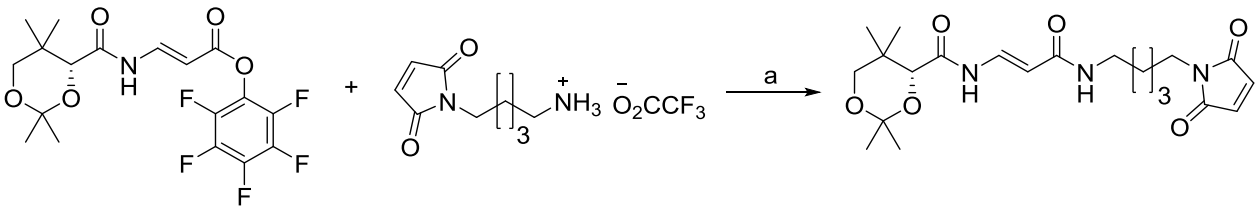

66 **62** **77**

Reagents and conditions: a) DIPEA, CH_2Cl_2, rt, 72 h, 80%.

Scheme 37. Synthesis of the five-carbon linker maleimide derivative **77.**

Gratifyingly, the same reaction conditions were also successfully applied for the coupling of the pentanamine derived maleimide **62** to the activated ester units **67**, **72** and **73**. Thus, we were able to generate the protein coupling precursors **78**-**80** in working yields. The only exception was the (*S*)-*trans*-analogue **71**, for which there was not enough material to achieve a quantifiable conversion (Table 2).

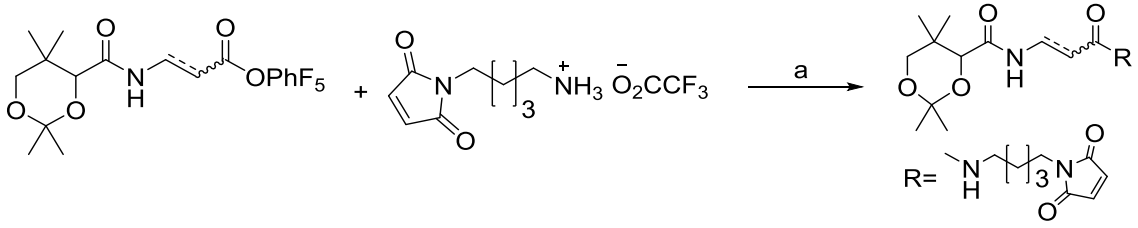

Starting material	***Product***	***Yield***	***Starting material***	***Product***	***Yield***
67	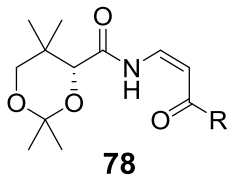 **78**	80%	**73**	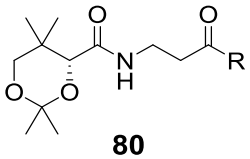 **80**	95%
72	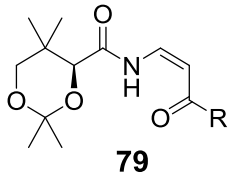 **79**	70%			

Reagents and conditions: a) DIPEA, CH_2Cl_2, rt, 72 h.

Table 2. Synthesis of the five-carbon linker maleimide derivatives **78**-**80**.

Having completed the synthesis of the CJ-15,801 derivatives **63**, **64**, **74**-**80**, our attention focused on the removal to the ketal protecting group to unmask the desired diol functionality. Previous efforts

in the group had shown that the ketal unit could be selectively removed without affecting the enamide unit through the careful use of $BiCl_3$ in wet CH_3CN.

Excitingly, initial attempts to deprotect acetonide **63** with $BiCl_3$ under standard conditions proved successful, yielding the desired diol adduct **81** after 24 h. Diol **81** was easily purified by flash column chromatography. ^1H NMR analysis confirmed the structure of the complete framework (Scheme 38).

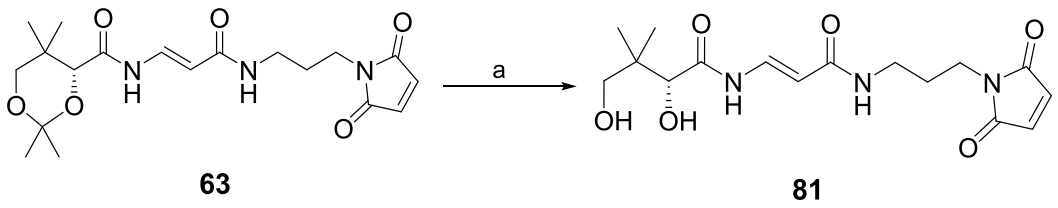

63 **81**

Reagents and conditions: a) $BiCl_3$, CH_3CN, H_2O, rt, 24 h, 92%.

Scheme 38. Synthesis of maleimide probe **81**.

The same procedure was replicated to other acetonides to afford the expected diol derivatives **82** to **86,** in enough quantities to carry on for testing (Table 3). Unfortunately, the (*S*)-acetonides were used for biological evaluation without any attempt to deprotect because of small amounts of material available.

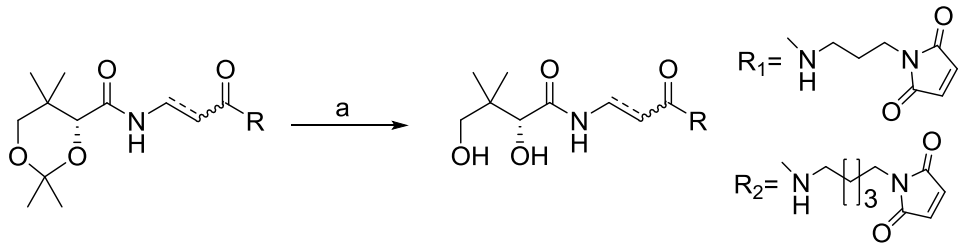

Starting material	***Product***	***Yield***	***Starting material***	***Product***	***Yield***
64	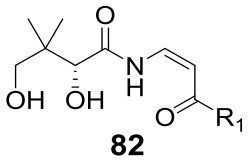 **82**	31%	**77**	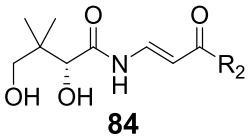 **84**	33%
73	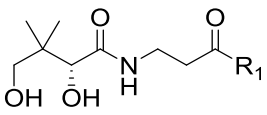 **83**	92%	**78**	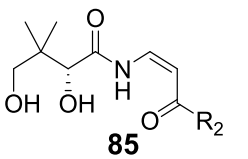 **85**	87%
			80	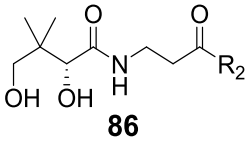 **86**	47%

Reagents and conditions: a) $BiCl_3$, CH_3CN, H_2O, rt, 24 h.

Table 3. Synthesis of maleimide probes **82-86**.

2.4 Bioconjugation of CJ-15,801 and pantothenic acid derived analogues with phiLOV(R475G, K476C).

Having completed the synthesis of the CJ-15,801 and pantothenic derivatives incorporating a maleimide unit, the key bioconjugation step with the phiLOV protein was attempted. As part of our efforts to design a mutant suitable for linking with the maleimide unit, we decided to carry out two single point mutations on phiLOV.

Thus, using site-directed mutagenesis,[65] arginine (R) 475 was mutated into a glycine (G) residue, and lysine (K) 476 was mutated into cysteine (C). R475 is located within a flexible extension loop (residues 476-483), and as such the R475G mutation was expected to reduce the phiLOV width. K476 on the other hand, is located at what can be considered to be the bottom and narrow end of phiLOV. The K476C mutation would provide the required nucleophilic residue for binding selectively with the maleimide unit at the narrowest part of protein.[55b, 56] Binding at the narrowest part of the protein was expected to help transport the protein through the putative transporter (Figure 26).

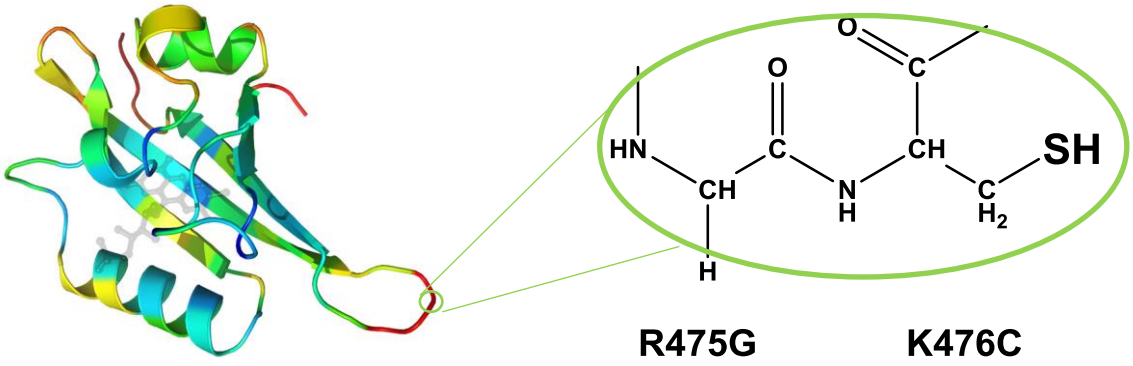

Figure 26. Crystal structure of phiLOV and the expected double mutagenesis position.[51a]

Design of the DNA primers to achieve the desired phiLOV mutations was performed in collaboration with B. Joanne Power and Jan Petersen from the Christie group in the Institute of Molecular Cell and Systems Biology (UoG). The phiLOV double mutant phiLOV(R475G, K476C) was isolated (6 mg/mL) in pH 8 buffer (Tris-HCl 50 mM, NaCl 150 mM). The success of the mutations was determined via proteomics analysis in the laboratory of Professor W. Mullen from the Institute of Cardiovascular and Medical Sciences (UoG). The primary structure of the double mutant contained 230 amino acids, of which 119 belonged to the SUMO-tag, and had a molecular weight of 26458.8 Da. (Figure 27). The fluorescence properties of both the wild type and the double mutant proteins were verified by measuring the fluorescence excitation spectrum. The spectrum is consistent with that reported in the literature (Figure 27).[48b]

```
phiLOVRGKC MKHHHHHHHGAWSHPQFEKGSLQDSEVNQEAKPEVKPEVKPETHINLKVSDGSSEIFFKI 60
phiLOVWT   MKHHHHHHHGAWSHPQFEKGSLQDSEVNQEAKPEVKPEVKPETHINLKVSDGSSEIFFKI 60
           ************************************************************

phiLOVRGKC KKTTPLRRLMEAFAKRQGKEMDSLRFLYDGIRIQADQAPEDLDMEDNDIIEAHREQIGGA 120
phiLOVWT   KKTTPLRRLMEAFAKRQGKEMDSLRFLYDGIRIQADQAPEDLDMEDNDIIEAHREQIGGA 120
           ************************************************************

phiLOVRGKC MEKSFVITDPRLPDYPIIFASDGFLELTEYSREEIMGRNARFLQGPETDQATVQKIRDAI 180
phiLOVWT   MEKSFVITDPRLPDYPIIFASDGFLELTEYSREEIMGRNARFLQGPETDQATVQKIRDAI 180
           ************************************************************

phiLOVRGKC RDQRETTVQLINYTKSGKKFWNLLHLQPVRDGCGGLQYFIGVQLVGSDHV 230
phiLOVWT   RDQRETTVQLINYTKSGKKFWNLLHLQPVRDRKGGLQYFIGVQLVGSDHV 230
           ******************************  *****************
```

SUMO-tag mutation

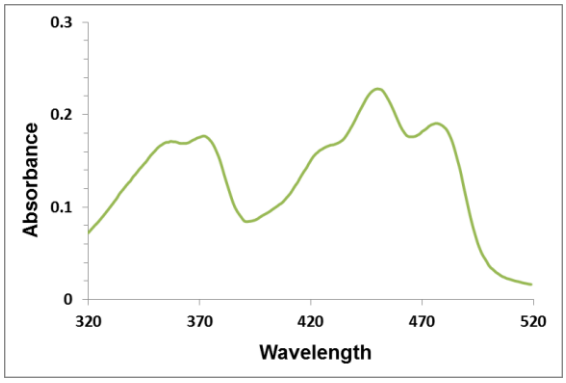

Figure 27. Multiple sequence alignment and fluorescence confirmation of phiLOV(R475G, K476C). Top: Sequence alignment for wild type (WT) and double mutant (R475G, K476C). Bottom: SUMO-tag-phiLOV(R475G, K476C) fluorescence excitation spectrum using an emission wavelength of 495 nm.

The Marquez group reported the reactivity of the α,β-unsaturated carbonyl moiety in CJ-15,801 as Michael acceptor. The samples after 2 h incubation with glutathione or *L*-cysteine were analysed by ^{1}H NMR to investigate directly the reactivity. They were enable to detect any reaction of CJ-15,801 and analogues. On the other hand, under the same conditions, *N*-ethylmaleimide (a reactive Michael acceptor) reacted rapidly, detecting addition products few minutes after mixing with the thiols.[66] Thus, the high reactivity of the maleimide unit compared to CJ-15,801 frame will provide selectivity in the bioconjugation with phiLOV(R475G, K476C).

Practically, for the key bioconjugation step, it was decided to take advantage of the differential reactivity of amino acid residues towards maleimide units. It has been reported that cysteine residues selectively react with maleimides at physiological pH (6.5-7.5), with the best selectivity being observed at pH 7 to generate thiol ethers. On the other hand, primary amines have been reported to be much better nucleophiles at higher pH values (>8).[56,65] Thus, in an attempt to increase the selectivity and efficiency of the coupling, the buffer was exchanged to pH 7 (phosphates buffer) and the protein concentrated to 10 mg/mL.

For the actual couplings, phiLOV(R475G, K476C) was incubated separately with each maleimide derivative, and the unreacted derivatives were eluted. Subsequent cleavage of the SUMO-tag through the use of a SUMO protease then released the coupled proteins. Initial characterisation attempts involved the use of SDS page technology, to see if a difference between the protein before (12690 Da) and after the coupling (>13000 Da) could be detected (Figure 28).

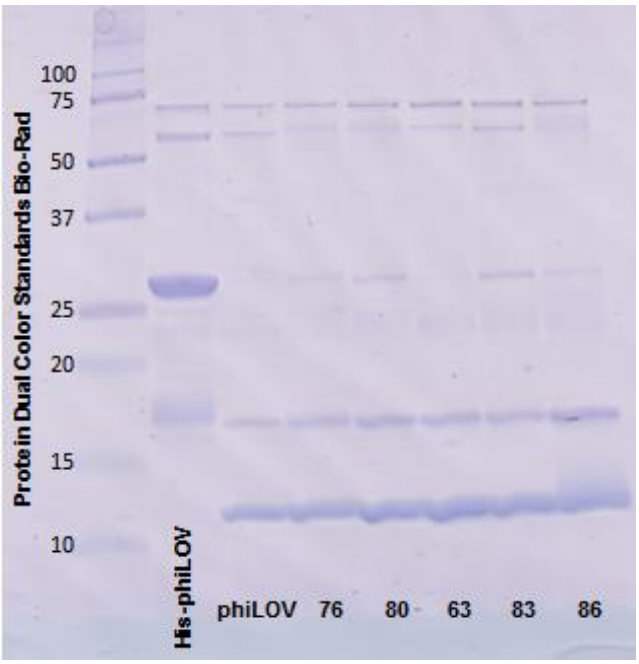

Figure 28. SDS page of the SUMO-tag-phiLOV(R745G, K476C), phiLOV(R475G, K476C) as well as pantothenic acid and CJ-15,801 coupled to phiLOV(R475G, K476C).

The SDS page (Figure 28) clearly showed the SUMO-tag-phiLOV(R745G, K476C) protein, as well as the SUMO cleaved phiLOV(R475G, K476C). Unfortunately, the increase in molecular weight provided by the derivatives was not enough to be detectable by this technique. Changing the speed and/or concentration of gel failed to help increase the resolution.

The lack of success of using the SDS page approach meant that a different approach had to be taken to determine whether the coupling had been successful. Thus, it was decided to resort to MALDI sequencing in collaboration with Dr. Mullen.

In MALDI, the choice of matrix is a key factor to ensure the technique performs as designed. Common matrices, for peptides and proteins analysis in MALDI, are α-cyano-4-hydroxycinnamic acid (CCA) **87,** sinapic acid (SA) **88**, and 2,5-dihydroxybenzoic acid (DHB) **89**.[67] Sinapic acid **88,** is best suited for the analysis of high-mass peptides (> 2500 Da.) and was selected as our matrix of choice. Plate preparation consisted in the deposition of a thin layer of matrix (SA dissolved in EtOH) followed by a layer of sample to be analysed (in 0.1% TFA) and then a final layer of matrix (SA dissolved in CH_3CN) on top (Figure 29).

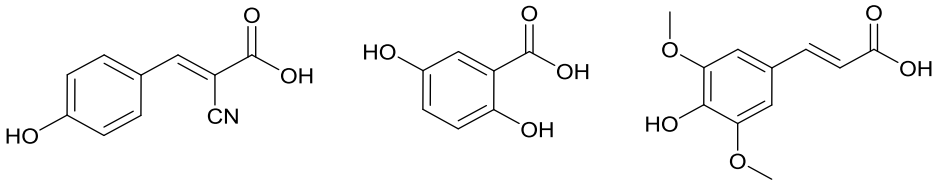

87 **88** **89**

Figure 29. Typical MALDI matrices for peptides and proteins analysis.

Gratifyingly, MALDI analysis of phiLOV(R475G, K476C) showed a molecular ion of 12690.20 Da, with the calculated molecular mass being 12690.41 Da (Figure 30). The rest of the samples were also analysed under the same conditions, and the results confirmed the coupling of protein with the different maleimide derivatives (Tables 4 and 5, appendix).

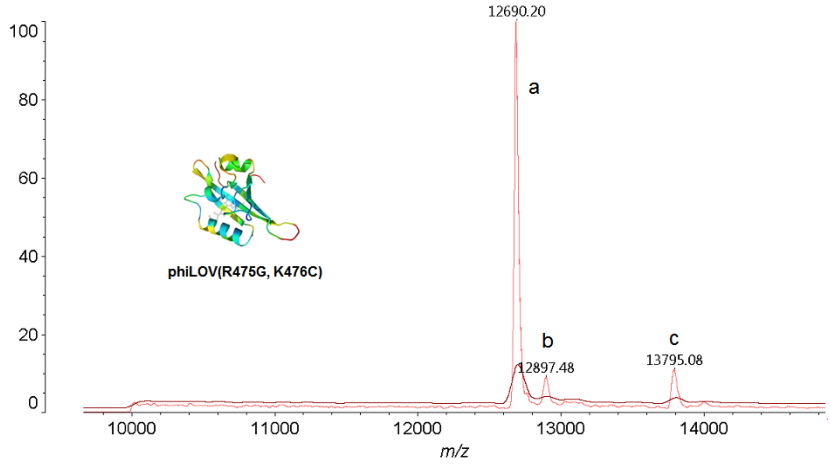

Peak a) $[M]^+$: calculated *m/z* 12690.41, found *m/z* 12690.20. Peak b) $[M+H+sinapic\ acid+H_2O]^+$: calculated *m/z* 12897.47, found *m/z* 12897.48. Peak c) $[M+H+sinapic\ acid+H_2O]^+$ plus Tween impurity, calculated *m/z* 13795.02, found *m/z* 13795.08.[68]

Figure 30. MALDI analysis of phiLOV(R475G, K476C).

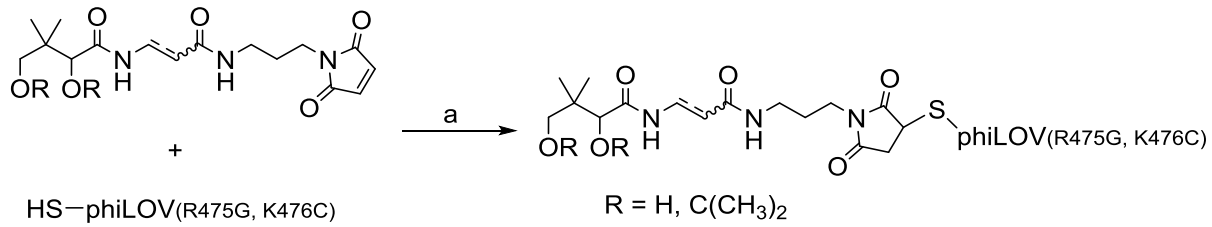

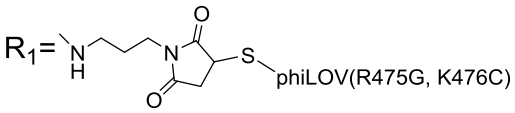

SM	*Product*	*Calc. mass/ adduct*	*Found mass*	*SM*	*Product*	*Calc. mass/ adduct*	*Found mass*
63	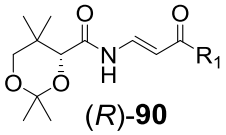 (*R*)-**90**	13082.60 $[M-H]^+$	13082.16	**76**	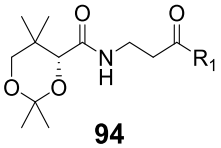 **94**	13084.60 $[M-H]^+$	13084.61
64	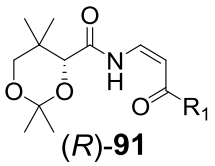 (*R*)-**91**	13084.60 $[M+H]^+$	13084.07	**81**	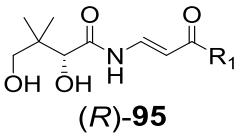 (*R*)-**95**	13811.03* $[M+((C_2H_4O)_{17}+H_2O+H)]^+$	13811.03
74	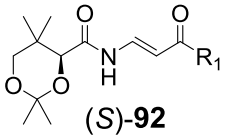 (*S*)-**92**	13084.60 $[M+H]^+$	13084.41	**82**	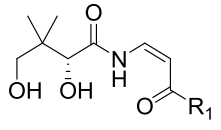 (*R*)-**96**	13066.57 $[M+Na]^+$	13066.45
75	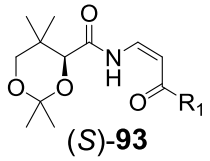 (*S*)-**93**	13082.60 $[M-H]^+$	13082.74	**83**	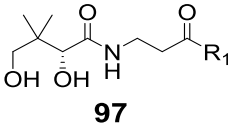 **97**	13043.59 $[M-2H]^+$	13043.62

Reagents and conditions: a) pH 7 buffer, rt, 1 h. SM= Starting material. *Reference 68.

Table 4. Synthesis of phiLOV(R475G, K476C) coupled to three-carbon linker maleimide derivatives **90-97**.

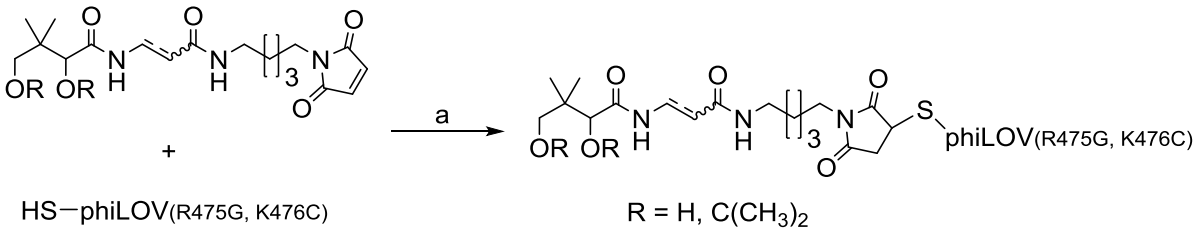

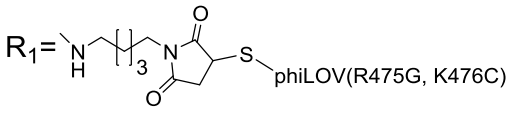

SM	*Product*	*Calc. mass/ adduct*	*Found mass*	*SM*	*Product*	*Calc. mass/ adduct*	*Found mass*
77	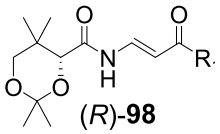 (*R*)-**98**	13114.63 $[M+3H]^+$	13114.57	**84**	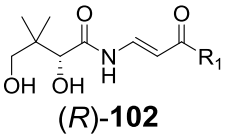 (*R*)-**102**	13078.61* $[M+Li]^+$	13078.68
78	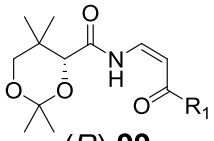 (*R*)-**99**	13296.74* $[M+GE+Na]^+$	13296.05	**85**	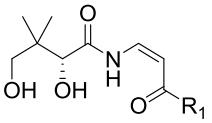 (*R*)-**103**	13085.60 $[M+CH_2]^+$	13085.06
79	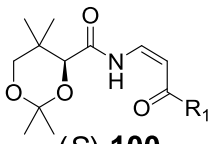 (*S*)-**100**	13110.63 $[M-H]^+$	13110.46	**86**	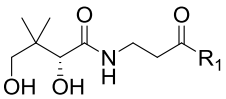 **104**	13073.62 $[M]^+$	13073.47
80	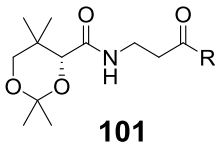 **101**	13111.63 $[M-2H]^+$	13111.50				

Reagents and conditions: a) pH 7 buffer, rt, 1 h. SM= Starting material. *References 68 and 69.

Table 5. Synthesis of phiLOV(R475G, K476C) coupled to five-carbon linker maleimide derivatives **98-104**.

The synthesis of the (*R*)-CJ-15,801 derivatives coupled to the phiLOV double mutant, was subsequently reproduced at the University of Nagasaki (Institute of Tropical Medicine) and bioconjugation adducts were confirmed by MALDI analysis at the University of Liverpool (XJTLU), thus proving the reliability of this approach.

In conclusion, we demonstrated an efficient and reproducible route for the synthesis of new CJ-15,801 and pantothenic acid derived analogues coupled to phiLOV. This library was generated from commercially available materials in a short period of time; the confirmation of each intermediate and final products was determined by NMR and MALDI.

2.5 Evaluation of CJ-15,801 and pantothenic acid derived analogues coupled to phiLOV(R475G, K476C) in *C. elegans*.

Considering the favourable results with the BODIPY derivatives, it was decided to move forward and test the uptake of pantothenic acid and CJ-15,801 analogues coupled to phiLOV(R475G, K476C) in *C. elegans.* Using the same procedure as for the BODIPY derivatives, *C. elegans* was incubated with the phiLOV constructs for 20 h. After incubation was completed, fluorescence microscopy revealed that *C. elegans* cultures incubated with phiLOV(R475G, K476C) showed no uptake, with only autofluorescence being detected. However, incubation with the phiLOV-CJ-15,801 complex (*R*)-**90** resulted in significant fluorescence being detected in the pharynx, gut lumen and gut cells of the worm. The worms were viable and fully motile (Figure 31).

The fluorescence intensities were measured from images using ImageJ software, and most of the derivatives exhibited values close to phiLOV control, due to the worm's autofluorescence.

Notably, microscopy and quantitative analysis reveal lower fluorescence intensities with phiLOV derivatives compared with BODIPY constructs. The fluorescent properties of both fluorophores, BODIPY and phiLOV, are important to notice: BODIPY core is a chemical compound of ~ 220 Da molecular weight with high efficiency as a dye ($\Phi \sim 1$ and $\varepsilon \sim 80{,}000\ M^{-1}cm^{-1}$), phiLOV on the other hand, is a protein of ~12 KDa with lower fluorescent capacity ($\Phi \sim 0.2$ and $\varepsilon \sim 13{,}500\ M^{-1}cm^{-1}$) but with a proved effectivity for *in-vivo* monitoring protein expression and localization.[52b,70] Thus, in addition to the uptake processes, the fluorescence intensities will be related to the fluorophore properties.

Interestingly, the length of the linker has a marked effect on the ability of the complex to be recognised and taken up by the worm. Incubation with complex (*R*)-**90** results in a much larger fluorescence reading compared to that of the five-carbon unit (*R*)-**98**.

Based on these results, it seems that the uptake process in *C. elegans* is selective for the lipophilic derivative (ketal) with *R* configuration, but the CJ-15,801 analogue was required to be linked to the phiLOV through a three-carbon linker. This restriction would be related with a reduced time required for the transporter to move the CJ-phiLOV derivative, being the three carbon linker –with a reduced length compared to the five-carbon- which provides the better conditions to cross rapidly the barrier.

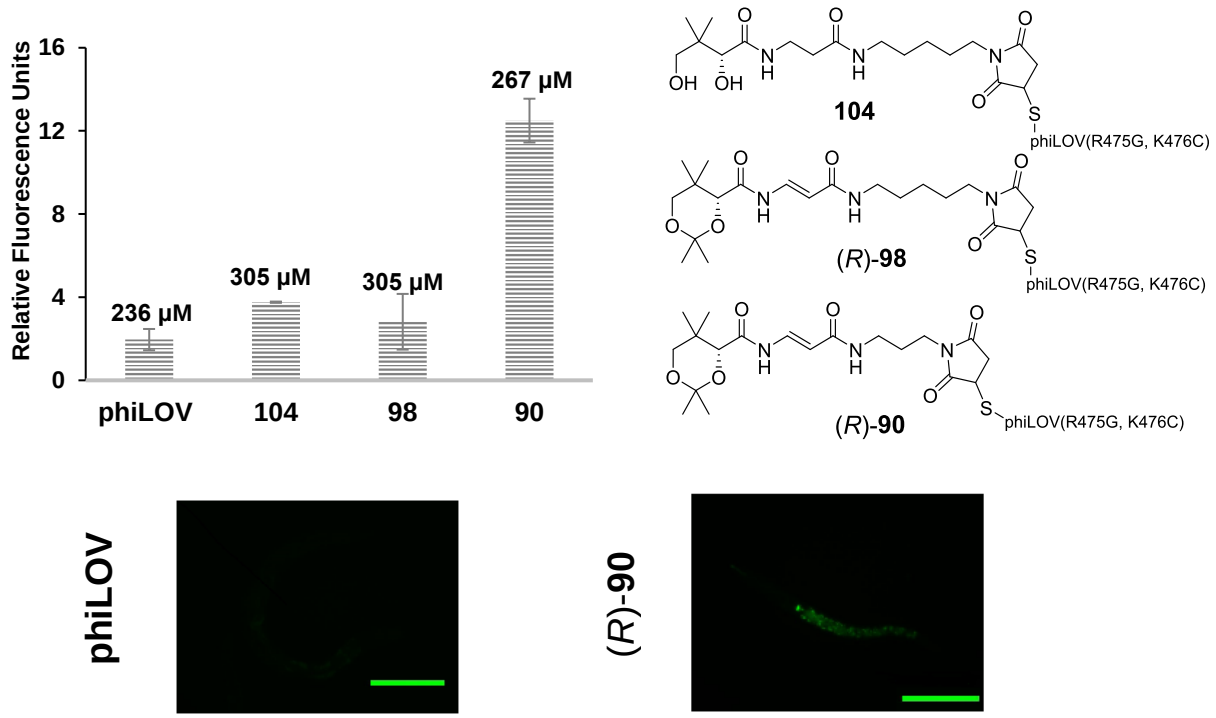

Figure 31. Uptake test of phiLOV(R475G, K476C)-pantothenic acid **104**, and CJ-15,801 derivatives (*R*)-**98** and (*R*)-**90** in *C. elegans*.

Bar chart represents RFU's from experiments performed at 20 °C for 20 h incubation. RFU were calculated from images using ImageJ software. (Units x10^6). Photos were taken through FITC filter, size bar: 100 µm.

Summing up the results from the pantothenate and CJ-15,801 derivatives attached to BODIPY and phiLOV(R475G, K476C), it seems that during the uptake process, the (*R*)-trans ketal CJ-15,801 core **28** is recognised and transported selectively inside the worm. Framework **28** is able to carry both a small molecule (BODIPY core) as well as a complex protein, being the linker length a crucial factor for biomolecules delivery. In both cases, the nematodes remain viable. Thus, CJ-15,801 analogue **28** has the potential to be used as a tool to deliver small molecules and biomolecules safely, into *C. elegans* in both short and long term studies.

2.6 Efforts towards the selective delivery of ivermectin B1a.

The combined uptake studies showed that the (*R*)-ketal protected CJ-15,801 analogue **28** (Figure 32) was very efficient at delivering both BODIPY units as well as the much larger phiLOV(R475G, K476C) protein into *C. elegans*. These results raised the tantalising possibility of being able to use analogue **28** as a platform for the efficient delivery of drugs and biomolecules into different worm species. Such a platform would be able to increase the effective dose of current drugs, and to deliver biomolecules which are currently problematic (i.e. nanobodies).

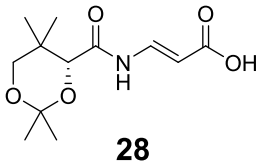

28

Figure 32. (*R*)-*trans* Ketal CJ-15,801 analogue **28**.

As a proof of concept, it was decided to attempt the selective delivery of ivermectin B1a. This 16-membered macrocyclic nematocide belongs to the family of avermectins (*a* without + *verm* worm + *ect* ectoparasites + *in* pharmaceutical product), which are closely related with the family of milbemycins (i.e. moxidectin), and are produced by a soil actinomycetes from the genus *Streptomyces* (Figure 33). Ivermectin is currently used to control nematodes and ectoparasitic infections in domestic animals, as well as to treat microfilarial infections, onchocerciasis and lymphatic filariasis in humans.[71] The glutamate-gated chloride channels (GluCls) in nerve cells and muscles of invertebrates is considered to be the target for the avermectins. Biologically, an increase in the permeability of Cl^- ion is observed after avermectin binds to the GluCls, which causes hyperpolarization of the cell, and leads to paralysis and death. Unfortunately, neurotoxicity in humans and domestic animals, as well as the emergence of anthelmintic resistant nematodes have proven to be a significant barrier for their use.[72]

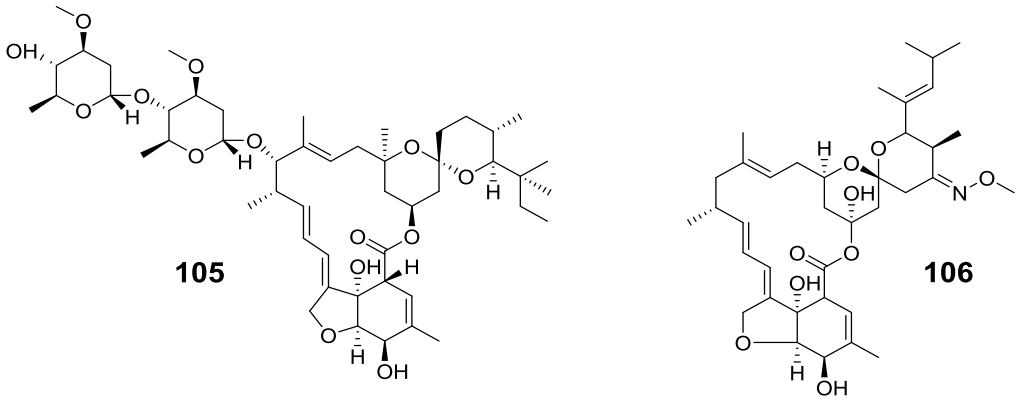

105 **106**

Figure 33. Ivermectin B1a **105** and moxidectin **106**.

Thus, as a proof of concept we decided to label ivermectin B1a with our drug delivery system. Retrosynthetically, it was envisioned that protected ivermectin B1a **107** would be covalently linked to the *trans*-ketal delivery vehicle **28** via the C4" alcohol (Scheme 39). The decision to introduce the delivery unit at the C4" position emanated from the published SAR studies on ivermectin B1a, which showed that substitutions at this position were tolerated without loss in activity. Alkylation of the C5 position, on the other hand, resulted in significant loss of nematocidal activity.[71a, 73]

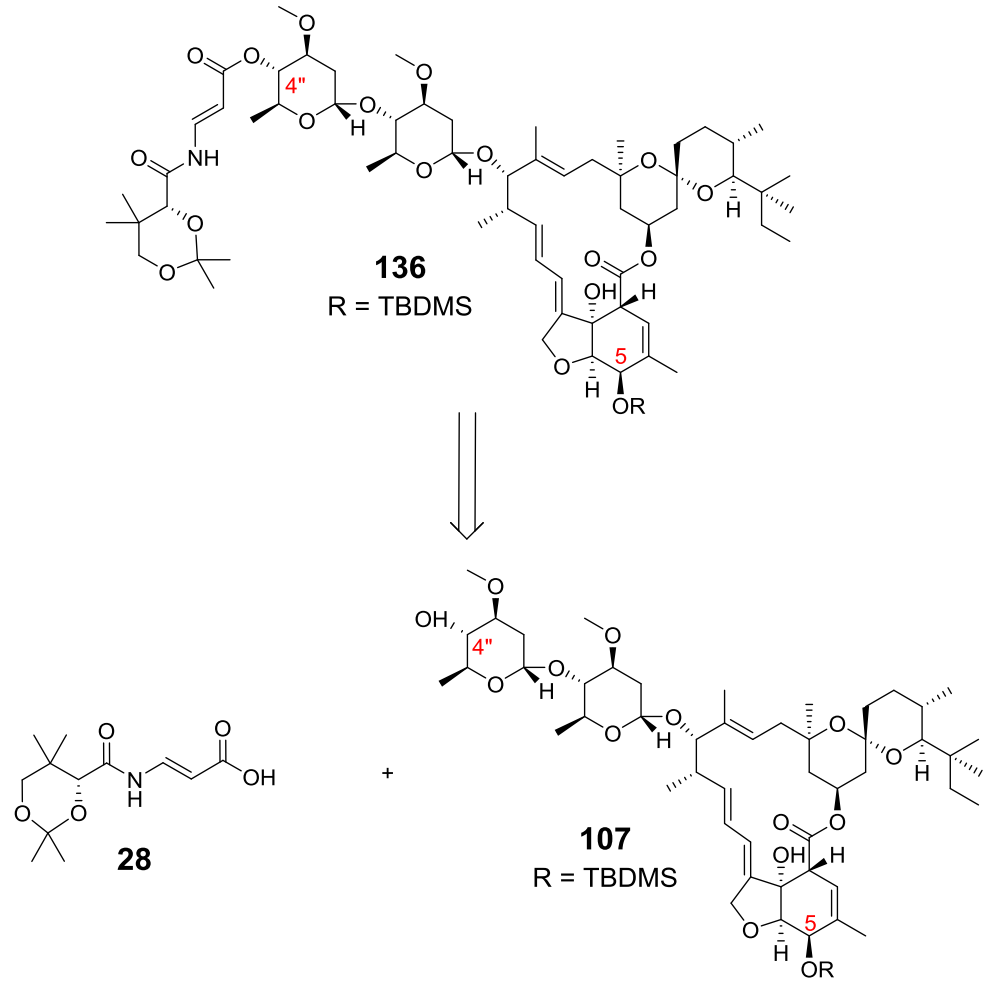

Scheme 39. Retrosynthesis of (*R*)-*trans*-ketal CJ-ivermectin B1a analogue**.**

Synthesis of the ivermectin B1a coupling precursor began with the selective protection of the C5 alcohol **105** using TBDMSCl to afford the desired silyl-ether **107**.[74] Coupling of silyl ether **107** with the (*R*)-*trans*-ketal-CJ analogue **28** through a Steglich esterification[75] then generated a new compound in reasonable yield in which the ^{1}H NMR chemical shift for the hydrogen on the C4" position had shifted from 3.14 ppm to 4.77 ppm. This change in chemical shift is consistent that reported by Mrozik during his synthesis of C4'' substituted ivermectin derivatives.[76] However, close inspection of the ^{1}H NMR spectra showed that the double bond within the enamide unit had isomerised to the *cis*-isomer **108** (Scheme 40).

The reaction was repeated several times, and in each case only the *cis*-enamide was isolated. The exclusive formation of the *cis*-enamide can be explained by a combination of the extra stabilisation provided by the intramolecular hydrogen bond (analogous to that proposed during the enamide isomerisation observed during the synthesis of the pentafluorophenyl ester derivatives, section 2.3), together with the steric hindrance provided by the neighbouring groups on the ivermectin framework. As a comparison, coupling of the (*R*)-*cis*-ketal enamide **54** with TBDMS protected ivermectin **107** afforded the expected *cis*-enamide-ivermectin derivative **108** as a single isomer in moderate yield (Scheme 40).

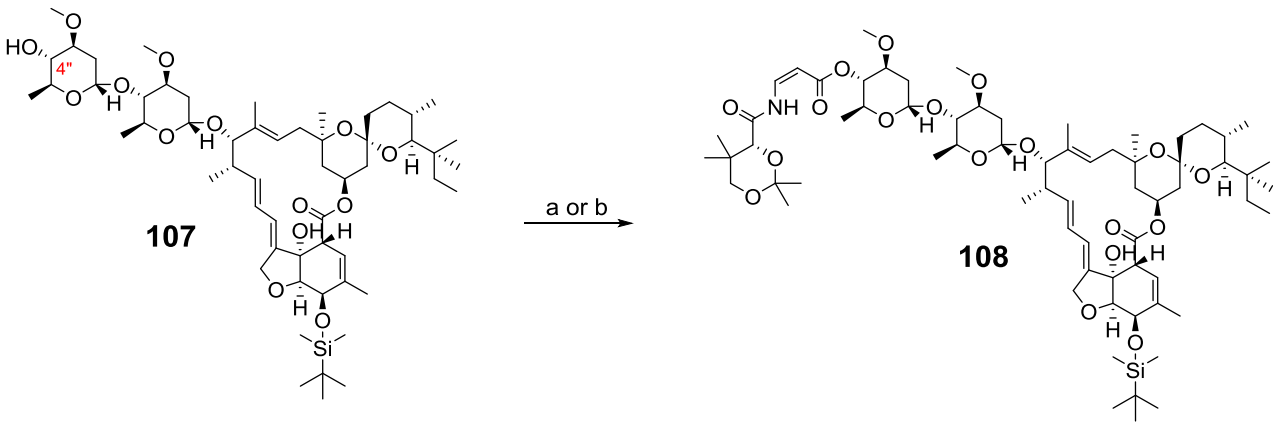

Reagents and conditions: a) **28** (1 eq.), DCC, DMAP, CH_2Cl_2, rt, 18 h, 40-55%. b) **54** (1 eq.), DCC, DMAP, CH_2Cl_2, rt, 18 h, 61%.

Scheme 40. Coupling of CJ-15,801 analogues **28** and **54**, with TBDMS ether-ivermectin B1a **107**.

Even though the (*R*)-*cis*-ketal enamide **54** did not show significant uptake in *C. elegans*, we determined to continue the deprotection of sylyl ether on derivative **108** to study the effect of the chemical reactions applied to ivermectin B1a for further biological tests.

Deprotection of the C5 TBDMS ether **108** using *p*-TsOH then afforded the desired (*R*)-cis-ketal-CJ-ivermectin B1a derivative **109** in good yield (Scheme 41).[74] ^{1}H NMR showed that the C5 hydroxyl signal, had shifted from a broad singlet at 4.46 ppm to a sharp doublet at 4.32 ppm, consistent with previous reports.[76,77] Significantly, the enamide and ketal units remained intact during the acidic conditions used for the deprotection (Scheme 41).

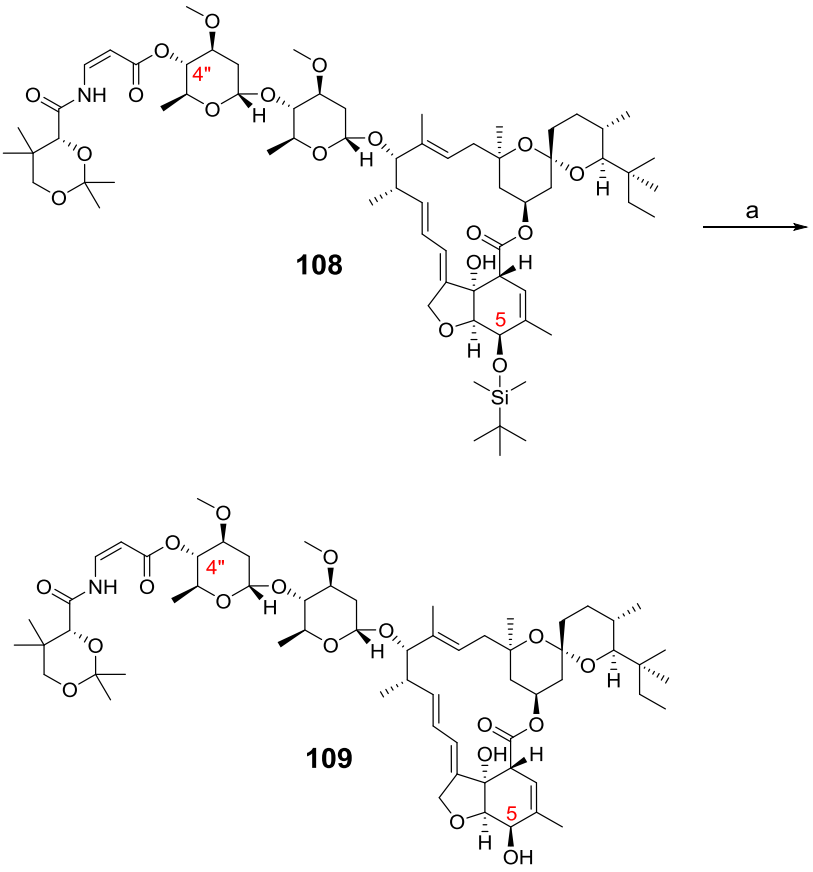

Reagents and conditions: a) *p*-TsOH, MeOH, 18 ºC, 0.5 h, 58%.

Scheme 41. Synthesis of (*R*)-*cis*-ketal CJ-ivermectin B1a analogue **109**.

2.7 Design and synthesis of new *bis*-functionalised BODIPY derivatives attached to ivermectin B1a.

With the (*R*)-cis-ketal-CJ-ivermectin derivative **109** at hand, a strategy for the assessment of its nematocidal activity began to take shape. According with our results, CJ derivatives revealed a selective uptake into *C. elegans*, which provided us with a golden opportunity to use them as selective drug carriers in *C. elegans.* However, there were still two issues that needed to be addressed. The first issue revolved around having the ability to efficiently cleave the drug from the carrier post-delivery. The second issue related to being able to detect that the expected transport had taken place (i.e. that the drug had indeed been delivered inside the nematode).

Although in the case of ivermectin, cleaving of the delivery unit from the actual pharmacophore should not be an issue due to the ability of ivermectin to tolerate substituents at the C4'' position without losing potency, there was still the need to develop a method to track the ivermectin uptake. With this in mind, we once again turned to the BODIPY core as a possible solution. It was reasoned that a *bis*-functionalised BODIPY unit could be used to link both the CJ-derivative and the ivermectin core (Figure 34), and would provide an easily readable visualisation method.

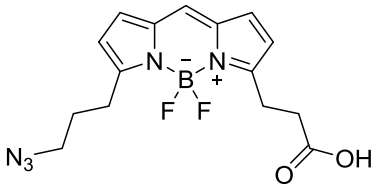

113

Figure 34. *Bis*-functionalised BODIPY **113**.

Thus, it was decided to generate a pseudo-C2 symmetric *bis*-functionalised BODIPY unit bearing substituents at the C3 and C5 positions. The substituent at the C3 position was envisioned to be an azido group at the end of a three-carbon aliphatic tether. The linker at the C5 position on the other hand, was designed to contain a carboxylate group linked to the BODIPY core through a two-carbon aliphatic linker. The carboxylate group was chosen as a coupling partner for the C4'' hydroxyl group of ivermectin B1a, whilst the azido group was included as the "click" partner for alkyne containing CJ-15,801 derivatives (Scheme 42).

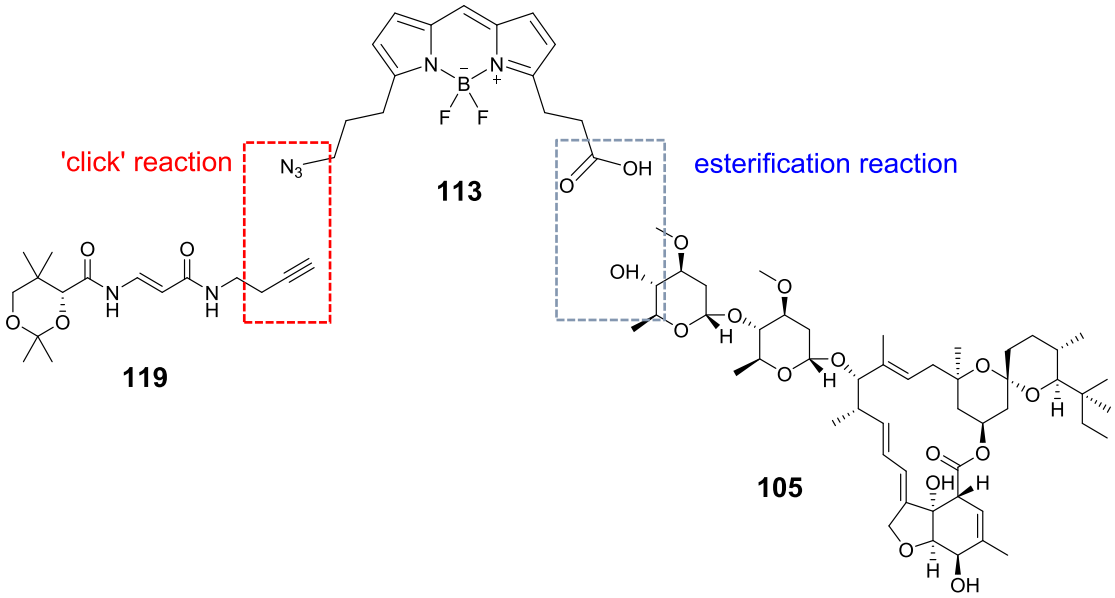

Scheme 42. Coupling strategy through *bis*-functionalised BODIPY linker.

The synthesis of the *bis*-functionalised BODIPY unit began with the Wittig reaction of pyrrole **34** with (*tert*-butoxycarbonylmethylene)triphenylphosphorane **133** to yield the vinylogous ester **134**. Hydrogenation of ester **134** with Pd/C, then afforded the desired *tert*-butyl ester **111** in good yield. The synthesis of the left hand side of the BODIPY unit began with previously generated azido-pyrrole **34** which was formylated by a Vilsmeier-Haack reaction to afford the desired aldehyde **110** in moderate yield. Aldehyde **110** was then condensed with *tert*-butyl ester **111** using $POCl_3$, and the resulting heterodimer was treated with $BF_3.Et_2O$ to generate the desired BODIPY unit **112** in low yield. However, despite the low yield, the reaction yielded enough material to carry forward.

Hydrolysis of the *tert*-butyl ester unit was then attempted, unfortunately despite extensive experimentation, only starting material decomposition was observed, with none of the desired BODIPY acid being detected (Scheme 43).

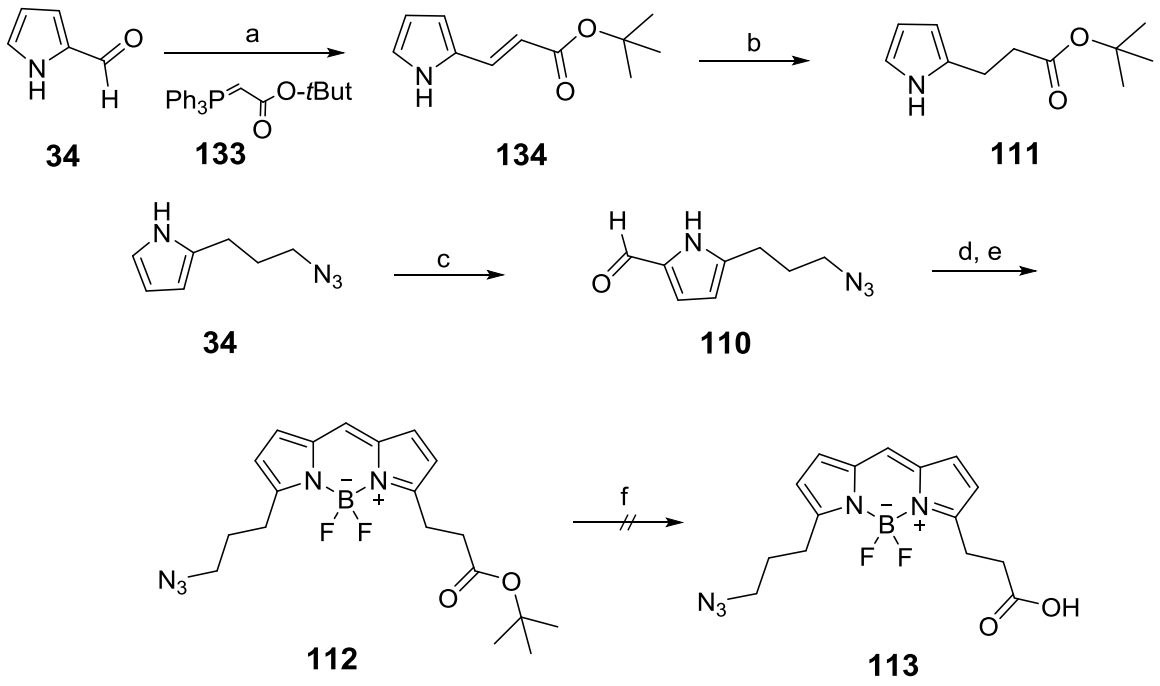

Reagents and conditions: a) **133**, benzene, 80 °C, 22 h, 83%. b) MeOH, Pd/C 10%, H_2, rt, 18 h. 92%. c) $POCl_3$, DMF, 0 °C to 50 °C, 18 h, 51%. d) **111**, $POCl_3$, DMF, 0 °C to rt, 6.5 h. e) $BF_3.Et_2O$, DIPEA, 0 °C to rt, 18 h, 9% after two steps. f) TFA, CH_2Cl_2, rt, 2 h, 0%.

Scheme 43. Synthesis of *bis*-functionalised BODIPY **113**.

The lack of success in the hydrolysis step prompted us to reconsider our choice of ester in the synthesis. Thus, as part of our modified approach, the known methyl ester **36** was formylated to afford the desired ester **114** in moderate yield. Excitingly, condensation of methyl ester **114** with azido-pyrrole **39** proceded to generate the desired BODIPY unit **115** in acceptable yield.

With the key BODIPY in hand, the key hydrolysis step was undertaken. Gratifyingly, treatment of methyl ester **115** with aqueous HCl afforded the desired free carboxylic acid **113** cleanly,[78] and with no need for purification (Scheme 44). The structure was corroborated by NMR spectroscopy, including ^{19}F NMR.

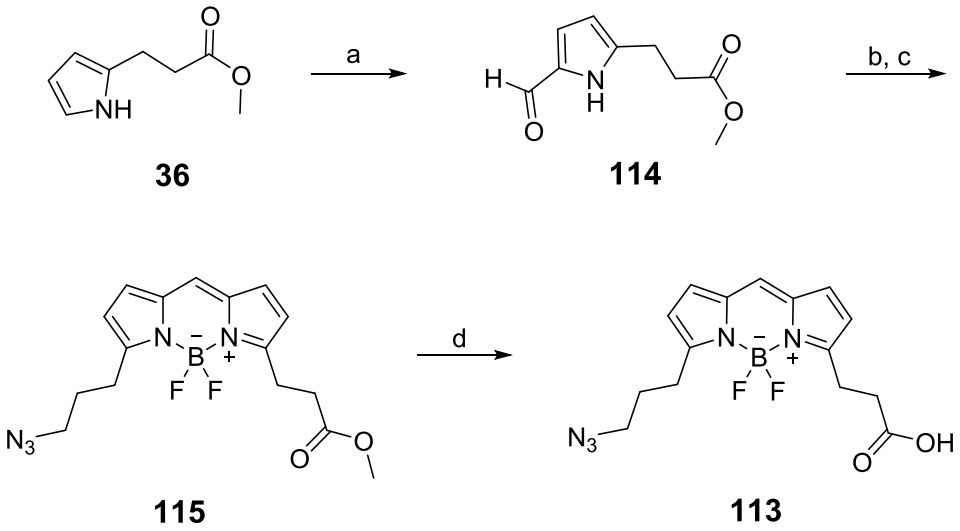

Reagents and conditions: a) $POCl_3$, DMF, 0 °C to 45 °C, 14 h, 66%. b) **39**, $POCl_3$, DMF, 0 °C to rt, 6.5 h. c) $BF_3.Et_2O$, DIPEA, 0 °C to rt, 18 h, 26% after two steps. d) HCl, THF/H_2O (2:1), rt, 18 h, 52%.

Scheme 44. Synthesis of *bis*-functionalised BODIPY **113**.

Gratifyingly, both the azide-BODIPY-methyl ester **115** and the azide-BODIPY-carboxylic acid **113** exhibit a maximum emission at 510 nm and excitation at 487 nm (~23 nm Stokes shift) (Figure 35). Thus, they are both suitable for use in fluorescence microscopy, as well as in intensity measurements.

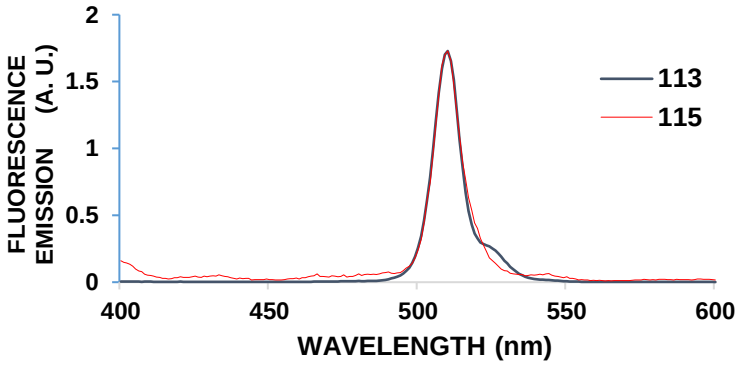

Figure 35. Normalized emission of compounds **113** and **115**.
Measurements were taken in MeOH. Fluorescence emission was measured at 315 nm, **113** c=5 nM, **115** c=0.2 nM. (Units x10^6).

Armed with the *bis*-functionalised BODIPY acid **113**, the Steglich esterification with the C5 TBDMS-protected ivermectin derivative **107** was attempted. Excitingly, the reaction afforded the desired fluorescent silylether **116** in moderate yield. As expected, ^{1}H NMR shows that the C4" proton signal has shifted from 3.14 ppm to 4.74 ppm. The fluorescent nature of the compound together with the ^{19}F NMR confirmed that the BODIPY core remained intact during the transformation (Scheme 45).

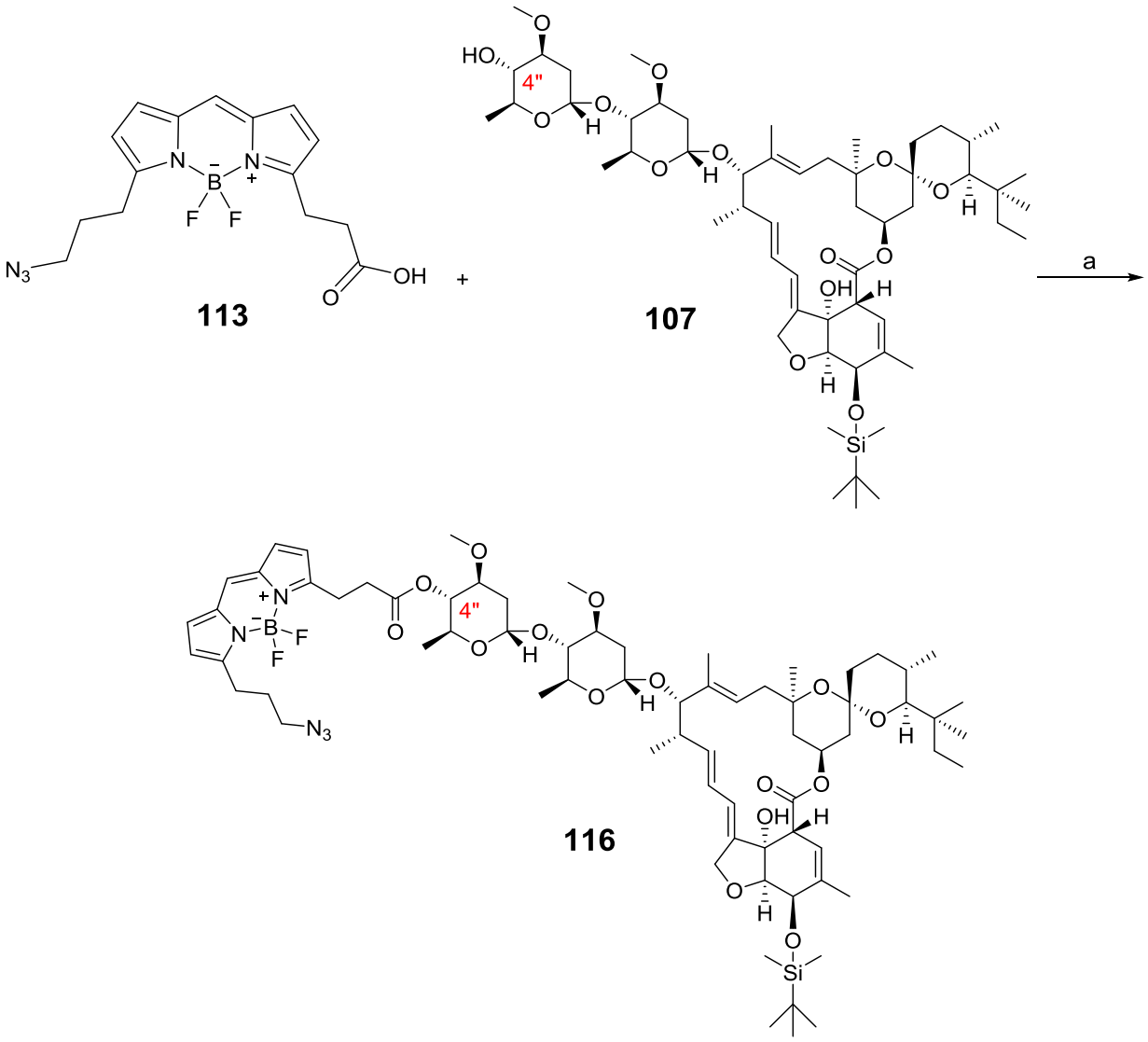

Reagents and conditions: a) DCC, DMAP, CH_2Cl_2, rt, 18 h, 39%.

Scheme 45. Synthesis of BODIPY linked TBS-protected ivermectin B_{1a} **116**.

Acid catalysed removal of the C5 TBDM silyl ether, afforded the desired free alcohol **117**. The BODIPY derived ivermectin B1a **117** was then confirmed by mass spectrometry. Unfortunately, the small amount of material generated meant that it was not possible to fully characterise the compound, but it was enough material to test in worm cultures (Scheme 46).

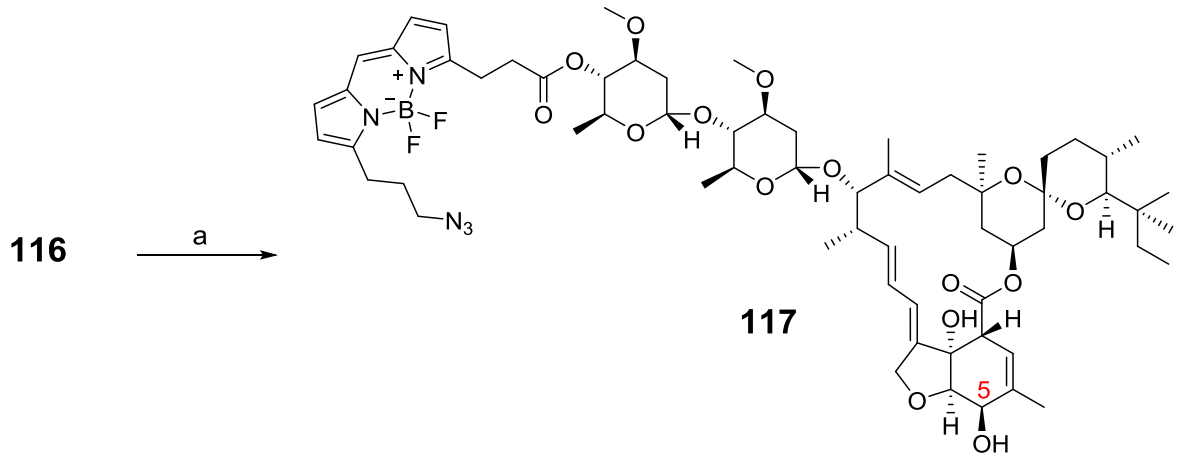

Reagents and conditions: a) *p*-TsOH, MeOH, 18 ºC, 1 h, 72%.

Scheme 46. Synthesis of BODIPY **117**.

For the generation of the desired CJ-BODIPY-ivermectin construct **137**, it was decided to pursue a 'click' strategy, in which the TBS-protected ivermectin-BODIPY unit **116** bearing the azido unit would react with the alkyne functionalised (*R*)-*trans*-CJ **119**. The alkyne unit **119**, in turn, envisioned as originating from the free acid **28** (Scheme 47).

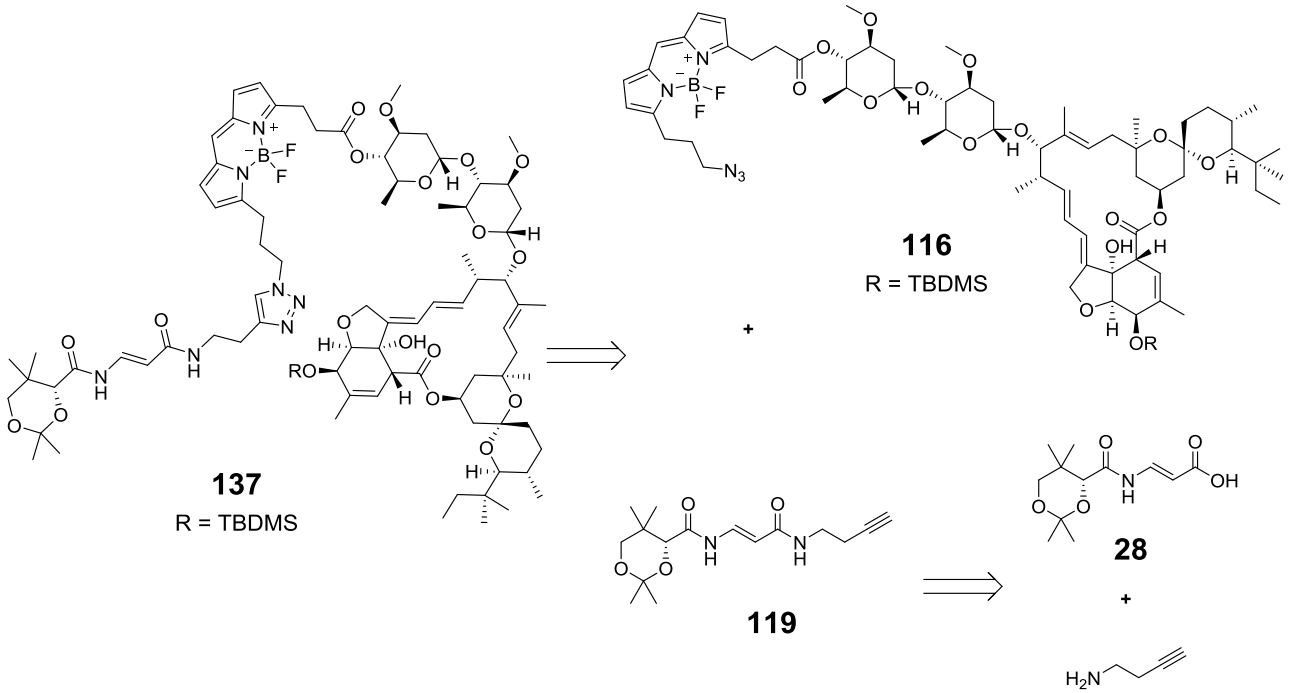

Scheme 47. Retrosynthesis of (*R*)-*trans*-ketal CJ-BODIPY-ivermectin B1a complex **137**.

The forward synthesis of the alkyne unit **119**, began with (*R*)-trans-ketal CJ-15,801 derivative **28** which was coupled with 1-amino-3-butyne **118** in the presence of BTFFH under microwave conditions to generate the desired amide **119** in good yield. Unfortunately, initial attempts to achieve the 'click' reaction between alkyne **119** and azido-ivermectin **116** failed to yield the desired CJ-BODIPY-ivermectin complex **120**, affording instead only unreacted starting material (Scheme 48).

Unfortunately, time constrains prevented the exploration of this key coupling. Alternative approaches could involve attempting the ‘click’ reaction before the esterification step (Scheme 49).

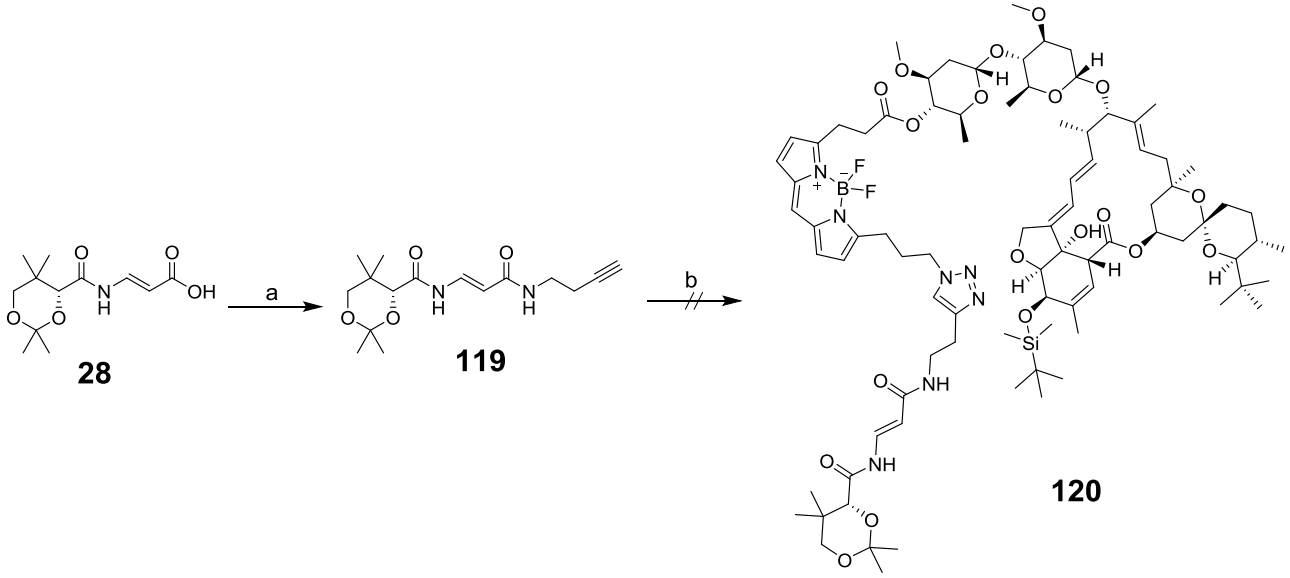

Reagents and conditions: a) 1-amino-3-butyne, BTFFH, DIPEA, CH_2Cl_2, mW, 80 °C, 2.5 h, 68%. b) **116**, CH_2Cl_2, DIPEA, CuI, rt, 18 h.

Scheme 48. Efforts towards the synthesis of CJ-BODIPY-ivermectin complex **120**.

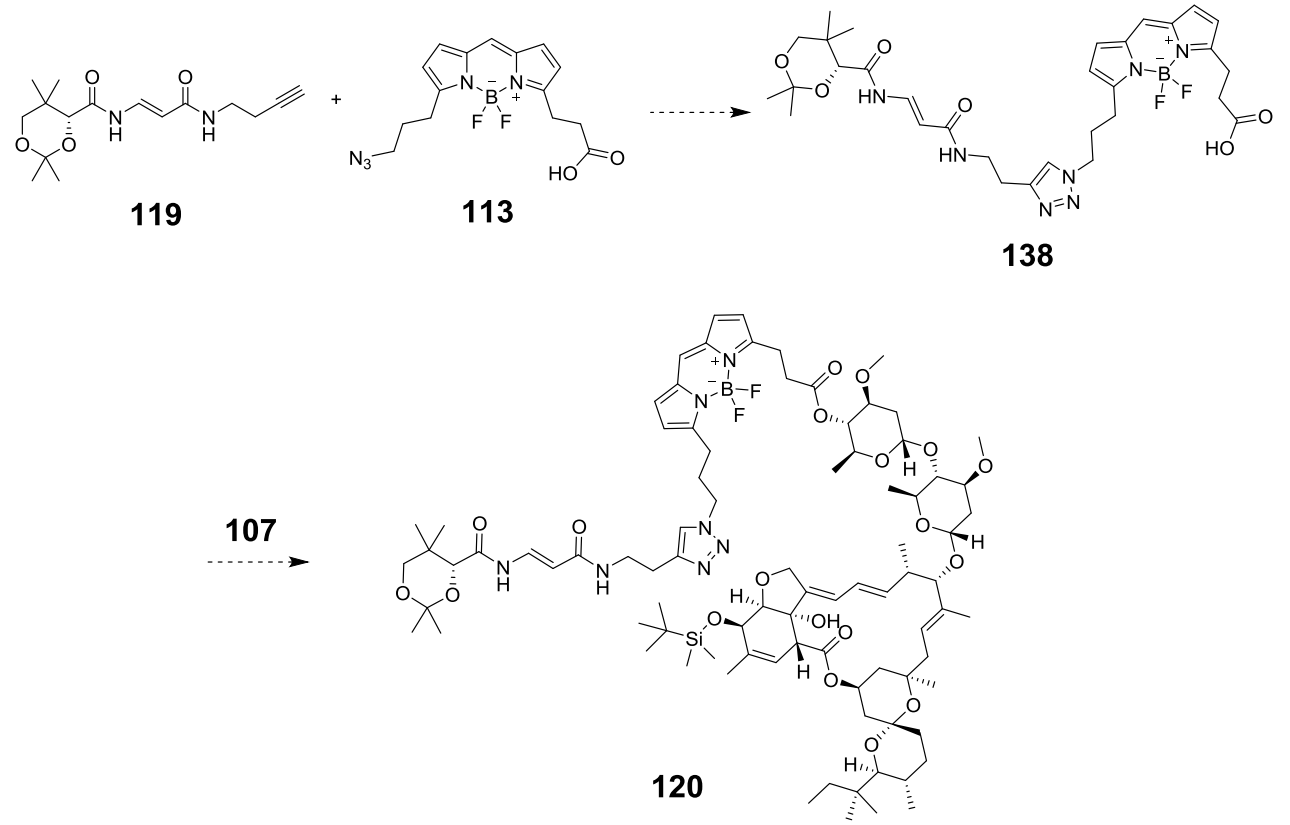

Scheme 49. Alternative approach for the synthesis of CJ-BODIPY-ivermectin complex **120**.

2.8 Bio-activity tests of ivermectin B1a-CJ-15,801 analogue 109, and BODIPY-ivermectin B1a 117 in *C. elegans.*

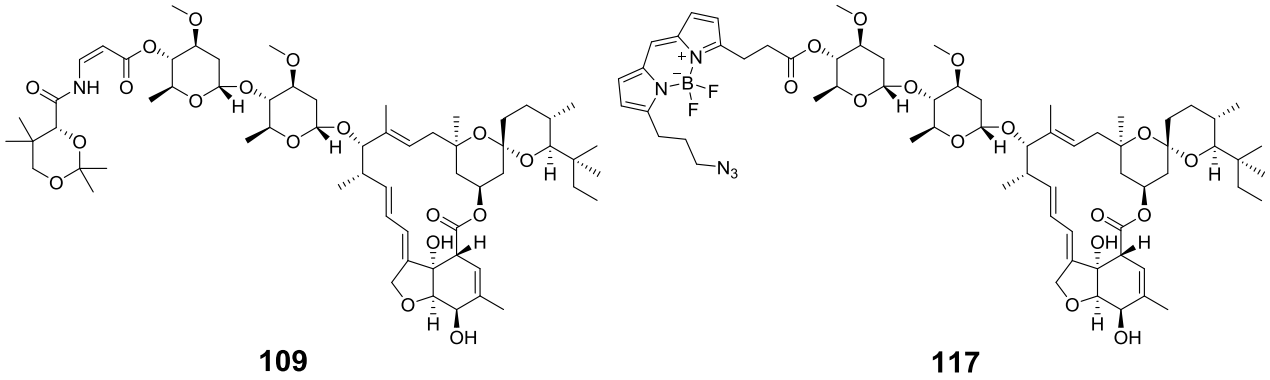

Figure 36. (*R*)-*cis*-ketal CJ-ivermectin analogue **109** and BODIPY-ivermectin B_{1a} **117.**

Having the ivermectin B1a derivatives in hand and based on the promising results obtained with the BODIPY and phiLOV(R475G, K476C) derivatives, a new collaboration was initiated with Professor Bill Pomroy, from the School of Veterinary Science, Massey University. An experiment was designed to test the bioactivity of (*R*)-*cis*-ketal CJ-ivermectin analogue **109**, BODIPY-ivermectin B1a **117** and a commercial veterinary ivermectin B1a solution, as control, in *C. elegans* (Figure 36).

To perform the test, a mixed culture of wild type nematodes, obtained from the University's sheep farm, were incubated for 20 h with the derivatives and the control at 5 and 50 μM, following the protocol described in section 5.

Nematodes treated with (*R*)-*cis*-ketal CJ-ivermectin analogue **109**, showed a similar pattern as the ivermectin B1a control, i.e. the worms exhibited paralysis at both concentrations, with most individuals dead at 50 μM. These findings reveal that this compound was taken into the organism, and that the drug's bioactivity was preserved (Figure 37).

On the other hand, worms treated with BODIPY-ivermectin B1a **117**, exhibited fluorescence at both concentrations. As expected, higher intensities were detected with the 50 μM concentration. Paralysis and death patterns were similar to those of ivermectin B1a**,** confirming the drug's bioactivity. Thus, this derivative would be used as fluorescent control for further tests (Figure 37).

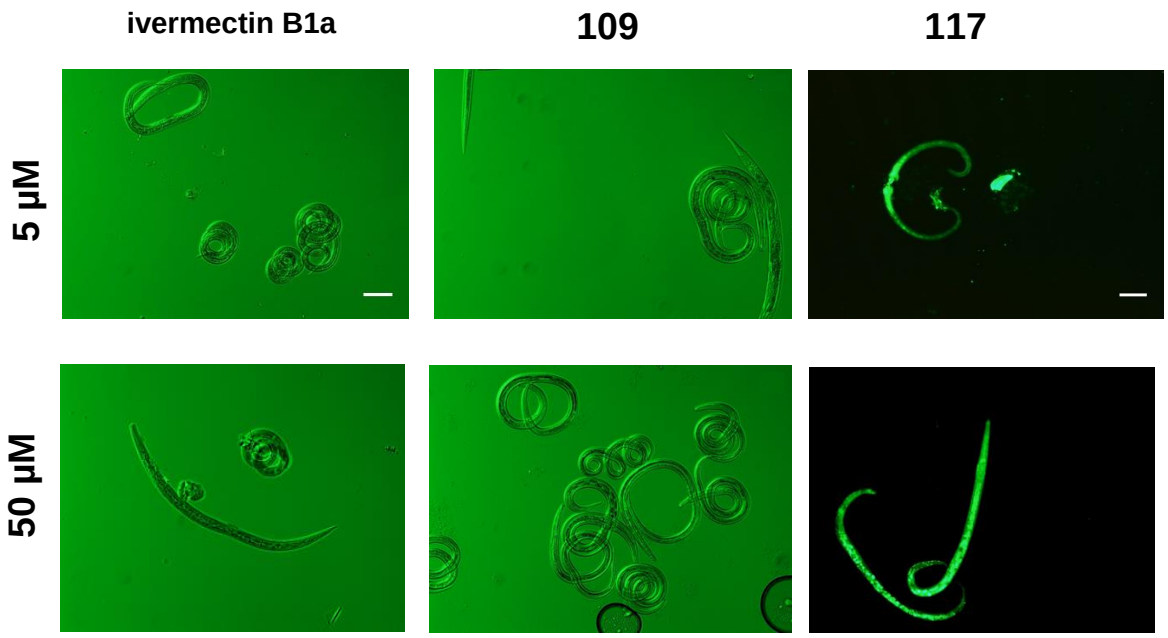

Figure 37. Bio-activity test of ivermectin B1a, *cis*-CJ-15,801 analogue-ivermectin B1a complex **109** and BODIPY-ivermectin B1a **117**

Photos were taken through brighthfield (for ivermectin B1a and derivative **109**) and FITC filter (for derivative **117**), from experiments performed at 50 and 5 µM concentrations and 25 °C for 24 h incubation, size bar: 100 µm. Results from a single experiment done in a single sample.

2.9 Evaluation of PZQ-BODIPY-CJ-15,801 complex 129 in *C. elegans.*

Praziquantel **131** (PZQ) has been in the market for more than 30 years, and this drug is still the first choice treatment against schistosomiasis.[79] After promising results with the CJ-15,801 analogue **28** to deliver BODIPY core and phiLOV in *C. elegans*; it was decided to test, as a probe of concept, the delivery of praziquantel derived complex **129**.

Dr. Silva, from the Marquez group, achieved the synthesis of complex CJ-BDP-PZQ **129** and derivative BODIPY-PZQ **132** (Figure 38). Following previously used protocols described in section 5, a mixed stage culture of *C. elegans* was incubated with a 50 µM solution of compounds **129** and **132**. After 3 h, the samples were analysed under the microscope, and fluorescence intensities were calculated from images using ImageJ software.

Samples treated with derivative BODIPY-PZQ **132**, showed slight fluorescence in the gut cells of larvae and adult worms, whilst in the samples incubated with CJ-BDP-PZQ **129** high fluorescence was observed in the pharynx, gut cells and gut lumen of both larvae and adults (Figure 39).

Fluorescence intensities readings are consistent with microscope findings. The samples treated with complex CJ-BDP-PZQ **129** exhibited more than two times higher intensities compared to the group treated with derivative BODIPY-PZQ **132**, and without apparent detrimental effect (Figure 39).

Thus, these results suggest that CJ-15,801 analogue **28** is able to deliver safely, small molecular weight drugs such as praziquantel, into *C. elegans*.

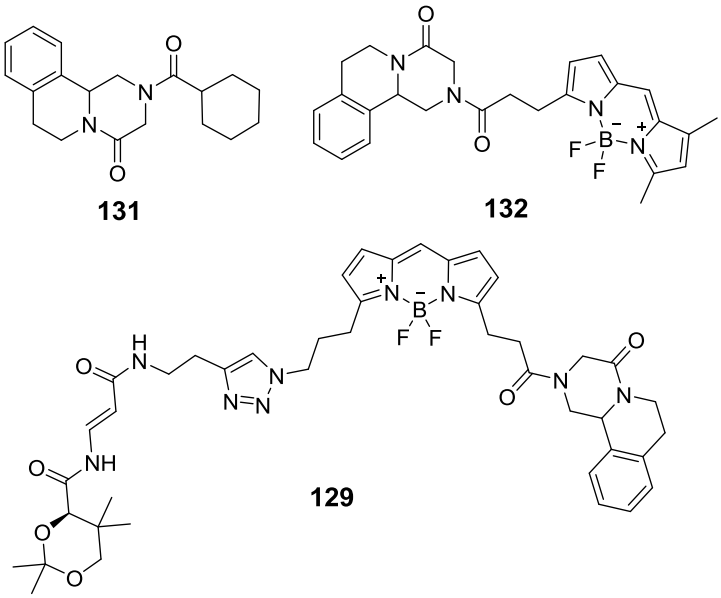

Figure 38. Praziquantel **131**, BODIPY-PZQ derivative **132** and CJ-BDP-PZQ complex **129**.

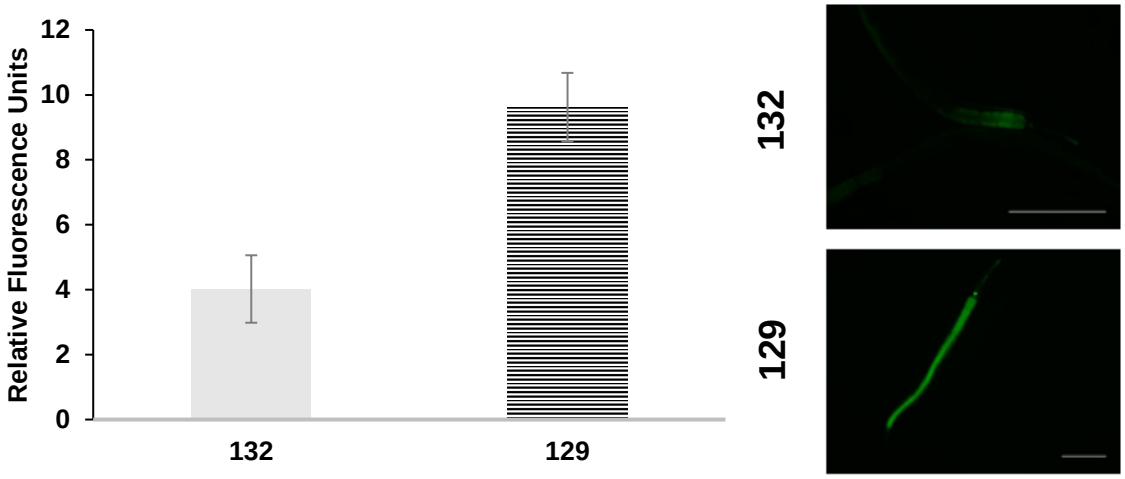

Figure 39. Uptake evaluation of BODIPY-PZQ derivative **132** and CJ-BDP-PZQ complex **129** in *C. elegans*.

Bar chart represents RFU's from experiment performed at 50 µM and 20 °C, samples were taken after 3 h incubation. RFU were calculated from images using ImageJ software. (Units $x10^6$). Photo were taken through FITC filter, size bar: 200 µm.

In conclusion, we have shown that it is possible to use CJ-15,801 analogue **28** to deliver selectively small molecules, as well as proteins, into *C. elegans*.

The synthesis of the CJ-15,801 analogues and their related constructs is reproducible, and can be modified to bind different ligands and biomolecules.

The synthesis of a new *bis*-functionalised BODIPY **113** has been achieved. A *bis*-functionalised BODIPY core has the potential to be extremally useful in drug delivery and selectivity studies.

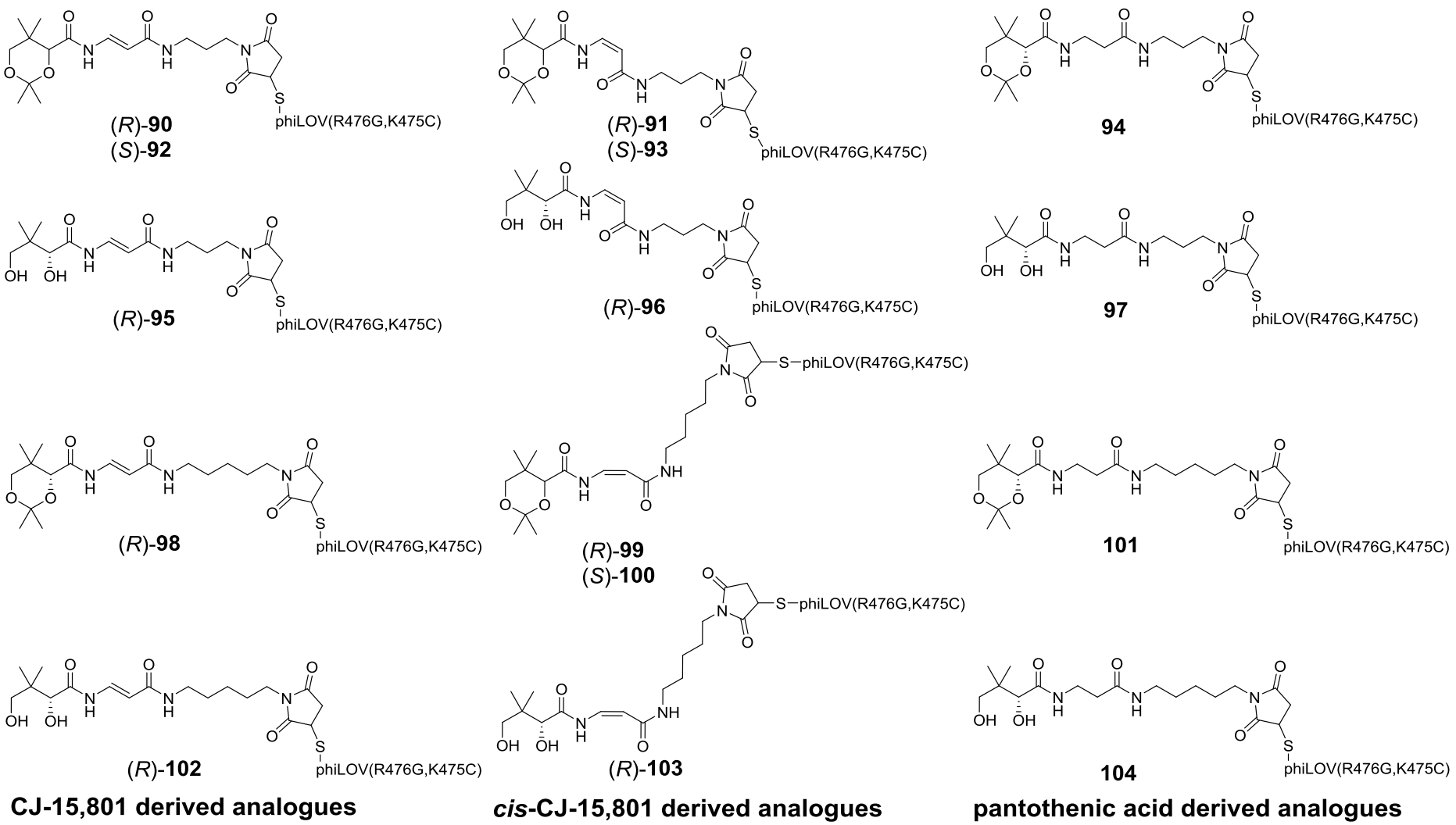

Figure 40. CJ-15,801 and pantothenic acid derivatives coupled to phiLOV(R475G, K476C) for biological evaluation.

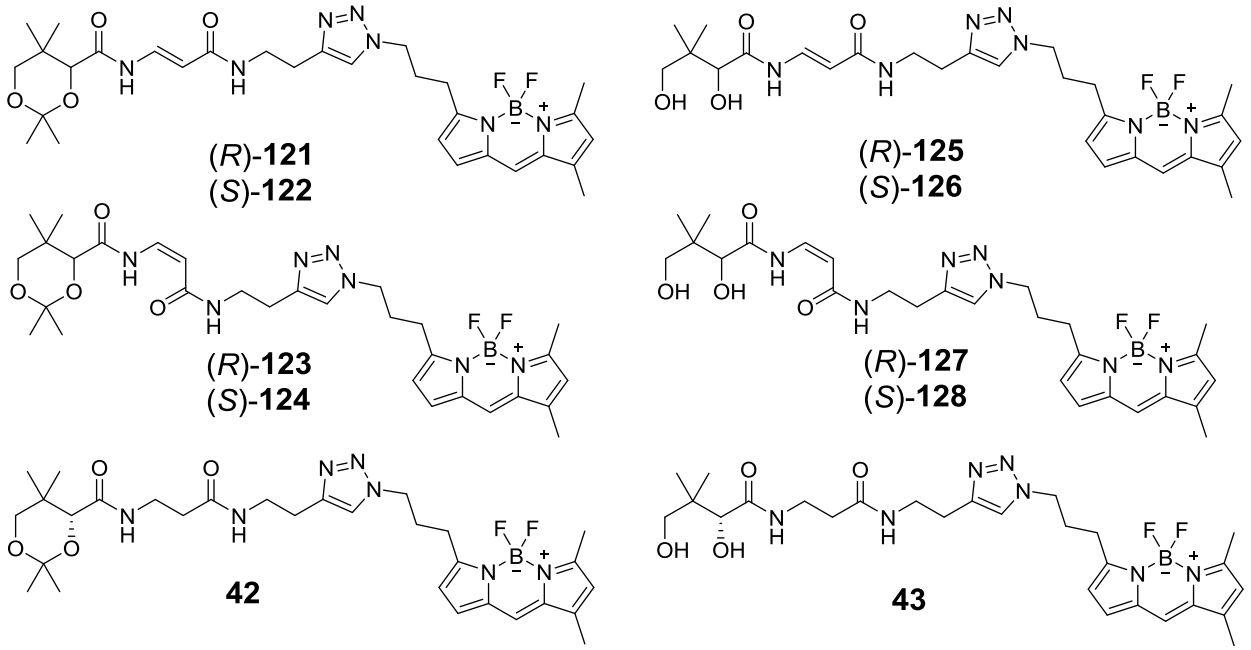

Figure 41. CJ-15,801 and pantothenic acid derivatives coupled to BODIPY FL for biological evaluation.

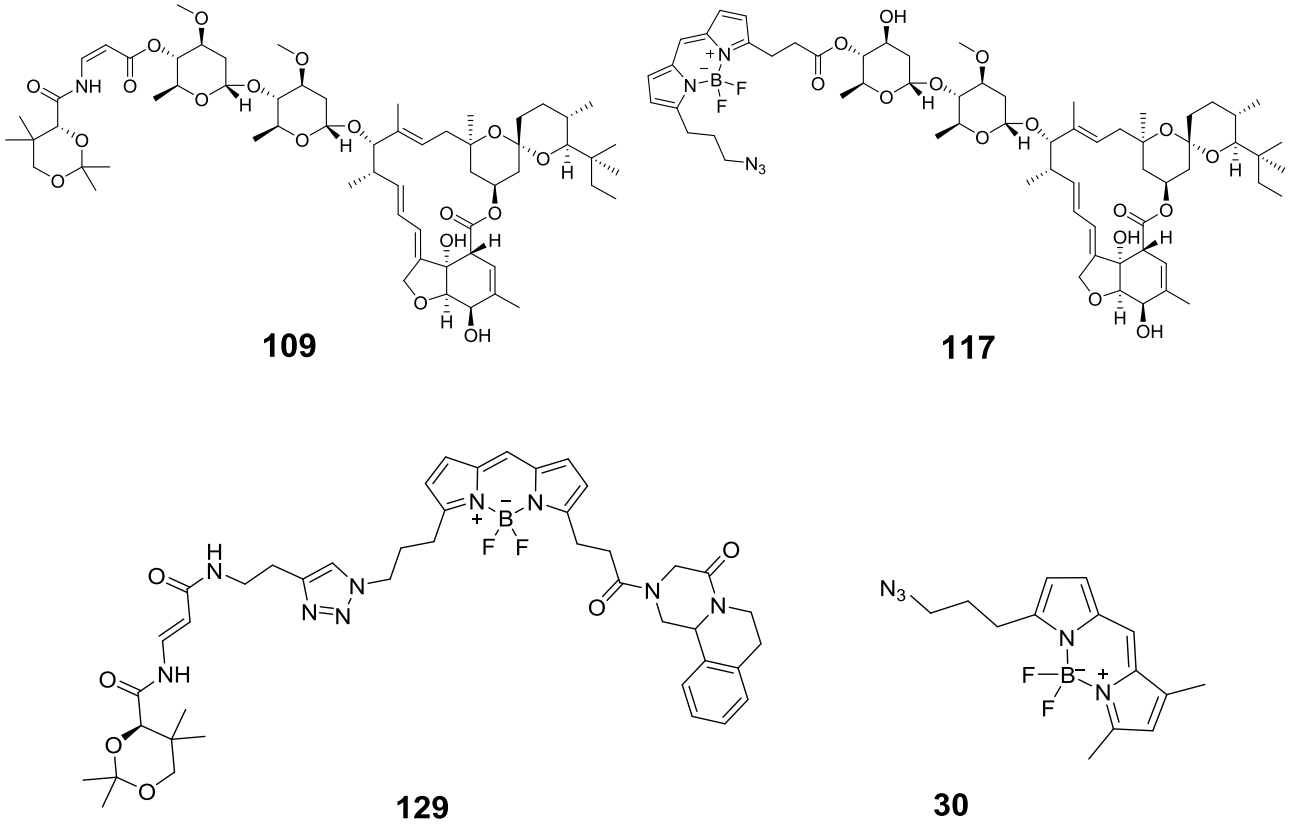

Figure 42. Ivermectin and praziquantel CJ-15,801 analogues complexes **109**,**129**. Ivermectin-BODIPY complex **117** and azido-BODIPY **30** for biological evaluation.

3. Biological evaluation.

3.1 *Lotmaria passim*

3.1.1. Evaluation of CJ-15,801 and Pantothenic acid analogues coupled to BODIPY FL in *L. passim.*

"*… without realising that you were carelessly watching the venerable ancestor to whom we probably owe most of our flowers and fruits (for it is actually estimated that more than a hundred thousand varieties of plants would disappear if the bees did not visit them), and possibly even our civilisation, for in these mysteries all things intertwine.*" The Life of the Bee by Maurice Maeterlinck, 1901

Previously, Dr. Sewell from the Marquez group reported promising results when a library of enamides, including CJ-15,801, were evaluated for activity against *Trypanosoma brucei*.[46]
Lotmaria passim, is *a* kinetoplastid related to *T. brucei* and has been identified as a possible cause for bee colony collapse disorder.[80]
In collaboration with the Kadowaki group from the Department of Biological Sciences at XJTLU, *Lotmaria passim* cultures obtained from honey bees (*Apis mellifera*) were incubated with BODIPY-CJ-15,801, and BODIPY-pantothenate analogues at 10 and 500 µM (Figure 41). After 45 min incubation, the samples were washed following the protocol described in section 5, and slides were prepared and analysed under the fluorescence microscope.

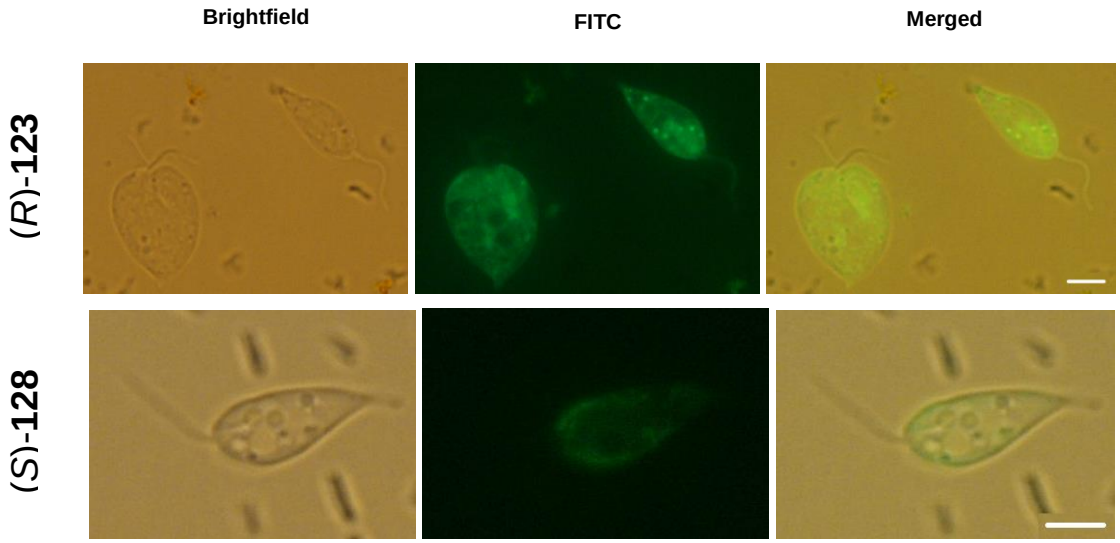

Figure 43. Uptake test of BODIPY-CJ-15,801 derivatives (*R*)-**123** and (*S*)-**128** in *L. passim*. Photos were taken from experiments performed at 500 µM for (*R*)-**123** and 10 µM for (*S*)-**128**, and incubation at rt for 45 min, size bar: 5 µm. Results from a single experiment done in triplicate.

Excitingly, parasites treated with ketal derivative (*R*)-**123** at 500 µM exhibited fluorescence in the parasite's cytosol, with the derivative forming fluorescence dots. Interestingly, parasites incubated with the diol derivative (*S*)-**128** at 10 µM displayed fluorescence surrounding the cell membrane but not in the cytoplasm (Figure 43). Although these results were promising, we needed to compare the fluorescence emission by a quantitative method. Thus, it was decided to use the Varioskan LUX microplate reader. The high sensitivity of the equipment meant that the experiment conditions had to be modified. Thus, the initial uptake screen was repeated with all the derivatives at 1 µM and 45 min incubation time.

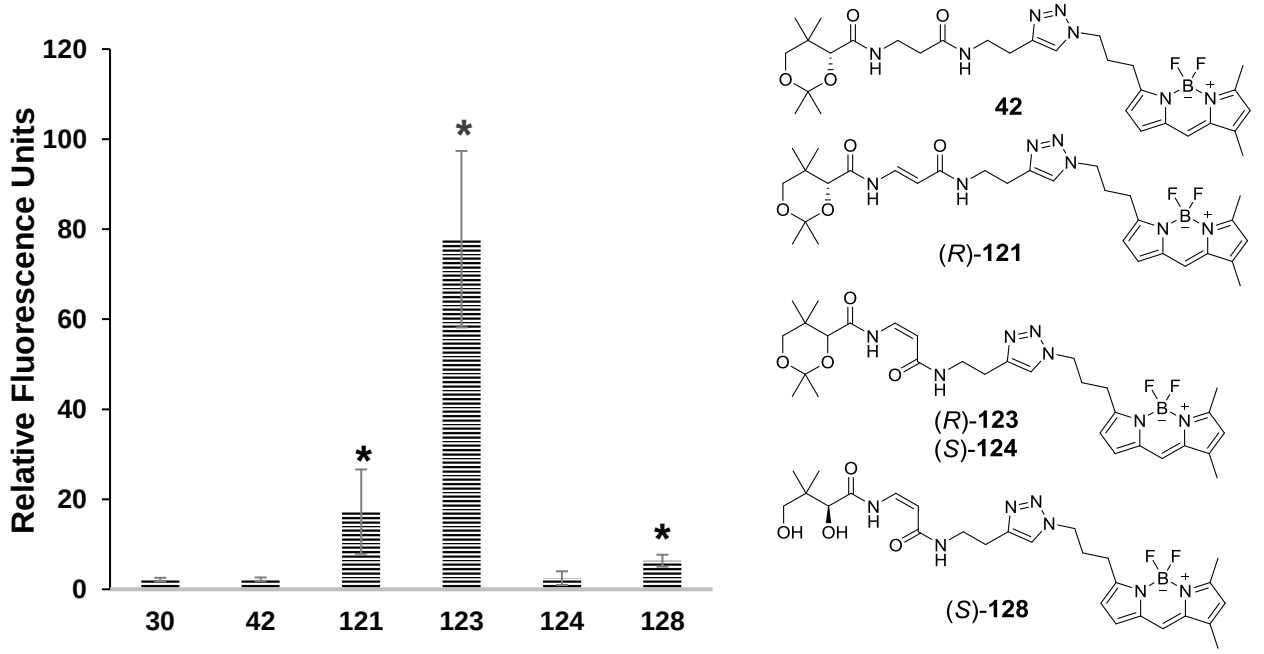

Figure 44. Uptake evaluation of BODIPY-CJ-15,801 derivatives and BODIPY **30** in *L. passim*. Bar chart represents RFU's from experiments performed at 1 µM and rt for 45 min incubation. (Units x10^6). The asterisks indicate significant differences (∗P< 0.03) between the samples and BODIPY control **30**, analysed using an independent Student's t-test. The figure represents a single experiment done in triplicate.

The plate reader results confirmed the fluorescence microscope findings which suggested the preferential uptake of the ketal derivatives. Consistent with a selective transport mechanism, derivative (*R*)-*cis*-**123** showed the highest reading amongst all the compounds tested, whilst derivative (S)-*cis*-**124** showed one of the lowest amounts of uptake. The diols performed very poorly, with the *cis* isomers being slightly better than the *trans* counterparts. On the other hand, the pantothenate derivates displayed not significant fluorescence readings (Figure 44).

Uptake studies at higher concentrations, using a small subset of the compounds including CJ-15,801 derivatives (*R*)-**121** and (*R*)-**123**, as well as the pantothenic acid ketal **42**, showed a similar pattern to the low concentration study (i.e. the (*R*)-*cis* ketal analogue **123** was selectively taken up by the parasites). Interestingly, incubation with the pantothenic acid ketal derivative **42** resulted in similar

intensity readings as those generated by the unsaturated analogue (*R*)-**121** (Figure 45). Thus, *L. passim* showed selective uptake for lipophilic derivatives (ketals), on the contrary to *C. elegans* results, with significant preference for the *cis*-geometry derivative (*R*)-**123**.

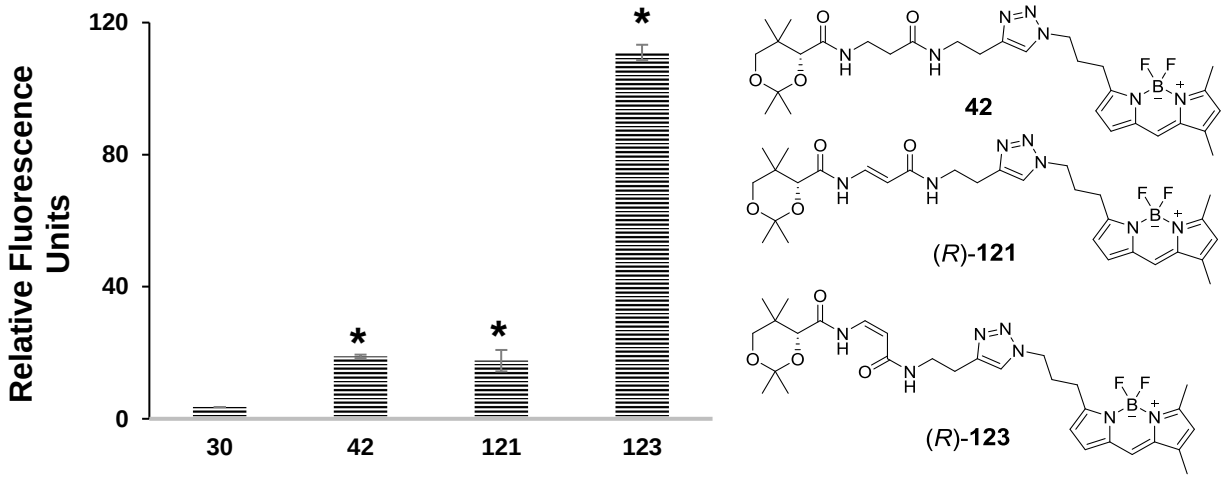

Figure 45. Uptake evaluation of BODIPY-pantothenate derivative **42**, CJ-15,801 derivatives (*R)*-**121**, (*R)*-**123** and BODIPY **30** in *L. passim*.

Bar chart represents RFU's from experiments performed at 100 µM and rt for 45 min incubation. (Units x10^2). The asterisks indicate significant differences (∗P<0.03) between the samples and BODIPY control **30**, analysed using an independent Student's t-test. The figure represents a single experiment done in triplicate.

3.1.2. Evaluation of CJ-15,801 and pantothenic acid analogues coupled to BODIPY FL in honey bee guts (*Apis mellifera*).

Having confirmed uptake of CJ-15,801 derivatives (*R*)-**123** and (*R*)-**121** into the *Lotmaria* parasites, their selectivity was explored by looking at their permeability into the guts of the bees.

For the gut test, the gastrointestinal system (crop, midgut and rectum) of adult honey bees was extracted, and incubated with ketals (*R*)-**123** and (*R*)-**121**, as well as BODIPY **30** and (*S*)-**128** as controls, for 45 min at 33 ˚C (Figure 46).

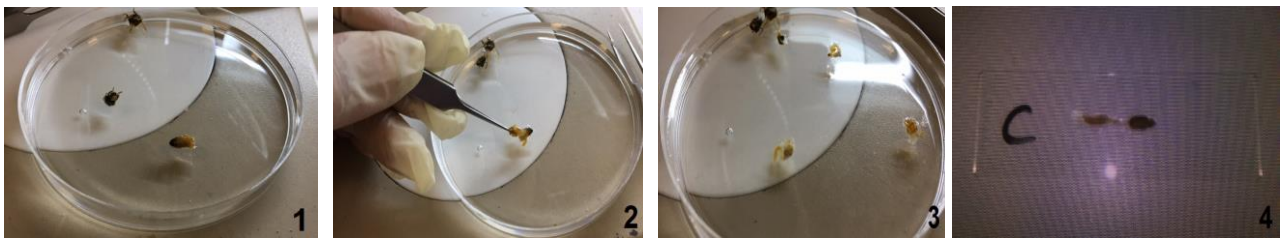

1,2: Disection, 3: Gut, 4: Slide before microscopic analysis.

Figure 46. Honey bee gut extraction.

Initially, the bee's gastrointestinal system was incubated with ketals (*R*)-**121** and (*R*)-**123** at 500 µM concentration. As expected, the DMSO control exhibited slight autofluorescence in the midgut and rectum. Not surprisingly, the high concentrations of ketals used resulted in fluorescence uptake in both the midgut and rectum. Thinking that this concentration was too high to detect any difference, we decided to reduce the concentration to 100 µM.

Clearly, reducing the concentration changed the output in the assay; guts treated with BODIPY **30** only, showed only autofluorescence. Incubation with derivative (*R*)-**121** resulted in high fluorescence in the midgut and rectum, but not the crop. Excitingly, ketal (*R*)-**123** and diol (*S*)-**128** displayed slight fluorescence in midgut and rectum, with none in the crop. Of particular interest is the uptake of ketal (*R*)-**123** as the fluorescence seems to be on the surface of the gut, but not inside of it (Figure 47).

Cells in midgut and rectum areas have an increased ability to absorb nutrients comparing to those in the crop. This correlates with the results obtained at different concentrations, in which the crop was always free of fluorescence even at high concentrations. The results also suggest that using derivatives under 100 µM would diminish the probability of distributing the compounds outside of the gastrointestinal system, and would maintain the compounds close the parasite.

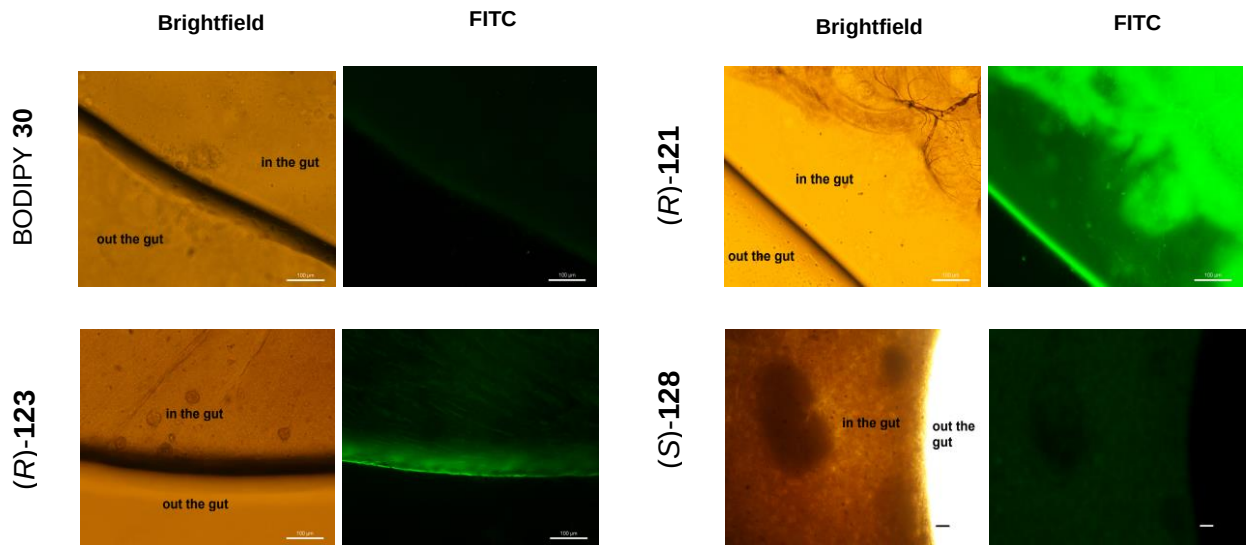

Figure 47. Uptake test of BODIPY-CJ-15,801 derivatives and BODIPY **30** in honey bee guts. Photos were taken from experiments performed at 100 µM and 33 ˚C for 45 min. incubation, size bar: 100 µm. Results from a single experiment done in triplicate.

A final experiment measuring the uptake into the parasites by FACS, could not be carried out due to time constrains. Using single cell measurements, would have provided more compelling evidence of the differential uptake.

In conclusion, in order to reach the parasite's cytosol, the BODIPY derivatives were transported through the cell membrane by a selective uptake mechanism, based on the selectivity of one enantiomer over another. Compound *R*- **123** was preferentially transported, and showed specific accumulation within the parasite. Potential localisation site is the acidocalcisome, which functions

as storage for phosphorus (as pyrophosphate and poly-phosphate) as well as Ca^{+2} and Mg^{+2} cations[81] (Figure 48).

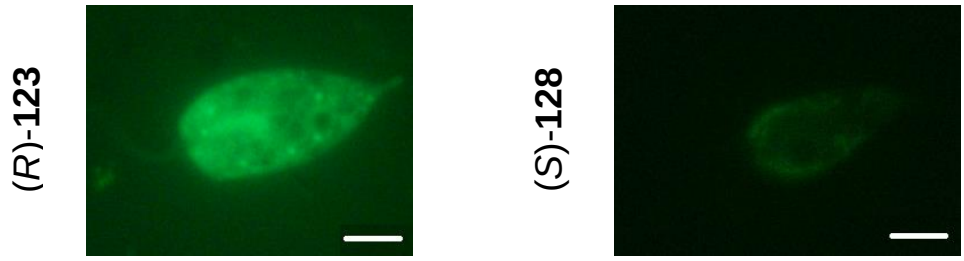

Figure 48. Uptake evaluation of BODIPY-CJ-15,801 derivatives (*R*)-**123** and (*S*)-**128** in *L. passim*. Photos were taken through FITC filter, from experiments performed at 500 µM for (*R*)-**123** and 10 µM for (*S*)-**128**, and incubation at rt for 45 min, size bar: 5 µm. Results from a single experiment done in triplicate.

On the other hand, according with the microscope findings, derivative diol *S*-**128** was able to bind the cell membrane, but was not able to be transported into the cytosol, possibly due to the strong interactions of the free diol with components on the cell membrane (Figure 48).
Crucially, the CJ-15,801 analogues **54** and **130** are unable to be transported through the gut cells possibly due to their geometry. Thus, this apparent low permeation represents a valuable property as a potential drug carrier for honey bee intestinal infections (Figure 49).

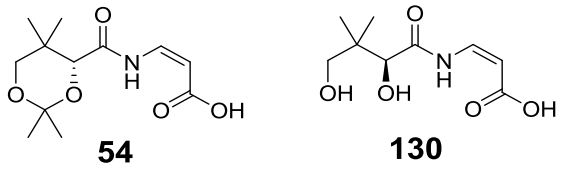

Figure 49. Promising CJ-15,801 analogues as drug carriers in kinetoplastid *Lotmaria passim*.

3.2 *Babesia bovis.*

3.2.1. Evaluation of CJ-15,801 and pantothenic acid analogues coupled to BODIPY FL in RBCs infected with *B. bovis.*

In collaboration with Dr. Osamu Kaneko and his group at the Institute of Tropical Medicine at the University of Nagasaki, the library of BODIPY and phiLOV(R475G, K476C) pantothenic and CJ-15,801 derivatives were tested in *Babesia bovis*. *B. bovis* is a protozoan parasite, which shares the taxonomic group with *Theileria,* and is placed in the *Piroplasmida* order due to its pear-shaped appearance within the infected erythrocytes. *Babesia* reproduces by binary fission, causing the characteristic presence of pairs or tetrads in stained infected erythrocytes.Two species, *B.bovis* and *B. bigemina,* cause considerable economic impact in the cattle industry.[82]

Dr. Sewell, from the Marquez group had originally reported the uptake of BODIPY derivative **135** into the apicomplexan parasite, *P. falciparum* 3D7.[46] *Plasmodium* and *Babesia* share a common intraerythrocytic stage as part of their life cycles.[83] However, it is important to notice, that *Plasmodium* exhibits an extra membrane*,* the parasitophorous vacuolar membrane (PVM). This membrane represents a barrier to control the trafficking of nutrients and metabolites in and out of the parasite, and may offer additional protection to the parasite from external conditions.[29b]

An initial test was performed on a *B. bovis* Texas strain sample using pantothenic acid and CJ-15,801 analogues attached to BODIPY. The *B. bovis* sample (~5% Parasitized Erythrocytes (PPE)) was incubated with different analogues (25 μM) for 45 min, following the protocol described in section 5.

Using the confocal microscope, weak fluorescence signal was observed in parasites incubated with BODIPY derivative **30**. In contrast, parasites exposed to (*R*)-ketal derivative **121** (25 μM) exhibited very high intensity. Interestingly, the (*S)*-enantiomer **122** showed lower uptake. The polar analogue (*R*)-**125** on the other hand, showed even less fluorescence. Most importantly, healthy erythrocytes did not show any uptake, and when the compounds were transported into the infected red blood cells, they were concentrated in the parasite's cytosol (Figure 50). Our findings in non-infected RBCs match with previous uptake studies of pantothenic acid. Saliba reported 26-times reduced uptake of [^{14}C] pantothenate into non-infected erythrocytes compared to *P. falciparum*-infected erythrocytes.[84]

In order to measure the fluorescence intensities and compare the uptake of CJ-15,801 derivatives, the images were analysed by ImageJ 1.50b software following the procedure reported by Miller.[49] Gratifyingly, the microscope findings are consistent with the calculated intensities. Comparing these fluorescence intensities, derivative (*R*)-**121** exhibited the highest uptake, whilst (*S*)-**122** derivative (20% less) and (*R*)-**125** derivative (30% less) showed lower values, compared to (*R*)-**121** derivative. BODIPY derivative **30** on other hand, exhibited much lower uptake (2 times less) compared also to (*R*)-**121** derivative (Figure 50). It seems that the BODIPY-CJ derivatives uptake is increased when CJ-15,801 core bears the ketal group, *trans* geometry and *R* configuration. Based on these results, the BODIPY-CJ-15,801 derivatives revealed a selective uptake mechanism in *B. bovis*.

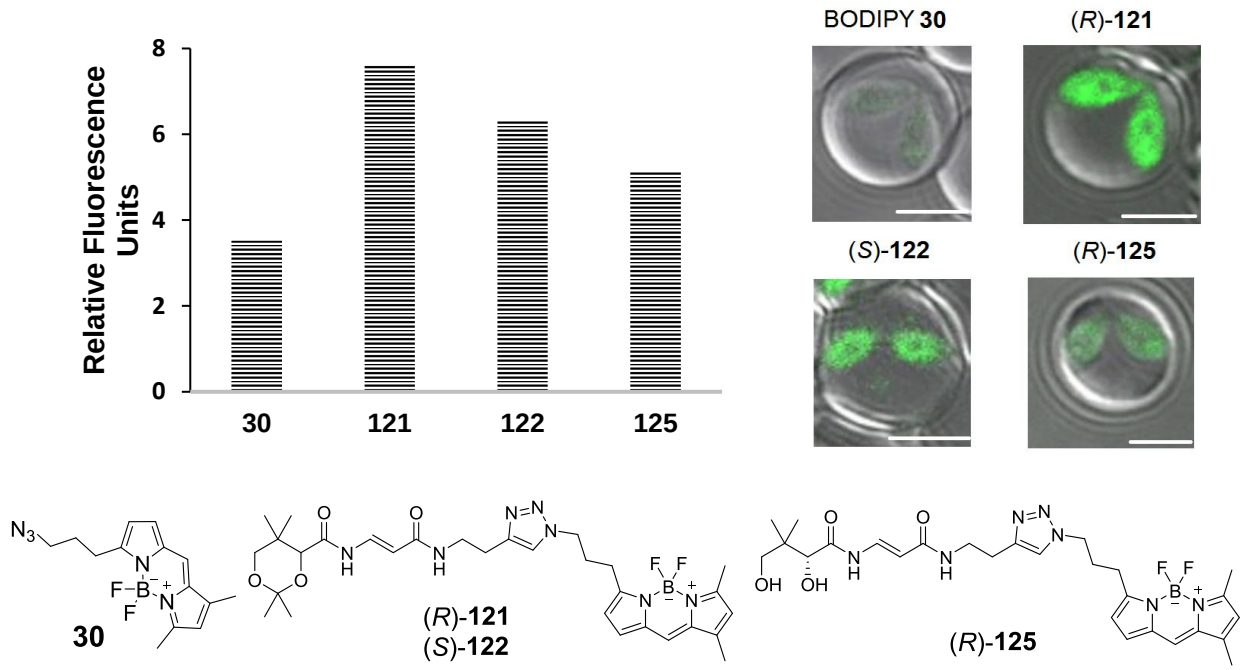

Figure 50. Uptake evaluation of BODIPY-CJ-15,801 derivatives in RBCs infected with *B. bovis*. Bar chart represents RFUs from experiment performed at 25 µM and 37 °C, after 45 min incubation. RFU were calculated from images using ImageJ software. (Units x10^6). Photos are merged results from brigthfield and FITC filter, size bar: 5 µm. Results from a single experiment.

3.2.2. Evaluation of CJ-15,801 and pantothenic acid derived analogues coupled to phiLOV(R475G, K476C) in RBCs infected with *B. bovis.*

Following the same protocol applied to the BODIPY derivatives, a set of CJ-phiLOV(R475G, K476C) derivatives were tested at 50 µM and incubated for 45 min incubation. Based on the results obtained with the BODIPY derivatives, only the (*R*)-isomers coupled to phiLOV were selected for this evaluation. Interestingly, initial microscopic analysis showed no fluorescence uptake with any of the samples. However, some red blood cells exhibited cell membrane rupture (both uninfected and infected), and many parasites were out of the host cells.

Upon careful consideration of all the experimental conditions, it was determined that media could be the source of this problem. During the storage process, the buffer had been exchanged to Creek's minimal medium (CMM), rich in Na^{+1}, K^{+1} and Ca^{+2} ions. High levels of these cations were likely to affect the osmotic pressure of the erythrocyte, causing lysis of the cell, as well as, representing a hostile environment for the parasite. This in turn, could reduce the trafficking of nutrients and waste compounds in and out of the parasite. Thus, considering the osmotic balance for RBCs, it was decided to change the buffer to PBS buffer (pH 7), and to test again at 100 µM following the protocol reported in section 5.

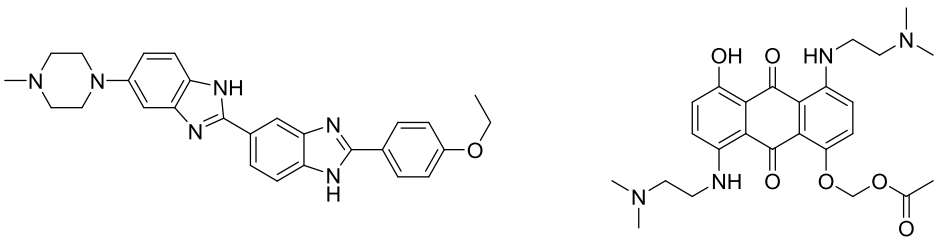

Figure 51. Nuclear stains used in *B. bovis* experiments.

The permeable nuclear stain, Hoechst 33342 (355/465) (Figure 51), was added as a co-stain in order to help to visualize and corroborate the localization of living parasites within the cells. Excitingly, the change of buffer significantly altered the output of the experiment, and fluorescence signals were detected in some of the samples.

Derivatives bearing the 5-carbon linker derivatives **104** and (*R*)-**102** exhibited uptake into merozoites located outside RBC, which appeared alive during the analysis. Interestingly, in a sample containing merozoites inside RBCs, the characteristic binary form of *B. bovis* became fluorescent when treated with derivative (R)-**102** (Figure 52). Based on these results, it seems that only the free diol derivatives were able to reach the parasite's cytosol. Probably, the ketal group presents a rigid structure, additional to the complex structure of phiLOV, making difficult the interaction with the transporter and causing that the uptake process decrease significantly.

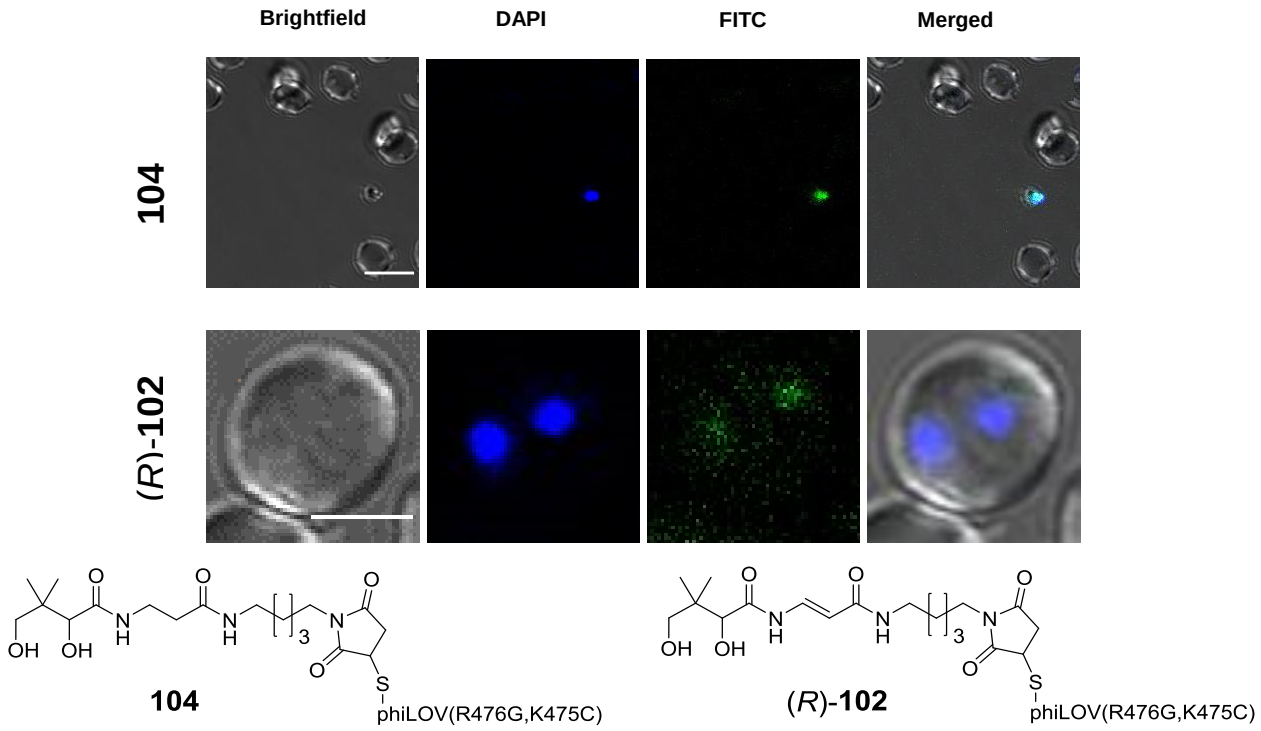

Figure 52. Uptake evaluation of phiLOV(R475G, K476C)-pantothenic acid **104** and CJ-15,801 derivative (*R*)-**102** in RBC's infected with *B. bovis*.

Photos are results from experiment performed at 100 μM and 37 °C, for 45 min. incubation. **104** Photo: Parasite outside of RBC, size bar: 10 μm. (*R*)-**102** Photo: RBC infected by parasites, size bar: 5 μm. Results from a single experiment done in triplicate.

In order to confirm these microscope findings that suggest preference for certain chemical group (free diol) and bearing the five-carbon linker, when CJ-15,801 core is coupled to phiLOV, a similar technique as the COPAS Bio-sort used in *C. elegans* was used to analyse the samples. FACS (Fluorescence-activated cell sorting) works by counting individual RBCs, and then differentiating them from uninfected cells using a nuclear dye, in the process measuring fluorescence signals through the use of an appropriate filter.

In our experiment, the phiLOV emission was measured using a FITC filter. DRAQ5 (600/697, Figure 51) was used as a co-stain, and was detected using a far red filter. Parasitemia during the experiment was approximately 9%.

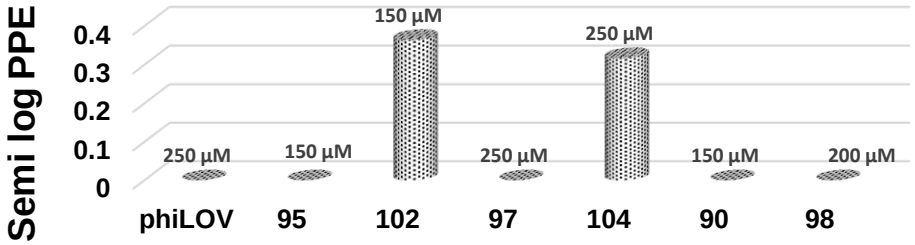

Figure 53. Uptake evaluation of phiLOV(R475G, K476C)-pantothenic acid derivatives and CJ-15,801 derivatives in RBCs infected with *B. bovis*.

Bar chart represents PPE from experiments performed at 37 °C after 45 min incubation with derivatives, cells were sorted by FACS. Results from a single experiment done in a single sample.

The FACS results were consistent with the confocal findings in which derivatives with a three-carbon linker did not show significant fluorescence. Excitingly, the 5-carbon linker derivatives (*R*)-**102** and **104**, exhibited a marked uptake into the infected erythrocytes (Figure 53). The distance from the carrier to the protein is crucial to cross the RBC membrane. It is possible that the 3-carbon unit does not allow the cellular receptor to identify the pantothenic/CJ ligand as a substrate, and instead "sees" it as a part of phiLOV.

Having been able to measure the uptake into the parasite, it became imperative to determine if the uptake had any impact on parasite growth. Thus, an initial assay was performed with all the phiLOV derivatives in RBCs infected with *B. bovis*, and incubated at the same concentration (100 µM) for 45 min (initial parasitemia of approximately 3%). Samples were then taken at 24 and 48 h after exposure. Interestingly, the parasites exposed to derivative (*R*)-**102** did not grow during the first 24 h, whilst all the other cultures showed similar growth levels to the phiLOV control. However, after 24 h, growth resumed and reached similar levels to those in the control group (Figure 54).

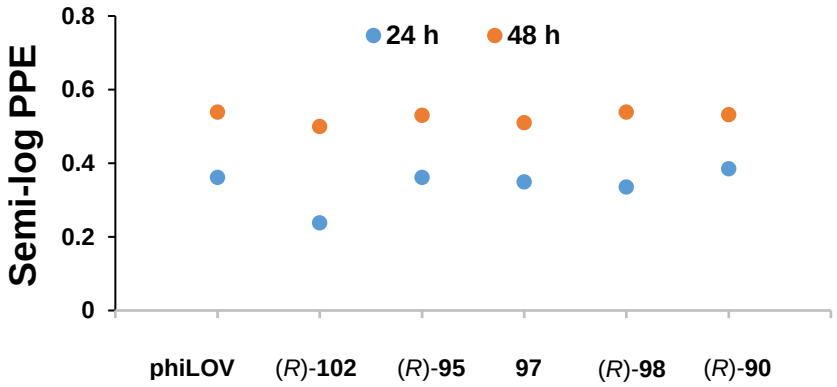

Figure 54. Growth test of *B. bovis* incubated with phiLOV(R475G, K476C)-pantothenic acid derivatives and CJ-15,801 derivatives.

Scatter chart represents PPEs from experiments performed at 100 µM and 37 °C after 45 min incubation with derivatives, samples were evaluated after 24 h and 48 h post-incubation. The figure represents a single experiment done in a single sample.

Considering the low impact of derivatives at 100 µM, we decided to evaluate the library at 5 µM in order to get a full impact profile. Thus, an additional experiment was carried out in which the concentration of the sample was 5 µM, and PPE was ~1.1%. Fresh media was added at 24 h, and post-incubation was continued to 48 h. The samples were analysed under the microscope, and weak fluorescence was detected in samples (*R*)-**102** and **104**. The rest of the samples only displayed autofluorescence (Figure 55).

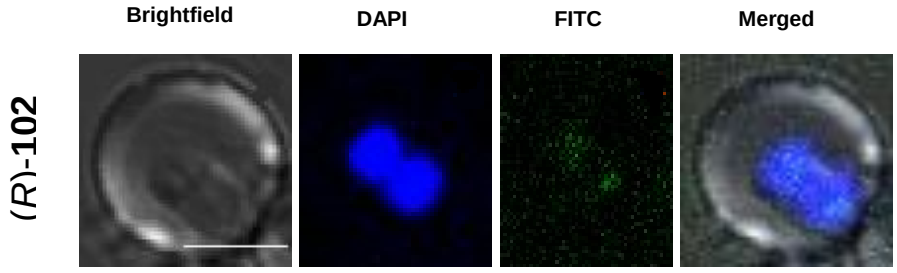

Figure 55. Growth evaluation of *B. bovis* incubated with phiLOV(R475G, K476C)-CJ-15,801 derivative (*R*)-**102**.

Photos are results from experiments performed at 5 µM and 37 °C, after 45 min. incubation, and 48 h post-incubation, size bar: 5 µm. Results from a single experiment done in triplicate.

PPE were calculated at 48 h post-incubation and differences in the percentage of parasitemia were statistically analysed by the independent Student's t-test, in which $P<0.03$ was considered to be of significant difference. All derivatives exhibited similar cell growth, showing no significant difference with the phiLOV control. Notably, the parasite reproduction reached comparable levels with the rest of the samples when microorganisms were incubated with compound (*R*)-**102**. Thus, pantothenic

acid and CJ-15,801 derived analogues did not display toxic effects on the parasite in long-term experiments (Figure 56).

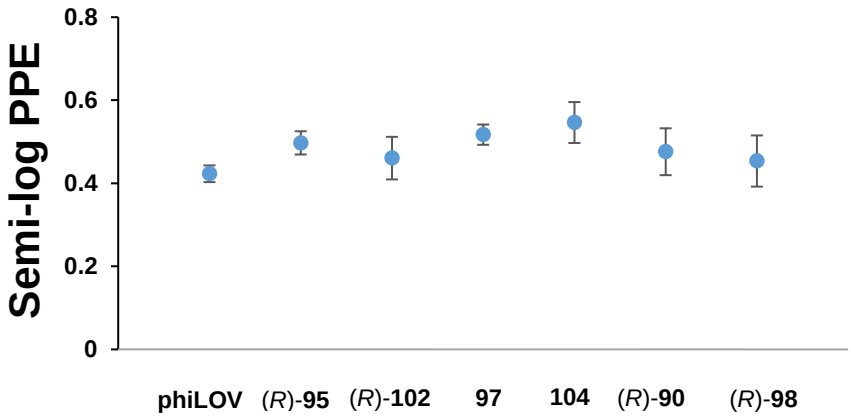

Figure 56. Growth evaluation of *B. bovis* incubated with phiLOV(R475G, K476C)-pantothenic acid derivatives and CJ-15,801 derivatives.

Scatter chart represents PPE's from experiments performed at 5 µM, 37 °C and 45 min incubation with derivatives, the samples were evaluated after 48 h post-incubation. The figure represents a single experiment done in triplicate.

Based on results from BODIPY and phiLOV derivatives, CJ-15,801 and pantothenate analogues showed a selective uptake mechanism, in which the transporter is able to differentiate one enantiomer over another. Additionally, when the ligand is more complex (i.e. phiLOV), the length of the linker also demonstrated to be crucial in order to allow the uptake.

In conclusion, we have demonstrated that CJ-15,801 analogues can be used to deliver small molecules as well as complex biomolecules, to the parasite's cytosol. This delivery system can also be used in short and long-term studies, providing a new approach for *B. bovis* studies.

3.3 *Mycobacterium*

3.3.1 Evaluation of CJ-15,801 and pantothenic acid analogues coupled to BODIPY FL in *M. smegmatis* and *M. tuberculosis.*

"If the importance of a disease for mankind is measured by the number of fatalities it causes, then tuberculosis must be considered much more important than those most feared infectious diseases, plague, cholera and the like. One in seven of all human beings dies from tuberculosis. If one only considers the productive middle-age groups, tuberculosis carries away one-third, and often more." (Robert Koch, 1882)[85]

Mycobacterium tuberculosis complex (MTC or MTBC) is known for its robust cell envelope which efficiently protects the bacilli from external intruders. *Mycobacterium* is a genus of actinobacteria and includes the species *M. tuberculosis, M. bovis, M. africanum.* All these species can cause tuberculosis (TB), and were the ninth leading cause of death for humans in 2016. M. bovis is also a major economic problem in the veterinary field.[5a, 86] *Mycobacterium leprae*, responsible for Hansen's disease or leprosy, caused more than 200,000 reported new cases globally in 2016.[87]

In collaboration with Dr. Boris Tefsen at XJTLU, it was decided to evaluate the uptake of the BODIPY-CJ and BODIPY-pantothenate analogues in *M. smegmatis*. *M. smegmatis* is a non-pathogenic specie that has been used as mycobacterial model, due to its fast-growth and ease to manipulate genetically.[88]

According to the literature, the mycobacterial machinery is able to bio-synthesise pantothenic acid *de-novo* starting from amino-acid intermediates. Only when the *panC* and *panD*, genes involved in vitamin B_5 synthesis, are deleted, the resultant mutant become auxotrophic for pantothenate.[89]

Due to the lacking of previous reports of CJ-15,801 on *M. smegmatis,* an initial experiment was designed to assess the possible impact of CJ-BODIPY derivatives on cell growth. The experiment involved incubating *M. smegmatis* wild type mc^2155 at 37 °C with 250 µM and 100 µM ligand concentrations. The optical density (OD) was measured at 600 nm after 24 h incubation, following the protocol described in section 5.

The microorganisms treated with BODIPY **30** were not affected, and their growth remained similar to the DMSO treated control group. Interestingly, cell growth decreased in the range of 35-50% when incubated with 250 µM ligand concentration. When the mycobacteria were treated with a 100 µM concentration of the ligands, the cells were largely unaffected and grew normally. A notable exception however, was the (*R*)-**121** derivative which reduced the cell growth by only (6% ±) with 250 µM concentration compared to the control. At 100 µM there was virtually no change between (*R*)-**121** and the control (Figure 57).

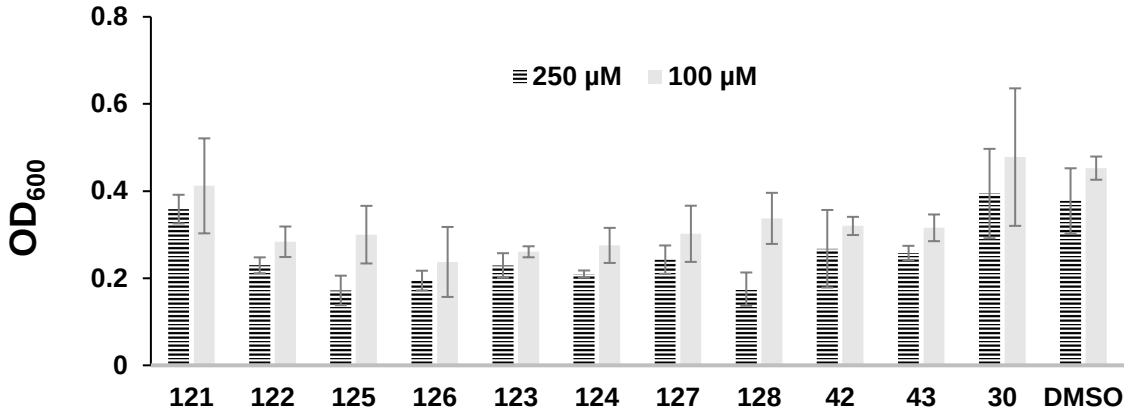

Figure 57. Growth evaluation of *M. smegmatis* incubated with BODIPY-pantothenic acid and CJ-15,801 derivatives and BODIPY **30**.

Bar chart represents Optical Densities (ODs) from experiments performed at 250 µM, 100 µM, 37 °C and 24 h incubation. ODs were analysed at 600 nm. The figure represents a single experiment done in triplicate.

Based on these results, a pilot assay was performed, in which *M. smegmatis* wild type mc^2155 was incubated with the BODIPY derivatives **42**, **43**, **121**-**128** at a 50 µM concentration for 48 h, followed by microscopic analysis using bright field and FITC filters to monitor uptake. As part of the microscopic analysis, the samples were transferred to glass slides without the use of fixating agents. Under the microscope, the samples incubated with DMSO did not show autofluorescence, and only minor levels of fluorescence were detected in the bacteria after incubation with BODIPY **30**. The bacteria incubated with the pantothenic acid derivatives did not show fluorescence, except for ketal analogue **42**. On the other hand, the CJ-15,801 analogues provided interesting findings, especially in the case of the *trans*-ketals (*R*)-**121** and (S)-**122**, which displayed high fluorescence around the cell envelope, but no emission from the cytosol, thereby clearly outlining the shape of the bacteria. Chemically, these compounds are enantiomers to each other sharing the *trans*-enamide geometric arrangement which might have played a role in preventing transport across the cell wall. However, it must be pointed out that at this point it was not possible to determine whether in any cleavage of the CJ-BODIPY complex had taken place.

Interestingly, when *M. smegmatis* was incubated with *cis*-derivatives (*S*)-**124** and (*S*)-**128,** both compounds exhibited fluorescence in the cytosol. In the case of compound (*S*)-**124**, fluorescent signals were focalized on the poles of the cell (dots); which might indicate preferred colocalization to certain lipids or proteins in the cell envelope (Figure 58).

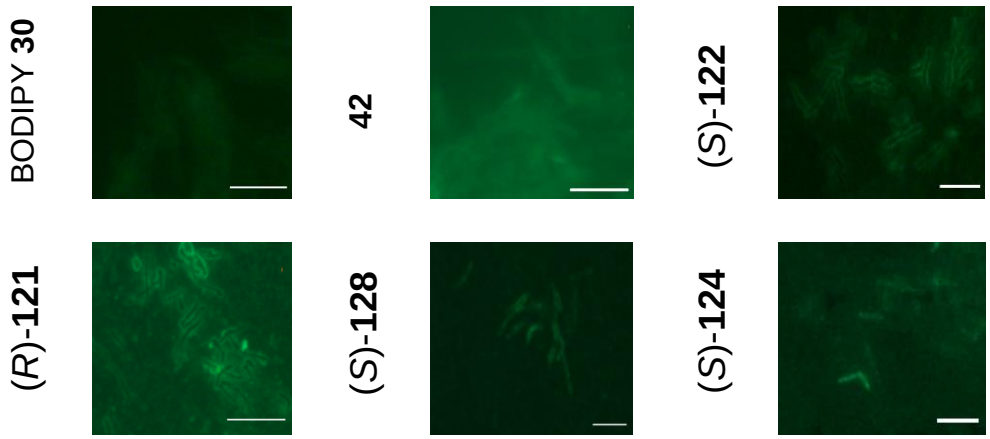

Figure 58. Uptake test of BODIPY-pantothenic acid derivatives and CJ-15,801 derivatives in *M.smegmatis*.

Photos were taken through FITC filter, from experiments performed at 50 µM and 37 °C for 48 h. incubation, size bar: 10 µm. Results from a single experiment done in triplicate.

Following from the microscopic studies, it was decided to measure the fluorescence intensities by a different quantitative method. This allow us to link the microscope readings with a second set of data, and reliability identity of compounds to be used as potential carriers. Thus, a new incubation experiment was performed at 250 µM ligand concentration, and readings were taken using a microreader.

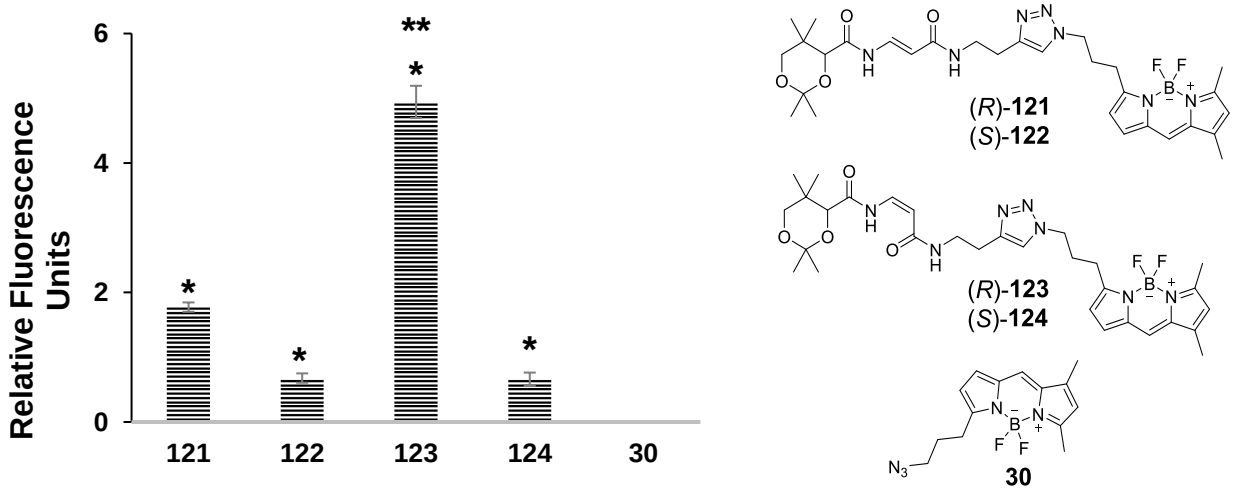

Figure 59. Uptake evaluation of BODIPY- CJ-15,801 derivatives **121-124** and BODIPY **30** in *M. smegmatis*

Bar chart represents RFU's from the experiment performed at 37 °C for 24 h incubation and 250 µM ligand concentrations. (Units x10^3). The asterisks indicate significant differences (∗P< 0.05) between the sample and BODIPY **30** control, and (∗∗P< 0.05) between the sample (*R*)-**121** and sample **123**, differences determined via an independent Student's t-test. The figure represents a single experiment done in triplicate.

Gratifyingly, the fluorescence readings obtained in this experiment correlated extremely well with the microscopy results, as the bacteria incubated with either DMSO, unbound BODIPY or the pantothenic acid analogues emitted low or no detectable fluorescence. Excitingly, the *trans*-isomers (*R*)-**121** and (*S*)-**122** exhibited clearly detectable fluorescence, with the (*R*)-derivative **121** showing a two fold higher fluorescence reading (RFU 1.9 ±0.1) compared to the (*S*)-derivative **122** (RFU 0.8 ±0.2). In the case of the *cis*-isomers, the (*S*)-enantiomer **124** also showed fluorescence readings (RFU 0.8 ±0.2) as expected from the microscopy results. The *cis*-(*R*)-enantiomer **123** on the other hand, displayed readings seven-fold larger than(*S*)-**122** (RFU 5.0 ±0.2) (Figure 59).

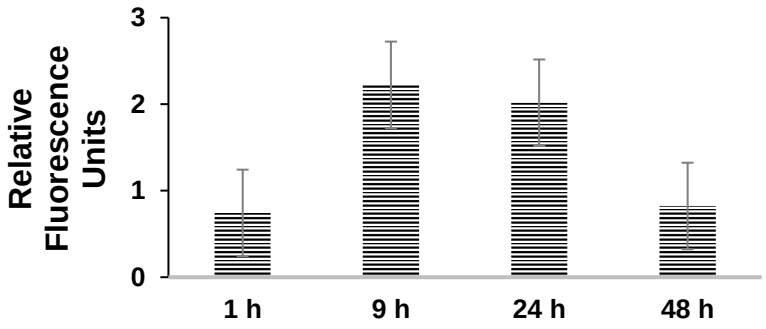

Figure 60. Time-course uptake evaluation of CJ-15,801 derivative (*R*)-**121** in *M. smegmatis.* Bar chart represents RFU's from experiment performed at 10 µM, 37 °C and 48 h incubation. (Units $x10^2$). The figure represents a single experiment done in triplicate.

After the confirmation of differential uptake by the bacilli, we decided to measure uptake after different incubation times using the (*R*)-*trans* derivative **121**. The ligand concentration was reduced to improve the conditions for the cell reproduction. Thus, *M. smegmatis* cultures were incubated at 37 °C with 10 µM concentrations of ligand and readings were taken after 1, 9, 24 and 48 h incubation, all done in triplicate.

Excitingly, significant uptake was detected after 1 h, and the maximum values were reached between 9 and 24 h. This bell shaped curve could be explained by a fast uptake, followed by saturation and then quenching or degradation of the BODIPY core (Figure 60).

To see whether the compounds would show similar characteristics in *M. tuberculosis* as in *M. smegmatis*, a set of compounds was sent to the Tuberculosis Research Laboratory (University of Queensland). The model used for evaluation, strain H37Rv, has been studied extensively in biomedical purposes due to its relatively simple manipulation, and its virulence in animal models, and susceptibility to drugs.[90]

Uptake experiments were performed by incubating the bacteria with 50 µg/mL of each derivative at room temperature for 45 min. The results revealed a similar pattern as found in *M. smegmatis*; with compounds (*R*)-**123** and (*R*)-**121** providing the highest fluorescence signals. Compound (*R*)-**123** exhibited around 2.5 times larger intensity compared to (*R*)-**121**. In *M. smegmatis* this difference in

signal was 2.7x. Interestingly, the shape of bacteria is clear in the case of compound (*R*)-**123**, and fluorescence was localised at the poles (Figure 61).

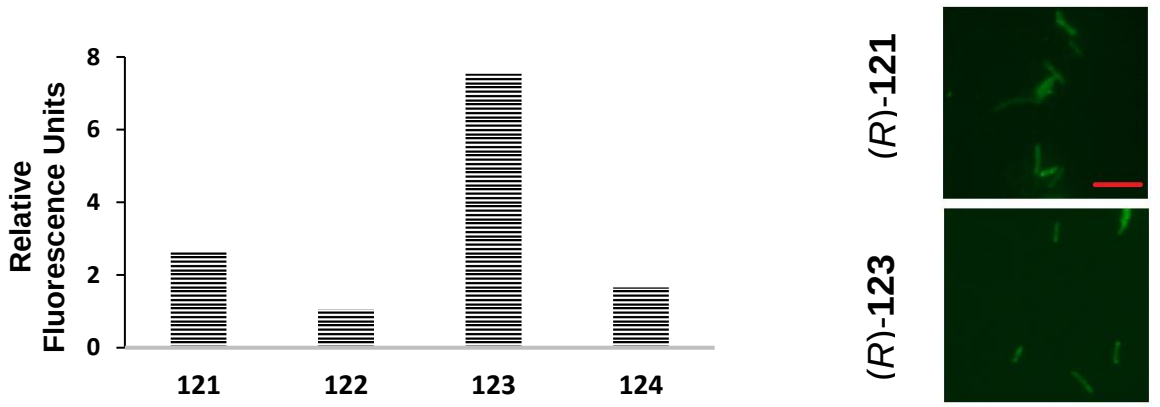

Figure 61. Uptake test of BODIPY-CJ-15,801 derivatives **121**-**124** in *M. tuberculosis.* Bar chart represents RFU's from experiment performed at 50 µg/mL and rt for 45 min incubation in *M. tuberculosis* strain H37Rv. (Units x10^4). Photos were taken through FITC filter, size bar: 10 µm. The figure represents a single experiment done in a single sample.

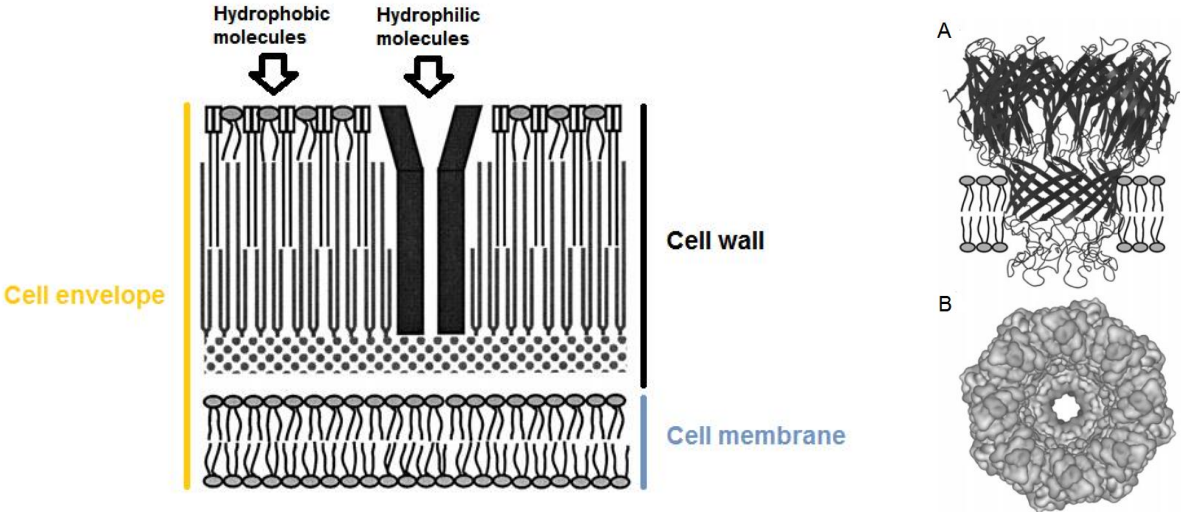

Figure 62. The cell envelope and MspA porin.
A) Side view of MspA integrated into a lipid bilayer B) Electrostatic potential of MspA in top view.[91]

Mycobacteria possess a cell envelope which offers protection against hostile conditions, and allows permeation of limited compounds into the cell. The wall consists of mycolic acids from the outer leaflet linked to an arabinogalactan-peptidoglycan complex in the inner leaflet[92] (Figure 62). This composition makes the bacterium less-permeable and susceptible to drugs compared to other bacteria. Even though lipophilic drugs would be predicted to cross this barrier easily, the unusual low fluidity and thickness of the wall hampers this *in-vivo*.[93] However, work by Niederweis showed

that drugs such as isoniazid, ethambutol, and ampicillin, were able to penetrate the cell wall when the number of porins was increased by gene insertion of the *M. smegmatis MspA* gene into *M. tuberculosis* and *M. bovis* BCG (Figure 63).[94] Draper reported the isolation of the porin-like protein, OmpA which is involved in the transport of hydrophilic molecules into *M. tuberculosis.* Draper was able to calculate that the porin channel had an exclusion limit to molecules around 600-800 Da.[92, 95]

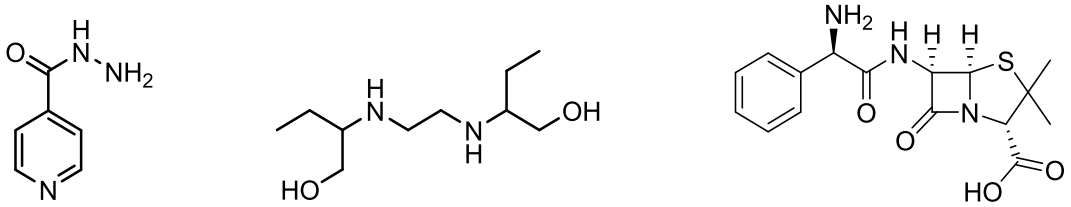

Figure 63. Isoniazid, ethambutol and ampicillin.

We propose that the BODIPY derivatives tested in *M. smegmatis* undertake two possible processes. The first one would be "the hydrophobic like pathway",[94] in which the ligands diffuse into the cell envelope, where they get trapped in the cell wall or cell membrane (Figure 64).

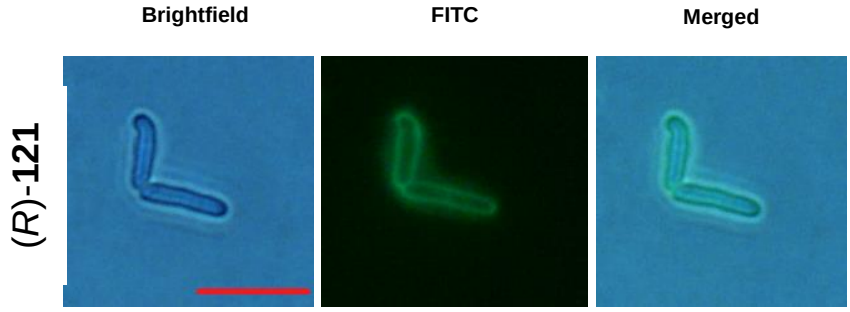

Figure 64. Uptake test of BODIPY-CJ-15,801 derivative (*R*)-**121** in *M. smegmatis*.
Photos were taken from experiments performed at 100 μM and 37 °C for 24 h. incubation, size bar: 10 μm. Results from a single experiment done in triplicate.

The second process, would be a facilitated uptake, in which the ligand interacts with a porin (or other transporter), and is transported through the cell wall, and across the cell membrane to end up in the cytosol.

Interestingly, the fluorophore also accumulates in patches in the cell wall, which might be caused by clogging or inhibiting the pores in their specific locations. Other possibility, it could be the accumulation of the BODIPY core after degradation of the compound by the enzymatic machinery in the cytosol (Figure 65).

Assuming the porin mediated transport, the lack of uptake of the hydrophilic CJ-15,801 derivatives could be explained by the low affinity of diol groups with the highly negative charge in the constriction zone of the transporter.[91]

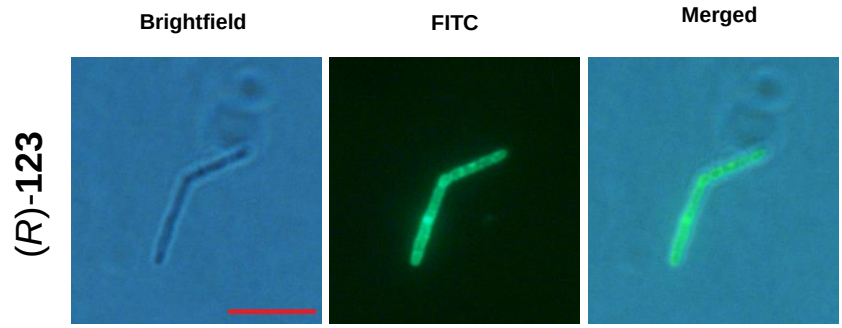

Figure 65. Uptake test of BODIPY-CJ-15,801 derivative (*R*)-**123** in *M. smegmatis*. Photos were taken from experiments performed at 100 μM and 37 °C for 24 h. incubation, size bar: 10 μm. Results from a single experiment done in triplicate.

Summarizing, the difference in fluorescence intensities and localization of the fluorescent signals initially observed by microscopy analysis, revealed a selective uptake process in which (*R*)-**123** is transported into the mycobacterial cytosol. Thus, CJ-15,801 analogue **54** might be useful as a carrier for drugs or biomolecules which are not able to cross the mycobacterial cell wall. Moreover, it might be interesting to investigate possible colocalization of the ligand with different porins in order to understand the apparent facilitated transport of this compound.

3.3.2 Evaluation of CJ-15,801 and pantothenic acid analogues coupled to BODIPY FL in THP-1 cells.

Having identified several promising derivatives that showed uptake in two mycobacterial species, our next goal was to investigate whether this finding could potentially have medical implications. Thus, we decided to evaluate the uptake of the CJ-derived compounds into *M. smegmatis* that had been taken up by THP-1 cells differentiated into macrophage-like cells. If the compounds were able to cross both the cell membrane of the THP-1 cells and subsequently that of the bacteria, this could provide an interesting approach for the delivery of drugs into latent tuberculosis cases.

THP-1 cells are widely used as a model system to understand the function and regulation of macrophages and monocytes.[96] THP-1 cells are fast-growing, and have low variability. They can also be transfected efficiently, and can be stored indefinitely in liquid nitrogen without obvious effects on the cellular features.[97] Importantly in 1999, Doxsee and Stokes[98] reported that *M.tb* infected THP-1 was a good model for evaluation of isoniazid, and was comparable to human monocyte-derived macrophages (MDM).[99] Thus, THP-1 cells are a robust and convenient approach to evaluate antimycobacterial activity when infected with pathogenic and non-pathogenic bacteria.

In order to investigate if CJ-15,801 derivatives are able to cross THP-1 cell membranes, a new experiment was designed in collaboration with the Tefsen group, using THP-1 cells differentiated with PMA (phorbol 12-myristate 13-acetate), as an activator. Only the compounds which had shown

promising results in the mycobacterial studies were included: compounds (*R*)-**123**, (*R*)-**121** and (*S*)-**126,** as negative control.

Practically, activated THP-1 cells were treated with the CJ-BODIPY derivatives at 200 µM, and then incubated for 24 h at 37 °C. The samples were washed, and transferred to a microplate to measure fluorescence intensities. Samples incubated with compound (*S*)-**126** showed low intensities in all the cases. However, compounds (*R*)-**123** and (*R*)-**121** clearly were able to enter into the THP-1 macrophage-like cells (Figure 66).

Interesting fluorescence microscopic results were found which could be correlated with microplate readings. Cells incubated with compounds (*R*)-**123** and (*R*)-**121**, appeared as a translucent cells, revealing the green fluorescence in the cytosol, whilst the nucleus and lipids dots were non-fluorescent. In contrast, in samples incubated with (*S*)-**126**, the THP-1 cell displayed an opaque fluorescent membrane; thus, it seems that this derivative interacts with the cell membrane and gets trapped on the surface, resulting in low fluorescence readings (Figure 66).

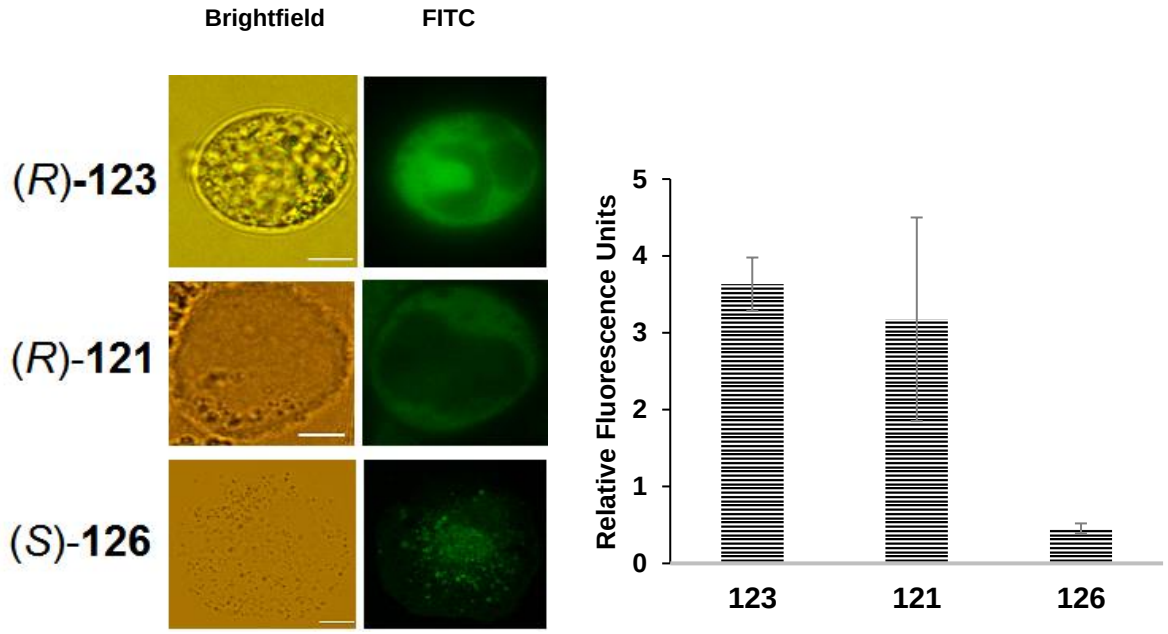

Figure 66. Uptake evaluation of BODIPY-CJ-15,801 derivatives in THP-1 cells.
Bar chart represents RFU's from experiments performed at 200 µM and 37 °C for 24 h incubation. (Units x10^3). Photos size bar: 10 µm. The figure represents a single experiment done in triplicate.

After the promising results using activated THP-1 cells, we decided to evaluate the uptake in activated THP-1 cells infecting with different multiplicity of infection (MOI). Thus, the BODIPY derivatives were added to the THP-1 cells after 3 h infection with *M. smegmatis* wild type mc^2155 at MOI5 and MOI10. The samples were then incubated at 37 °C for 24 h and 200 µM ligand concentration. The cells incubated with compound (*S*)-**126** again exhibited low intensities at both MOI's, and a fluorescence increment of just ~18% compared to non-infected cells. Again, it is

possible that this derivative interacts with a limited number of transporters and sticks to the THP-1 cell membrane. On the other hand, compounds (*R*)-**123** and (*R*)-**121** were able to access the non-infected as well as infected THP-1 cells. Significantly, MOI5 infected cells had fluorescence readings 30% larger than the non-infected. For infected cells treated with (*R*)-**121**, when the MOI increased, the intensities were higher (Figure 67).

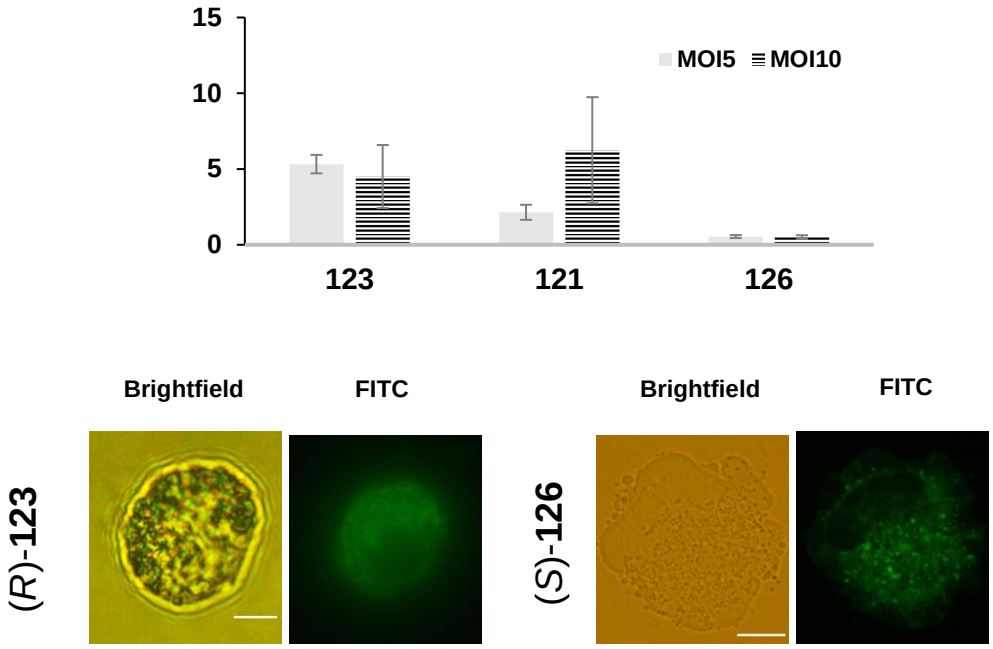

Figure 67. Uptake evaluation of BODIPY-CJ-15,801 derivatives in THP-1 cells infected with *M. smegmatis*.

Bar chart represents RFU's from experiments performed at 200 µM, 37 °C and 24 h incubation and MOI5 and MOI10 *M. smegmatis* infection (multiplicity of infection, MOI). (Units x10^3). Photos were taken from experiments at MOI5 for (*R*)-**123** and MOI 10 for (*S*)-**126**, size bar: 10 µm. The figure represents a single experiment done in triplicate.

Significantly, incubation with both ligands (*R*)-**123** and (*R*)-**121** resulted in fluorescence being located in the bacterial area. Unfortunately, magnification could not be increased in the conventional fluorescence microscope in order to expose the shape of bacillus; however, we could infer that after accumulation in the THP-1 cytosol, both compounds travelled through the guest, and accumulate in/on bacteria. Many activated THP-1 cells exhibited the characteristic mobility of pseudopodia, showing that the ligands are non-toxic. On the other hand, samples incubated with (*S*)-**126** showed the similar pattern observed in non-infected THP-1 cells (Figure 66), in which the cell displayed an opaque fluorescent membrane. Thus, it was no possible to look inside the (*S*)-**126** treated THP-1 cells (both infected and non-infected) (Figure 67).

After having established that (*R*)-**123** and (*R*)-**121** were able to reach the bacteria that were inside the THP-1 macrophage-like cells, we decided to evaluate the uptake of compound (*R*)-**123** at 20 and 200 µM with MOI5 at different time points and using uninfected THP-1 cells as controls. Results at

200 μM revealed a similar pattern for both infected and uninfected cells; i.e. during the first hours the maximum was reached rapidly, and the fluorescence began to be quenched after 4 h. However, when the concentration was reduced by an order of magnitude to 20 μM, the uptake was increased over the time for both infected and uninfected cells (Figure 68).

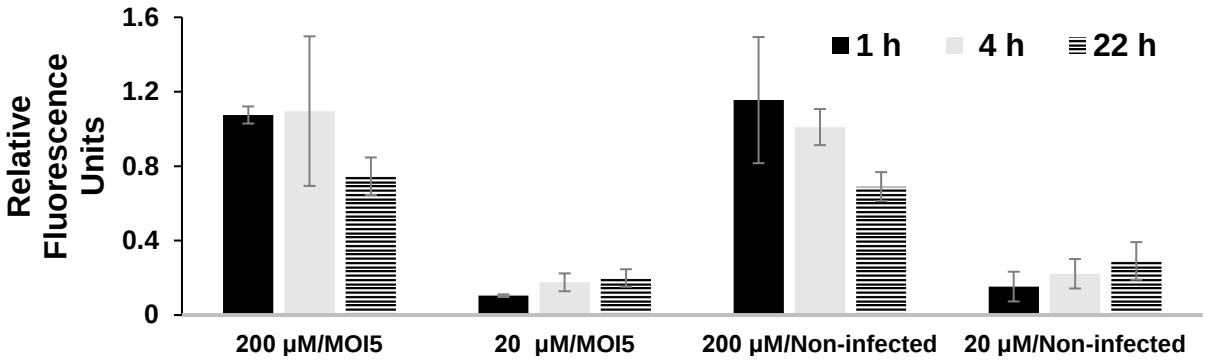

Figure 68. Time-course uptake evaluation of CJ-15,801 derivative (*R*)-**123** in THP-1 cells. Bar chart represents RFU's from experiments performed at 200 and 20 μM and 37 °C after 22 h incubation. MOI5 and MOI10 *M. smegmatis* infection (multiplicity of infection, MOI). (Units $x10^3$). The figure represents a single experiment done in triplicate.

In order to obtain more accurate measurements, the uptake was monitored using Flow Cytometry using a 200 μM concentration of ligands (*R*)-**123** and (*S*)-**126** after 21 h incubation. Samples incubated with compound (*R*)-**123** were consistent with the microplate results, in which uninfected cells exhibited higher fluorescence compared to the infected macrophages. We believe that could be due to the bacilli quenching the fluorophore of derivatives after they get delivered (Figure 69). Results from cells incubated with compound (*S*)-**126** are also important; in previous experiments we notice very similar intensities between uninfected and infected macrophages, with no difference if MOI was increased, and FACS results correlated perfectly (Figure 69).

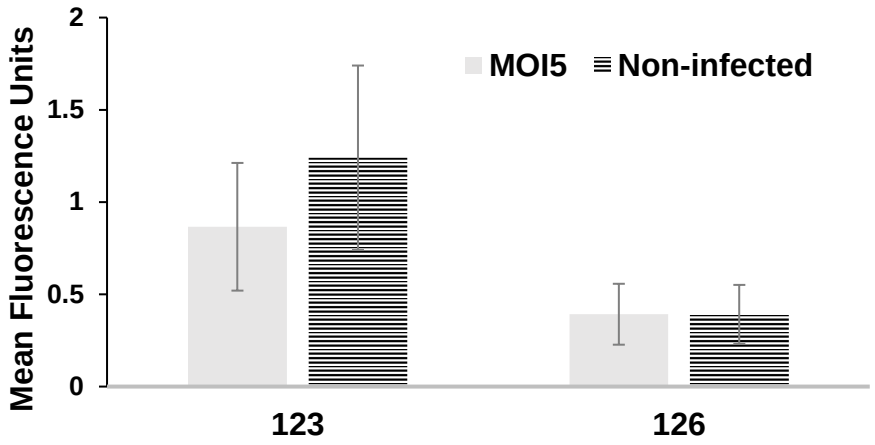

Figure 69. Uptake evaluation of BODIPY-CJ-15,801 derivatives (*R*)-**123** and (*S*)-**126** in THP-1 cells.

Bar chart represents mean fluorescence intensities from experiments performed at 200 µM and 37 °C after 21 h incubation, and MOI5 *M. smegmatis* infection; sorted by FACS. (Units x 10^3). The figure represents a single experiment done in triplicate.

In conclusion, evidence shows that CJ-15,801 analogues **28** and **54** are able to cross the THP-1 macrophage cell membrane, and reach the bacteria (Figure 70). Compound **54** is the able to cross the mycobacterial cell envelope, and accumulates in the cytosol. However, the exact localization of both compounds in the bacteria taken up by the THP-1 macrophage-like cells could not be established, although it is tempting to presume that they would follow the same pattern as shown in the bacteria-only uptake experiments. For derivative **28**, it is still not clear whether the ligand reaches the cytosol both in free bacteria and within marcophages, but clearly did not affect the bacteria growth.

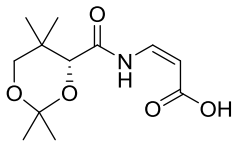

54

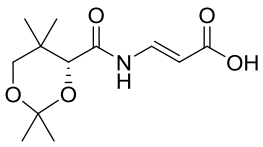

28

Figure 70. Promising CJ-15,801 analogues **28** and **54** as drug carriers in *Mycobacterium* research.

4. Conclusions and future work.

4.1 Conclusions.

The syntheses of new pantothenate and CJ-15,801 derivatives coupled to the fluorescent protein mutant phiLOV **90**-**104** was successfully completed. The synthesis of derivatives **90**-**104** proved to be reproducible and affordable, starting from commercially available materials. These new compounds were evaluated for uptake in *C. elegans* and *B. bovis*, and based on the quantitative and microscopy analysis, the organisms revealed a selective uptake mechanism. Thus, our delivery system can be used safely to carry complex biomolecules in aplicomplexan *B. bovis,* as well as *C. elegans* worm.

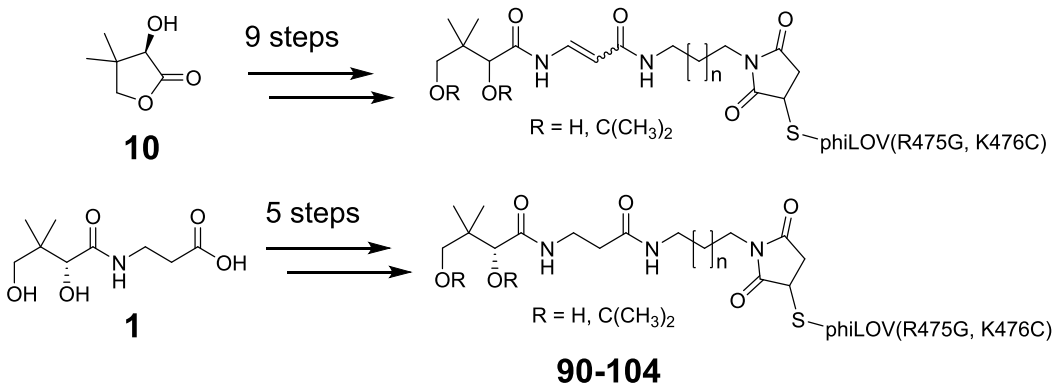

Figure 71. Synthesis of CJ-15,801 and pantothenic acid derivatives coupled to mutated phiLOV protein.

New pantothenate derivatives coupled to BODIPY FL **42** and **43** were also synthesized successfully, from pantothenic acid **1** in 4 steps and 12% yield. These new compounds, and derivatives BODIPY-CJ-15,801 **121**-**128** were evaluated for uptake in *C. elegans*, *B. bovis*, *L. passim*, *M. smegmatis* and *M. tuberculosis*. Different pantothenate and CJ-15,801 analogues displayed selective uptake in different organisms, in the process giving us an understanding of the structural features required for uptake.

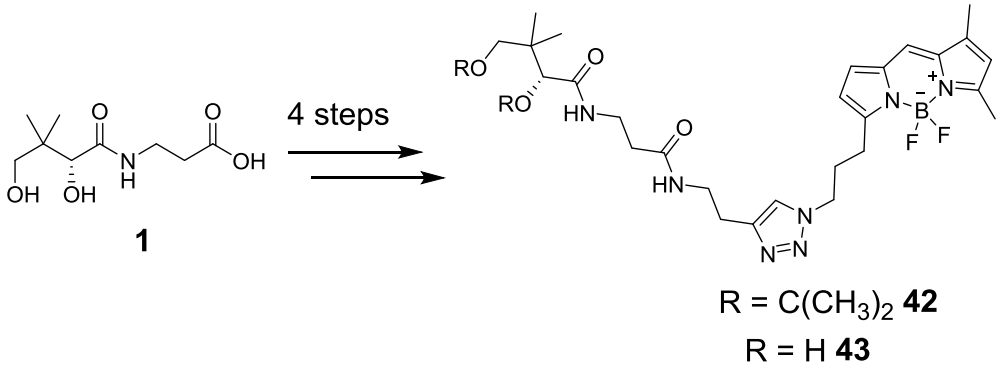

Figure 72. Synthesis of pantothenic acid derivatives coupled to BODIPY FL.

In order to connect the CJ-15,801 and pantothenate analogues to potential drugs, the synthesis of a new *bis*-functionalised BODIPY **113** was also completed. Starting from commercially available pyrrole **28**, this fluorophore can be connected through 'click' reaction and an amide/ester bond. The carrier and the desired drug could react under mild conditions.

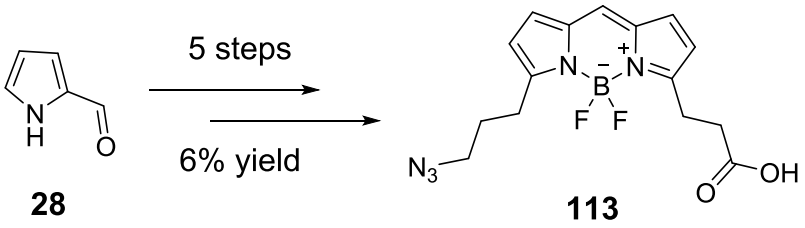

Figure 73. Synthesis of *bis*-functional BODIPY **113**.

Finally, BODIPY-ivermectin B1a derivative **117** and *cis*-CJ analogue-ivermectin B1a **109** were synthetized, and tested in *C. elegans*. Both derivatives **117** and **109** retain the characteristic paralysis effect of ivermectin B1a. Also, successful uptake was observed with derived praziquantel probe **129** in *C. elegans*.

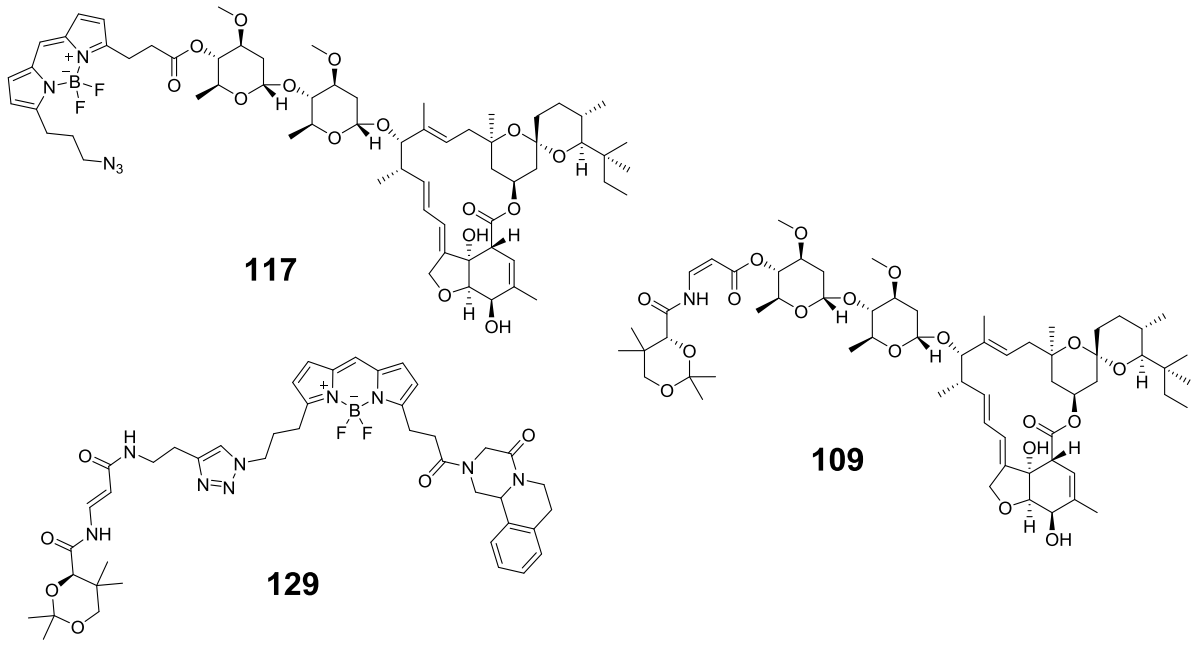

Figure 74. Ivermectin B1a derivatives **109** and **107**, and derived praziquantel complex **129**.

In summary, a new drug delivery system has been developed, using CJ-15,801 and pantothenate analogues as carriers, which is able to carry safely small and complex molecules, in unicellular or multicellular organisms.

4.2 Future work.

Having established that CJ-15,801 analogue **28** is a realiable carrier to deliver ligands into *C. elegans,* more work is needed to determine the selectivity of the uptake, and to generate derivatives coupled to ivermectin B1a **105** and moxidectin **106** for future testing.

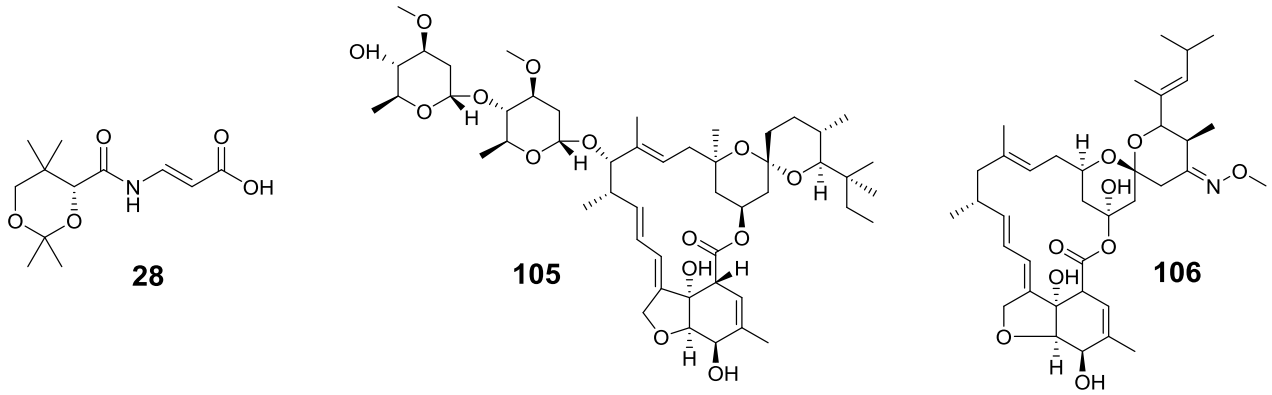

Figure 75. CJ-15,801 analogue **54**, ivermectin B1a **105** and moxidectin **106**.

As part of our future work, CJ-15,801 analogues **54** and **130** will be used in experiments to deliver drugs in bees and their parasites. The *bis*-functionalised BODIPY **113** could also be used to connect the CJ-carrier and the drug, providing a method to track the uptake under the microscope, and to measure the fluorescence by FACS.

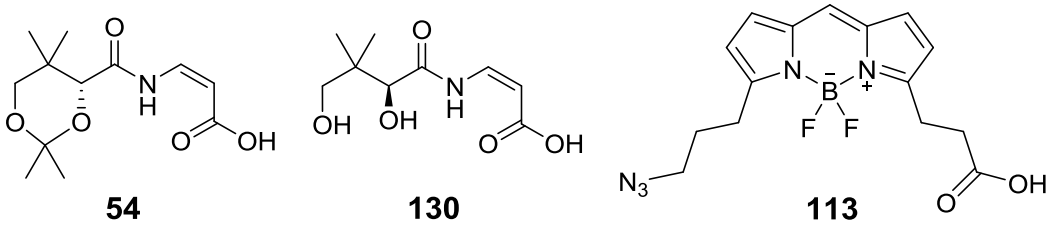

Figure 76. CJ-15,801 analogues **54** and **130**, *bis*-functionalised BODIPY **113**.

For further experiments, it will be interesting to evaluate the phiLOV derivatives **90**-**104** in *Plasmodium*, in order to investigate the ability to cross the extra barrier (PVM) when the carrier bears a complex biomolecule such as phiLOV. Future work will also focus on the ability of the CJ-15,801 analogues to deliver anti-mycobacterial drugs effectively inside infected macrophages.

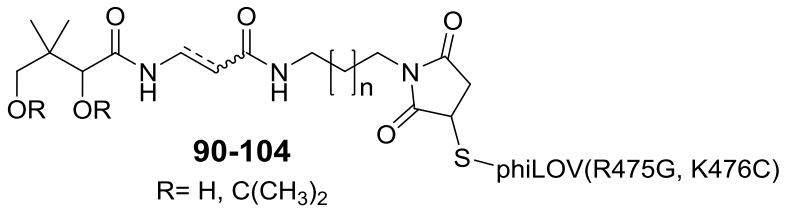

Figure 77. CJ-15,801 and pantothenic acid derivatives coupled to mutated phiLOV protein.

5. Experimental.

Biological evaluations.

C. elegans.

Short-term test (CJ-15,801 and pantothenic acid derivatives coupled to BODIPY FL, phiLOV(R475G, K476C and derived praziquantel complex 129)).

75 mM stock solutions of Bodipy derivatives were prepared with DMSO. *C. elegans* wild type Bristol N2 strain was cultured on *E. coli* strain OP50 at 20°C on NGM plates and a sterile synchronized population was obtained as described previously.[100] The worms were grown at 25°C on OP50/NGM plates, until the L4 or young adult stage, then washed off and resuspended in liquid culture medium (50 mM NaCl containing a 10x concentration of OP50 grown to stationary phase and ampicillin at 100 µg/ml), to which was added the sample (final concentration 50 µM for BODIPY derivatives and 200-305 µM for phiLOV derivatives) or a DMSO control (0.2%). Incubate at 20°C in dark. After 3 or 20 h, aliquots were removed, centrifuged to pellet the worms, washed with 50 mM NaCl, and transferred to slides with agarose 1% and sodium azide to inhibit the motility and analysed by brightfield and fluorescence microscopy.

Long-term test (BODIPY-CJ-15,801 derived analogue (*R*)-121 and BODIPY 24).

The *C. elegans* conditionally sterile strain *fer-15(b26ts)* was cultured on *E. coli* strain OP50 at 20°C on NGM plates and a sterile synchronized population was obtained as described previously.[100] The worms were grown at 25°C on OP50/NGM plates, until the L4 or young adult stage, then washed off and resuspended in liquid culture medium (50 mM NaCl containing a 10x concentration of OP50 grown to stationary phase and ampicillin at 100 µg/ml), to which was added the sample (final concentration 50 µM) or a DMSO control (0.2%) at 25°C with gentle shaking. After 3 or 20 h, aliquots were removed, centrifuged to pellet the worms, washed with 50 mM NaCl, resuspended in 50 mM NaCl, transferred to OP50/NGM plates at incubated further at 25°C before analysis, analysed directly with the COPAS Biosort or by brightfield and fluorescence microscopy.

Ivermectin B1a derivatives test.

A mixture stage of *C. elegans* wild type, worms from the sheep farm of Massey University, were washed off, cuticle was removed using a freshly prepared NaClO solution, resuspended in liquid culture medium (50 mM NaCl containing a 10x concentration of OP50 grown to stationary phase and ampicillin at 100 µg/ml), to which was added the sample or ivermectin control (final concentration 50 and 5 µM). Incubate at 20°C in dark. After 20 h, aliquots were removed, centrifuged to pellet the worms, washed with 50 mM NaCl, transferred to slides and analysed by brightfield and fluorescence microscopy.

Babesia bovis.

Short-term test in *B. bovis* (CJ-15,801 and pantothenic acid derivatives coupled to BODIPY FL and phiLOV(R475G, K476C)).

100 mM stock solutions of Bodipy derivatives were prepared with DMSO. B. bovis Texas strain was cultured in GIT medium with 10% Bovine RBC by a microaerophilic stationary-phase culture system.[101] The parasite culture was centrifuged and washed once with GIT medium. RBC's were pellet down and 20 µl infected RBC mixture (10 µl packed infected RBC+ 10 µl GIT) was prepared. Then, 180 µl GIT medium with compound (final concentration 25 µM for BODIPY derivatives and 100 µM for phiLOV derivatives) or DMSO (0.1%)/PBS control. Incubate for 45 min at 37 °C. (Samples were stained 1 µg/mL diluted Hoechst 33342 in GIT medium). After the incubation, the samples were centrifuged and pellet washed with GIT medium (3 x), and 50% haematocrit infected RBC mixture was transferred for slide to be observed by confocal laser microscopy (Nikon A1). Level of parasitemia was monitored by staining thin blood smears with Giemsa solution.

FACS experiment in *B. bovis* (CJ-15,801 and pantothenic acid derivatives coupled to phiLOV(R475G, K476C)).

B. bovis Texas strain was cultured in GIT medium with 10% Bovine RBC by a microaerophilic stationary-phase culture system.[101] The parasite culture was centrifuged and washed once with GIT medium. RBC's were pellet down and 20 µl infected RBC mixture (10 µl packed infected RBC+ 10 µl GIT) was prepared. Then, 180 µl GIT medium with compound (final concentration 150-250 µM) or DMSO (0.1%)/PBS control. Incubate for 45 min at 37 °C. (Samples were stained at 20 µM final concentration DRAQ5 in GIT medium). After the incubation, the samples were centrifuged and pellet washed with GIT medium (3 x), and transferred to FACS tubes to be analysed by BD FACS Verse.

Long-term test in *B. bovis* (CJ-15,801 and pantothenic acid derivatives coupled to phiLOV(R475G, K476C)).

B. bovis Texas strain was cultured in GIT medium with 10% Bovine RBC by a microaerophilic stationary-phase culture system.[101] The parasite culture was centrifuged and washed once with GIT medium. RBC's were pellet down and 20 µl infected RBC mixture (10 µl packed infected RBC+ 10 µl GIT) was prepared. Then, 180 µL GIT medium with compound (final concentration 100 or 5 µM for phiLOV derivatives) or DMSO (0.1%)/PBS control. Incubate for 45 min at 37 °C. After the incubation, the samples were centrifuged and pellet washed with GIT medium (3 x), 180 µL GIT were added and incubated at 37 °C. Microscope samples were stained 200× diluted Hoechst 33342 in GIT medium, 50% haematocrit infected RBC mixture was transferred for slide to be observed by confocal laser microscopy (Nikon A1) at 5 h and 48 h. At 24 h fresh GIT media was added to the samples. Level of parasitemia was monitored by staining thin blood smears with Giemsa solution.

Lotmaria passim.

Parasite uptake test (CJ-15,801 and pantothenic acid derivatives coupled to BODIPY FL).

100 mM stock solutions of Bodipy derivatives were prepared with DMSO. *L. passim* strain *PRA-403* was cultured in modified medium for *C. bombi*.[102] The parasite culture was centrifuged, supernatant was removed and 500 µL of *L. passim* medium with compound (final concentration 500, 100, 10 or 1 µM for BODIPY derivatives) or DMSO (0.1%) control were added. Incubated for 45 min at room temperature. After the incubation, the samples were centrifuged and pellet washed with PBS (3 x 500 µL), samples were transferred to slide and be observed by fluorescent microscope (NIKON ECLIPSE Ni) or added 100 µL to transfer to 96-wells microplate and fluorescence intensities were measure by Varioskan LUX or BioTek microplate reader.

Honey bee gut uptake test (CJ-15,801 and pantothenic acid derivatives coupled to BODIPY FL).

Honey bee (*A. mellifera*) hives were obtained from honey bee keepers in Jiangsu Province, China. The honey bee colonies are maintained at XJTLU campus and can feed ab libitum during April to November. During December to March, pollen mixed with 50% (v/v) sucrose is added to the honey bee hives in order to provide sufficient food. Honey bees were dissected and gastrointestinal system was removed including the crop, midgut and rectum, and added immediately to 500 µL of sample diluted with PBS at 100 µM final concentration or DMSO (0.1%) control. Incubated for 45 min at 33 °C. After the incubation, the samples were centrifuged and guts washed with PBS (3 x 500 µL), samples were transferred to slide to be observed by fluorescent microscope (NIKON ECLIPSE Ni).

Mycobacterium.

Uptake test in *M. smegmatis* (CJ-15,801 and pantothenic acid derivatives coupled to BODIPY FL).

100 mM stock solutions of BODIPY derivatives were prepared with DMSO. *M. smegmatis* wild type strain mc^2155 was cultured in Middlebrook 7H9,10% ADS and 0.05% Tween-80 medium in Falcon tube, incubated at 37 °C/200 rpm and collected in mid-logarithmic growth phase. BODIPY derivatives and DMSO (0.1%) control were diluted (concentration are described in the results) using the bacteria media before added to the 96-well microplate with bacteria culture to final volume of 100 µL. Incubated at 37 °C. After the incubation, the samples were transferred to Eppendorf tubes, centrifuged and pellet washed with PBS (3 x 100 µL), samples were transferred to 96-well microplate to evaluate the fluorescence intensities in BioTek reader. Aliquots of 5-10 µL were taken after fluorescence measurements and transferred to glass slides protected with coverslip without fixation process in order to be observed by fluorescent microscope (NIKON ECLIPSE Ni).

Uptake test in *M. tuberculosis* (CJ-15,801 and pantothenic acid derivatives coupled to BODIPY FL).

20 mg/mL stock solutions of BODIPY derivatives were prepared with DMSO. *M. tuberculosis* strain H37Rv centrifuged, media was removed and pellet resuspended with PBS/ 0.02% tyloxapol, 1 mL aliquots were transferred to Eppendorf tubes, centrifuged, supernatant was removed and pellet was resuspended with 1 mL of BODIPY derivatives (final concentration 50µg/ml) incubated at room temperature for 45 min, with agitation and protected from light. After the incubation, the samples were centrifuged and pellet washed with PBS (3 x 100 µL), samples were transferred to 96-well microplate to evaluate the fluorescence intensities in the microplate reader. 25 µL were spotted on glass slides before dried over a heat block at 90 °C for 10 min. Cells were fixed by immersing in 10% formalin for 30 min. Slides were then air dried and mounted with DAKO mounting media before being observed under fluorescence microscopy.

Uptake test in THP-1 cells (CJ-15,801 and pantothenic acid derivatives coupled to BODIPY FL).

100 mM stock solutions of BODIPY derivatives were prepared with DMSO. THP-1 cells (T25 culture Corning) were grown in RPMI 1640, 10% (v/) FCS (fetal calf serum), 100 U/mL penicillin and 0,1 mg/mL streptomycin over 96-well microplate. The cells were treated with phorbol myristate acetate (PMA; Promega) final concentration 10 ng/mL, incubated at 5% CO_2 and 37°C. Differentiate cells were infected with overnight culture of *M. smegmatis*, diluted with infection media to ensure ratio of 5 of 10 bacilli per macrophage (MOI 5) or MOI10, infecting for 3 h. BODIPY derivatives were diluted (concentration are described in the results) using the infection media before added to the microplate to final volume of 100 µL. Incubated at 5% CO_2 and 37 °C. After the incubation, infection media was removed and samples were washed with PBS (3 x 100 µL) before fluorescence measurement in the BioTek reader. 50 µL of trypsin solution was added to remove the cells and transferred to FACS tubes and sort the samples. Finally, Aliquots of 5-10 µL were taken after fluorescence measurements and transferred to glass slides protected with coverslip without fixation process in order to be observed by fluorescent microscope (NIKON ECLIPSE Ni).

Chemistry. General information

Reactions involving air sensitive reagents and anhydrous solvents were performed in oven dried glassware (130 °C) and carried out under an argon atmosphere. Dichloromethane, tetrahydrofuran and toluene were purified through a Pure Solv 400-5MD (UoG) and PS-MD-50N7 (XJTLU) solvent purification system (Innovative Technology, Inc).

All reagents were used as received, unless otherwise stated. Solvents were evaporated under reduced pressure at 40 °C using a Rotavapor. Column chromatography was performed under pressure using silica gel (Fluoro Chem or Merck Silica LC 60A) as the stationary phase and technical grade solvents as eluent.

Reactions were monitored by thin layer chromatography. TLC was performed on aluminium sheets pre-coated with silica gel (Merck or Fluorochem Silica Gel 60 F254). The plates were visualised by the quenching of UV fluorescence (λ_{max} 254 nm) and/ or by staining with a $KMnO_4$ and/or anysaldehyde solution dips.

Proton magnetic resonance spectra (^{1}H NMR) and carbon magnetic resonance spectra (^{13}C NMR) were recorded at 400 MHz and 100 MHz or at 500 MHz and 125 MHz respectively, using either a Bruker DPX Avance400 instrument (UoG), Bruker Ascend 400 (XJTLU) or a Bruker AvanceIII500 instrument (UoG). DEPT 135 and two-dimensional (COSY, HSQC) NMR spectroscopy were used in novel compounds to assist in the assignment of signals in the ^{1}H and ^{13}C NMR spectra. Structures have been given an arbitrary numbering system to enable ^{1}H and ^{13}C NMR assignment. Chemical shifts (δ) are reported in parts per million (ppm) and are referenced to the residual solvent peak. NMR signals are described by multiplicity as singlet (s), doublet (d), triplet (t), quartet (q), quintet (quin) or multiplet (m), apparent (app) and broad (br) or by a combination of these terms. Coupling constant (*J*) are quoted in Hertz to the nearest 0.1 Hz.

IR spectra were obtained employing a Golden Gate^{TM}attachment that uses a type IIa diamond as a single reflection element so that IR spectrum of the compound (solid o liquid) could be detected directly (thin layer) without any sample preparation (Shimadzu FTIR-8400S, Agilent Technologies Cary660 FTIR). Only significant absorptions are reported in wavenumbers with the following terms to describe intensity: w (weak), m (medium), s (strong) or br (broad).

High resolution mass spectra (HRMS) were recorded by the analytical group of the Chemistry Department at UoG on JEOL JMS-700 and Bruker micrOTOFQ mass spectrometers by electrospray and chemical ionisation operating at a resolution of 15000 full widths at half heights. HRMS at XJTLU were recorded on a Bruker micrOTOF-Q II mass spectrometer by electrospray ionisation operating at a resolution of 10000 full widths at half heights.

Melting points were recorded on a Stuart Scientific Melting Point SMPI apparatus, and are uncorrected.

Initator Biotage (UoG) and Discover-SPW/Activent CEM (XJTLU) were used to perform microwave assisted reactions according, with the settings described in each procedure.

MALDI analysis were obtained using either a Shimadzu Biotech AXIMA Confidence (UoG) or a Bruker Autoflex speed (XJTLU). Specific optical rotations were calculated using AutopolV Rudolph Research Analytical polarimeter.

Experimental details.

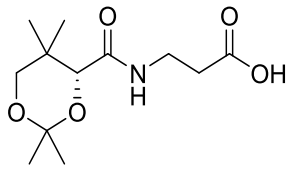

(*R*)-3-(2,2,5,5-Tetramethyl-1,3-dioxane-4-carboxamido)propanoic acid, 32.

A solution of *D*-pantothenic acid hemicalcium salt **1** (500 mg, 1.0 mmol) in acetone (25 mL) was treated with *p*-TsOH.H_2O (560 mg, 3.0 mmol) and 1.0 g of 4 Å molecular sieves. The reaction was stirred at rt until completion by TLC analysis (18 h). The suspension was then filtered through a celite bed, washed with acetone (2x15 mL) and the organic phases combined. The combined organic washes were concentrated *in vacuo* before addition of EtOAc (30 mL) to the crude residue. The resulting solution was then washed with brine (2x30 mL), dried over Na_2SO_4 and concentrated under reduced pressure. Before total reduction of solvent, a few drops of hexane were added until crystallization was induced to afford acetonide **32** as white solid (300 mg, 55%), which required no further purification. The NMR data matches the literature data for this compound.[39, 47]

^{1}H NMR ($CDCl_3$, 400 MHz) δ: 7.04 (1H, appt, N*H*), 4.12 (1H, s, C*H*), 3.71 (1H, d, *J* = 11.6 Hz, CH_2Cq), 3.66-3.47 (2H, m, NHCH_2), 3.30 (1H, d, *J* = 11.6 Hz, CH_2Cq), 2.65 (2H, t, *J* = 6.0 *Hz,* CH_2CO_2H), 1.48 (3H, s, Cq(CH_3)$_2$), 1.45 (3H, s, Cq(CH_3)$_2$), 1.06 (3H, s, Cq(CH_3)$_2$), 1.00 (3H, s, Cq(CH_3)$_2$). ^{13}C NMR ($CDCl_3$, 100 MHz) δ: 174.7 (*C*O), 170.1 (*C*O), 99.0 (*Cq*(CH_3)$_2$), 77.2 (O*C*H), 71.4 (O*C*H_2), 34.1 (CH_2*Cq*), 33.7 (HN*C*H_2), 32.9 (*C*H_2CO_2H), 29.4 (Cq(*C*H_3)$_2$), 22.0 (Cq(*C*H_3)$_2$), 18.8 (Cq(*C*H_3)$_2$), 18.7 (Cq(*C*H_3)$_2$).

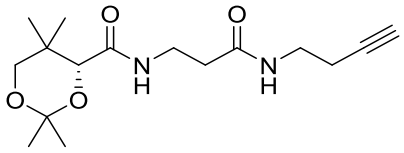

***(R)-N*-(3-(But-3-yn-1-ylamino)-3-oxopropyl)-2,2,5,5-tetramethyl-1,3-dioxane-4-carboxamide, 33.**

A solution of (*R*)-3-(2, 2, 5, 5-tetramethyl-1,3-dioxane-4-carboxamido)propanoic acid **32** (160 mg, 0.6 mmol) in CH_2Cl_2 (1.5 mL) was treated with HBTU (340 mg, 0.9 mmol), followed by 1-amino-3-butyne (70 µL, 0.9 mmol) and *N,N*-diisopropylethylamine (150 µL, 0.9 mmol). The reaction mixture was then heated to 80 °C for 3.5 h in the microwave oven. The reaction was then concentrated under reduced pressure. Purification of the crude residue by flash column chromatography (0-5% MeOH/CH_2Cl_2) gave the desired alkyne **33** as a red oil (175 mg, 90%).

^{1}H NMR ($CDCl_3$, 400 MHz) δ: 7.05 (1H, br s, N*H*), 6.24 (1H, br s, N*H*), 4.10 (1H, s, C*H*), 3.71 (1H, d, *J* = 12.0 Hz, CH_2Cq), 3.65-3.50 (2H, m, CH_2NH), 3.30 (1H, d, *J* = 12.0 Hz, CH_2Cq), 3.24-3.17 (2H, m, CH_2CO), 2.50 (2H, t, *J* = 8.0 Hz, NHCH_2), 2.42 (2H, td, *J* = 6.4 Hz, 2.4 Hz, CH_2Cq), 2.03 (1H, t, *J* = 2.4 Hz, CqC*H*),1.48 (3H, s, Cq(CH_3)$_2$), 1.46 (3H, s, Cq(CH_3)$_2$), 1.06 (3H, s, Cq(CH_3)$_2$), 0.99 (3H, s, Cq(CH_3)$_2$). ^{13}C NMR ($CDCl_3$, 100 MHz) δ: 171.4 (*C*O), 170.5 (*C*O), 99.1 (*Cq*(CH_3)$_2$), 88.1 (*Cq*CH), 77.2 (O*C*H), 71.4 (O*C*H_2), 70.2 (Cq*C*H), 38.1 (HN*C*H_2), 35.9 (*C*H_2CO), 34.8 (NH*C*H_2), 33.0 (*C*H_2Cq), 29.4 (Cq(*C*H_3)$_2$), 22.1 (Cq(*C*H_3)$_2$), 18.9 (Cq(*C*H_3)$_2$), 18.6 (Cq(*C*H_3)$_2$). HRMS (ESI) calculated for $C_{16}H_{26}N_2O_4$ [M+Na]$^+$: *m/z* 333.1785, found *m/z* 333.1765. IR υ_{max} (film)/cm^{-1}: 3293 (m), 2989 (m), 1740 (s), 1650 (m), 1536 (m), 1368 (m), 1232 (s), 1090 (s). $[\alpha]_D$ +9.500 (*c* = 0.5, $CHCl_3$, T = 23.0 °C).

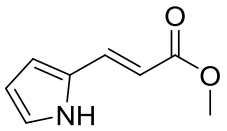

(*E*)-Methyl-3-(1*H*-pyrrol-2-yl)acrylate, 35.

A suspension of 1*H*-pyrrole-2-carboxaldehyde **34** (2.0 g, 21.0 mmol) in benzene (160 mL) was treated with methyl (triphenylphosphoranylidene)acetate (10.9 g, 32.5 mmol). The resulting mixture was heated to 80 ° C until completion by TLC analysis (18 h). The reaction mixture was cooled down to rt and concentrated *in vacuo* to give a crude orange oil. Purification of the crude residue by flash column chromatography (0-20% EtOAc/PE) gave the desired vinilogous ester **35** as a white solid (2.33 g, 73%). The NMR data matches the literature data for this compound.[45]

^{1}H NMR ($CDCl_3$, 400 MHz) δ: 8.93 (1H, br s, N*H*), 7.58 (1H, d, *J* = 16.0 Hz, CqC*H*), 6.97-6.94 (1H, m, C$H_{pyrrole}$), 6.60-6.57 (1H, m, C$H_{pyrrole}$), 6.32-6.29 (1H, m, C$H_{pyrrole}$), 6.06 (1H, d, *J* = 16.0 Hz, C*H*CO), 3.80 (3H, s, OCH_3). ^{13}C NMR ($CDCl_3$, 100 MHz) δ: 168.0 (*C*O), 134.3 (Cq*C*H), 128.3 (Ar*Cq*), 122.4 (*C*HCO), 114.5 (Ar*C*H), 111.0 (Ar*C*H), 110.8 (Ar*C*H), 51.5 (OCH_3).

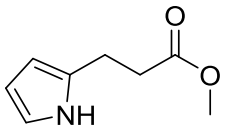

Methyl 3-(1*H*-pyrrol-2-yl)propanoate, 36.

A solution of (*E*)-methyl-3-(1*H*-pyrrol-2-yl)acrylate **35** (2.33 g, 15.4 mmol) in anhydrous MeOH (100 mL) was stirred for 5 minutes under an argon atmosphere. Pd/C (10%, 240 mg, 14 mol%) was added before replacing the argon with a hydrogen atmosphere, and stirred at rt until completion by TLC analysis (18 h). The reaction was then filtered through a celite bed, and washed with MeOH (2x25 mL). The organic phases were combined and concentrated *in vacuo* to afford the desired ester **36** as a brown oil (2.2 g, 93%), which required no further purification. The NMR data matches the literature data for this compound.[45]

^{1}H NMR ($CDCl_3$, 400 MHz) δ: 8.54 (1H, br s, N*H*), 6.71-6.69 (1H, m, ArC$H_{pyrrole}$), 6.14-6.11 (1H, m, ArC$H_{pyrrole}$), 5.96-5.93 (1H, m, ArC$H_{pyrrole}$), 3.72 (3H, s, OCH_3), 2.94 (2H, t, *J* = 8.0 Hz, Cq*C*H_2), 2.67 (2H, t, *J* = 8.0 Hz, CH_2CO). ^{13}C NMR ($CDCl_3$, 100 MHz) δ: 174.5 (*C*O), 130.9 (Ar*Cq*), 116.8 (Ar*C*H), 108.0 (Ar*C*H), 105.5 (Ar*C*H), 51.8 (O*C*H_3), 34.3 (Cq*C*H_2), 22.5 (*C*H_2CO).

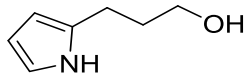

3-(1*H*-Pyrrol-2-yl)propan-1-ol, 37.

A 0 ° C solution of methyl 3-(1*H*-pyrrol-2-yl)propanoate **36** (2.1 g, 13.7 mmol) in Et_2O (110 mL) was stirred for 15 minutes before being treated slowly with $LiAlH_4$ (1.0 g, 26.3 mmol). The solution was allowed to warm up to rt until completion by TLC analysis (16 h). The reaction was quenched by the dropwise addition of 1M NaOH solution until pH neutral. The solvent was decanted off, and the lithium/aluminium salts were washed with Et_2O (2x100 mL). The combined organic washes were dried over Na_2SO_4, and concentrated *in vaccuo* to afford the expected alcohol **37** as a brown oil (1.7 g, 100%), which required no further purification. The NMR data matches the literature data for this compound.[45]

^{1}H NMR ($CDCl_3$, 400 MHz) δ: 8.16 (1H, br s, N*H*), 6.72-6.68 (1H, m, ArC$H_{pyrrole}$), 6.18-6.13 (1H, m, ArC$H_{pyrrole}$), 5.98-5.94 (1H, m, ArC$H_{pyrrole}$), 3.74 (2H, t, *J* = 6.0 Hz, CH_2OH), 2.76 (2H, t, *J* = 8.0 Hz, CqCH_2), 2.00-1.80 (2H, m, $CH_2CH_2CH_2$). ^{13}C NMR ($CDCl_3$, 100 MHz) δ: 130.9 (Ar*Cq*), 116.4 (Ar*C*H), 108.4 (Ar*C*H), 105.3 (Ar*C*H), 63.7 (*C*H_2OH), 28.9 (Cq*C*H_2), 24.0 ($CH_2CH_2CH_2$).

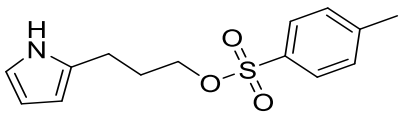

3-(1*H*-Pyrrol-2-yl)propyl 4-methylbenzenesulfonate, 38.

A 0 °C solution of 3-(1*H*-pyrrol-2-yl)propan-1-ol **37** (1.2 g, 10.0 mol) and *p*-TsCl (2.9 g, 15.0 mol) in CH_2Cl_2 (75 mL) was treated with triethylamine (2.8 mL, 20.0 mol). The resultant mixture was then stirred at rt until completion by TLC analysis (2 h). The reaction was then washed with 1M HCl (3x75 mL), $NaHCO_3$ saturated solution (2x75 mL) and brine (75 mL). The organic phase was dried over Na_2SO_4, and concentrated *in vacuo* to afford the expected product **38** as a brown oil (1.66 g, 60%). The crude product was used without further purification.

^{1}H NMR ($CDCl_3$, 400 MHz) δ: 8.05 (1H, br s, N*H*), 7.81 (2H, d, *J* = 8.0 Hz, ArC$H_{benzene}$), 7.37 (2H, d, *J* = 7.6 Hz, ArC$H_{benzene}$), 6.69-6.65 (1H, m, ArC$H_{pyrrole}$), 6.14-6.10 (1H, m, ArC$H_{pyrrole}$), 5.88-5.84 (1H, m, ArC$H_{pyrrole}$), 4.08 (2H, t, *J* = 6.0 Hz, CH_2O), 2.71 (2H, t, *J* = 7.0 Hz, CqCH_2), 2.48 (3H, s, CH_3), 2.01-1.92 (2H, m, CH_2). ^{13}C NMR ($CDCl_3$, 100 MHz) δ: 144.8 (Ar*Cq*), 133.0 (Ar*Cq*), 130.3 (Ar*Cq*), 129.9 (2 x Ar*C*H), 127.9 (2 x Ar*C*H), 116.6 (Ar*C*H), 108.4 (Ar*C*H), 105.5 (Ar*C*H), 69.5 (*C*H_2O), 29.3 (Cq*C*H_2), 23.3 ($CH_2CH_2CH_2$), 21.6 (Cq*C*H_3). HRMS (ESI) calculated for $C_{14}H_{17}NO_3S$

$[M+(CH_3CN+NH_4)^+]^+$: *m/z* 338.1532, found *m/z* 338.3412. IR υ_{max} (film)/cm^{-1}: 3362 (br), 2920 (m), 2848 (m), 1645 (s), 1469 (m), 1025 (s).

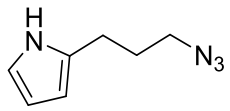

2-(3-Azidopropyl)-1*H*-pyrrole, 39.

A solution of 3-(1*H*-pyrrol-2-yl)propyl 4-methylbenzenesulfonate **38** (1.0 g, 3.6 mmol) in DMF (30 mL) was treated with NaN_3 (980 mg, 15.0 mmol), and the resultant mixture was heated to 70 °C until completion by TLC analysis (16 h). The reaction was then cooled down to rt, and diluted with EtOAc (60 mL) followed by H_2O (30 mL). The phases were separated, and the aqueos layer was extracted with EtOAc (2x60 mL). The combined organic layers were washed with brine (5x100 mL), dried over Na_2SO_4 and concentrated under reduced pressure. The crude residue was purified by flash column chromatography (0-20% EtOAc/PE) to afford the desired azide **39** as a yellow oil (370 mg, 68%). The NMR data matches the literature data for this compound.[45]

^{1}H NMR ($CDCl_3$, 400 MHz) δ: 7.98 (1H, br s, N*H*), 6.73-6.69 (1H, m, ArC$H_{pyrrole}$), 6.19-6.14 (1H, m, ArC$H_{pyrrole}$), 5.98-5.94 (1H, m, ArC$H_{pyrrole}$), 3.35 (2H, t, *J* = 6.8 Hz, CH_2N_3), 2.74 (2H, t, *J* = 7.6 Hz, CqCH_2), 1.98-1.89 (2H, m, $CH_2CH_2CH_2$). ^{13}C NMR ($CDCl_3$, 100 MHz) δ: 130.2 (Ar*C*q), 127.5 (Ar*C*H), 108.5 (Ar*C*H), 105.5 (Ar*C*H), 50.6 (*C*H_2N_3), 28.8 (Cq*C*H_2), 24.6 ($CH_2CH_2CH_2$).

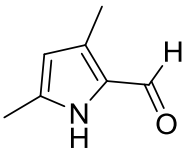

3,5-Dimethyl-1*H*-pyrrole-2-carbaldehyde, 41.

Anhydrous DMF (20 mL) was cooled down to 0 °C and treated with $POCl_3$ (1.0 mL, 11.0 mmol). The solution was stirred at 0 °C for 5 min., and then at rt for 30 min. The reaction mixture was cooled back down to 0 °C, and treated with 2,4-dimethyl-1*H*-pyrrole **40** (1.0 mL, 10.0 mmol). The reaction was then heated to 40 °C until completion by TLC analysis (18 h). The mixture was cooled down to rt, and diluted with EtOAc (40 mL) followed by H_2O (20 mL). The phases were separated, and the aqueos layer was extracted with EtOAc (2x40 mL). The combined organic layers were washed with H_2O (5x100 mL), brine (2x100 mL) and dried over Na_2SO_4. The resulting solution was concentrated under reduced pressure, and the crude residue was purified by flash column chromatography (0-50% Et_2O/PE) to afford the desired aldehyde **41** as a white solid (540 mg, 45%). The NMR data matches the literature data for this compound.[41]

^{1}H NMR ($CDCl_3$, 400 MHz) δ: 9.93 (1H, br, N*H*), 9.49 (1H, s, C*H*O), 5.88 (1H, s, ArC$H_{pyrrole}$), 2.36 (3H, s, CH_3), 2.33 (3H, s, CH_3). ^{13}C NMR ($CDCl_3$, 100 MHz) δ: 175.8 (*C*O), 138.3 (Ar*Cq*), 134.6 (Ar*Cq*), 128.7 (Ar*Cq*), 112.0 (Ar*C*H), 13.1 (*C*H_3Cq), 10.5 (Cq*C*H_3).

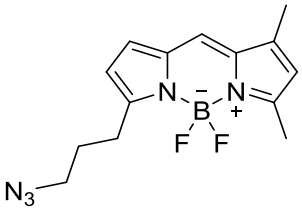

3-Azido [4,4-difluoro-5,7-dimethyl-4-bora-3a,4a-diaza-*s*-indacene-3-yl]propane, 30.

A 0 °C solution of 2-(3-azidopropyl)-*1H*-pyrrole **39** (270 mg, 1.8 mmol) in CH_2Cl_2 (10 mL), was treated with a solution of 3,5-dimethyl-1*H*-pyrrole-2-carbaldehyde **41** (203 mg, 1.6 mmol) in CH_2Cl_2 (2 mL). The solution was then treated with the dropwise addition of $POCl_3$ (100 µL, 1.0 mmol), and the mixture was stirred at rt for 6.5 h before being cooled back down to 0 °C. The reaction mixture was then treated sequentially with $BF_3.Et_2O$ (0.5 mL, 4.0 mmol) followed by *N,N*-diisopropylethylamine (0.7 mL, 4.0 mmol). The resulting reaction mixture was stirred at rt until completion by TLC analysis (18 h). The reaction was then quenched with H_2O (15 mL), diluted with CH_2Cl_2 (5 mL) and filtered through a bed of celite. The celite was washed thoroughly with CH_2Cl_2 (2x10 mL), and the organic phases combined. The combined organic washes were dried over Na_2SO_4, and concentrated *in vacuo* to give the crude residue as a red oil. Purification of the crude residue by flash column chromatography (0-20% EtOAc/PE) yielded the expected azide **30** as a red oil (290 mg, 59%). The NMR data matches the literature data for this compound.[45]

^{1}H NMR ($CDCl_3$, 400 MHz) δ: 7.11 (1H, s, ArC$H_{BODIPY\text{-}C8}$), 6.94 (1H, d, *J* = 4.0 *Hz*, ArC$H_{BODIPY\text{-}C1}$), 6.31 (1H, d, *J* = 4.0 *Hz*, ArC$H_{BODIPY\text{-}C2}$), 6.14 (1H, s, ArC$H_{BODIPY\text{-}C6}$), 3.41 (2H, t, *J* = 8.0 *Hz* CH_2N_3), 3.07 (2H, t, *J* = 8.0 Hz C_qCH_2), 2.59 (3H, s, CH_3), 2.28 (3H, s, CH_3), 2.06 (2H, m, C$H_2CH_2N_3$).

^{13}C NMR ($CDCl_3$, 100 MHz) δ: 160.5 (Ar*Cq*), 156.5 (Ar*C*q), 146.7 (Ar*C*q), 143.7 (Ar*C*q), 134.1 (Ar*C*q), 128.3 (Ar*C*H), 123.8 (Ar*C*H), 120.2 (Ar*C*H), 116.6 (Ar*C*H), 50.9 (*C*H_2N_3), 28.2 ($CH_2CH_2CH_2$), 25.8 (Cq*C*H_2), 14.9 (*C*H_3Cq), 11.4 (*C*H_3Cq).

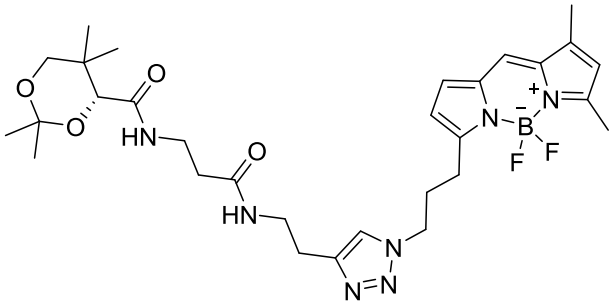

(*R*)-*N*-((((3-[4,4-Difluoro-5,7-dimethyl-4-bora-3a,4a-diaza-*s*-indacene-3-yl]propyl)-1*H*-1,2,3-triazol-4-yl)ethylamino)-3-oxopropyl)-2,2,5,5-tetramethyl-1,3-dioxane-4-carboxamide, 42.

A solution of 3-azido [4,4-difluoro-5,7-dimethyl-4-bora-3a,4a-diaza-*s*-indacene-3-yl]propane **30** (40 mg, 0.1 mmol) in THF (2.5 mL) was treated with a solution of *N*-(3-(but-3-yn-1-ylamino)-3-oxopropyl)-2,2,5,5-tetramethyl-1,3-dioxane-4-carboxamide **33** (43 mg, 0.1 mmol) in THF (2.5 mL). The resulting mixture was treated with a catalytic amount of CuI (5 mg) followed by *N,N*-diisopropylethylamine (0.1 mL, 0.6 mmol). The reaction was then heated to 70 ^{o}C until completion by TLC analysis (18 h). The reaction mixture was cooled down to rt, and diluted with H_2O (5 mL). The aqueos phase was extracted with EtOAc (3x10 mL) and the combined organics were washed with brine (3x30 mL), dried over $MgSO_4$ and concentrated under reduced pressure. Purification of the crude residue by flash column chromatography (0-5% MeOH/CH_2Cl_2) afforded the expected triazole **42** as a red oil (74 mg, 87%).

^{1}H NMR ($CDCl_3$, 400 MHz) δ: 7.45 (1H, s, ArC*H*$_{Triazole}$), 7.13 (1H, s, ArC*H*$_{BODIPY-C8}$), 6.91 (1H, d, *J* = 4.0 Hz, ArC*H*$_{BODIPY-C1}$), 6.61 (1H, t, *J* = 5.0 Hz, CON*H*), 6.28 (1H, d, *J* = 4.0 Hz, ArC*H*$_{BODIPY-C2}$), 6.15 (1H, s, ArC*H*$_{BODIPY-C6}$), 4.44 (2H, t, *J* = 8.0 Hz, C*H*$_2$N), 4.07 (1H, s, C*H*), 3.70 (1H, d, *J* = 12.0 Hz, C*H*$_2$Cq), 3.62-3.56 (2H, m, NHC*H*$_2$), 3.54-3.45 (2H, m, NHC*H*$_2$), 3.28 (1H, d, *J* = 12.0 Hz, C*H*$_2$Cq), 3.01 (2H, t, *J* = 8.0 Hz, C*H*$_2$Cq), 2.90 (2H, t, *J* = 6.4 Hz, C*H*$_2$CO), 2.56 (3H, s, C*H*$_3$), 2.43 (2H, t, *J* = 6.0 Hz, C*H*$_2$Cq), 2.39-2.33 (2H, m, CH_2C*H*$_2$$CH_2$), 2.28 (3H, s, C*H*$_3$),1.46 (3H, s, Cq(C*H*$_3$)$_2$), 1.44 (3H, s, Cq(C*H*$_3$)$_2$), 1.03 (3H, s, Cq(C*H*$_3$)$_2$), 0.96 (3H, s, Cq(C*H*$_3$)$_2$). ^{13}C NMR ($CDCl_3$, 100 MHz) δ: 171.2 (*C*O), 169.9 (*C*O), 160.5 (Ar*C*q), 156.5 (Ar*C*q), 145.2 (Ar*C*q), 135.0 (Ar*C*q), 133.1 (ArCq), 132.0 (Ar*C*q), 128.8 (Ar*C*H), 123.9 (Ar*C*H), 121.9 (Ar*C*H), 120.6 (Ar*C*H), 116.5 (Ar*C*H), 99.1 (*C*q(CH$_3$)$_2$), 77.1 (O*C*H), 71.4 (O*C*H$_2$), 49.7 (N*C*H$_2$), 38.7 (HN*C*H$_2$), 35.9 (*C*H$_2$CO), 34.8 (NH*C*H$_2$), 32.9 (CH$_2$*C*q), 29.4 (Cq(*C*H$_3$)$_2$), 29.3 (CH$_2$*C*H$_2$CH$_2$), 25.8 (*C*H$_2$ArCq), 25.4 (*C*H$_2$Cq), 22.1 (Cq(*C*H$_3$)$_2$), 18.9 (Cq(*C*H$_3$)$_2$), 18.6 (Cq(*C*H$_3$)$_2$),14.9 (*C*H$_3$Cq), 11.3 (*C*H$_3$Cq). ^{19}F NMR ($CDCl_3$, 376 MHz) δ: -70.1, -72.0. HRMS (ESI) calculated for $C_{29}H_{44}BF_2N_7O_4$ [M+H+Na]$^{+}$: *m/z* 637.3252, found *m/z* 637.3214. IR υ_{max} (film)/cm^{-1}: 3357 (br), 2922 (m), 2850 (m), 1740 (s), 1650 (m). $[\alpha]_D$ -15.500 (*c* = 0.1, $CHCl_3$, T = 23.0 °C).

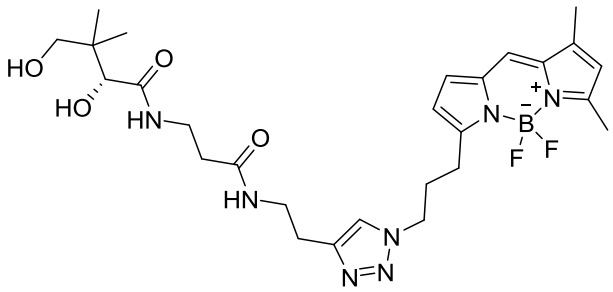

(*R*)-*N*-((((3-[4,4-Difluoro-5,7-dimethyl-4-bora-3a,4a-diaza-*s*-indacene-3-yl]propyl)-1*H*-1,2,3-triazol-4-yl)ethylamino)-3-oxopropyl)-2,4-dihydroxy-3,3-dimethylbutanamide, 43.

A solution of (*R*)-*N*-((((3-[4,4-Difluoro-5,7-dimethyl-4-bora-3a,4a-diaza-s-indacene-3-yl]propyl)-1*H*-1,2,3-triazol-4-yl)ethylamino)-3-oxopropyl)-2,2,5,5-tetramethyl-1,3-dioxane-4-carboxamide **42** (40 mg, 60 μmol) in CH_3CN (3 mL) was treated with a catalytic amount of $BiCl_3$ (5 mg) followed by H_2O (0.1 mL). The reaction mixture was stirred at rt until completion by TLC analysis (17 h). The reaction was then quenched by the addition of five drops of sat. aq. $NaHCO_3$, and diluted with EtOAc (5 mL). The resulting suspension was filtered through a bed of celite, and the celite was washed with EtOAc (2x5 mL). The organic phases were combined, dried over Na_2SO_4, and concentrated under reduced pressure. Purification of the crude residue by flash column chromatography (0-10% 2M NH_3 in MeOH/CH_2Cl_2) afforded the expected diol **43** as a red oil (10 mg, 28%).

^{1}H NMR (CD_3OD, 400 MHz) δ: 8.57 (1H, s, N*H*), 7.45 (1H, s, ArC$H_{Triazole}$), 7.06 (1H, s, ArC$H_{BODIPY-C8}$), 7.00 (1H, d, *J* = 4.0 *Hz*, ArC$H_{BODIPY-C1}$), 6.71 (1H, br s, CON*H*), 6.43 (1H, d, *J* = 4.0 Hz, ArC$H_{BODIPY-C2}$), 6.24 (1H, s, ArC$H_{BODIPY-C6}$), 4.51 (2H, t, *J* = 8.0 Hz, NCH_2), 4.09 (1H, s, C*H*), 3.69 (1H, d, *J* = 12.0 Hz, CH_2Cq), 3.63-3.59 (2H, m, NHCH_2), 3.56-3.53 (2H, m, NHCH_2), 3.15 (1H, d, *J* = 12.0 Hz, CH_2Cq), 3.00 (2H, t, *J* = 8.0 Hz, CH_2Cq), 2.92 (2H, t, *J* = 6.4 Hz, CH_2CO), 2.51 (3H, s, CqCH_3), 2.31 (2H, t, *J* = 6.0 Hz, CH_2Cq), 2.20-2.12 (2H, m, $CH_2CH_2CH_2$), 2.07 (3H, s, CqCH_3), 1.04 (3H, s, Cq(CH_3)$_2$), 0.74 (3H, s, Cq(CH_3)$_2$). ^{13}C NMR (CD_3OD, 100 MHz) δ: 179.0 (*C*O), 167.8 (*C*O), 160.3 (Ar*C*q), 155.8 (Ar*C*q), 145.4 (Ar*C*q), 134.2 (Ar*C*q), 132.4 (Ar*C*q), 130.8 (Ar*C*q), 129.6 (Ar*C*H), 124.3 (Ar*C*H), 122.5 (Ar*C*H), 120.9 (Ar*C*H), 116.2 (Ar*C*H), 100.5 (*C*q(CH_3)$_2$), 77.4 (O*C*H), 71.8 (O*C*H_2), 50.1 (N*C*H_2), 38.7 (HN*C*H_2), 35.9 (*C*H_2CO), 35.1 (NH*C*H_2), 31.6 (CH_2*C*q), 29.0 (CH_2C*H*$_2CH_2$), 25.5 (*C*H_2Cq), 25.4 (*C*H_2Cq),18.7 (Cq(*C*H_3)$_2$), 18.4 (Cq(*C*H_3)$_2$),13.0 (*C*H_3Cq), 11.4 (*C*H_3Cq). ^{19}F NMR (CD_3OD, 376 MHz) δ: -74.1, -76.0. HRMS (ESI) calculated for $C_{27}H_{38}BF_2N_7O_4$ $[M]^+$: *m/z* 573.3046, found *m/z* 573.3890. IR υ_{max} (film)/cm^{-1}: 3491 (br), 2927 (m), 1843 (m), 1644 (m), 1557 (m), 1411 (s), 1258 (s). $[\alpha]_D$ -26.000 (*c* = 0.02, $CHCl_3$, T = 23.0 °C).

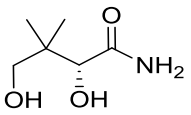

(*R*)-2,4–Dihydroxy-3,3-dimethylbutanamide, 23.

A -78 °C solution of (*D*)-(−)-pantolactone **10** (5.0 g, 38.2 mmol) in MeOH (20 mL) was treated with liquid ammonia (80 mL), and the reaction was refluxed until completion by TLC analysis (16 h). The

reaction mixture was then concentrated under reduced pressure, to afford the expected amide **23** as a white solid (5.5 g, 97%), which required no further purification. The NMR data matches the literature data for this compound.[39]

^{1}H NMR ($(CD_3)_2SO$, 400 MHz) δ: 7.10 (2H, s, NH_2), 5.25 (1H, d, *J* = 5.6 Hz, CHO*H*), 4.50 (1H, t, *J* = 5.6 Hz, CH_2O*H*), 3.66 (1H, d, *J* = 5.5 Hz, C*H*OH), 3.30 (1H, dd, *J* = 10.4, 5.6 Hz, CH_2OH), 3.17 (1H, dd, *J* = 10.4, 5.6 Hz, CH_2OH), 0.82 (3H, s, Cq(CH_3)$_2$), 0.80 (3H, s, Cq(CH_3)$_2$). ^{13}C NMR ($(CD_3)_2SO$, 100 MHz) δ: 176.0 (*C*O), 75.5 (*C*HOH), 68.5 (*C*H_2OH), 39.2 (*Cq*CH_2), 21.4 (Cq(*C*H_3)$_2$), 20.9 (Cq(*C*H_3)$_2$).

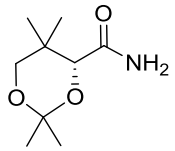

(*R*)-2,2,5,5-Tetramethyl-1,3-dioxane-4-carboxamide, 44.

A 0 °C solution of 2-methoxypropene (3.9 mL, 61.2 mmol) in acetone (30 mL) was treated with *p*-TsOH (114 mg, 0.6 mmol), and the resulting solution was diluted with acetone (60 mL) and CH_2Cl_2 (30 mL). The mixture was treated with (*R*)-2,4-dihydroxy-3,3-dimethylbutanamide **23** (3.0 g, 20.4 mmol) and reaction mixture was stirred at rt until completion by TLC analysis (16 h). The reaction was quenched by dropwise addition of triethylamine, until a pale yellow solution was obtained. The solution was then dried over Na_2SO_4, and concentrated under reduced pressure. The crude residue was then triturated with PE to afford a yellow solid. The solvent was decanted off and the crude residue was purified by flash column chromatography (0-20% EtOAc/PE) to yield the expected acetonide **44** as a white solid (1.76 g, 47%). The NMR data matches the literature data for this compound.[39]

^{1}H NMR ($CDCl_3$, 400 MHz) δ: 6.49 (1H, br s, NH_2), 5.42 (1H, br s, NH_2), 4.13 (1H, s, C*H*), 3.73 (1H, d, *J* = 11.7 Hz, CH_2OH), 3.33 (1H, d, *J* = 11.7 Hz, CH_2OH), 1.48 (3H, s, Cq(CH_3)$_2$), 1.46 (3H, s, Cq(CH_3)$_2$), 1.08 (3H, s, Cq(CH_3)$_2$), 1.07 (3H, s, Cq(CH_3)$_2$) ^{13}C NMR ($CDCl_3$, 100 MHz) δ: 172.6 (*C*O), 99.0 (*Cq*(CH$_3$)$_2$), 77.3 (O*C*H), 71.4 (O*C*H_2), 32.8 (CH_2*Cq*), 29.5 (Cq(*C*H_3)$_2$), 22.0 (Cq(*C*H_3)$_2$), 18.9 (Cq(*C*H_3)$_2$, 18.6 (Cq(*C*H_3)$_2$.

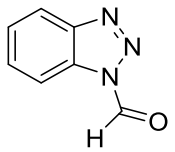

1*H*-Benzotriazole-1-carboxaldehyde, 49.

A mixture of formic acid **45** (2.4 mL, 64.0 mmol) and acetic anhydride **46** (3.1 mL, 32.0 mmol) was heated to 55 °C for 3 h under anhydrous conditions.^{1}H NMR analysis of the crude reaction mixture was used to calculate the mass ratio of acetic formic anhydride **47** formed (2.08 g, 23.6 mmol). The

solution was then cooled to −10 °C, and was treated with a solution of 1*H*-benzotriazole **48** (2.5 g, 21.2 mmol) in anhydrous THF (7 mL). The reaction was then stirred at −10 °C until completion by TLC analysis (2 h). The mixture was then concentrated under reduced pressure, and then kept under high vaccum for 36 h to afford the expected *N*-formylated product **49** as a white solid (3.3 g, 97%). The NMR data matches the literature data for this compound.[57]

^{1}H NMR ($CDCl_3$, 400 MHz) δ: 9.89 (1H, s, C*H*O), 8.28 (1H, d, *J* = 8.2 Hz, Ar*H*), 8.17 (1H, dt, *J* = 8.3, 0.9 Hz, Ar*H*), 7.74 (1H, ddd, *J* = 8.2, 7.2, 1.0 Hz, Ar*H*), 7.61 (1H, ddd, *J* = 8.2, 7.2, 1.0 Hz, Ar*H*) ^{13}C NMR ($CDCl_3$, 100 MHz) δ: 159.7 (*C*O), 146.5 (Ar*Cq*), 130.7 (Ar*C*H), 129.8 (Ar*Cq*), 126.0 (Ar*C*H), 120.4 (Ar*C*H), 113.6 (Ar*C*H).

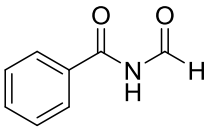

***N*-Formylbenzamide, 51.**

A 0 °C solution of benzamide **50** (50 mg, 0.4 mmol) in anhydrous THF (1.5 mL) was treated by the dropwise addition of *n*-BuLi (1.6 M in hexanes, 0.2 mL, 0.4 mmol). The reaction mixture was allowed to warm up to rt and stirred for 1 h at rt. The resulting mixture was then treated by the dropwise addition of a solution of *N*-formylbenzotriazole **49** (64 mg, 0.4 mmol) in anhydrous THF (0.5 mL). The resulting reaction mixture was then stirred at rt until completion as indicated by TLC analysis (20 h), and the reaction was then quenched with 2-propanol (0.2 mL), and diluted with sat. aq. $NaHCO_3$ (2 mL). The phases were separated, and the aqueous phase was extracted with Et_2O (2x4 mL). The combined organics were washed with brine (2x8 mL), dried over Na_2SO_4, and concentrated under reduced pressure. Purification of the crude residue by flash column chromatography (0-20% EtOAc/PE) afforded the expected *N*-formylated product **51** as a white solid (25 mg, 36%). The NMR data matches the literature data for this compound.[39]

^{1}H NMR ($CDCl_3$, 400 MHz) δ: 9.87 (1H, br s, N*H*), 9.43 (1H, d, *J* = 9.7 Hz, C*H*O), 8.01 (2H, dt, *J* = 8.5, 1.6 Hz, Ar*H*), 7.77-7.63 (1H, m, Ar*H*), 7.62-7.53 (2H, m, Ar*H*). ^{13}C NMR ($CDCl_3$, 100 MHz) δ: 166.5 (*C*O), 162.9 (*C*O), 132.9 (Ar*Cq*), 131.4 (Ar*C*H), 128.2 (2 x Ar*C*H), 127.8 (2 x Ar*C*H).

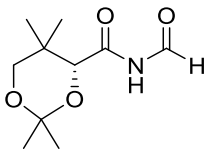

***N*-Formyl-(*R*)-2,2,5,5-tetramethyl-[1,3]dioxane-4-carboxylic acid amide, 24.**

A 0 °C solution of (*R)*-2,2,5,5-tetramethyl-1,3-dioxane-4-carboxamide **44** (1.3 g, 7.0 mmol) in anhydrous THF (40 mL) was treated by the dropwise addition of *n*-BuLi (2.4M in hexanes, 3.2 mL, 7.6 mmol). The reaction mixture was allowed to warm up to rt and stirred for 1 h at rt. The reaction was then treated by the dropwise addition of a solution of *N*-formylbenzotriazole **49** (1.7 g, 11.5

mmol) in anhydrous THF (5 mL). The mixture was then stirred at rt until completion by TLC analysis (20 h). The reaction was quenched with 2-propanol (0.5 mL), and diluted with sat. aq. $NaHCO_3$ (18 mL). The aqueous phase was extracted with EtOAc (3x60 mL), and the combined organics were washed with brine (2x180 mL). The combined organic washes were dried over Na_2SO_4, and concentrated under reduced pressure. Purification of the crude residue by flash column chromatography (0-20% EtOAc/PE) afforded the expected *N*-formylated product **24** as a white solid (60 mg, 87%). The NMR data matches the literature data for this compound.[39]

^{1}H NMR ($CDCl_3$, 400 MHz) δ: 9.09 (1H, d, *J* = 10.4 Hz, C*H*O), 8.85 (1H, br s, N*H*), 4.13 (1H, s, C*H*), 3.65 (1H, d, *J* = 11.8 Hz, CH_2), 3.26 (1H, d, *J* = 11.8 Hz, CH_2), 1.42 (3H, s, Cq(CH_3)$_2$), 1.38 (3H, s, Cq(CH_3)$_2$), 0.99 (3H, s, Cq(CH_3)$_2$), 0.98 (3H, s, Cq(CH_3)$_2$). ^{13}C NMR ($CDCl_3$, 100 MHz) δ: 170.6 (*C*HO), 161.4 (*C*O), 99.6 (*Cq*O), 77.1 (O*C*H), 71.1 (*C*H_2), 33.3 (CH$_2$*Cq*), 29.3 (Cq(*C*H_3)$_2$), 21.7 (Cq(*C*H_3)$_2$, 18.9 (Cq(*C*H_3)$_2$, 18.6 (Cq(*C*H_3)$_2$).

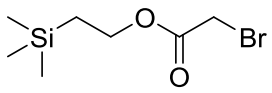

2-(Trimethylsilyl)ethyl 2-bromoacetate, 48.

A 0 °C solution of 2-(trimethylsilyl)ethan-1-ol **47** (0.8 mL, 5.6 mmol) in CH_2Cl_2 (16 mL) was treated sequentially with triethylamine (0.8 mL, 5.6 mmol), followed by solution of bromoacetylbromide (0.5 mL, 5.6 mmol) in CH_2Cl_2 (16 mL). The resulting solution was allowed to warm up to rt and then stirred at rt until completion by TLC analysis (16 h). The reaction mixture was then diluted with H_2O (32 mL), and the organic phase was separated. The aqueos phase was extracted with CH_2Cl_2 (3x30 mL), and the combined organics were washed with brine (2x100 mL). The organic phase was dried over Na_2SO_4 and concentrated under reduced pressure. Purification of the crude residue by flash column chromatography (0-2% EtOAc/PE) yielded the expected ester product **48** as a yellow oil (0.53 g, 40%). The NMR data matches the literature data for this compound.[39]

^{1}H NMR ($CDCl_3$, 400 MHz) δ: 4.23-4.19 (2H, m, OCH_2), 3.77 (2H, s, CH_2Br), 1.00-0.96 (2H, m, CH_2Si), 0.00 (9H, s, Si(CH_3)$_3$). ^{13}C NMR ($CDCl_3$, 100 MHz) δ: 168.9 (*C*O), 66.3 (O*C*H$_2$), 27.6 (*C*H$_2$Br), 18.7 (*C*H$_2$Si), 0.0 (3 x Si(*C*H_3)$_3$).

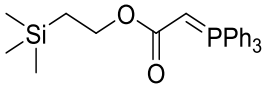

2-(Trimethylsilyl)ethyltriphenylphosphoranylidene acetate, 25.

A solution of 2-(trimethylsilyl)ethyl 2-bromoacetate **48** (500 mg, 2.1 mmol) in toluene (10 mL) was treated with PPh_3 (500 mg, 2.1 mmol), and the resulting reaction mixture was stirred at rt until completion by TLC analysis (4 days). The reaction was filtered through a filtration funnel, and the

crude solid was washed with toluene (2x5 mL). The solid was dissolved in CH_2Cl_2 (10 mL) and the solution was treated with sat. aq. $NaHCO_3$ (10 mL), and stirred at rt for 2 h. The organic phase was then separated, and the aqueous phase was extracted with CH_2Cl_2 (2x10 mL). The combined organics were washed with brine (2x30 mL) and dried over Na_2SO_4. The resulting solution was concentrated under reduced pressure, and afforded the expected ylide **25** as a yellow oil (0.44 g, 50%). The product required no further purification. The NMR data matches the literature data for this compound.[39]

^{1}H NMR ($CDCl_3$, 400 MHz) δ : 7.72-7.66 (6H, m, Ar*H*), 7.59-7.54 (3H, m, Ar*H*), 7.49-7.46 (6H, m, Ar*H*), 4.04 (2H, br s, OCH_2), 2.92 (1H, br s, PC*H*), 0.91 (2H, br s, CH_2Si), 0.00 (9H, s, Si(CH_3)$_3$). ^{13}C NMR ($CDCl_3$, 100 MHz) δ: 167.2 (*C*O), 134.4 (6 x Ar*C*H), 133.5 (3 x Ar*C*H), 130.0 (6 x Ar*C*H), 129.8 (3 x Ar*Cq*) 54.9 (OCH_2), 29.9 (P*C*H), 19.1 (*C*H_2Si), 0.0 (3 x Si(*C*H_3)$_3$).

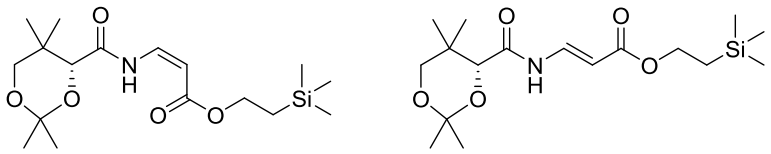

(*R*,*Z*)-2-(Trimethylsilyl)ethyl3-(2,2,5,5-tetramethyl-1,3-dioxane-4-carboxamido)acrylate, 26 and (*R*,*E*)-2-(Trimethylsilyl)ethyl3-(2,2,5,5-tetramethyl-1,3-dioxane-4-carboxamido)acrylate, 27.

A solution of *N*-formyl-(*R*)-2,2,5,5-tetramethyl-[1,3]dioxane-4-carboxylic acid amide **24** (145 mg, 0.7 mmol) in benzene (6 mL) was treated with a solution of 2-(trimethylsilyl)ethyltriphenylphosphoranylidene acetate **25** (566 mg,1.3 mmol) in benzene (5 mL). The reaction mixture was heated to 80 °C until completion by TLC analysis (18 h). The reaction was then cooled down to rt and concentrated under reduced pressure. Purification of the crude residue by flash column chromatography (0-20% EtOAc/PE) afforded the expected *cis*-isomer **26** as a yellow oil (72 mg, 30%), and the *trans*-isomer **27** as a white solid (157mg, 65%). The NMR data matches the literature data for these compounds.[39]

(*R*,*Z*) -2- (Trimethylsilyl)ethyl3-(2,2,5,5-tetramethyl -1,3-dioxane-4-carboxamido)acrylate, 26.

^{1}H NMR ($CDCl_3$, 400 MHz) δ: 11.04 (1H, d, *J* = 11.5 Hz, N*H*), 7.36 (1H, dd, *J* = 11.6, 8.9 Hz, NC*H*), 5.10 (1H, d, *J* = 9.0 Hz, C*H*CO_2), 4.21-4.20 (2H, m, OCH_2), 4.16 (1H, s, C*H*), 3.67 (1H, d, *J* = 11.7 Hz, CH_2Cq), 3.28 (1H, d, *J* = 11.7 Hz, CH_2Cq), 1.53 (3H, s, Cq(CH_3)$_2$), 1.41 (3H, s, Cq(CH_3)$_2$), 0.99 (3H, s, Cq(CH_3)$_2$), 0.98 (3H, s, Cq(CH_3)$_2$), 0.96 (2H, m, CH_2Si(CH_3)$_3$), 0.00 (9H, s, Si(CH_3)$_3$). ^{13}C NMR ($CDCl_3$, 100 MHz) δ: 170.2 (*C*O), 169.8 (*C*O), 137.2 (N*C*H), 100.7 (*C*HCO_2), 99.7 (*Cq*(CH_3)$_2$), 78.7 (O*C*H), 72.8 (OCH_2), 63.7 (OCH_2), 34.7 (CH_2*Cq*), 30.8 (Cq(*C*H_3)$_2$), 23.3 (Cq(*C*H_3)$_2$), 20.4 (Cq(*C*H_3)$_2$), 20.1 (Cq(*C*H_3)$_2$), 18.8 (*C*H_2Si), 0.0 (3 x Si(*C*H_3)$_3$).

26: [α]$_D$ +33.500 (*c* = 0.6, $CHCl_3$, T = 24.3 °C).

(*R*,*E*) -2- (Trimethylsilyl)ethyl3-(2,2,5,5- tetramethyl -1,3-dioxane-4-carboxamido)acrylate, 27.

^{1}H NMR ($CDCl_3$, 400 MHz) δ: 8.32 (1H, d, *J* = 11.9 Hz, N*H*), 7.92 (1H, dd, *J* = 14.2, 12.0 Hz, NC*H*), 5.53 (1H, d, *J* = 14.1 Hz, C*H*CO_2), 4.21-4.16 (2H, m, OCH_2), 4.15 (1H, s, OC*H*), 3.67 (1H, d, *J* = 11.7 Hz, CH_2Cq), 3.27 (1H, d, *J* = 11.8 Hz, CH_2Cq), 1.51 (3H, s, Cq(CH_3)$_2$), 1.46 (3H, s, Cq(CH_3)$_2$), 1.05 (3H, s, Cq(CH_3)$_2$), 1.04 (2H, m, CH_2Si), 1.01 (3H, s, Cq(CH_3)$_2$), 0.01 (9H, s, Si(CH_3)$_3$). ^{13}C NMR ($CDCl_3$, 100 MHz) δ: 169.3 (*C*O), 168.7 (*C*O), 137.3 (NCH), 104.6 (*C*HCO_2), 100.9 (*Cq*(CH$_3$)$_2$), 78.7 (O*C*H), 72.7 (O*C*H$_2$), 63.8 (O*C*H$_2$), 34.8 (CH$_2$*Cq*), 30.9 (Cq(*C*H$_3$)$_2$), 23.3 (Cq(*C*H$_3$)$_2$), 20.4 (Cq(*C*H$_3$)$_2$), 20.1 (Cq(*C*H$_3$)$_2$), 18.8 (*C*H$_2$Si), 0.0 (3 x Si(*C*H$_3$)$_3$).

27: [α]$_D$ +53.125 (*c* = 0.8, $CHCl_3$, T = 24.4 °C).

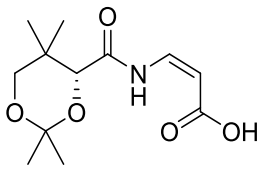

(*R,Z*)-3-(2,2,5,5-Tetramethyl-1,3-dioxane-4-carboxamido)acrylic acid, 54.

A 0° C solution of (*R*,*Z*) -2- (trimethylsilyl)ethyl3-(2,2,5,5-tetramethyl -1,3-dioxane-4-carboxamido)acrylate **26** (72 mg, 0.2 mmol) in anhydrous DMF (2.0 mL) was treated with TASF (66 mg, 0.2 mmol), and the reaction mixture was stirred at rt until completion by TLC analysis (20 h). The reaction was then diluted with EtOAc (6 mL) and treated with a LiCl solution (10% aq., 4 mL). The organic phase was separated, and the aqueos layer was extracted with EtOAc (2x6 mL). The combined organics were washed with a LiCl solution (10% aq., 2x18 mL). The combined organic washes were dried over Na_2SO_4, and concentrated under reduced pressure to afford the expected carboxylic acid **54** as a colorless oil (37 mg, 78%). The product required no further purification. The NMR data matches the literature data for this compound.[46]

^{1}H NMR ($CDCl_3$, 400 MHz) δ: 11.25 (1H, d, *J* = 12.0 Hz, N*H*), 7.54 (1H, dd, *J* = 12.0, 8.8 Hz, NHC*H*), 5.23 (1H, d, *J* = 8.8 Hz, C*H*CO_2), 4.22 (1H, s, OC*H*), 3.74 (1H, d, *J* = 11.6 Hz, CH_2Cq), 3.34 (1H, d, *J* = 11.6 Hz, CH_2Cq), 1.54 (3H, s, Cq(CH_3)$_2$), 1.47 (3H, s, Cq(CH_3)$_2$), 1.06 (3H, s, Cq(CH_3)$_2$), 1.04 (3H, s, Cq(CH_3)$_2$). ^{13}C NMR ($CDCl_3$, 125 MHz) δ: 173.1 (*C*O), 168.7 (*C*O), 138.2 (NCH), 99.2 (*C*HCO$_2$), 96.8 (*Cq*(CH$_3$)$_2$), 77.2 (O*C*H), 71.2 (O*C*H$_2$), 33.2 (CH$_2$*Cq*), 29.1 (Cq(*C*H$_3$)$_2$), 21.7 (Cq(*C*H$_3$)$_2$), 18.9 (Cq(*C*H$_3$)$_2$), 18.6 (Cq(*C*H$_3$)$_2$).

54: [α]$_D$ +35.000 (*c* = 1.75, $CHCl_3$, T = 24.4 °C).

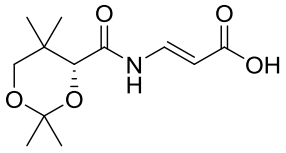

(*R,E*)-3-(2,2,5,5-Tetramethyl-1,3-dioxane-4-carboxamido)acrylic acid, 28.

A 0° C solution of (*R*,*E*)-2-(trimethylsilyl)ethyl3-(2,2,5,5-tetramethyl-1,3-dioxane-4-carboxamido)acrylate **27** (60 mg, 0.2 mmol) in anhydrous DMF (2.0 mL) was treated with TASF

(50 mg, 0.2 mmol), and the reaction mixture was stirred at rt until completion by TLC analysis (24 h). The reaction was then diluted with EtOAc (6 mL) and treated with a LiCl solution (10% aq., 4 mL). The organic phase was separated, and the aqueos layer was extracted with EtOAc (2x6 mL). The combined organics were washed with a LiCl solution (10% aq., 2x18 mL). The combined organic washes were dried over Na_2SO_4, and concentrated under reduced pressure. Purification of the crude residue by flash column chromatography (0-2% MeOH/CH_2Cl_2) afforded the expected carboxylic acid **28** as a white solid (40 mg, 97%). The NMR data matches the literature data for this compound.[39]
^{1}H NMR ($CDCl_3$, 400 MHz) δ: 8.49 (1H, d, *J* = 12.0 Hz, N*H*), 8.00 (1H, app t, *J* = 14.0, 12.0 Hz, NHC*H*), 5.62 (1H, d, *J* = 14.0 Hz, C*H*CO_2), 4.23 (1H, s, OC*H*), 3.73 (1H, d, *J* = 12.0 Hz, C*H*$_2$Cq), 3.35 (1H, d, *J* = 11.6 Hz, C*H*$_2$Cq), 1.54 (3H, s, Cq(C*H*$_3$)$_2$), 1.48 (3H, s, Cq(C*H*$_3$)$_2$), 1.07 (3H, s, Cq(C*H*$_3$)$_2$), 1.03 (3H, s, Cq(C*H*$_3$)$_2$). ^{13}C NMR ($CDCl_3$, 100 MHz) δ: 172.2 (*C*O), 167.9 (*C*O), 138.0 (N*C*H), 101.8 (*C*HCO$_2$), 99.6 (*Cq*(CH$_3$)$_2$), 77.0 (O*C*H), 71.2 (O*C*H$_2$), 33.4 (CH$_2$*Cq*), 29.4 (Cq(*C*H$_3$)$_2$), 21.8 (Cq(*C*H$_3$)$_2$), 18.8 (Cq(*C*H$_3$)$_2$), 18.6 (Cq(*C*H$_3$)$_2$).
28: [α]$_D$ +67.800 (*c* = 0.6, $CHCl_3$, T = 24.6 °C).

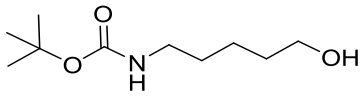

***tert*-Butyl (5-hydroxypenthyl)carbamate, 56.**
A solution of 5-aminopentanol **55** (500 mg, 4.8 mmol) in CH_2Cl_2 (10 mL) was treated sequentially with triethylamine (1.3 mL, 9.6 mmol), followed by solution of di-*tert*-butyl dicarbonate (1.2 g, 5.3 mmol) in CH_2Cl_2 (10 mL). The reaction mixture was stirred at rt until completion by TLC analysis (16 h). The reaction was then diluted with H_2O (20 mL), and the organic phase was separated. The aqueos phase was extracted with CH_2Cl_2 (2 x 20 mL). The combined organics were washed with brine (60 mL), and dried over Na_2SO_4. The resulting solution was concentrated under reduced pressure. Purification of the crude residue by flash column chromatography (0-5% MeOH/CH_2Cl_2) yielded the expected carbamate **56** as a yellow oil (730 mg, 74%). The NMR data matches the literature data for this compound.[60]
^{1}H NMR ($CDCl_3$, 400 MHz) δ: 4.50 (1H, br s, N*H*), 3.67 (2H, t, *J* = 6.4 Hz, C*H*$_2$OH), 3.15 (2H, dd, *J* = 12.8, 6.3 Hz, C*H*$_2$NH), 1.60-1.49 (4H, m, NCH$_2$C*H*$_2$, C*H*$_2$CH$_2$OH), 1.45 (9H, s, Cq(C*H*$_3$)$_3$), 1.44-1.39 (2H, m, CH$_2$C*H*$_2$CH$_2$). ^{13}C NMR ($CDCl_3$, 100 MHz) δ: 156.0 (*C*O), 79.1 (O*Cq*), 62.75 (*C*H$_2$OH), 40.4 (*C*H$_2$N), 32.2 (*C*H$_2$CH$_2$OH), 29.8 (NCH$_2$*C*H$_2$), 28.4 (3 x Cq(*C*H$_3$)$_3$), 22.9 (CH$_2$*C*H$_2$CH$_2$).

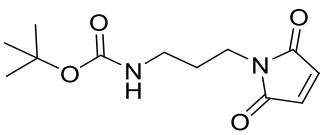

***tert*-Butyl(3-(2,5-dioxo-2,5-dihydro-1*H*-pyrrol-1-yl)propyl)carbamate, 59.**
A solution of *tert*-butyl(3-hydroxypropyl)carbamate **58** (0.2 mL, 1.5 mmol) in THF (7 mL) was treated sequentially with maleimide **57** (175 mg, 1.8 mmol), followed by PPh_3 (472mg, 1.8 mmol) and DIAD

(0.4 mL, 1.8 mmol). The reaction mixture was stirred at rt until completion by TLC analysis (18 h). The reaction was then concentrated under reduced pressure, to give a crude yellow oil. Purification of the crude residue by flash column chromatography (0-30% EtOAc/PE) afforded the desired substituted maleimide **59** as a colorless oil (257 mg, 69%). The NMR data matches the literature data for this compound.[103]

^{1}H NMR ($CDCl_3$, 400 MHz) δ: 6.63 (2H, s, C*H*$_{maleimide}$), 5.08 (1H, br s, N*H*), 3.55-3.42 (2H, t, *J* = 6.8 Hz, C*H*$_2$N), 3.06-2.90 (2H, appq, *J* = 6.0 Hz, C*H*$_2$NH), 1.73-1.63 (2H, q, *J* = 6.4 Hz, $CH_2CH_2CH_2$), 1.38 (9H, s, Cq(C*H*$_3$)$_3$). ^{13}C NMR ($CDCl_3$, 100 MHz) δ: 170.9 (*C*O), 170.3 (*C*O), 134.1 (2 x *C*H$_{maleimide}$), 79.3 (*Cq*(CH$_3$)$_3$), 70.1 (*C*H$_2$N), 37.3 (NH*C*H$_2$), 34.9 ($CH_2CH_2CH_2$), 28.4 (3 × Cq(*C*H$_3$)$_3$).

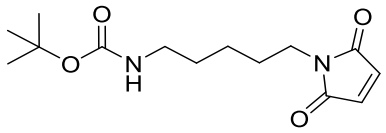

***tert*-Butyl(5-(2,5-dioxo-2,5-dihydro-1*H*-pyrrol-1-yl)pentyl)carbamate, 60.**

A solution of *tert*-butyl(5-hydroxypenthyl)carbamate **56** (203 mg, 1.0 mmol) in THF (5mL) was treated sequentially with maleimide **57** (107 mg, 1.1 mmol), followed by triphenylphosphine (283mg, 1.1 mmol) and DIAD (0.2 mL, 1.2 mmol). The reaction was stirred at rt until completion by TLC analysis (16 h). The reaction was then concentrated under reduced pressure, to give a crude yellow oil. Purification of the crude residue by flash column chromatography (0-1% MeOH/CH_2Cl_2) yielded the expected substituted maleimide **60** as a pale yellow oil (with DIAD traces) (124 mg, 40%). The NMR data matches the literature data for this compound.[104]

^{1}H NMR ($CDCl_3$, 400 MHz) δ: 6.70 (2H, s, C*H*$_{maleimide}$), 4.50 (1H, br s, N*H*), 3.53 (2H, t, *J* = 7.2 Hz, C*H*$_2$N), 3.12 (2H, appq, *J* = 6.4 Hz, C*H*$_2$NH), 1.67-1.57 (2H, m, C*H*$_2$CH$_2$N),1.56-1.47 (2H, m, NHCH$_2$C*H*$_2$), 1.46 (9H, s, Cq(C*H*$_3$)$_3$),1.36-1.30 (2H, m, $CH_2CH_2CH_2$). ^{13}C NMR ($CDCl_3$, 100 MHz) δ: 170.8 (*C*O), 170.1 (*C*O), 134.0 (2 x *C*H$_{maleimide}$), 79.1 (O*Cq*), 70.1 (N*C*H$_2$), 40.3 (*C*H$_2$NH), 37.6 (NCH$_2$*C*H$_2$), 29.8 (NHCH$_2$*C*H$_2$), 28.4 (3 × Cq(*C*H$_3$)$_3$), 23.9 ($CH_2CH_2CH_2$).

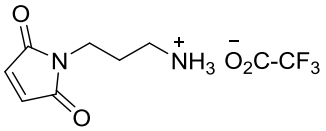

3-(2,5-Dioxo-2,5-dihydro-1*H*-pyrrol-1-yl)propan-1-aminium 2,2,2-trifluoroacetate salt, 61.

A solution of *tert*-butyl(3-(2,5-dioxo-2,5-dihydro-1*H*-pyrrol-1-yl)propyl)carbamate **59** (250 mg, 1 mmol) in CH_2Cl_2 (1.5 mL) was treated with trifluoroacetic acid (1.5 mL, 20 mmol), and the reaction mixture was stirred at rt until completion by TLC analysis (3 h). The reaction was then diluted with CH_2Cl_2 (3 mL), followed by H_2O (5 mL). The aqueos layer was separated, and the organic phase was extracted with H_2O (3x3 mL). The combined aqueous layers were then washed with CH_2Cl_2 (3x15 mL). The combined aqueous washes were concentrated under reduced pressure, and kept

under high vaccum for 36 h, to afford the desired substituted maleimide **61** as a white solid (250 mg, 95%).

^{1}H NMR (CD_3OD, 500 MHz) δ: 6.86 (2H, s, C$H_{maleimide}$), 3.63 (2H, t, *J* = 7.0 Hz, NCH_2), 2.95 (2H, t, *J* = 7.5 Hz, CH_2NH), 1.97-1.91 (2H, m, $CH_2CH_2CH_2$). ^{13}C NMR (CD_3OD, 125 MHz) δ: 171.1 (2 X *C*O), 134.1 (2 x *C*H$_{maleimide}$), 37.0 (NCH_2), 34.0 (*C*H_2NH), 26.5 ($CH_2CH_2CH_2$). ^{19}F NMR (CD_3OD, 470 MHz) δ: -76.8 (3F). HRMS (ESI) calculated for $C_9H_{11}F_3N_2O_4$ $[M\text{-}CO_2CF_3]^+$: *m/z* 155.0815, found *m/z* 155.0863. IR υ_{max} (neat)/cm^{-1}: 3426 (s br), 2950 (m), 2870 (m), 1623 (s), 1135 (m), 1032 (m). m.p.: 93-96 ^{o}C.

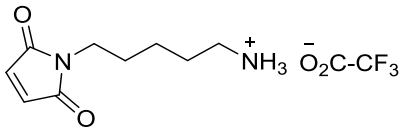

1-(5-Aminopentyl)-1*H*-pyrrole-2,5-dione 2,2,2-trifluoroacetate salt, 62.

A solution of *tert*-butyl (5-(2,5-dioxo-2,5-dihydro-1*H*-pyrrol-1-yl)pentyl)carbamate **60** (140 mg, 0.5 mmol) in CH_2Cl_2 (0.6 mL) was treated with trifluoroacetic acid (0.6 mL, 8 mmol), and the resulting mixture was stirred at rt until completion by TLC analysis (2.5 h). The reaction mixture was diluted with CH_2Cl_2 (2 mL), followed by H_2O (5 mL). The aqueos layer was separated, and the organic phase was extracted with H_2O (3x3 mL). The combined aqueous layers were washed with CH_2Cl_2 (3x15 mL). The combined aqueous washes were concentrated under reduced pressure, and kept under high vaccum for 36 h, to afford the desired amine **62** as a yellow oil (107 mg, 73%).

^{1}H NMR (CD_3OD, 400 MHz) δ: 6.71 (2H, s, C$H_{maleimide}$), 3.40 (2H, t, *J* = 7.2 Hz, NCH_2), 2.80 (2H, t, *J* = 7.2 Hz, CH_2NH), 1.62-1.49 (4H, m, NCH_2CH_2, CH_2CH_2NH), 1.30-1.23 (2H, m, $CH_2CH_2CH_2$). ^{13}C NMR (CD_3OD, 125 MHz) δ: 171.2 (2 x *C*O), 133.9 (2 x *C*H), 39.1 (NCH_2), 36.65 (*C*H_2NH), 27.6 (*C*H_2CH_2NH), 26.5 (NCH_2CH_2), 23.1 ($CH_2CH_2CH_2$). ^{19}F NMR (CD_3OD, 470 MHz) δ: -76.8 (3F). HRMS (ESI) calculated for $C_{11}H_{15}F_3N_2O_4$ $[M\text{-}CO_2CF_3]^+$: *m/z* 183.1128, found *m/z* 183.1158. IR υ_{max} (neat)/cm^{-1}: 3400 (m), 3091 (m), 2948 (m), 1709 (s), 1680 (s), 1204 (m), 1174 (m), 1136 (m).

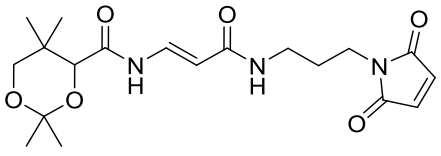

(*R,E*)-*N*-(3-((3-(2,5-Dioxo-2,5-dihydro-1*H*-pyrrol-1-yl)propyl)amino)-3-oxoprop-1-en-1-yl)-2,2,5,5-tetramethyl-1,3-dioxane-4-carboxamide, 63 and (*S,E*)-*N*-(3-((3-(2,5-Dioxo-2,5-dihydro-1*H*-pyrrol-1-yl)propyl)amino)-3-oxoprop-1-en-1-yl)-2,2,5,5-tetramethyl-1,3-dioxane-4-carboxamide, 74.

Method A

A solution of (*R,E*)-3-(2,2,5,5-tetramethyl-1,3-dioxane-4-carboxamido)acrylic acid **28** (25 mg, 0.1 mmol) in CH_2Cl_2 (0.3 mL) was treated sequentially with solution of 3-(2,5-dioxo-2,5-dihydro-1*H*-pyrrol-1-yl)propan-1-aminium 2,2,2-trifluoroacetate salt **61** (39 mg, 0.1 mmol) in CH_2Cl_2 (0.3 mL),

followed by BTFFH (46 mg, 0.1 mmol) and *N,N*-diisopropylethylamine (25 µL, 0.1 mmol). The reaction was then heated to 80 °C for 2.5 h in the microwave oven. The reaction mixture was concentrated under reduced pressure, to give a crude red oil. Purification of the crude residue by flash column chromatography (0-5% MeOH/CH_2Cl_2) afforded the desired substituted maleimide **63** as a pink oil (12.6 mg, 33%).

Method B

A solution of perfluorophenyl (*R,E*)-3-(2,2,5,5-tetramethyl-1,3-dioxane-4-carboxamido)acrylate **66** (25 mg, 60 µmol) in CH_2Cl_2 (1.0 mL) was treated with suspension of 3-(2,5-dioxo-2,5-dihydro-1*H*-pyrrol-1-yl)propan-1-aminium 2,2,2-trifluoroacetate salt **61** (25 mg, 80 µmol) in CH_2Cl_2 (0.5 mL), followed by *N,N*-diisopropylethylamine (25 µL, 150 µmol). The reaction mixture was stirred at rt until completion by TLC analysis (72 h). The reaction was then concentrated under reduced pressure. Purification of the crude residue by flash column chromatography (0-4% MeOH/CH_2Cl_2) afforded the desired substituted maleimide **63** as a pink oil (21 mg, 90%).

^{1}H NMR ($CDCl_3$, 400 MHz) δ: 8.23 (1H, d, *J* = 10.8 Hz, N*H*), 7.77 (1H, appt, *J* = 13.6 Hz, NHC*H*), 6.65 (2H, s, C*H*$_{maleimide}$), 5.95 (1H, br s, N*H*CH_2), 5.75 (1H, d, *J* = 14.0 Hz, C*H*CO), 4.12 (1H, s, OC*H*), 3.64 (1H, d, *J* = 11.6 Hz, C*H*$_2$Cq), 3.52 (2H, t, *J* = 6.0 Hz, C*H*$_2$N), 3.24 (1H, d, *J* = 11.6 Hz, C*H*$_2$Cq), 3.22-3.17 (2H, m, NHC*H*$_2$), 1.76-1.70 (2H, m, CH_2C*H*$_2$$CH_2$), 1.44 (3H, s, Cq(C*H*$_3$)$_2$), 1.38 (3H, s, Cq(C*H*$_3$)$_2$), 0.98 (3H, s, Cq(C*H*$_3$)$_2$), 0.93 (3H, s, Cq(C*H*$_3$)$_2$). ^{13}C NMR ($CDCl_3$, 100 MHz) δ: 171.1 (*C*O), 168.0 (*C*O), 162.99 (*C*O), 134.2 (2 x *C*H$_{maleimide}$),123.0 (N*C*H), 105.9 (*C*HCO), 99.4 (*Cq*$(CH_3)_2$), 77.2 (O*C*H), 71.3 (O*C*H_2), 35.9 (*C*H_2N), 34.7 (NH*C*H_2), 33.4 (CH_2*Cq*), 29.4 (Cq(C*H*$_3$)$_2$), 28.3 (CH_2*C*$H_2$$CH_2$), 21.9 (Cq(*C*$H_3$)$_2$), 18.8 (Cq(*C*$H_3$)$_2$), 18.7 (Cq(*C*$H_3$)$_2$). HRMS (EI$^+$) calculated for $C_{19}H_{27}N_3O_6$ $[M]^+$: *m/z* 393.1900, found *m/z* 393.1903. IR υ_{max} (neat)/cm^{-1}: 3323 (m), 3050 (m), 2926 (m), 1705 (s), 1664 (s), 1600 (m), 1097 (m).

(*R*)-**63**: $[\alpha]_D$ +54.667 (*c* = 0.3, $CHCl_3$, T = 23.9 °C).

(*S*)-**74**: $[\alpha]_D$ -48.000 (*c* = 0.5, $CDCl_3$, T = 26.0 °C).

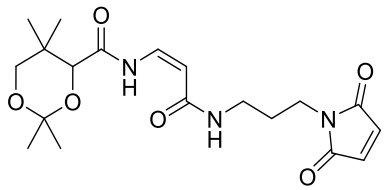

(*R,Z*)-*N*-(3-((3-(2,5-dioxo-2,5-dihydro-1*H*-pyrrol-1-yl)propyl)amino)-3-oxoprop-1-en-1-yl)-2,2,5,5-tetramethyl-1,3-dioxane-4-carboxamide, 64 and (*S,Z*)-*N*-(3-((3-(2,5-dioxo-2,5-dihydro-1*H*-pyrrol-1-yl)propyl)amino)-3-oxoprop-1-en-1-yl)-2,2,5,5-tetramethyl-1,3-dioxane-4-carboxamide, 75.

Method A

A solution of (*R,Z*)-3-(2,2,5,5-tetramethyl-1,3-dioxane-4-carboxamido)acrylic acid **54** (10 mg, 40 µmol) in CH_2Cl_2 (0.3 mL) was treated sequentially with solution of 3-(2,5-dioxo-2,5-dihydro-1*H*-pyrrol-1-yl)propan-1-aminium 2,2,2-trifluoroacetate salt **61** (15 mg, 50 µmol) in CH_2Cl_2 (0.3 mL),

followed by HBTU (23 mg, 60 μmol) and *N,N*-diisopropylethylamine (10 μL, 60 μmol). The reaction was then heated to 80 °C for 2.5 h in the microwave oven. The reaction mixture was concentrated under reduced pressure, to give a crude purple oil. Purification of the crude residue by flash column chromatography (0-4% MeOH/CH_2Cl_2) afforded the desired substituted maleimide **64** as a yellow oil (4 mg, 26%).

Method B

A solution of perfluorophenyl (*R,Z*)-3-(2,2,5,5-tetramethyl-1,3-dioxane-4-carboxamido)acrylate **67** (43 mg, 100 μmol) in CH_2Cl_2 (1.0 mL) was treated with suspension of 3-(2,5-dioxo-2,5-dihydro-1*H*-pyrrol-1-yl)propan-1-aminium 2,2,2-trifluoroacetate salt **61** (9.75 mg, 30 μmol) in CH_2Cl_2 (1.4 mL), followed by *N,N*-diisopropylethylamine (31 μL, 180 μmol). The reaction mixture was stirred at rt until completion by TLC analysis (72 h), and then concentrated under reduced pressure. Purification of the crude residue by flash column chromatography (0-3% MeOH/CH_2Cl_2) afforded the desired substituted maleimide **64** as a yellow oil (30 mg, 40%).

^{1}H NMR ($CDCl_3$, 400 MHz) δ: 11.58 (1H, d, *J* = 11.2 Hz, N*H*), 7.25-7.20 (1H, dd, *J* = 11.2, 9.2 Hz, NHC*H*), 6.65 (2H, s, C$H_{maleimide}$), 5.89 (1H, t, *J* = 6.0 Hz, N*H*CH_2), 4.98 (1H, d, *J* = 9.2 Hz, C*H*CO), 4.12 (1H, s, OC*H*), 3.65 (1H, d, *J* = 11.6 Hz, CH_2Cq), 3.53 (2H, t, *J* = 6.4 Hz, CH_2N), 3.25 (1H, d, *J* = 11.6 Hz, CH_2Cq), 3.23-3.13 (2H, m, HNCH_2), 1.77-1.70 (2H, m, CH_2C$H_2$$CH_2$), 1.53 (3H, s, Cq(C$H_3$)$_2$), 1.39 (3H, s, Cq(C$H_3$)$_2$), 0.98 (6H, s, Cq(C$H_3$)$_2$). ^{13}C NMR ($CDCl_3$, 100 MHz) δ: 171.0 (*C*O), 168.8 (*C*O), 167.8 (CO), 134.2 (2 x C$H_{maleimide}$), 133.4 (N*C*H), 100.5 (*C*HCO), 99.2 (*Cq*$(CH_3)_2$), 77.2 (O*C*H), 71.4 (O*C*H_2), 33.5 (*C*H_2N), 34.8 (NH*C*H_2), 33.3 (*Cq*$(CH_3)_2$), 29.3 (Cq(*C*H_3)$_2$), 28.3 (CH_2*C*$H_2$$CH_2$), 22.0 (Cq(*C*$H_3$)$_2$), 19.0 (Cq(*C*$H_3$)$_2$), 18.6 (Cq(*C*$H_3$)$_2$). HRMS (EI$^+$) calculated for $C_{19}H_{27}N_3O_6$ $[M]^+$: *m/z* 393.1900, found *m/z* 393.1898. IR υ_{max} (neat)/cm^{-1}: 3311 (m), 3050 (m), 2928 (m), 1705 (s), 1654 (s), 1097 (m), 696 (m).

(*R*)-**64**: $[\alpha]_D$ +24.000 (*c* = 0.5, $CHCl_3$, T = 23.8 °C).

(*S*)-**75**: $[\alpha]_D$ -29.470 (*c* = 1.9, $CDCl_3$, T = 26.1 °C).

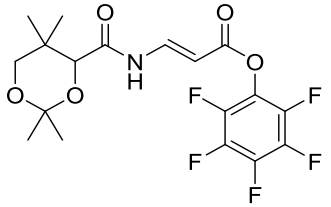

Perfluorophenyl (*R,E*)-3-(2,2,5,5-tetramethyl-1,3-dioxane-4-carboxamido)acrylate, 66 and Perfluorophenyl (*S,E*)-3-(2,2,5,5-tetramethyl-1,3-dioxane-4-carboxamido)acrylate, 71.

A solution of (*R,E*)-3-(2,2,5,5-tetramethyl-1,3-dioxane-4-carboxamido)acrylic acid **28** (100 mg, 0.4 mmol) in CH_2Cl_2 (1.5 mL) was treated sequentially with a solution of 2,3,4,5,6-pentafluorophenol **65** (90 mg, 0.5 mmol) in CH_2Cl_2 (1.5 mL), followed by EDC.HCl (88 mg, 0.5 mmol) and a catalytic amount of DMAP (3 mg). The reaction mixture was then stirred at rt until completion by TLC analysis (24h), and then concentrated under reduced pressure. Purification of the crude residue by flash

column chromatography (100% CH_2Cl_2) afforded the expected *trans*-ester **66** as a yellow oil (60 mg, 41%), followed by the *cis*-ester **67** as a yellow oil (60 mg, 41%) and unreacted starting material **28** (10 mg, 10%).

^{1}H NMR ($CDCl_3$, 500 MHz) δ: 8.61 (1H, d, *J* = 12.0 Hz, N*H*), 8.10 (1H, dd, *J* = 14.0, 12.5 Hz, NHC*H*), 5.76 (1H, d, *J* = 14.0 Hz, C*H*CO_2), 4.18 (1H, s, OC*H*), 3.66 (1H, d, *J* = 12.0 Hz, CH_2Cq), 3.27 (1H, d, *J* = 12.0 Hz, CH_2Cq), 1.45 (3H, s, Cq(CH_3)$_2$), 1.40 (3H, s, Cq(CH_3)$_2$), 0.99 (3H, s, Cq(CH_3)$_2$), 0.96 (3H, s, Cq(CH_3)$_2$). ^{13}C NMR ($CDCl_3$, 125 MHz) δ: 168.1 (*C*O), 162.9 (*C*O), 142.4 (Ar*C*F), 140.3 (2 x Ar*C*F),140.0 (N*C*H), 138.9 (2 x Ar*C*F), 138.3 (Ar*C*F), 99.70 (*C*HCO$_2$), 98.88 (*Cq*(CH$_3$)$_2$), 77.0 (O*C*H), 71.18 (O*C*H$_2$), 33.49 (OCH$_2$*Cq*), 29.40 (Cq(*C*H$_3$)$_2$), 21.77 (Cq(*C*H$_3$)$_2$), 18.95 (Cq(*C*H$_3$)$_2$), 18.84 (Cq(*C*H$_3$)$_2$). ^{19}F NMR ($CDCl_3$, 470 MHz) δ: -152.0, -158.0, -163.0. HRMS (ESI) calculated for $C_{18}H_{18}F_5NO_5$ [M+Na]$^+$: *m/z* 446.0997, found *m/z* 446.0979. IR υ_{max} (neat)/cm^{-1}: 3350 (m), 3050 (m), 2933 (m), 1752 (m), 1718 (m), 1630 (m), 1518 (s), 1087 (m), 1005 (m).

(*R*)-**66**: $[\alpha]_D$ +38.909 (*c* = 2.2, $CHCl_3$, T = 22.9 °C).

(*S*)-**71**: $[\alpha]_D$ -36.000 (*c* = 0.8, $CHCl_3$, T = 22.8 °C).

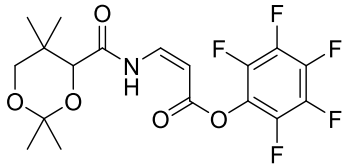

Perfluorophenyl (*R,Z*)-3-(2,2,5,5-tetramethyl-1,3-dioxane-4-carboxamido)acrylate, 67 and Perfluorophenyl (*S,Z*)-3-(2,2,5,5-tetramethyl-1,3-dioxane-4-carboxamido)acrylate, 72.

A solution of (*R,Z*)-3-(2,2,5,5-tetramethyl-1,3-dioxane-4-carboxamido)acrylic acid **54** (35 mg, 0.1 mmol) in CH_2Cl_2 (1.0 mL) was treated sequentially with a solution of 2,3,4,5,6-pentafluorophenol **65** (38 mg, 0.2 mmol) in CH_2Cl_2 (1.0 mL), followed by EDC.HCl (38 mg, 0.2 mmol) and a catalytic amount of DMAP (3 mg). The reaction mixture was then stirred at rt until completion by TLC analysis (18 h), and then concentrated under reduced pressure. Purification of the crude residue by flash column chromatography (0-20% EtOAc/PE) afforded the expected *cis*-ester **67** as a yellow oil (40 mg, 64%) followed by the *trans*-ester **66** as a yellow oil (22 mg, 35%).

^{1}H NMR ($CDCl_3$, 500 MHz) δ: 10.80 (1H, d, *J* = 11.5 Hz, N*H*), 7.63-7.59 (1H, dd, *J* = 12.0, 8.5 Hz, NHC*H*), 5.39 (1H, d, *J* = 8.5 Hz, C*H*CO_2), 4.16 (1H, s, OC*H*), 3.64 (1H, d, *J* = 12.0 Hz, CH_2Cq), 3.25 (1H, d, *J* = 12.0 Hz, CH_2Cq), 1.42 (3H, s, Cq(CH_3)$_2$), 1.37 (3H, s, Cq(CH_3)$_2$), 0.97 (3H, s, Cq(CH_3)$_2$), 0.96 (3H, s, Cq(CH$_3$)$_2$). ^{13}C NMR ($CDCl_3$, 125 MHz) δ: 168.9 (*C*O), 163.6 (*C*O), 142.3 (Ar*C*F), 140.4 (2 x Ar*C*F), 140.2 (N*C*H), 138.8 (2 x Ar*C*F), 136.8 (Ar*C*F), 99.4 (*C*HCO$_2$), 93.8 (*Cq*(CH$_3$)$_2$), 77.2 (O*C*H), 71.1 (O*C*H$_2$), 33.3 (CH$_2$*Cq*), 29.2 (Cq(*C*H$_3$)$_2$), 21.7 (Cq(*C*H$_3$)$_2$), 18.9 (Cq(*C*H$_3$)$_2$), 18.5 (Cq(*C*H$_3$)$_2$). ^{19}F NMR (CDCl3, 470 MHz) δ: -151.6, -158.6, -162.7. HRMS (ESI) calculated for $C_{18}H_{18}F_5NO_5$ [M+Na]$^+$: *m/z* 446.0997, found *m/z* 446.0978. IR υ_{max} (neat)/cm^{-1}: 3351 (m), 2956 (m), 2928 (m), 1723 (m), 1621 (m), 1519 (s), 1117 (m), 1001 (m).

(*R*)-**67**: $[\alpha]_D$ +10.286 (*c* = 1.4, $CHCl_3$, T = 23.0 °C).

(*S*)-**72**: $[\alpha]_D$ -19.652 (*c* = 2.3, $CHCl_3$, T = 22.8 °C).

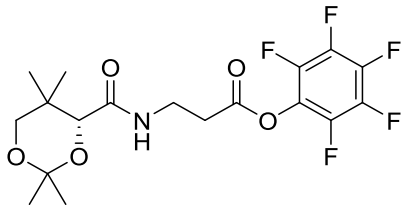

Perfluorophenyl (*R*)-3-(2,2,5,5-tetramethyl-1,3-dioxane-4-carboxamido)propanoate, 73.

A solution of (*R*)-3-(2,2,5,5-tetramethyl-1,3-dioxane-4-carboxamido)propanoic acid **32** (150 mg, 0.6 mmol) in CH_2Cl_2 (2.0 mL) was treated sequentially with a solution of 2,3,4,5,6-pentafluorophenol **65** (141 mg, 0.8 mmol) in CH_2Cl_2 (2.0 mL), followed by EDC.HCl (132 mg, 0.7 mmol) and a catalytic amount of DMAP (3 mg). The reaction mixture was then stirred at rt until completion by TLC analysis (18 h), and then concentrated under reduced pressure. Purification of the crude residue by flash column chromatography (0-40% EtOAc/PE) afforded the expected ester **73** as a colorless oil (200 mg, 81%).

^{1}H NMR ($CDCl_3$, 500 MHz) δ: 7.01 (1H, br s, N*H*), 4.13 (1H, s, C*H*), 3.78-3.60 (2H, m, NHCH_2), 3.71 (1H, d, *J* = 12.0 Hz, CH_2Cq), 3.31 (1H, d, *J* = 11.5 Hz, CH_2Cq), 2.98 (2H, t, *J* = 6.5 Hz, CH_2CO_2), 1.47 (3H, s, Cq(CH_3)$_2$), 1.45 (3H, s, Cq(CH_3)$_2$), 1.08 (3H, s, Cq(CH_3)$_2$), 1.00 (3H, s, Cq(CH_3)$_2$). ^{13}C NMR ($CDCl_3$, 100 MHz) δ: 170.1 (*C*O), 168.1 (*C*O), 142.3 (Ar*C*F), 139.8 (2 x Ar*C*F), 139.2 (2 x Ar*C*F), 136.8 (Ar*C*F), 99.1 (*Cq*(CH$_3$)$_2$), 77.2 (O*C*H), 71.4 (O*C*H$_2$), 34.1 (CH$_2$*Cq*), 33.5 (HN*C*H$_2$), 33.0 (*C*H$_2$CO$_2$), 29.3 (Cq(*C*H$_3$)$_2$), 22.0 (Cq(*C*H$_3$)$_2$), 18.7 (Cq(*C*H$_3$)$_2$), 18.6 (Cq(*C*H$_3$)$_2$). ^{19}F NMR ($CDCl_3$, 470 MHz) δ: -152.6, -157.6, -162.0. HRMS (ESI) calculated for $C_{18}H_{20}F_5NO_5$ [M+Na]$^+$: *m/z* 448.1154, found *m/z* 448.1135. IR υ_{max} (neat)/cm^{-1}: 3439 (m), 2991 (m), 2956 (m), 1787 (m), 1679 (m), 1517 (s), 1094 (m), 1001 (m).

73: $[\alpha]_D$ +19.956 (*c* = 9.0, $CHCl_3$, T = 23.1 °C).

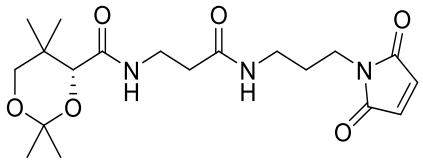

(*R*)-*N*-(3-((3-(2,5-Dioxo-2,5-dihydro-1*H*-pyrrol-1-yl)propyl)amino)-3-oxopropyl)-2,2,5,5-tetramethyl-1,3-dioxane-4-carboxamide, 76.

A solution of perfluorophenyl (*R*)-3-(2,2,5,5-tetramethyl-1,3-dioxane-4-carboxamido)propanoate **73** (95 mg, 0.2 mmol) in CH_2Cl_2 (4.0 mL) was treated with a suspension of 3-(2,5-dioxo-2,5-dihydro-1*H*-pyrrol-1-yl)propan-1-aminium 2,2,2-trifluoroacetate salt **61** (80 mg, 0.3 mmol) in CH_2Cl_2 (4.0 mL), followed by *N,N*-diisopropylethylamine (70 µL, 0.4 mmol). The reaction mixture was then stirred at rt until completion by TLC analysis (72 h), and then concentrated under reduced pressure. Purification of the crude residue by flash column chromatography (0-3% MeOH/CH_2Cl_2) afforded the desired substituted maleimide **76** as a colorless oil (52 mg, 59%).

^{1}H NMR ($CDCl_3$, 500 MHz) δ: 7.00 (1H, appt, *J* = 5.6 Hz, N*H*), 6.65 (2H, s, C*H*$_{maleimide}$), 6.32 (1H, app t, *J* = 5.6 Hz, N*H*CH_2), 4.01 (1H, s, OCH), 3.67 (1H, d, *J* = 12.0 Hz, C*H*$_2$Cq), 3.55-3.42 (2H, m, NHC*H*$_2$), 3.50 (2H, t, *J* = 8.0 Hz, C*H*$_2$N), 3.21 (1H, d, *J* = 12.0 Hz, C*H*$_2$Cq), 3.16-3.11 (2H, m, NHC*H*$_2$), 2.39 (2H, t, *J* = 7.5 Hz, C*H*$_2$CO), 1.74-1.68 (2H, m, CH_2C*H*$_2$$CH_2$), 1.38 (3H, s, Cq(C*H*$_3$)$_2$), 1.34 (3H, s, Cq(C*H*$_3$)$_2$), 0.96 (3H, s, Cq(C*H*$_3$)$_2$), 0.90 (3H, s, Cq(C*H*$_3$)$_2$). ^{13}C NMR ($CDCl_3$, 125 MHz) δ: 171.1 (CO), 170.9 (CO), 170.0 (CO), 134.2 (2 x *C*H$_{maleimide}$), 99.0 (*Cq*(CH$_3$)$_2$), 77.2 (OCH), 71.4 (O*C*H$_2$), 36.1 (*C*H$_2$CO), 36.0 (*C*H$_2$N), 34.8 (HN*C*H$_2$), 32.9 (*Cq*(CH$_3$)$_2$), 30.9 (HN*C*H$_2$) 29.4 (Cq(*C*H$_3$)$_2$), 28.2 (CH_2*C*H$_2$$CH_2$), 22.1 (Cq(*C*H$_3$)$_2$), 18.8 (Cq(*C*H$_3$)$_2$), 18.6 (Cq(*C*H$_3$)$_2$). HRMS (ESI) calculated for $C_{19}H_{29}N_3O_6$ [M+Na]$^+$: *m/z* 418.1949, found *m/z* 418.1931. IR υ_{max} (neat)/cm^{-1}: 3310 (m), 3098 (m), 2945 (m), 1706 (s), 1647 (s), 1533 (m), 1097 (m), 696 (m).

76: $[\alpha]_D$ +21.231 (*c* = 1.3, $CHCl_3$, T = 23.7 °C).

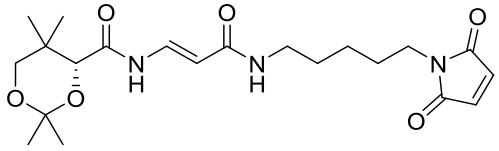

(*R,E*)-*N*-(3-((5-(2,5-dioxo-2,5-dihydro-1*H*-pyrrol-1-yl)pentyl)amino)-3-oxoprop-1-en-1-yl)-2,2,5,5-tetramethyl-1,3-dioxane-4-carboxamide, 77.

A solution of perfluorophenyl (*R,E*)-3-(2,2,5,5-tetramethyl-1,3-dioxane-4-carboxamido)acrylate **66** (35 mg, 0.1 mmol) in CH_2Cl_2 (1.0 mL) was treated with a solution of 1-(5-aminopentyl)-1*H*-pyrrole-2,5-dione trifluoroacetate salt **62** (34 mg, 0.1 mmol) in CH_2Cl_2 (1.0 mL), followed by *N,N*-diisopropylethylamine (30 µL, 0.2 mmol). The reaction mixture was then stirred at rt until completion by TLC analysis (72 h), and then concentrated under reduced pressure. Purification of the crude residue by flash column chromatography (0-4% MeOH/CH_2Cl_2) afforded the desired substituted maleimide **77** as a colorless oil (28 mg, 80%).

^{1}H NMR ($CDCl_3$, 400 MHz) δ: 8.30 (1H, d, *J* = 10.8 Hz, N*H*), 7.78 (1H, dd, *J* = 13.9, 10.9 Hz, NHC*H*), 6.72 (2H, s, C*H*$_{maleimide}$), 5.84 (1H, d, *J* = 13.9 Hz, C*H*CO), 5.49 (1H, t, *J* = 5.5 Hz, N*H*CH_2), 4.21 (1H, s, OCH), 3.73 (1H, d, *J* = 11.8 Hz, C*H*$_2$Cq), 3.54 (2H, t, *J* = 7.0 Hz, C*H*$_2$N), 3.36-3.30 (3H, m, NHC*H*$_2$, C*H*$_2$Cq), 1.65-1.56 (4H, m, C*H*$_2$$CH_2$N, NHCH$_2$C*H*$_2$), 1.53 (3H, s, Cq(C*H*$_3$)$_2$), 1.47 (3H, s, Cq(C*H*$_3$)$_2$), 1.37-1.31 (2H, m, CH_2C*H*$_2$$CH_2$), 1.07 (3H, s, Cq(C*H*$_3$)$_2$), 1.02 (3H, s, Cq(C*H*$_3$)$_2$). ^{13}C NMR ($CDCl_3$, 100 MHz) δ: 170.9 (*C*O), 168.1 (*C*O), 166.3 (*C*O), 134.1 (2 x *C*H$_{maleimide}$),132.8 (N*C*H), 106.2 (*C*HCO), 99.4 (*Cq*(CH$_3$)$_2$), 77.2 (O*C*H), 71.3 (O*C*H$_2$), 39.3 (CH_2N), 37.4 (NH*C*H$_2$), 33.3 (CH_2*Cq*), 29.4 (Cq(*C*H$_3$)$_2$), 28.9 (*C*H$_2$$CH_2$N), 28.1 (*C*H$_2$$CH_2$NH), 23.8 ($CH_2$*C*H$_2$$CH_2$), 21.9 (Cq(*C*H$_3$)$_2$), 18.8 (Cq(*C*H$_3$)$_2$), 18.7 (Cq(*C*H$_3$)$_2$). HRMS (ESI) calculated for $C_{21}H_{31}N_3O_6$ [M+Na]$^+$: *m/z* 444.2105, found *m/z* 444.2101. IR υ_{max} (neat)/cm^{-1}: 3329 (m), 3050 (m), 2933 (m), 1701 (s), 1662 (s), 1097 (m), 720 (m).

(*R*)-**77**: $[\alpha]_D$ +25.090 (*c* = 2.2, $CHCl_3$, T = 23.8 °C).

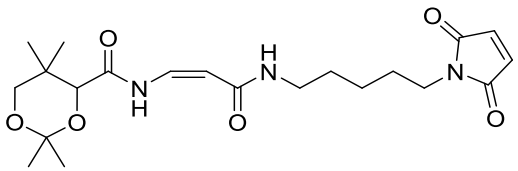

(*R,Z*)-*N*-(3-((5-(2,5-dioxo-2,5-dihydro-1*H*-pyrrol-1-yl)pentyl)amino)-3-oxoprop-1-en-1-yl)-2,2,5,5-tetramethyl-1,3-dioxane-4-carboxamide, 78 and (*S,Z*)-*N*-(3-((5-(2,5-dioxo-2,5-dihydro-1*H*-pyrrol-1-yl)pentyl)amino)-3-oxoprop-1-en-1-yl)-2,2,5,5-tetramethyl-1,3-dioxane-4-carboxamide, 79.

A solution of perfluorophenyl (*R,Z*)-3-(2,2,5,5-tetramethyl-1,3-dioxane-4-carboxamido)acrylate **67** (5 mg, 10 μmol) in CH_2Cl_2 (0.5 mL) was treated with a solution of 1-(5-aminopentyl)-1*H*-pyrrole-2,5-dione trifluoroacetate salt **62** (5 mg, 11 μmol) in CH_2Cl_2 (0.5 mL), followed by *N,N*-diisopropylethylamine (10 μL, 60 μmol). The resulting reaction mixture was stirred at rt until completion by TLC analysis (72 h), and then concentrated under reduced pressure. Purification of the crude residue by flash column chromatography (0-3% MeOH/CH_2Cl_2) afforded the desired substituted maleimide **78** as a colorless oil (4 mg, 80%).

^{1}H NMR ($CDCl_3$, 400 MHz) δ: 11.59 (1H, d, *J* = 11.2 Hz, N*H*), 7.23-7.18 (1H, dd, *J* = 11.2, 8.4 Hz, NHC*H*), 6.63 (2H, s, C*H*$_{maleimide}$), 5.37 (1H, appt, *J* = 5.2 Hz, CON*H*), 4.92 (1H, d, *J* = 8.4 Hz, C*H*CO), 4.12 (1H, s, OC*H*), 3.64 (1H, d, *J* = 11.6 Hz, C*H*$_2$Cq), 3.46 (2H, t, *J* = 6.8 Hz, C*H*$_2$N), 3.25 (1H, d, *J* = 11.6 Hz, C*H*$_2$Cq), 3.22-3.19 (2H, m, HNC*H*$_2$), 1.58-1.43 (4H, m, C*H*$_2$CH$_2$N, NHCH$_2$C*H*$_2$), 1.53 (3H, s, Cq(C*H*$_3$)$_2$), 1.37 (3H, s, Cq(C*H*$_3$)$_2$), 1.28-1.25 (2H, m, CH$_2$C*H*$_2$CH$_2$), 1.18 (3H, s, Cq(C*H*$_3$)$_2$), 0.97 (3H, s, Cq(C*H*$_3$)$_2$). ^{13}C NMR ($CDCl_3$, 100 MHz) δ: 170.9 (*C*O), 168.9 (*C*O), 167.9 (CO), 134.1 (2 x *C*H$_{maleimide}$), 133.2 (N*C*H), 100.5 (*C*HCO$_2$), 99.2 (*Cq*(CH$_3$)$_2$), 77.2 (O*C*H), 71.4 (O*C*H$_2$), 38.9 (CH$_2$N), 37.3 (NH*C*H$_2$), 33.3 (*Cq*(CH$_3$)$_2$), 29.7 (Cq(*C*H$_3$)$_2$), 28.7 (*C*H$_2$CH$_2$N), 28.1 (NHCH$_2$*C*H$_2$), 23.8 (CH$_2$*C*H$_2$CH$_2$), 22.0 (Cq(*C*H$_3$)$_2$), 19.0 (Cq(*C*H$_3$)$_2$), 18.6 (Cq(*C*H$_3$)$_2$). HRMS (ESI) calculated for $C_{21}H_{31}N_3O_6$ [M+Na]$^+$: *m/z* 444.2105, found *m/z* 444.2087. IR υ_{max} (neat)/cm^{-1}: 3323 (m), 2926 (s), 2854 (m), 1703 (s), 1656 (m), 1465 (m), 1097 (m), 720 (m).

(*R*)-**78**: $[\alpha]_D$ +12.500 (*c* = 0.8, $CHCl_3$, T = 23.9 °C).

(*S*)-**79**: $[\alpha]_D$ -68.240 (*c* = 1.7, $CDCl_3$, T = 26.4 °C).

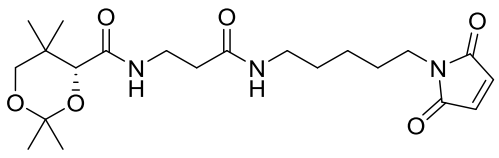

(*R*)-*N*-(3-((5-(2,5-dioxo-2,5-dihydro-1*H*-pyrrol-1-yl)pentyl)amino)-3-oxopropyl)-2,2,5,5-tetramethyl-1,3-dioxane-4-carboxamide, 80.

A solution of perfluorophenyl (*R*)-3-(2,2,5,5-tetramethyl-1,3-dioxane-4-carboxamido)propanoate **73** (95 mg, 0.2 mmol) in CH_2Cl_2 (2.5 mL) was treated with a solution of 1-(5-aminopentyl)-1*H*-pyrrole-2,5-dione trifluoroacetate salt **62** (60 mg, 0.2 mmol) in CH_2Cl_2 (2.5 mL), followed by

N,N-diisopropylethylamine (60 µL, 0.4 mmol). The reaction mixture was then stirred at rt until completion by TLC analysis (72 h), and then concentrated under reduced pressure. Purification of the crude residue by flash column chromatography (0-3% MeOH/CH_2Cl_2) afforded the desired substituted maleimide **80** as a colorless oil (90 mg, 95%).

^{1}H NMR ($CDCl_3$, 500 MHz) δ: 6.97 (1H, appt, *J* = 5.5 Hz, NH), 6.63 (2H, s, C*H*$_{maleimide}$), 5.98 (1H, br s, N*H*CH_2), 4.00 (1H, s, OCH), 3.61 (1H, d, *J* = 11.5 Hz, C*H*$_2$Cq), 3.58-3.46 (2H, m, NHC*H*$_2$), 3.44 (2H, t, *J* = 7.0 Hz, C*H*$_2$N), 3.21 (1H, d, *J* = 11.5 Hz, C*H*$_2$Cq), 3.17-3.12 (2H, m, NHC*H*$_2$), 2.36 (2H, t, *J* = 6.0 Hz, C*H*$_2$CO), 1.56-1.42 (4H, m, C*H*$_2$CH$_2$N, NHCH$_2$C*H*$_2$), 1.39 (3H, s, Cq(C*H*$_3$)$_2$), 1.34 (3H, s, Cq(C*H*$_3$)$_2$), 1.26-1.18 (2H, m, CH$_2$C*H*$_2$CH$_2$), 1.03 (3H, s, Cq(C*H*$_3$)$_2$), 0.80 (3H, s, Cq(C*H*$_3$)$_2$). ^{13}C NMR ($CDCl_3$, 125 MHz) δ: 170.9 (CO), 170.8 (CO), 170.2 (CO), 134.2 (2 x *C*H$_{maleimide}$), 99.0 (*Cq*(CH$_3$)$_2$), 77.2 (O*C*H), 71.4 (O*C*H$_2$), 39.3 (*C*H$_2$N), 37.4 (HN*C*H$_2$), 36.1 (*C*H$_2$CO), 34.9 (HN*C*H$_2$), 32.9 (*Cq*(CH$_3$)$_2$), 29.4 (Cq(*C*H$_3$)$_2$), 29.2 (*C*H$_2$CH$_2$N), 28.1 (NHCH$_2$*C*H$_2$), 23.9 (CH$_2$*C*H$_2$CH$_2$), 22.1 (Cq(*C*H$_3$)$_2$), 18.8 (Cq(*C*H$_3$)$_2$), 18.6 (Cq(*C*H$_3$)$_2$). HRMS (ESI) calculated for $C_{21}H_{33}N_3O_6$ [M+Na]$^+$: *m/z* 446.2262, found *m/z* 446.2240. IR υ_{max} (neat)/cm^{-1}: 3330 (m), 2930 (m), 1706 (s), 1656 (s), 1521 (s), 1097 (m), 696 (m).

80: $[\alpha]_D$ +24.267 (*c* = 1.5, $CHCl_3$, T = 23.7 °C).

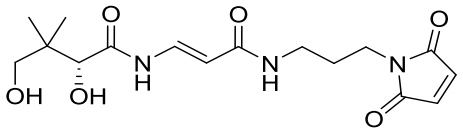

(*R,E*)-*N*-(3-((3-(2,5-dioxo-2,5-dihydro-1*H*-pyrrol-1-yl)propyl)amino)-3-oxoprop-1-en-1-yl)-2,4-dihydroxy-3,3-dimethylbutanamide, 81.

A solution of (*R,E*)-*N*-(3-((3-(2,5-dioxo-2,5-dihydro-1*H*-pyrrol-1-yl)propyl)amino)-3-oxoprop-1-en-1-yl)-2,2,5,5-tetramethyl-1,3-dioxane-4-carboxamide **63** (12 mg, 30 µmol) in CH_3CN (0.2 mL) was treated with $BiCl_3$ (1 mg, 3 µmol), followed by H_2O (10 µL). The reaction mixture was then stirred at rt until completion by TLC analysis (24 h). The reaction was then quenched by addition of five drops of sat. aq. $NaHCO_3$ and diluted with EtOAc (1 mL). The resulting suspension was filtered through a bed of celite, and the celite was washed with EtOAc (2x2 mL). The organic washes were combined, dried over Na_2SO_4, and concentrated under reduced pressure. Purification of the crude residue by flash column chromatography (0-5% 6M NH_3 in MeOH/CH_2Cl_2) afforded the expected diol **81** as a colourless oil (10 mg, 92%).

^{1}H NMR ($CDCl_3$, 400 MHz) δ: 9.02 (1H, d, *J* = 11.2 Hz N*H*), 7.79 (1H, dd, *J* = 14.0, 11.6 Hz, NHC*H*), 6.66 (2H, s, C*H*$_{maleimide}$), 6.32 (1H, t, *J* = 5.8 Hz, N*H*CH_2), 5.75 (1H, d, *J* = 13.9 Hz, C*H*CO), 4.10 (1H, s, OC*H*), 3.65 (1H, d, *J* = 11.8 Hz, C*H*$_2$Cq), 3.30 (2H, appt, *J* = 6.8 Hz C*H*$_2$N), 3.25 (1H, d, *J* = 11.8 Hz, CH_2Cq), 3.21-3.17 (2H, m, C*H*$_2$NH), 1.76-1.71 (2H, m, CH$_2$C*H*$_2$CH$_2$), 0.98 (3H, s, Cq(CH$_3$)$_2$), 0.93 (3H, s, Cq(CH$_3$)$_2$). ^{13}C NMR ((CD$_3$)$_2$CO), 100 MHz) δ: 170.8 (*C*O), 169.8 (*C*O), 169.1 (*C*O), 134.2 (2 x *C*H$_{maleimide}$), 133.0 (HN*C*H), 105.4 (*C*HCO), 76.5 (O*C*H), 69.4 (O*C*H$_2$), 39.3 (*Cq*(CH$_3$)$_2$), 36.4 (*C*H$_2$N), 35.2 (*C*H$_2$NH), 28.9 (CH$_2$*C*H$_2$CH$_2$), 20.4 (Cq(*C*H$_3$)$_2$), 19.7 (Cq(*C*H$_3$)$_2$). HRMS (ESI)

calculated for $C_{16}H_{23}N_3O_6$ [M+Na]$^+$: *m/z* 376.1479, found *m/z* 376.1460. IR υ_{max} (neat)/cm^{-1}: 3323 (m, br), 2924 (m), 1701 (s), 1654 (s), 1329 (m), 1188 (m).
(*R*)-**81**: $[\alpha]_D$ +16.800 (*c* = 0.5, acetone, T = 25.7 °C).

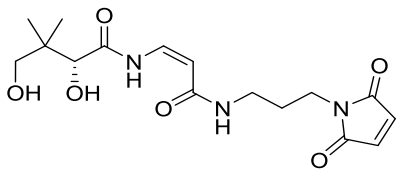

(*R,Z*)-*N*-(3-((3-(2,5-Dioxo-2,5-dihydro-1*H*-pyrrol-1-yl)propyl)amino)-3-oxoprop-1-en-1-yl)-2,4-dihydroxy-3,3-dimethylbutanamide, 82.

A solution of (*R,Z*)-*N*-(3-((3-(2,5-dioxo-2,5-dihydro-1*H*-pyrrol-1-yl)propyl)amino)-3-oxoprop-1-en-1-yl)-2,2,5,5-tetramethyl-1,3-dioxane-4-carboxamide **64** (18 mg, 40 μmol) in CH_3CN (1.6 mL) was treated with $BiCl_3$ (8 mg, 20 μmol), followed by H_2O (80 μL). The reaction mixture was then stirred at rt until completion by TLC analysis (24 h). The reaction was then quenched by addition of five drops of sat. aq. $NaHCO_3$ and diluted with EtOAc (1 mL). The resulting suspension was filtered through a bed of celite, and the celite was washed with EtOAc (2x2 mL). The organic washes were combined, dried over Na_2SO_4, and concentrated under reduced pressure. Purification of the crude residue by flash column chromatography (0-5% 6M NH_3 in MeOH/CH_2Cl_2) afforded the expected diol **82** as a yellow oil (5 mg, 31%).
^{1}H NMR ($CDCl_3$,400 MHz) δ: 11.76 (1H, d, *J* = 12.0 Hz, N*H*), 7.30-7.25 (1H, dd, *J* = 12.0, 8.0 Hz, NHC*H*), 6.67 (2H, s, C*H*$_{maleimide}$), 6.06 (1H, appt, *J* = 8.0 Hz, N*H*CH$_2$), 5.04 (1H, d, *J* = 8.0 Hz, C*H*CO), 4.13 (1H, s, OC*H*), 3.98 (1H, d, *J* = 8.8 Hz, C*H*$_2$Cq), 3.89 (1H, d, *J* = 8.8 Hz, C*H*$_2$Cq), 3.55 (2H, appt, *J* = 6.4 Hz, C*H*$_2$N), 3.22-3.17 (2H, m, HNC*H*$_2$), 1.79-1.73 (2H, m, CH$_2$C*H*$_2$CH$_2$), 1.00 (3H, s, Cq(C*H*$_3$)$_2$), 0.94 (3H, s, Cq(C*H*$_3$)$_2$). ^{13}C NMR ((CD$_3$)$_2$CO), 100 MHz) δ: 170.8 (*C*O), 168.5 (*C*O), 167.9 (CO), 134.2 (2 x *C*H$_{maleimide}$), 132.8 (N*C*H), 100.1 (*C*HCO), 76.3 (O*C*H), 69.4 (O*C*H$_2$), 39.3 (*Cq*(CH$_3$)$_2$), 36.1 (*C*H$_2$N), 35.1 (NH*C*H$_2$), 29.6 (CH$_2$*C*H$_2$CH$_2$), 20.4 (Cq(*C*H$_3$)$_2$), 19.7 (Cq(*C*H$_3$)$_2$). HRMS (ESI) calculated for $C_{16}H_{23}N_3O_6$ [M+Na]$^+$: *m/z* 376.1479, found *m/z* 376.1465. IR υ_{max} (neat)/cm^{-1}: 3300 (br), 2953 (m), 2924 (m), 1720 (s), 1703 (s), 1658 (m), 1178 (m), 1101 (m).
(*R*)-**82**: $[\alpha]_D$ -32.000 (c =0.5, acetone, T = 25.6 °C).

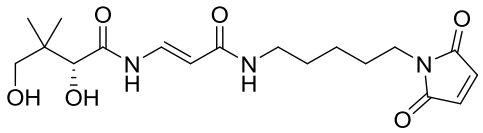

(*R,E*)-*N*-(3-((5-(2,5-dioxo-2,5-dihydro-1*H*-pyrrol-1-yl)pentyl)amino)-3-oxoprop-1-en-1-yl)-2,4-dihydroxy-3,3-dimethylbutanamide, 84.

A solution of (*R,E*)-*N*-(3-((5-(2,5-dioxo-2,5-dihydro-1*H*-pyrrol-1-yl)pentyl)amino)-3-oxoprop-1-en-1-yl)-2,2,5,5-tetramethyl-1,3-dioxane-4-carboxamide **77** (10 mg, 20 μmol) in CH_3CN (0.2 mL) was treated with $BiCl_3$ (1 mg, 3 μmol), followed by H_2O (10 μL). The reaction mixture was then stirred at

rt until completion by TLC analysis (24 h). The reaction was quenched by addition of five drops of sat. aq. $NaHCO_3$ and diluted with EtOAc (1 mL). The resulting suspension was filtered through a bed of celite, and the celite was washed with EtOAc (2x1 mL). The organic washes were combined, dried over Na_2SO_4, and concentrated under reduced pressure. Purification of the crude residue by flash column chromatography (0-5% 6M NH_3 in $MeOH/CH_2Cl_2$) afforded the expected diol **84** as a colourless oil (3 mg, 33%).

^{1}H NMR ($CDCl_3$, 500 MHz) δ: 8.00 (1H, br s, N*H*), 7.62 (1H, m, NHC*H*), 6.62 (2H, s, 2 x C$H_{maleimide}$), 6.46 (1H, d, *J* = 9.0 Hz, C*H*CO), 5.28 (1H, br s, N*H*CH_2), 4.06 (1H, s, OC*H*), 3.65-3.20 (6H, m, CH_2Cq, CH_2N, CH_2NH), 1.57-1.47 (4H, m, CH_2CH_2N, CH_2CH_2NH),1.27-1.23 (2H, m, $CH_2CH_2CH_2$), 1.0 (6H, s, Cq(CH_3)$_2$). ^{13}C NMR ($CDCl_3$, 125 MHz) δ: 178.7 (*C*O), 177.8 (*C*O), 170.9 (*C*O), 134.1 (2 x C$H_{maleimide}$), 132.3 (NCH), 102.5 (*C*HCO), 76.4 (OCH), 75.7 (OCH_2), 40.9 (*Cq*(CH_3)$_2$), 38.3 (CH_2N), 37.5 (NHCH_2), 29.7 (CH_2CH_2N), 29.1 ($NHCH_2CH_2$), 24.2 ($CH_2CH_2CH_2$), 22.8 (Cq(CH_3)$_2$),18.5 (Cq(CH_3)$_2$. HRMS (ESI) calculated for $C_{18}H_{27}N_3O_6$ [M+Na]$^+$: *m/z* 404.1792, found *m/z* 404.1778. IR υ_{max} (neat)/cm^{-1}: 3300 (br), 2929 (m), 2850 (m), 1699 (s), 1631 (m), 1120 (m), 1004 (m).

(*R*)-**84**: $[\alpha]_D$ -83.300 (*c* = 2.4, acetone, T = 25.6 °C).

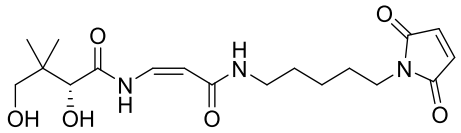

(*R,Z*)-*N*-(3-((5-(2,5-dioxo-2,5-dihydro-1*H*-pyrrol-1-yl)pentyl)amino)-3-oxoprop-1-en-1-yl)-2,4-dihydroxy-3,3-dimethylbutanamide, 85.

A solution of (*R,Z*)-N-(3-((5-(2,5-dioxo-2,5-dihydro-1*H*-pyrrol-1-yl)pentyl)amino)-3-oxoprop-1-en-1-yl)-2,2,5,5-tetramethyl-1,3-dioxane-4-carboxamide **78** (14 mg, 30 μmol) in CH_3CN (0.7 mL) was treated with $BiCl_3$ (8 mg, 20 μmol), followed by H_2O (30 μL). The reaction mixture was then stirred at rt until completion by TLC analysis (24 h). The reaction was quenched by addition of five drops of sat. aq. $NaHCO_3$ and diluted with EtOAc (1 mL). The resulting suspension was filtered through a bed of celite, and the celite was washed with EtOAc (2x1 mL). The organic washes were combined, dried over Na_2SO_4, and concentrated under reduced pressure. Purification of the crude residue by flash column chromatography (0-5% 6M NH_3 in $MeOH/CH_2Cl_2$) afforded the expected diol **85** as a yellow oil (11 mg, 87%).

^{1}H NMR ($(CD_3)_2CO$, 400 MHz) δ: 11.94 (1H, d, *J* = 12.0 Hz, N*H*), 7.14 (1H, dd, *J* = 12.0, 8.8 Hz, NHC*H*), 6.78 (2H, s, C$H_{maleimide}$), 5.11 (1H, d, *J* = 8.8 Hz, C*H*CO), 4.05 (1H, s, OC*H*), 3.45 (1H, d, *J* = 10.8 Hz, CH_2Cq), 3.39 (2H, t, *J* = 7.2 Hz, CH_2N), 3.36 (1H, d, *J* = 10.4 Hz, CH_2Cq), 3.16-3.13 (2H, m, HNCH_2), 1.54-1.50 (4H, m, CH_2CH_2N, $NHCH_2CH_2$), 1.25-1.22 (2H, m, $CH_2CH_2CH_2$), 0.89 (3H, s, Cq(CH_3)$_2$), 0.88 (3H, s, Cq(CH_3)$_2$). ^{13}C NMR ($CDCl_3$, 100 MHz) δ: 170.9 (*C*O), 169.4 (*C*O), 165.8 (CO), 134.6 (2 x C$H_{maleimide}$), 131.6 (NCH), 103.9 (*C*HCO), 76.6 (OCH), 70.9 (OCH_2), 47.0 (CH_2Cq), 35.7 (CH_2N), 34.1 (CH_2NH), 29.6 (CH_2CH_2N), 27.2 ($NHCH_2CH_2$), 22.6 ($CH_2CH_2CH_2$), 19.6 (Cq(CH_3)$_2$), 18.1 (Cq(CH_3)$_2$). HRMS (ESI) calculated for $C_{18}H_{27}N_3O_6$ [M+Na]$^+$: *m/z* 404.1792, found

m/z 404.1775. IR υ_{max}(neat)/cm^{-1}: 3300 (br), 2926 (m), 2854 (m), 1703 (s), 1641 (m), 1404 (m), 1166 (m), 694 (m).

(*R*)-**85**: $[\alpha]_D$ -44.000 (c= 1.0, acetone, T = 25.6 °C).

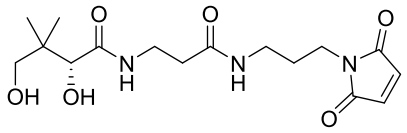

(*R*)-*N*-(3-((3-(2,5-Dioxo-2,5-dihydro-1*H*-pyrrol-1-yl)propyl)amino)-3-oxopropyl)-2,4-dihydroxy-3,3-dimethylbutanamide, 83.

A solution of (*R*)-*N*-(3-((3-(2,5-dioxo-2,5-dihydro-1*H*-pyrrol-1-yl)propyl)amino)-3-oxopropyl)-2,2,5,5-tetramethyl-1,3-dioxane-4-carboxamide **73** (90 mg, 230 μmol) in CH_3CN (3.0 mL) was treated with $BiCl_3$ (3 mg, 10 μmol), followed by H_2O (0.1 mL). The reaction mixture was then stirred at rt until completion by TLC analysis (24 h). The reaction was quenched by addition of five drops of sat. aq. $NaHCO_3$ and diluted with EtOAc (1 mL). The resulting suspension was filtered through a bed of celite, and the celite was washed with EtOAc (2x1 mL). The organic washes were combined, dried over Na_2SO_4, and concentrated under reduced pressure. Purification of the crude residue by flash column chromatography (0-5% 6M NH_3 in MeOH/CH_2Cl_2) afforded the expected diol **83** as a yellow oil (75 mg, 92%).

^{1}H NMR ($(CD_3)_2CO$, 400 MHz) δ: 7.64 (1H, br s, N*H*), 7.28 (1H, br s, N*H*), 6.88 (2H, s, C*H*$_{maleimide}$), 3.98 (1H, s, OCH), 3.93 (1H, br s, C*H*$_2$Cq), 3.57-3.43 (4H, m, NHC*H*$_2$, C*H*$_2$N), 3.40 (1H, br s, C*H*$_2$Cq), 3.24-3.15 (2H, m, NHC*H*$_2$), 2.41 (2H, t, *J* = 6.4 Hz, C*H*$_2$CO), 1.81-1.71 (2H, m, $CH_2CH_2CH_2$), 0.96 (3H, s, Cq(C*H*$_3$)$_2$), 0.87 (3H, s, Cq(C*H*$_3$)$_2$). ^{13}C NMR ($CDCl_3$, 100 MHz) δ: 177.3 (*C*O), 171.7 (*C*O), 171.1 (*C*O), 134.1 (2 x *C*H$_{maleimide}$), 76.3 (O*C*H), 75.7 (O*C*H$_2$), 40.9 (CH_2*Cq*), 39.3 (*C*H$_2$CO), 35.7 (*C*H$_2$N), 34.9 (HN*C*H$_2$), 31.9 (HN*C*H$_2$), 28.1 ($CH_2CH_2CH_2$), 22.9 (Cq(*C*H$_3$)$_2$), 18.7 (Cq(*C*H$_3$)$_2$). HRMS (ESI) calculated for $C_{16}H_{25}N_3O_6$ $[M+Na]^+$: *m/z* 378.1636, found *m/z* 378.1619. IR υ_{max} (neat)/cm^{-1}: 3300 (br), 2962 (m), 2931 (m), 1705 (s), 1651 (s), 1498 (m), 1004 (m).

83: $[\alpha]_D$ +56.220 (*c* = 3.7, acetone, T = 25.7 °C).

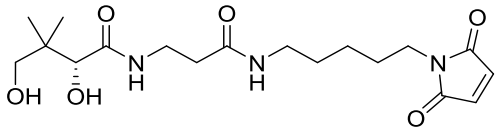

(*R*)-*N*-(3-((5-(2,5-Dioxo-2,5-dihydro-1*H*-pyrrol-1-yl)pentyl)amino)-3-oxopropyl)-2,4-dihydroxy-3,3-dimethylbutanamide, 86.

A solution of (*R*)-*N*-(3-((5-(2,5-dioxo-2,5-dihydro-1*H*-pyrrol-1-yl)pentyl)amino)-3-oxopropyl)-2,2,5,5-tetramethyl-1,3-dioxane-4-carboxamide **80** (100 mg, 0.23 mmol) in CH_3CN (1.6 mL) was treated with $BiCl_3$ (8 mg, 20 μmol), followed by H_2O (80 μL). The reaction mixture was then stirred at rt until completion by TLC analysis (24 h). The reaction was quenched by addition of five drops of sat. aq. $NaHCO_3$ and diluted with EtOAc (1 mL). The resulting suspension was filtered through a bed of

celite, and the celite was washed with EtOAc (2x2 mL). The organic washes were combined, dried over Na_2SO_4, and concentrated under reduced pressure. Purification of the crude residue by flash column chromatography (0-5% 6M NH_3 in MeOH/CH_2Cl_2) afforded the expected diol **86** as a yellow oil (43 mg, 47%).

^{1}H NMR ($(CD_3)_2CO$, 500 MHz) δ: 7.52 (1H, br, N*H*), 7.22 (1H, br, N*H*), 6.73 (2H, s, C$H_{maleimide}$), 4.81 (1H, br, O*H*), 3.80 (1H, s, OC*H*), 3.41-3.35 (2H, m, NHCH_2), 3.32 (2H, t, *J* = 5.6 Hz, CH_2N), 3.29 (1H, d, *J* = 8.4 Hz, CH_2Cq), 3.25 (1H, d, *J* = 8.8 Hz, CH_2Cq), 3.04 (2H, m, NHCH_2), 2.27 (2H, t, *J* = 5.2 Hz, CH_2CO), 1.45-1.36 (4H, m, CH_2CH$_2$N, NHCH$_2$CH_2), 1.18-1.15 (2H, m, CH$_2$CH_2CH$_2$), 0.81 (3H, s, Cq(CH$_3$)$_2$), 0.74 (3H, s, Cq(CH$_3$)$_2$). ^{13}C NMR ($(CD_3)_2CO$, 125 MHz) δ: 170.9 (CO), 170.8 (2 x CO), 134.2 (2 x C$H_{maleimide}$), 76.3 (OCH), 69.6 (OCH$_2$), 63.3 (CH$_2$*Cq*), 54.6 (CH$_2$N), 39.2 (*C*H$_2$CO), 38.8 (HN*C*H$_2$), 37.1 (HN*C*H$_2$), 28.5 (*C*H$_2$CH$_2$N), 28.0 (NHCH$_2$*C*H$_2$), 23.8 (CH$_2$*C*H$_2$CH$_2$), 21.1 (Cq(*C*H$_3$)$_2$), 19.8 (Cq(*C*H$_3$)$_2$). HRMS (ESI) calculated for $C_{18}H_{29}N_3O_6$ $[M+Na]^+$: m/z 406.1949, found m/z 406.1959. IR υ_{max} (neat)/cm^{-1}: 3310 (br), 2931 (m), 2870 (m), 1700 (s), 1646 (s), 1539 (s), 1043 (m), 829 (m).

86: $[\alpha]_D$ +13.023 (*c* = 4.3, acetone, T = 23.9 °C).

Bioconjugation of CJ-15,801 and pantothenic acid analogues with phiLOV(R475G,K476C).

General procedure

A solution of SUMO-tag-phiLOV(R475G,K476C) (10 mg, 0.7 mmol) in pH7 phosphates buffer (500 μL) was treated with a suspension of the desired CJ-15,801 or pantothenic acid analogue (12 mmol) in pH7 phosphates buffer (500 μL), and the resulting mixture was stirred at rt for 1 h. The reaction mixture was transfered into a plastic column, and treated with Strep-Tactin Superflow resin (1 mL) followed by pH8 buffer (150mM TRIS, 100mM NaCl; 1 mL). The column was sealed and incubated at 4 °C for 15 min on the rotor. The unreacted CJ-15,801 or pantothenate ligand was then eluted with pH8 buffer (150mM TRIS, 100mM NaCl; 4 mL). The protein attached to the resin was treated with SUMO protein (15 μL) followed by pH8 buffer (100mM TRIS, 150mM NaCl; 1 mL). The column was sealed and incubated at 4 °C for 18 h on the rotor. The resulting solution (now green color) was eluted on eppendorf tubes. The combined eluted solution was concentrated by centrifugation at 14000 rpm for 7 min (Amicon Ultra-4, centrifugal filters, ultracel-10K, Millipore tubes). The concentration was calculated by Bradford protein assay, and the phiLOV(R475G,K476C)-CJ-15,801 or pantothenate construct solutions were storaged at -80 °C.

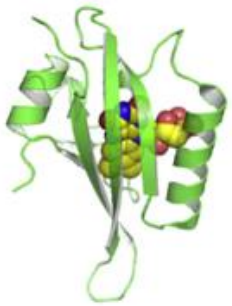

phiLOV(R475G,K476C)

HRMS (MALDI) calculated for phiLOV(R475G,K476C) $[M]^+$: *m/z* 12690.41, found *m/z* 12690.20.

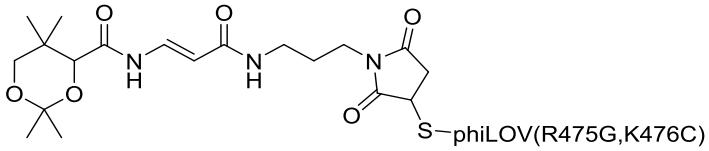

(*R,E*)-*N*-(3-((3-(2,5-Dioxo-2,5-dihydro-1*H*-pyrrol-1-yl)propyl)amino)-3-oxoprop-1-en-1-yl)-2,2,5,5-tetramethyl-1,3-dioxane-4-carboxamide coupled to phiLOV(R475G,K476C), (*R*)-90.

(*R*)-**90:** HRMS (MALDI) calculated for phiLOV(R475G,K476C)+$C_{19}H_{27}N_3O_6$ $[M-H]^+$: *m/z* 13082.60, found *m/z* 13082.16.

(*S,E*)-*N*-(3-((3-(2,5-Dioxo-2,5-dihydro-1*H*-pyrrol-1-yl)propyl)amino)-3-oxoprop-1-en-1-yl)-2,2,5,5-tetramethyl-1,3-dioxane-4-carboxamide coupled to phiLOV(R475G,K476C), (*S*)-92.

(*S*)-**92**: HRMS (MALDI) calculated for phiLOV(R475G,K476C)+$C_{19}H_{27}N_3O_6$ $[M+H]^+$: m/z 13084.60, found m/z 13084.41.

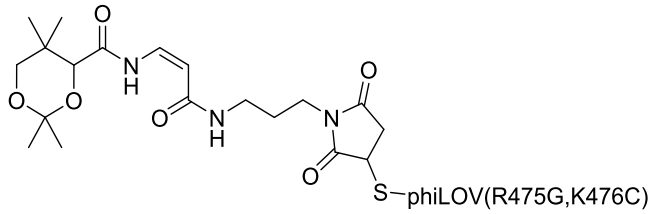

(*R,Z*)-*N*-(3-((3-(2,5-Dioxo-2,5-dihydro-1*H*-pyrrol-1-yl)propyl)amino)-3-oxoprop-1-en-1-yl)-2,2,5,5-tetramethyl-1,3-dioxane-4-carboxamide coupled to phiLOV(R475G,K476C), (*R*)-91.

(*R*)-**91**: HRMS (MALDI) calculated for phiLOV(R475G,K476C)+$C_{19}H_{27}N_3O_6$ $[M+H]^+$: *m/z* 13084.60, found *m/z* 13084.07

(*S,Z*)-*N*-(3-((3-(2,5-Dioxo-2,5-dihydro-1*H*-pyrrol-1-yl)propyl)amino)-3-oxoprop-1-en-1-yl)-2,2,5,5-tetramethyl-1,3-dioxane-4-carboxamide coupled to phiLOV(R475G,K476C), (*S*)-93.

(*S*)-**93**: HRMS (MALDI) calculated for phiLOV(R475G,K476C)+$C_{19}H_{27}N_3O_6$ $[M-H]^+$: *m/z* 13082.60, found *m/z* 13082.74.

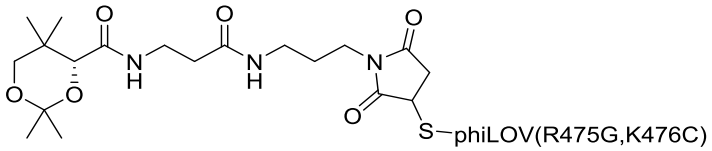

(*R*)-*N*-(3-((3-(2,5-Dioxo-2,5-dihydro-1*H*-pyrrol-1-yl)propyl)amino)-3-oxopropyl)-2,2,5,5-tetramethyl-1,3-dioxane-4-carboxamide coupled to phiLOV(R475G,K476C), 94.

94: HRMS (MALDI) calculated for phiLOV(R475G,K476C)+$C_{19}H_{29}N_3O_6$ [M-H]$^+$: *m/z* 13084.60, found *m/z* 13084.61.

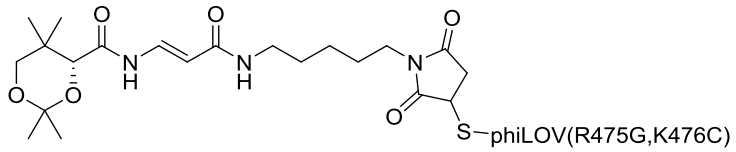

(*R,E*)-*N*-(3-((5-(2,5-Dioxo-2,5-dihydro-1*H*-pyrrol-1-yl)pentyl)amino)-3-oxoprop-1-en-1-yl)-2,2,5,5-tetramethyl-1,3-dioxane-4-carboxamide coupled to phiLOV(R475G,K476C), (*R*)-98.

(*R*)-**98**: HRMS (MALDI) calculated for phiLOV(R475G,K476C)+$C_{21}H_{31}N_3O_6$ [M+3H]$^+$: *m/z* 13114.63, found *m/z* 13114.57.

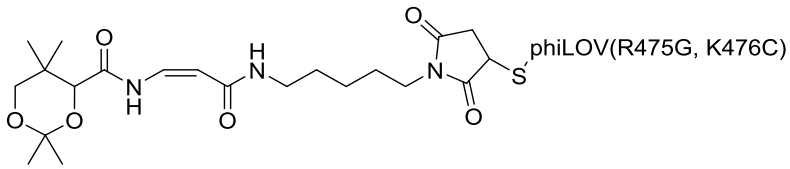

(*R,Z*)-*N*-(3-((5-(2,5-Dioxo-2,5-dihydro-1*H*-pyrrol-1-yl)pentyl)amino)-3-oxoprop-1-en-1-yl)-2,2,5,5-tetramethyl-1,3-dioxane-4-carboxamide coupled to phiLOV(R475G,K476C), (*R*)-99.

(*R*)-**99**: HRMS (MALDI)[68] calculated for phiLOV(R475G,K476C)+$C_{21}H_{31}N_3O_6$ [M+GE+Na]$^+$: *m/z* 13296.74, found *m/z* 13296.05.

(*S,Z*)-*N*-(3-((5-(2,5-Dioxo-2,5-dihydro-1*H*-pyrrol-1-yl)pentyl)amino)-3-oxoprop-1-en-1-yl)-2,2,5,5-tetramethyl-1,3-dioxane-4-carboxamide coupled to phiLOV(R475G,K476C), (*S*)-100.

(*S*)-**100**: HRMS (MALDI) calculated for phiLOV(R475G,K476C)+$C_{21}H_{31}N_3O_6$ [M-H]$^+$: *m/z* 13110.63, found *m/z* 13110.46.

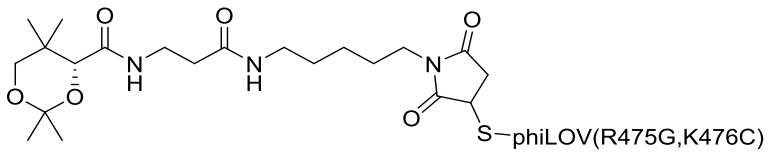

(*R*)-*N*-(3-((5-(2,5-Dioxo-2,5-dihydro-1*H*-pyrrol-1-yl)pentyl)amino)-3-oxopropyl)-2,2,5,5-tetramethyl-1,3-dioxane-4-carboxamide coupled to phiLOV(R475G,K476C), 101.

101: HRMS (MALDI) calculated for phiLOV(R475G,K476C)+$C_{21}H_{33}N_3O_6$ [M-2H]$^+$: *m/z* 13111.63, found *m/z* 13111.50.

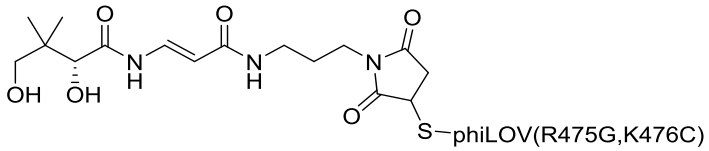

(*R,E*)-*N*-(3-((3-(2,5-Dioxo-2,5-dihydro-1*H*-pyrrol-1-yl)propyl)amino)-3-oxoprop-1-en-1-yl)-2,4-dihydroxy-3,3-dimethylbutanamide coupled to phiLOV(R475G,K476C), (*R*)-95.

(*R*)-**95**: HRMS (MALDI)[68] calculated for phiLOV(R475G,K476C)+$C_{16}H_{23}N_3O_6$ $[M+((C_2H_4O)_{17}+H_2O+H)]^+$: *m/z* 13811.03, found *m/z* 13811.03.

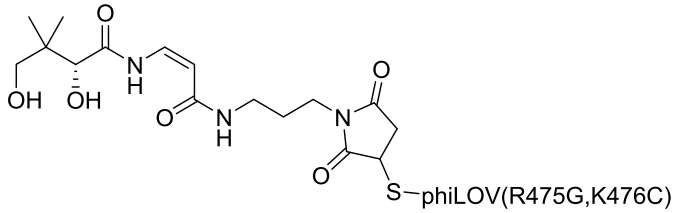

(*R,Z*)-*N*-(3-((3-(2,5-Dioxo-2,5-dihydro-1*H*-pyrrol-1-yl)propyl)amino)-3-oxoprop-1-en-1-yl)-2,4-dihydroxy-3,3-dimethylbutanamide coupled to phiLOV(R475G,K476C), (*R*)-96.

(*R*)-**96**: HRMS (MALDI) calculated for phiLOV(R475G,K476C)+$C_{16}H_{23}N_3O_6$ $[M+Na]^+$: *m/z* 13066.57, found *m/z* 13066.45.

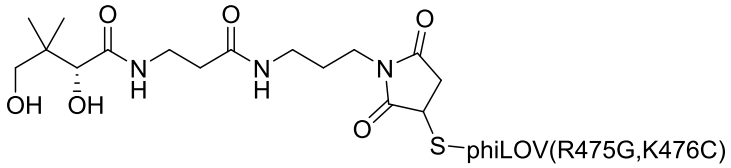

(*R*)-*N*-(3-((3-(2,5-Dioxo-2,5-dihydro-1*H*-pyrrol-1-yl)propyl)amino)-3-oxopropyl)-2,4-dihydroxy-3,3-dimethylbutanamide coupled to phiLOV(R475G,K476C), 97.

97: HRMS (MALDI) calculated for phiLOV(R475G,K476C)+$C_{16}H_{25}N_3O_6$ $[M-2H]^+$: *m/z* 13043.59, found *m/z* 13043.62.

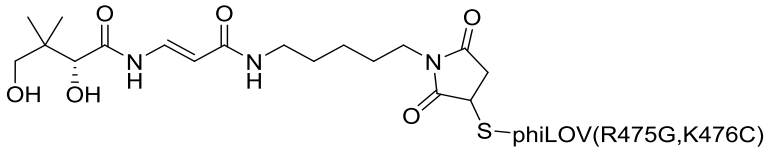

(*R,E*)-*N*-(3-((5-(2,5-Dioxo-2,5-dihydro-1*H*-pyrrol-1-yl)pentyl)amino)-3-oxoprop-1-en-1-yl)-2,4-dihydroxy-3,3-dimethylbutanamide coupled to phiLOV(R475G,K476C), (*R*)-102.

(*R*)-**102**: HRMS (MALDI)[69] calculated for phiLOV(R475G,K476C)+$C_{18}H_{27}N_3O_6$ $[M+Li]^+$: *m/z* 13078.61, found *m/z* 13078.68.

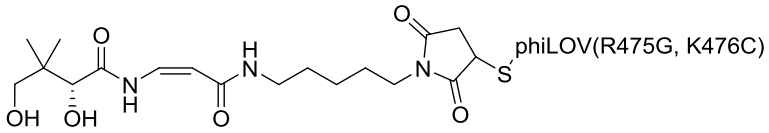

(*R,Z*)-*N*-(3-((5-(2,5-Dioxo-2,5-dihydro-1*H*-pyrrol-1-yl)pentyl)amino)-3-oxoprop-1-en-1-yl)-2,4-dihydroxy-3,3-dimethylbutanamide coupled to phiLOV(R475G,K476C), (*R*)-103.

(*R*)-**103**: HRMS (MALDI)[68] calculated for phiLOV(R475G,K476C)+$C_{18}H_{27}N_3O_6$ $[M+CH_2]^+$: *m/z* 13085.60, found *m/z* 13085.06.

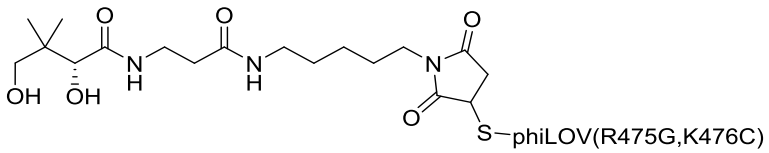

(*R*)-*N*-(3-((5-(2,5-Dioxo-2,5-dihydro-1*H*-pyrrol-1-yl)pentyl)amino)-3-oxopropyl)-2,4-dihydroxy-3,3-dimethylbutanamide coupled to phiLOV(R475G,K476C), 104.

104: HRMS (MALDI) calculated for phiLOV(R475G,K476C)+$C_{18}H_{29}N_3O_6$ $[M]^+$: *m/z* 13073.62, found *m/z* 13073.47.

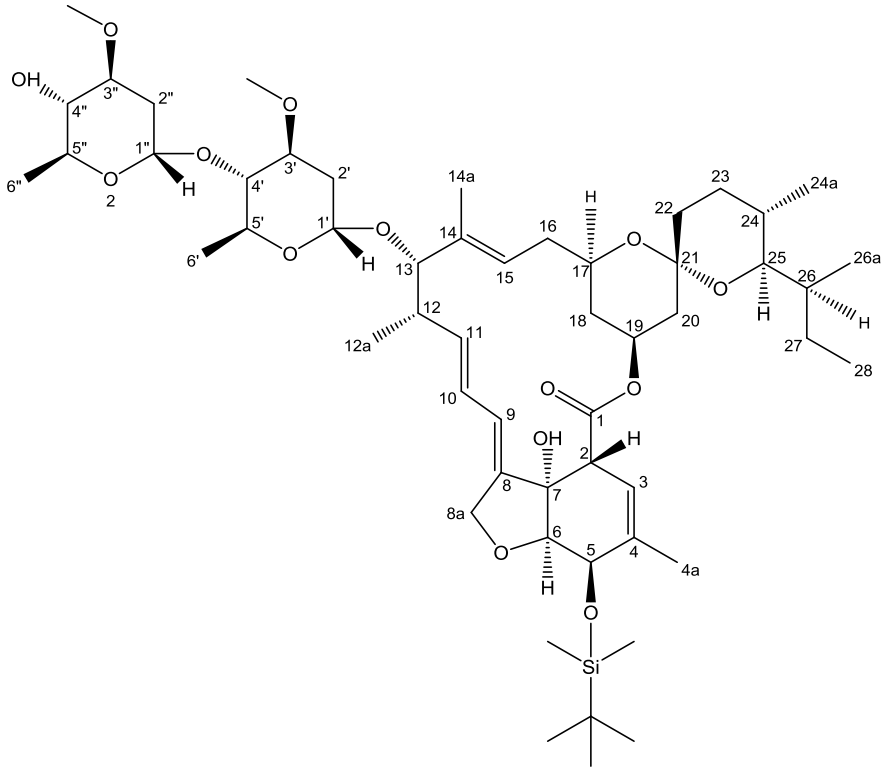

5-*O*-(*tert*-Butyldimethylsilyl)avermectin B_{1a}, 107.

A solution of ivermectin B_{1a} **105** (980 mg, 1.1 mmol) in anhydrous DMF (8.0 mL) was treated with imidazole (495 mg, 7.3 mmol), followed by a solution of TBDMSCl (560 mg, 3.28 mmol) in anhydrous DMF (2.0 mL). The reaction mixture was then stirred at rt until completion as indicated by TLC analysis (2.5 h). The reaction was then diluted with Et_2O (25 mL) followed by H_2O (15 mL), and the resulting emulsion was stirred for 0.5 h. The organic layer was separated, and aqueous phase was extracted with Et_2O (3x25 mL). The combined organics were washed with H_2O (5x100 mL) and brine (2x100 mL). The combined organic washes were dried over Na_2SO_4 and concentrated under reduced pressure. Purification of the crude residue by flash column chromatography (0-30% EtOAc/PE) yielded the expected product **107** as a white solid (638 mg, 58%). The NMR data matches the literature data for this compound.[74]

^{1}H NMR ($CDCl_3$, 400 MHz) δ: 5.83-5.78 (1H, m, C_9H), 5.73-5.69 (2H, m, $C_{10}H$,$C_{11}H$), 5.38 (1H, d, *J* = 3.2 Hz, $C_{1''}H$), 5.32 (1H, br s, C_3H), 5.29-5.28 (1H, m, $C_{19}H$), 4.97 (1H, d, *J* = 9.6 Hz, $C_{15}H$), 4.76 (1H, d, *J* = 3.2 Hz, $C_{1'}H$), 4.67 (1H, d, *J* = 14.4 Hz, $C_{8a}H_2$), 4.56 (1H, d, *J* = 14.8 Hz, $C_{8a}H_2$), 4.42 (1H, br s, C_5H), 3.92(1H, br s, $C_{13}H$), 3.85-3.78 (2H, m, C_6H, $C_{5'}H$), 3.77-3.72 (1H, m, $C_{5''}H$), 3.68-3.57 (2H, m, $C_{17}H$, $C_{3'}H$), 3.50-3.45 (1H, m, $C_{3''}H$), 3.41 (3H, s, $C_{3'}OCH_3$), 3.40 (3H, s, $C_{3''}OCH_3$), 3.36 (1H, br s, C_2H), 3.25-3.19 (2H, m, $C_{4'}H$, $C_{25}H$), 3.14 (1H, appt, *J* = 8.8 Hz, $C_{4''}H$), 2.53 (1H, appt, *J* = 6.8 Hz, $C_{12}H$), 2.35-2.29 (2H, m, $C_{2''}H_2$, $C_{16}H_2$), 2.28-2.25 (1H, m, $C_{16}H_2$), 2.21 (1H, dd, *J* = 13.2, 5.0 Hz, $C_{2'}H_2$), 1.98 (1H, dd, *J* = 12.0, 4.4 Hz, $C_{20}H_2$), 1.77 (3H, s, $C_{4a}H_3$), 1.74-1.71 (1H, m, $C_{18}H_2$), 1.64 (1H, d, *J* = 11.1 Hz, $C_{22}H_2$), 1.59-1.52 (7H, m, $C_{22}H_2$, $C_{23}H_2$, $C_{24}H$, $C_{2''}H_2$, $C_{2'}H_2$, $C_{26}H$), 1.49 (3H, s, $C_{14a}H_3$), 1.47-1.39 (2H, m, $C_{27}H_2$), 1.33 (1H, appt, *J* = 12.0 Hz, $C_{20}H_2$), 1.26 (3H, br s, $C_{6''}H_3$), 1.25

(3H, br s, $C_{6'}H_3$), 1.14 (3H, d, J = 6.8 Hz, $C_{12a}H_3$), 0.96-0.92 (3H, m, $C_{28}H_3$), 0.91 (9H, s, SiCq(CH_3)$_3$), 0.87-0.81 (4H, m, $C_{18}H_2$, $C_{26a}H_3$), 0.76 (3H, d, J = 4.4 Hz, $C_{24a}H_3$), 0.12 (6H, s, Si(CH_3)$_2$). ^{13}C NMR ($CDCl_3$, 100 MHz) δ: 174.0 (C_1O), 140.2 (Cq_8), 137.5 (C_{11}H), 137.4 (Cq_4), 135.0 (Cq_{14}), 124.8 (C_{10}H), 119.3 (C_9H), 118.3 (C_3H), 117.3 (C_{15}H), 98.4 ($C_{1'}$H), 97.4 (Cq_{21}), 94.7 ($C_{1'}$H), 81.8 (C_{13}H), 80.3 ($C_{4'}$H), 80.2 (Cq_7), 80.0 (C_6H), 79.3 ($C_{3'}$H), 78.1 ($C_{3''}$H), 76.5 ($C_{4''}$H), 76.0 (C_{25}H), 69.4 (C_{17}H), 68.6 ($C_{5''}$H), 68.1(C_{19}H), 67.9 ($C_{8a}H_2$), 67.2 (2 x C_5H,$C_{5'}$H), 56.4 ($C_{3''}OCH_3$), 56.3 ($C_{3'}OCH_3$), 45.7 (C_2H), 41.1 ($C_{20}H_2$), 39.6 (C_{12}H), 36.8 ($C_{18}H_2$), 35.7($C_{2'}H_2$), 35.4 (2 x C_{26}H, C_{24}H), 34.5 ($C_{2''}H_2$), 34.1 (2 x $C_{23}H_2$, $C_{16}H_2$), 31.2 (C_{22}H), 27.3 ($C_{27}H_2$), 26.8 (SiCq), 25.8 (3 x Cq(CH_3)$_3$), 20.2 ($C_{12a}H_3$), 20.0 ($C_{4a}H_3$), 18.4 ($C_{6'}H_3$), 17.6 (C_6H_3), 17.4 ($C_{24a}H_3$), 15.1 ($C_{14a}H_3$), 12.4 ($C_{26a}H_3$), 12.0 ($C_{28}H_3$), -4.6 (SiCH_3), -4.8 (SiCH_3).

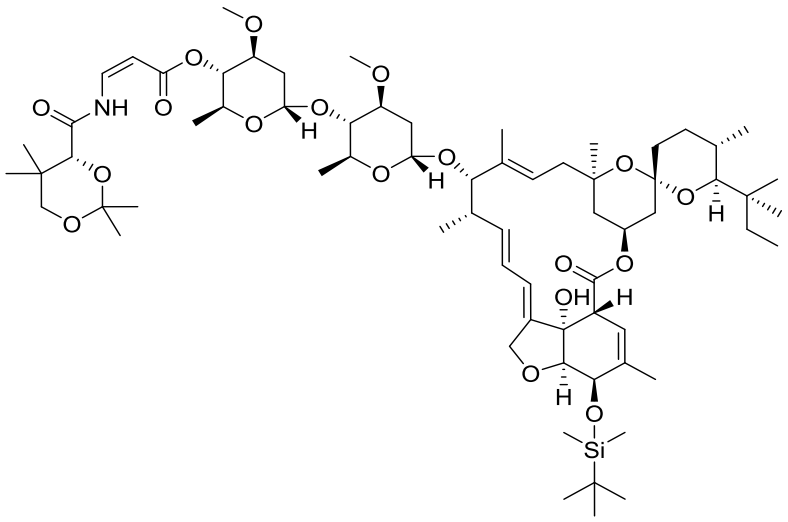

4''-*O*-[(*R,Z*)-3-(2,2,5,5-Tetramethyl-1,3-dioxane-4-carboxamido)acrylate]-5-*O*-(*tert*-butyldimethylsilyl)avermectin B_{1a}, 108.

A solution of 5-*O*-(*tert*-butyldimethylsilyl)avermectin B_{1a} **107** (45 mg, 40 μmol) in CH_2Cl_2 (1 mL) was treated sequentially with DCC (19 mg, 90 μmol), followed by DMAP (10 mg, 80 μmol), and solution of (*R,Z*)-3-(2,2,5,5-tetramethyl-1,3-dioxane-4-carboxamido)acrylic acid **54** (10 mg, 40 μmol) in CH_2Cl_2 (1.5 mL). The resulting reaction mixture was then stirred at rt until completion by TLC analysis (18 h). The reaction was then diluted with CH_2Cl_2 (5 mL), and washed with 1M HCl (7 mL), followed by sat. aq. $NaHCO_3$ (7 mL) and brine (7 mL). The organic layer was dried over Na_2SO_4 and concentrated under reduced pressure. Purification of the crude residue by flash column chromatography (0-10% EtOAc/PE) afforded the expected avermectin derived complex **108** as a colourless oil (30 mg, 61%).

^{1}H NMR ($CDCl_3$, 400 MHz) δ: 11.12 (1H, d, J = 11.6 Hz, NH), 7.52-743 (1H, m, NCH), 5.87-5.82 (1H, m, C_9H), 5.79-5.71 (2H, m, $C_{10}H$,$C_{11}H$), 5.42 (1H, br s, C_3H), 5.36-5.31 (2H, m, $C_{19}H$, $C_{1''}H$), 5.19 (1H, d, J = 8.9 Hz, CHCO$_2$), 5.00 (1H, d, J = 9.9 Hz, $C_{15}H$), 4.79 (1H, br s, $C_{1'}H$), 4.77 (1H, appt, J = 9.6 Hz, $C_{4''}H$), 4.70 (1H, d, J = 14.6 Hz, $C_{8a}H_2$), 4.60 (1H, d, J = 14.5 Hz, $C_{8a}H_2$), 4.46 (1H, br s, C_5H), 4.22 (1H, s, OCH), 3.96 (1H, br s, $C_{13}H$), 3.92-3.83 (3H, m, C_6H, $C_{5'}H$, $C_{5''}H$), 3.73 (1H, d, J =

11.7 Hz, CH_2Cq), 3.70-3.60 (3H, m, $C_{17}H$, $C_{3'}H$, $C_{3''}H$), 3.45 (3H, s, $C_{3'}OCH_3$), 3.42-3.38 (4H, m, C_2H, $C_{3''}OCH_3$), 3.34 (1H, d, *J* = 11.7 Hz, CH_2Cq), 3.28-3.20 (2H, m, $C_{25}H$, $C_{4'}H$,), 2.53 (1H, br s, $C_{12}H$), 2.38-2.32 (2H, m, $C_{2''}H_2$, $C_{16}H_2$), 2.31-2.22 (2H, m, $C_{16}H_2$, $C_{2'}H_2$), 2.00 (1H, dd, *J* = 11.7, 3.8 Hz, $C_{20}H_2$), 1.81 (3H, s, $C_{4a}H_3$), 1.79-1.62 (9H, m, $C_{18}H_2$, 2 x $C_{22}H_2$, 2 X $C_{23}H_2$, $C_{24}H$, $C_{2''}H_2$, $C_{2'}H_2$, $C_{26}H$,),1.59 (3H, s, Cq(CH_3)$_2$), 1.47 (3H, s, $C_{14a}H_3$), 1.44-1.41 (5H, br s, Cq(CH_3)$_2$, $C_{27}H_2$), 1.37 (1H, t, *J* = 12.4 Hz, $C_{20}H_2$), 1.28 (3H, br s, $C_{6''}H_3$), 1.27 (3H, br s, $C_{6'}H_3$), 1.18 (3H, d, *J* = 6.3 Hz, $C_{12a}H_3$), 1.07 (3H, s, Cq(CH_3)$_2$), 1.05 (3H, s, Cq(CH_3)$_2$), 0.99-0.96 (3H, m, $C_{28}H_3$), 0.94 (9H, s, SiC(CH_3)$_3$), 0.88-0.85 (4H, m, $C_{26a}H_3$, $C_{18}H_2$), 0.81-0.79 (1H, m, $C_{24a}H_3$), 0.15 (6H, s, Si(CH_3)$_2$). ^{13}C NMR ($CDCl_3$, 100 MHz) δ: 174.0 (C_1O), 168.9 (*C*ONH), 167.2(CH*C*O), 140.3 (Cq_8), 137.5 (C_{11}H), 137.4 (Cq_4), 136.6 (N*C*H),135.0 (Cq_{14}), 124.8 (C_{10}H), 119.3 (C_9H), 118.3 (C_3H), 117.2 (C_{15}H), 99.3 (*C*HCO$_2$), 98.4 ($C_{1''}$H), 98.2 (*Cq*(CH$_3$)$_2$), 97.5 (Cq_{21}), 94.8 ($C_{1'}$H), 81.9 (C_{13}H), 80.8 ($C_{4'}$H), 80.2 (Cq_7), 80.0 (C_6H), 79.2 ($C_{3'}$H), 77.2 ($C_{3''}$H), 77.1 (O*C*H), 76.6 ($C_{4''}$H), 75.7 (C_{25}H), 75.6 ($C_{5''}$H), 71.3 (O*C*H$_2$), 69.5 (C_{17}H,), 68.7 (C_{19}H), 67.9 (C_{8a}H$_2$), 67.1 (2 x C_5H, $C_{5'}$H), 57.2 (C$_{3''}$O*C*H$_3$), 56.5 (C$_{3'}$O*C*H$_3$), 45.7 (C_2H), 41.1 (C_{20}H$_2$), 39.6 (C_{12}H), 36.8 (C_{18}H$_2$), 35.7 ($C_{2'}$H$_2$), 35.4 (2 x C_{26}H, C_{24}H), 35.2 ($C_{2''}$H$_2$), 34.5 (C_{16}H), 34.1 (C_{23}H$_2$), 33.3 (CH$_2$*Cq*), 31.2 (C_{22}H), 29.3 (Cq(*C*H$_3$)$_2$), 27.2 (C_{27}H$_2$), 26.9 (Si*Cq*), 25.8 (3 x Cq(*C*H$_3$)$_3$), 21.9 (Cq(*C*H$_3$)$_2$), 20.3 (C_{12a}H$_3$), 20.0 (C_{4a}H$_3$), 18.9 (Cq(*C*H$_3$)$_2$), 18.6 (Cq(*C*H$_3$)$_2$),18.4 ($C_{6''}$H$_3$), 17.4 ($C_{6'}$H$_3$), 17.4 (C_{24a}H$_3$), 15.2 (C_{14a}H$_3$), 12.4 (C_{26a}H$_3$), 12.1 (C_{28}H$_3$), -4.5 (Si*C*H$_3$), -4.8 (Si*C*H$_3$). HRMS (ESI) calculated for $C_{68}H_{109}NO_{18}Si$ $[M\text{-}CO_2]^+$: *m/z* 1211.7516, found *m/z* 1211.6699. IR υ_{max} (film)/ cm^{-1}: 3420 (br), 2945 (m), 2879 (m), 1775 (s), 1670 (s), 1550 (m), 1392 (m), 1128 (s).

108: $[\alpha]_D$ +12.210 (*c* = 0.7, $CHCl_3$, T = 23.1°C).

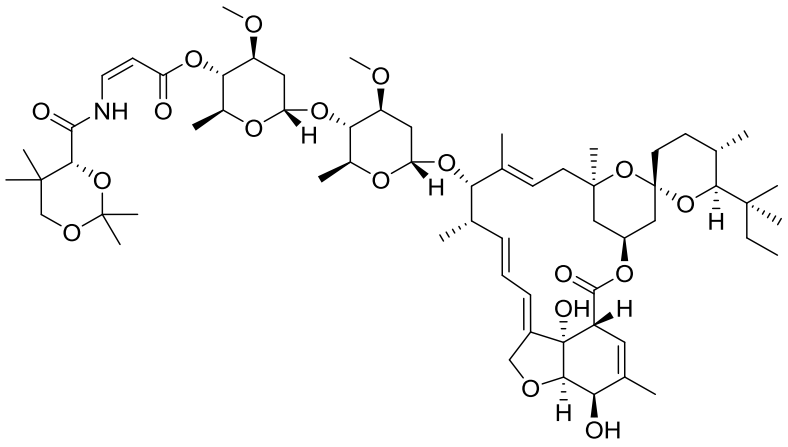

4”-*O*-[(*R,Z*)-3-(2,2,5,5-Tetramethyl-1,3-dioxane-4-carboxamido)acrylate]avermectin B$_{1a}$, 109.

A solution of 4”-*O*-[(*R,Z*)-3-(2,2,5,5-tetramethyl-1,3-dioxane-4-carboxamido)acrylate]-5-*O*-(*tert*-butyldimethylsilyl)avermectin B_{1a} **108** (30 mg, 20 μmol) in MeOH (2.5 mL) was treated with a catalytic amount of *p*-TsOH (3 mg). The reaction mixture was then stirred at 18 °C for 30 min, and was then diluted with H_2O (17 mL) and EtOAc (20 mL). The phases were separated, and the organic layer was washed with H_2O (3x20 mL) and brine (20 mL). The organic phase was dried over Na_2SO_4, and concentrated under reduced pressure. Purification of the crude residue by flash column

chromatography (0-3% MeOH/ CH_2Cl_2) afforded *cis*-CJ-15,801-ivermectin B_{1a} complex **110** as a yellow oil (16 mg, 58%).

^{1}H NMR ($CDCl_3$, 400 MHz) δ: 11.27 (1H, d, *J* = 11.6 Hz, N*H*), 7.52 (1H, dd, *J* = 11.6, 9.6 Hz, NC*H*), 5.89 (1H, d, *J* = 9.2 Hz, C_9*H*), 5.82-5.69 (2H, m, C_{10}*H*,C_{11}*H*), 5.44 (1H, br s, C_3*H*), 5.42-5.32 (2H, m, C_{19}*H,* $C_{1''}$*H*), 5.23 (1H, d, *J* = 9.2 Hz, C*H*CO_2), 5.00 (1H, d, *J* = 10.0 Hz, C_{15}*H*), 4.80 (1H, br s, $C_{1'}$*H*), 4.75 (1H, d, *J* = 9.5 Hz, $C_{4''}$*H*), 4.72-4.65 (2H, m, C_{8a}*H*$_2$), 4.32 (1H, d, *J* = 6.0 Hz, C_5*H*), 4.23 (1H, s, OC*H*), 4.13 (1H, br s, C_7O*H*), 3.99 (2H, m, C_{13}*H,* C_6*H*), 3.92-3.84 (2H, m, $C_{5'}$*H,* $C_{5''}$*H*), 3.73-3.62 (4H, m, C_{17}*H*, $C_{3'}$*H*, $C_{3''}$*H,* C*H*$_2$Cq), 3.58 (1H, d, *J* = 6.8 Hz, C*H*$_2$Cq), 3.45 (3H, br s, $C_{3'}$OC*H*$_3$), 3.38 (3H, br s, $C_{3''}$OC*H*$_3$), 3.30 (1H, br s, C_2*H*), 3.28-3.21 (3H, m, C_{25}*H*, $C_{4'}$*H*), 2.54 (1H, br s, C_{12}*H*), 2.39-2.32 (2H, m, $C_{2''}$*H*$_2$, C_{16}*H*$_2$), 2.32-2.22 (2H, m, C_{16}*H*$_2$, $C_{2'}$*H*$_2$), 2.00 (1H, dd, *J* = 12.0, 4.4 Hz, C_{20}*H*$_2$), 1.89 (3H, s, C_{4a}*H*$_3$),1.77 (1H, d, *J* = 11.6 Hz, C_{22}*H*$_2$), 1.67 (1H, d, J = 9.6 Hz, C_{18}*H*$_2$), 1.62-1.47 (16H, m, C_{22}*H*$_2$, 2 x C_{23}*H*$_2$, C_{24}*H*, $C_{2''}$*H*$_2$, $C_{2'}$*H*$_2$, C_{26}*H*, C_{14a}*H*$_3$, Cq(C*H*$_3$)$_2$), 1.47-1.34 (3H, m, 2 x C_{27}*H*$_2$, C_{20}*H*$_2$), 1.29-1.25 (3H, m, $C_{6''}$*H*$_3$), 1.20-1.15 (6H, m, C_{12a}*H*$_3$, $C_{6'}$*H*$_3$), 1.07 (3H, s, Cq(C*H*$_3$)$_2$), 1.00 (3H, s, Cq(C*H*$_3$)$_2$), 0.95 (3H, t, *J* = 7.2 Hz C_{28}*H*$_3$), 0.87 (3H, d, *J* = 6.6 Hz, C_{26a}*H*$_3$), 0.83-0.78 (4H, m, C_{18}*H*$_2$, C_{24a}*H*$_3$). ^{13}C NMR ($CDCl_3$, 100 MHz) δ: 174.0 (*C*$_1$O), 168.9 (*C*ONH), 167.2(CH*C*O), 140.3 (*Cq*$_8$), 138.0 (*C*$_{11}$H), 137.9 (*Cq*$_4$), 137.2 (NCH),135.0 (*Cq*$_{14}$), 124.7 (*C*$_{10}$H), 120.4 (*C*$_9$H), 118.3 (*C*$_3$H), 118.0 (*C*$_{15}$H), 107.0 (*Cq*$_{21}$), 98.5 (*Cq*(CH$_3$)$_2$), 98.3 (*C*$_{1''}$H), 97.4 (*C*HCO$_2$), 94.8 (*C*$_{1'}$H), 81.8 (*C*$_{13}$H), 80.7(*C*$_4$H), 80.4 (*Cq*$_7$), 79.2 (*C*$_{3'}$H), 79.0 (*C*$_6$H), 77.9 (*C*$_{3''}$H), 77.2 (OCH), 76.3 (*C*$_{4''}$H), 75.8 (*C*$_{25}$H), 75.7 (*C*$_{5''}$H), 71.3 (O*C*H$_2$), 68.6 (*C*$_{17}$H), 68.5 (*C*$_{8a}$H$_2$), 67.7 (*C*$_5$H), 67.2 (*C*$_{19}$H), 67.1 (*C*$_{5'}$H), 57.1 ($C_{3''}$O*C*H$_3$), 56.5 ($C_{3'}$O*C*H$_3$), 45.7 (*C*$_2$H), 41.1 (*C*$_{20}$H$_2$), 39.7 (*C*$_{12}$H), 36.9 (*C*$_{18}$H$_2$), 35.7 (*C*$_{2''}$H$_2$), 35.4 (*C*$_{26}$H), 35.1 (*C*$_{2'}$H$_2$), 34.5 (*C*$_{16}$H$_2$), 34.1 (2 x *C*$_{23}$H$_2$,CH$_2$*Cq*), 31.2 (*C*$_{24}$H), 28.0 (*C*$_{22}$H$_2$), 27.2 (*C*$_{27}$H$_2$), 22.9 (Cq(*C*H$_3$)$_2$), 20.8 (Cq(*C*H$_3$)$_2$), 20.5 (*C*$_{12a}$H$_3$), 20.2 (*C*$_{4a}$H$_3$), 20.0 (Cq(*C*H$_3$)$_2$), 18.8 (Cq(*C*H$_3$)$_2$), 18.4 ($C_{6''}$H$_3$), 17.4 (2 x C_{24a}H$_3$, $C_{6'}$H$_3$), 15.1 (*C*$_{14a}$H$_3$), 12.4 (*C*$_{26a}$H$_3$), 12.1 (*C*$_{28}$H$_3$). HRMS (ESI) calculated for $C_{62}H_{95}NO_{18}$ [M-CO_2]$^+$: *m/z* 1097.6651, found *m/z* 1097.1176. IR υ_{max} (film)/cm^{-1}: 3680 (br), 2947 (m), 2879 (m), 1783 (s), 1645 (m), 1498 (m), 1288 (m).

109: [α]$_D$ +4.500 (*c* = 0.2, $CHCl_3$, T = 23.0°C).

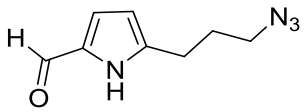

5-(3-Azidopropyl)-1*H*-pyrrole-2-carbaldehyde, 110.

Anhydrous DMF (20 mL) was cooled down to 0 °C and was then treated with $POCl_3$ (0.6 mL, 6.6 mmol). The resulting solution was then stirred at 0 °C for 5 min., and then at rt for an additional 30 min. The reaction was then cooled back down to 0 °C, and treated with a solution of 2-(3-azidopropyl)-1*H*-pyrrole **34** (805 mg, 5.3 mmol) in anhydrous DMF (2 mL). The mixture was then heated to 40 °C until completion by TLC analysis (18 h). The reaction was cooled back down to rt, and diluted with EtOAc (5 mL), and treated with 4M aq. NaOH solution (5 mL). The phases were separated, and the aqueous layer was extracted with EtOAc (3x5 mL). The combined organic layers

were washed with H_2O (5x20 mL), brine (2x20 mL) and dried over Na_2SO_4. The resulting solution was concentrated under reduced pressure, to afford the desired aldehyde **110** as a brown oil (490 mg, 51%). The product was used without further purification.

^{1}H NMR ($CDCl_3$, 400 MHz) δ: 9.95 (1H, br s, N*H*), 9.41 (1H, s, C*H*O), 6.93-6.91 (1H, m, ArC$H_{pyrrole}$), 6.13-6.12 (1H, m, ArC$H_{pyrrole}$), 3.01 (2H, t, *J* = 8.0 Hz, CH_2N_3), 2.72 (2H, t, *J* = 7.0 Hz, CqCH_2), 1.8-1.6 (2H, m, $CH_2CH_2CH_2$). ^{13}C NMR ($CDCl_3$, 100 MHz) δ: 178.3 (CO), 129.7 (Ar*C*q), 128.5 (Ar*C*q), 127.8 (Ar*C*H), 109.6 (Ar*C*H), 60.4 (*C*H_2N_3), 28.0 ($CH_2CH_2CH_2$), 24.4 (Cq*C*H_2). HRMS (ESI) calculated for $C_8H_{10}N_4O$ $[M]^+$: *m/z* 178.0855, found *m/z* 178.0851. IR υ_{max} (film)/cm^{-1}: 3233 (br), 2831 (m), 2099 (m), 1735 (s), 1653 (s), 1376 (m).

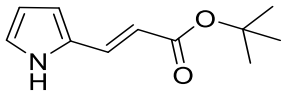

***tert*-Butyl (*E*)-3-(1*H*-pyrrol-2-yl)acrylate, 134.**

A solution of pyrrole-2-carboxaldehyde **34** (1.5 g, 15.2 mmol) in benzene (110 mL) was treated with (*tert*-butoxycarbonylmethylene)triphenylphosphorane **133** (10.0 g, 26.5 mmol). The reaction mixture was heated to 80 ^{o}C until completion by TLC analysis (22 h). The reaction was then cooled to rt, and concentrated under reduced pressure. Purification of the crude residue by flash column chromatography (0-20% EtOAc/PE) afforded the expected product **134** as an orange oil (2.45 g, 83%).

^{1}H NMR ($CDCl_3$, 400 MHz) δ: 9.00 (1H, br s, N*H*), 7.49 (1H, d, *J* = 16.0 Hz, CqC*H*), 6.92 (1H, apps, ArC$H_{pyrrole}$), 6.55 (1H, apps, ArC$H_{pyrrole}$), 6.29 (1H, apps, ArC$H_{pyrrole}$), 6.01 (1H, d, *J* = 16.0 Hz, C*H*CO), 1.55 (9H, s, Cq(CH_3)$_3$). ^{13}C NMR ($CDCl_3$, 100 MHz) δ: 167.1 (CO), 133.3 (Cq*C*H), 128.5 (Ar*C*q), 122.0 (*C*HCO), 113.7 (ArC*H*), 113.3 (ArC*H*), 110.8 (ArC*H*), 80.2 (*C*q(CH$_3$)$_3$), 28.2 (3 x Cq(*C*H$_3$)$_3$). HRMS (ESI) calculated for $C_{11}H_{15}NO_2$ $[M+Na]^+$: *m/z* 216.0995, found *m/z* 216.0966. IR υ_{max} (film)/cm^{-1}: 3358 (m), 2919 (m), 2848 (m), 1713 (m), 1632 (s), 1150 (m).

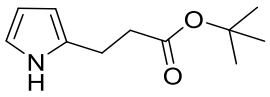

***tert*-Butyl 3-(1*H*-pyrrol-2-yl)propanoate, 111.**

A solution of (*E*)-3-(1*H*-pyrrol-2-yl)acrylate **134** (2.4 g, 12.4 mmol) in anhydrous MeOH (95 mL) was stirred for 5 minutes under an argon atmosphere. Pd/C (10%, 160 mg, 7 mol%) was added to the solution, and the reaction placed under a hydrogen atmosphere, and stirred at rt until completion by TLC analysis (18 h). The reaction was filtered through a celite bed, and washed with MeOH (2x25 mL). The organic phases were combined, and concentrated *in vacuo* to afford the desired ester **111** as a brown oil (2.23 g, 92%). The product obtained required no further purification.

^{1}H NMR ($CDCl_3$, 400 MHz) δ: 8.62 (1H, br s, N*H*), 6.69 (1H, apps, ArC$H_{pyrrole}$), 6.12 (1H, appd, *J* = 2.4 Hz ArC$H_{pyrrole}$), 5.93 (1H, apps, ArC$H_{pyrrole}$), 2.89 (2H, t, *J* = 6.4 Hz, CqCH_2), 2.57 (2H, t, *J* = 6.4 Hz, CH_2CO), 1.47 (9H, s, Cq(CH_3)$_3$). ^{13}C NMR ($CDCl_3$, 100 MHz) δ: 173.6 (*C*O), 131.3 (Ar*Cq*), 116.7 (Ar*C*H), 107.8 (Ar*C*H), 105.4 (Ar*C*H), 80.7 (*Cq*(CH_3)$_3$), 35.7 (*C*H_2CO), 28.1 (3 x Cq(*C*H_3)$_3$), 22.6 (Cq*C*H_2). HRMS (ESI) calculated for $C_{11}H_{17}NO_2$ $[M+Na]^+$: *m/z* 218.1151, found *m/z* 218.1168. IR υ_{max} (film)/cm^{-1}: 3394 (m), 2919 (m), 2848 (m), 1644 (m).

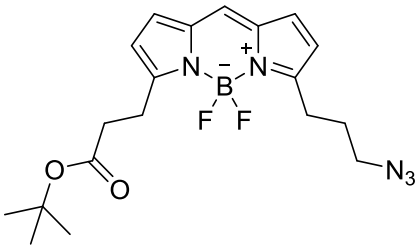

***tert*-Butyl 3-(5-(3-azidopropyl)-4,4-difluoro-4-bora-3a,4a-diaza-*s*-indacene-3-yl)propanoate, 112.**

A 0 °C solution of 5-(3-azidopropyl)-1*H*-pyrrole-2-carbaldehyde **110** (330 mg, 1.9 mmol) in CH_2Cl_2 (8 mL), was treated with a solution *tert*-butyl 3-(1*H*-pyrrol-2-yl)propanoate **111** (346 mg, 1.8 mmol) in CH_2Cl_2 (2 mL). The resulting mixture was then treated by the dropwise addition of $POCl_3$ (150 µL, 1.5 mmol), and was then stirred at rt for 6.5 h before being cooled back down to 0 °C. The reaction mixture was then treated sequentially with $BF_3.Et_2O$ (0.9 mL, 7.2 mmol) followed by *N,N*-diisopropylethylamine (1.5 mL, 8.5 mmol). The mixture was then stirred at rt until completion by TLC analysis (18 h). The reaction was quenched with H_2O (10 mL), diluted with CH_2Cl_2 (5 mL) and filtered through a bed of celite. The celite was washed with CH_2Cl_2 (2x10 mL), and the organic phases combined. The combined organic washes were dried over Na_2SO_4, and concentrated under reduced pressure. Purification of the crude residue by flash column chromatography (0-15% EtOAc/PE) yielded the expected ester **112** as a red oil (71 mg, 9%).

^{1}H NMR ($CDCl_3$, 400 MHz) δ: 7.13 (1H, s, ArC$H_{BODIPY-C8}$), 7.00-6.92 (2H, m, ArC$H_{BODIPY-C1,C2}$), 6.37-6.34 (2H, m, ArC$H_{BODIPY-C6,C7}$), 3.35-3.27 (4H, m, CqCH_2, CH_2N_3), 2.80 (2H, t, *J* = 8.0 Hz, CqCH_2), 2.67 (2H, t, *J* = 8.0 Hz, CH_2CO), 1.46 (9H, s, Cq(CH_3)$_3$),1.27 (2H, appt, *J* = 7.2 Hz, $CH_2CH_2CH_2$).

^{13}C NMR ($CDCl_3$, 100 MHz) δ: 172.7 (CO), 161.6 (Ar*Cq*), 161.1 (Ar*C*q), 134.7 (Ar*C*q), 134.6 (Ar*C*q), 130.6 (Ar*C*H), 130.2 (Ar*C*H), 127.8 (Ar*C*H), 118.7 (Ar*C*H), 118.1 (Ar*C*H), 80.7 (*C*q(CH_3)$_3$), 51.8 (*C*H_2N_3), 34.2 (*C*H_2CO), 32.8 (*C*H_2Cq), 29.7 ($CH_2CH_2CH_2$), 28.2 (Cq(*C*H_3)$_3$), 24.2 (Cq*C*H_2). ^{19}F NMR ($CDCl_3$, 376 MHz) δ: -144.17, -144.26, -144.35, -144.44. HRMS (ESI) calculated for $C_{19}H_{24}BF_2N_5O_2$ $[M-N_3]^+$: *m/z* 361.1899, found *m/z* 361.3293. IR υ_{max} (film)/cm^{-1}: 3172 (m), 2978 (m), 2150 (w), 1733 (s), 1609 (s), 1490 (m), 1439 (s), 1155 (m).

λ_{exc}= 467 nm. (at 510 nm emission, c= 0.2 nM, MeOH).

λ_{emis}= 516 nm. (at 315 nm excitation, c= 0.2 nM, MeOH).

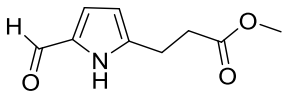

Methyl 3-(5-formyl-1*H*-pyrrol-2-yl)propanoate, 114.

Anhydrous DMF (10 mL) was cooled down to 0 °C and was treated with $POCl_3$ (0.6 mL, 6.6 mmol). The resulting solution was then stirred at 0 °C for 5 min., and then at rt for an additional 30 min. The reaction was cooled back down to 0 °C, and treated with a solution of methyl 3-(1*H*-pyrrol-2-yl)propanoate **36** (800 mg, 5.2 mmol) in anhydrous DMF (2 mL). The mixture was then heated to 40 °C until completion by TLC analysis (14 h). The reaction was cooled back down to rt and diluted with EtOAc (18 mL), and treated with 4M aq. NaOH solution (5 mL). The phases were separated, and the aqueous layer was extracted with EtOAc (3x18 mL). The combined organic layers were washed with H_2O (5x30 mL), brine (2x30 mL) and dried over Na_2SO_4. The resulting solution was concentrated under reduced pressure, to afford the desired aldehyde **114** as a brown oil (630 mg, 66%). The product was used without further purification.

^{1}H NMR ($CDCl_3$, 400 MHz) δ: 10.01 (1H, br, N*H*), 9.42 (1H, s, C*H*O), 6.89 (1H, appt, *J* = 4.0 Hz, ArC$H_{pyrrole}$), 6.1-6.0 (1H, appt, *J* = 4.0 Hz, ArC$H_{pyrrole}$), 3.73 (3H, s, OCH_3), 3.02 (2H, t, *J* = 7.0 Hz, Cq*C*H_2), 2.72 (2H, t, *J* = 7.1 Hz, CH_2CO). ^{13}C NMR ($CDCl_3$, 100 MHz) δ: 178.4 (*C*O), 173.3 (*C*O), 116.8 (Ar*C*q), 132.3 (Ar*C*q), 122.1 (Ar*C*H), 109.6 (Ar*C*H), 52.0 (O*C*H_3), 33.3 (*C*H_2CO), 22.8 (Cq*C*H_2). HRMS (ESI) calculated for $C_9H_{11}NO_3$ $[M+H]^+$: *m/z* 182.0739, found *m/z* 182.0828. IR υ_{max} (film)/ cm^{-1}: 3248 (br), 2924 (m), 2853 (m), 1735 (s), 1647 (m).

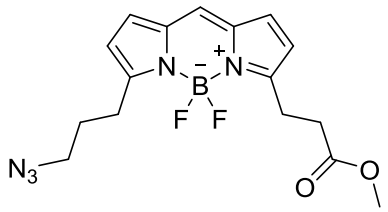

Methyl 3-[3-(3-azidopropyl)-4, 4-difluoro-4-bora-3a,4a-diaza-*s*-indacene-5-yl]propanoate, 115.

A 0 °C solution of 2-(3-azidopropyl)-1*H*-pyrrole **39** (100 mg, 0.7 mmol) in CH_2Cl_2 (5 mL), was treated with a solution of 3-(5-formyl-1*H*-pyrrol-2-yl)propanoate **114** (60 mg, 0.3 mmol) in CH_2Cl_2 (5 mL). The resulting mixture was then treated by the dropwise addition of $POCl_3$ (100 µL, 1.0 mmol), and was then stirred at rt for 6.5 h before being cooled back down to 0 °C. The reaction mixture was then treated sequentially with $BF_3.Et_2O$ (0.2 mL, 1.6 mmol) followed by *N,N*-diisopropylethylamine (0.3 mL, 1.7 mmol). The reaction was stirred at rt until completion by TLC analysis (18 h). The reaction mixture was then quenched with H_2O (10 mL), diluted with CH_2Cl_2 (5 mL) and filtered through a bed of celite. The celite was washed with CH_2Cl_2 (2x10 mL), and the organic phases combined. The combined organic washes were dried over Na_2SO_4, and concentrated under reduced pressure. Purification of the crude residue by flash column chromatography (0-30% EtOAc/PE) yielded the expected ester **115** as a red oil (31 mg, 26%).

^{1}H NMR ($CDCl_3$, 400 MHz) δ: 7.15 (1H, s, ArC*H*$_{BODIPY-C8}$), 7.04 (1H, d, *J* = 4.0 *Hz*, ArC*H*$_{BODIPY-C1}$), 7.01 (1H, d, *J* = 4.4 *Hz*, ArC*H*$_{BODIPY-C2}$), 6.3 (2H, appt, *J* = 4.0 *Hz*, ArC*H*$_{BODIPY-C6,C7}$), 3.72 (3H, s, OC*H*$_3$), 3.42 (2H, t, *J* = 6.8 Hz, C*H*$_2$N$_3$), 3.34 (2H, t, *J* = 7.6 Hz, C*H*$_2$Cq), 3.09 (2H, t, *J* = 7.6 Hz, C*H*$_2$Cq), 2.81 (2H, t, *J* = 7.6 Hz, C*H*$_2$CO), 2.09-2.02 (2H, m, $CH_2CH_2CH_2$). ^{13}C NMR ($CDCl_3$, 100 MHz) δ: 164.6 (*C*O), 159.9 (Ar*Cq*), 156.5 (Ar*C*q), 146.8 (Ar*C*q), 140.1 (Ar*C*q), 134.9 (Ar*C*H), 128.3 (Ar*C*H), 127.9 (Ar*C*H), 120.9 (Ar*C*H), 114.7 (Ar*C*H), 51.8 (O*C*H$_3$), 50.8 (*C*H$_2$N$_3$), 34.7 (*C*H$_2$CO), 28.0 ($CH_2CH_2CH_2$), 25.4 (*C*H$_2$Cq), 21.4 (Cq*C*H$_2$). ^{19}F NMR ($CDCl_3$, 376 MHz) δ: -143.7, -143.8, -143.9, -144.0. HRMS (ESI) calculated for $C_{16}H_{18}BF_2N_5O_2$ [M-H]$^+$: *m/z* 360.1522, found *m/z* 360.3250. IR υ_{max} (film)/cm^{-1}: 3171 (m), 2936 (m), 2098 (m), 1734 (s), 1609 (m), 1497 (m), 1175 (m).

λ_{exc}= 467 nm (at 510 nm emission, c= 0.2 nM, MeOH).

λ_{emis}= 509 nm (at 315 nm excitation, c= 0.2 nM, MeOH).

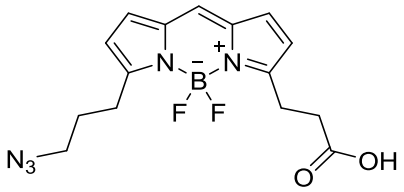

3-[3-(3-Azidopropyl)-4,4-difluoro-4-bora-3a,4a-diaza-*s*-indacene-5-yl]propionic acid, 113.

A 0 °C solution of methyl 3-[3-(3-azidopropyl)-4,4-difluoro-4-bora-3a,4a-diaza-*s*-indacene-5-yl]propanoate **115** (30 mg, 80 μmol) in THF (4 mL) was treated with H_2O (2.6 mL), followed by conc. HCl (1.6 mL). The reaction mixture was then stirred at rt until completion by TLC analysis (18 h). The reaction mixture was then diluted with CH_2Cl_2 (20 mL), and stirred at rt for 1 h. The organic layer was separated, and washed with H_2O (2x20 mL) followed by brine (2x25 mL). The resulting solution was dried over Na_2SO_4, and concentrated under reduced pressure to afford the expected carboxylic acid **113** as a red oil (15 mg, 52%). The product was used without further purification.

^{1}H NMR ($CDCl_3$, 400 MHz) δ: 7.16 (1H, s, ArC*H*$_{BODIPY-C8}$), 7.05 (1H, d, *J* = 4.0 Hz, ArC*H*$_{BODIPY-C1}$), 7.01 (1H, d, *J* = 3.2 Hz, ArC*H*$_{BODIPY-C2}$), 6.39-6.38 (2H, m, ArC*H*$_{BODIPY-C6,C7}$), 3.42 (2H, t, *J* = 6.8 Hz, C*H*$_2$N$_3$), 3.35 (2H, t, *J* = 7.6 Hz, C*H*$_2$Cq), 3.10 (2H, t, *J* = 7.6 Hz, C*H*$_2$Cq), 2.86 (2H, t, *J* = 7.6 Hz, C*H*$_2$CO), 2.10-2.02 (2H, m, $CH_2CH_2CH_2$). ^{13}C NMR ($CDCl_3$, 100 MHz) δ: 166.2 (CO), 161.6 (Ar*Cq*), 159.9 (Ar*Cq*), 153.1 (Ar*C*q), 149.0 (Ar*C*q), 134.9 (Ar*C*H), 130.8 (Ar*C*H), 128.8 (Ar*C*H), 127.9 (Ar*C*H), 118.5 (Ar*C*H), 50.9 (*C*H$_2$N$_3$), 31.9 ($CH_2CH_2CH_2$), 30.5 (*C*H$_2$CO), 26.0 (*C*H$_2$Cq), 23.8 (Cq*C*H$_2$). ^{19}F NMR ($CDCl_3$, 376 MHz) δ: -143.75, -143.84, -143.92, -144.01. HRMS (ESI) calculated for $C_{15}H_{16}BF_2N_5O_2$ [M-H]$^+$: *m/z* 346.1365, found *m/z* 346.3293. IR υ_{max} (film)/cm^{-1}: 3423 (br s), 2915 (m), 2850 (m), 1644 (s).

λ_{exc}= 467 nm (at 510 nm emission, c= 5 nM, MeOH).

λ_{emis}= 510 nm (at 315 nm excitation, c= 5 nM, MeOH).

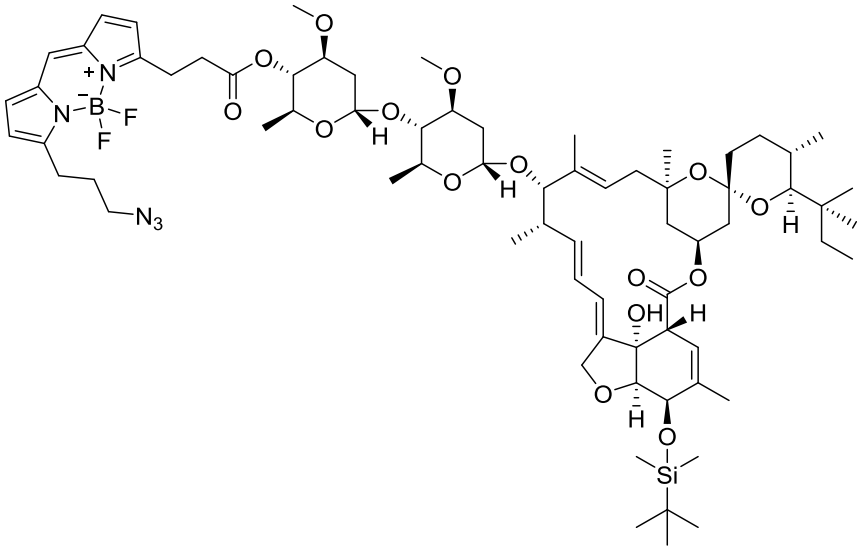

4”-*O*-[3-(5-(3-Azidopropyl)-4,4-difluoro-4-bora-3a,4a-diaza-s-indacene-3-yl)propanoate]-5-*O*-(*tert*-butyldimethylsilyl)avermectin B_{1a}, 116.

A solution of 5-*O*-(*tert*-butyldimethylsilyl)avermectin B_{1a} **107** (40 mg, 40 μmol) in CH_2Cl_2 (2.5 mL) was treated sequentially with solution of 3-(5-(3-azidopropyl)-4,4-difluoro-4-bora-3a,4a-diaza-*s*-indacene-3-yl)propanoic acid **113** (15 mg, 40 μmol) in CH_2Cl_2 (2.5 mL), followed by DCC (16 mg, 70 μmol) and DMAP (3 mg, 20 μmol). The resulting reaction mixture was then stirred at rt until completion by TLC analysis (18h). The reaction was then concentrated under reduced pressure, and the crude residue purified by flash column chromatography (0-20% EtOAc/PE) to yield the silyl-ivermectin complex **116** as a red oil (23 mg, 39%).

^{1}H NMR ($CDCl_3$, 400 MHz) δ: 7.14 (1H, s, ArC$H_{BODIPY\text{-}C8}$), 7.00 (2H, d, *J* = 4.4 Hz, ArC$H_{BODIPY\text{-}C1,C2}$), 6.43 (1H, d, *J* = 4.0 Hz, ArC$H_{BODIPY\text{-}C6}$), 6.37 (1H, d, *J* = 4.0 Hz, ArC$H_{BODIPY\text{-}C7}$), 5.85-5.82 (1H, m, C_9H), 5.77-5.72 (2H, m, $C_{10}H$,$C_{11}H$), 5.41 (1H, br s, C_3H), 5.36-5.31 (2H, m, $C_{19}H$, $C_{1''}H$), 5.00 (1H, d, *J* = 9.6 Hz, $C_{15}H$), 4.79 (1H, br s, $C_{1'}H$), 4.74 (1H, appt, *J* = 10.0 Hz, $C_{4''}H$), 4.71-4.68 (1H, m, $C_{8a}H_2$), 4.60 (1H, d, *J* = 14.4 Hz, $C_{8a}H_2$), 4.45 (1H, br s, C_5H), 3.96 (1H, br s, $C_{13}H$), 3.88-3.83 (3H, m, C_6H, $C_{5'}H$, $C_{5''}H$), 3.70-3.60 (3H, m, $C_{17}H$, $C_{3'}H$, $C_{3''}H$), 3.45 (6H, br s, $C_{3''}OCH_3$, $C_{3'}OCH_3$), 3.41-3.37 (4H, m, CH_2N_3, $CqCH_2$), 3.34-3.31 (1H, m, C_2H), 3.28-3.20 (2H, m, $C_{25}H$, $C_{4'}H$), 2.86-2.79 (4H, m, $CqCH_2$, CH_2CO), 2.53 (1H, br s, $C_{12}H$), 2.38-2.32 (2H, m, $C_{2''}H_2$, $C_{16}H_2$), 2.29 (1H, appd, *J* = 11.6 Hz, $C_{16}H_2$), 2.24 (1H, dd, *J* = 12.0, 4.0 Hz , $C_{2'}H_2$), 2.00 (1H, dd, *J* = 12.8, 4.4 Hz, $C_{20}H_2$), 1.98-1.93 (2H, m, $CH_2CH_2CH_2$), 1.81 (3H, s, $C_{4a}H_3$), 1.79-1.62 (9H, m, $C_{18}H_2$, 2 x $C_{22}H_2$, 2 X $C_{23}H_2$, $C_{24}H$, $C_{2''}H_2$, $C_{2'}H_2$, $C_{26}H$),1.53 (3H, s, $C_{14a}H_3$), 1.41-1.36 (3H, m, $C_{20}H_2$, $C_{27}H_2$), 1.29-1.27 (6H, br s, $C_{6''}H_3$, $C_{6'}H_3$),1.17 (1H, d, *J* = 6.8 Hz, $C_{12a}H_3$), 0.96-0.92 (12H, m, $C_{28}H_3$, $SiCq(CH_3)_3$), 0.89-0.86 (4H, m, $C_{26a}H_3$, $C_{18}H_2$), 0.81-0.79 (1H, m, $C_{24a}H_3$), 0.15 (6H, s, $Si(CH_3)_2$). ^{13}C NMR ($CDCl_3$, 100 MHz) δ: 174.0 (C_1O), 172.7 (CH_2CO_{BODIPY}), 162.1 (ArCq_{BODIPY}), 160.5 (ArCq_{BODIPY}), 140.2 (Cq_8), 137.5 x 2 ($C_{11}H$, Cq_4), 135.0 x 2 (ArCq_{BODIPY}, Cq_{14}), 134.8 (ArCq_{BODIPY}), 130.4 (ArCH_{BODIPY}), 127.9 (ArCH_{BODIPY}), 124.8 ($C_{10}H$), 119.3 (C_9H), 118.7 (ArCH_{BODIPY}), 118.4 (ArCH_{BODIPY}),118.3 (C_3H), 117.2 ($C_{15}H$), 98.5 ($C_{1''}H$), 97.5 (Cq_{21}), 94.8 ($C_{1'}H$), 81.9 ($C_{13}H$), 80.6 ($C_{4'}H$), 80.4 (Cq_7), 80.2 (C_6H), 80.0 (C_3H), 79.3

($C_{3''}$H), 79.2 ($C_{4''}$H), 77.2 (C_{25}H), 76.5 ($C_{5''}$H), 69.5 (C_{17}H), 68.7 (C_{19}H), 67.9 ($C_{8a}H_2$), 67.2 (C_5H), 67.1 (C_5H), 56.8 ($C_{3''}OCH_3$), 56.5 ($C_{3'}OCH_3$), 51.8 (CH_2N_3), 45.7 (C_2H), 41.1 ($C_{20}H_2$), 39.6 (C_{12}H), 36.8 ($C_{18}H_2$), 35.7 ($C_{2'}H_2$), 35.4 (C_{26}H, C_{24}H), 34.9 ($C_{2''}H_2$), 34.5 (C_{16}H), 34.1 ($C_{23}H_2$), 33.2 ($C_qCH_{2BODIPY}$), 33.0 ($CH_2C_{qBODIPY}$), 31.2 (C_{22}H), 29.7 ($CH_2CH_2N_3$), 28.1 (Si*Cq*), 27.3 ($C_{27}H_2$), 25.8 x 3 ($Cq(CH_3)_3$), 25.4 (CH_2CO_{BODIPY}), 20.3 ($C_{12a}H_3$), 20.0 ($C_{4a}H_3$), 18.4 ($C_{6''}H_3$), 17.7 ($C_{6'}H_3$), 17.4 ($C_{24a}H_3$), 15.2 ($C_{14a}H_3$), 12.4 ($C_{26a}H_3$), 12.1 ($C_{28}H_3$), -4.5 ($SiCH_3$), -4.8 ($SiCH_3$). ^{19}F NMR ($CDCl_3$, 376 MHz) δ: -144.21, -144.30, -144.39, -144.48. HRMS (ESI) calculated for $C_{71}H_{106}BF_2N_5O_{15}Si$ $[M-H]^+$: *m/z* 1344.7516, found *m/z* 1344.3033. IR υ_{max} (film)/cm^{-1}: 3360 (m), 2961 (m), 2921 (m), 2851 (m), 1632 (m).

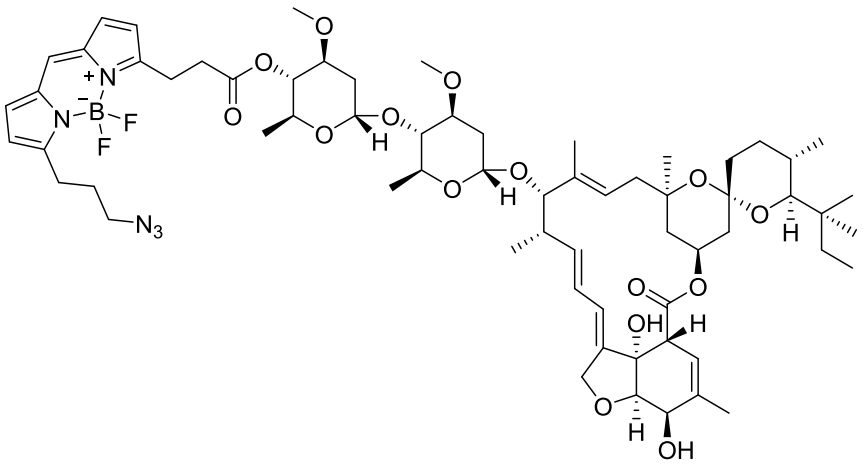

4”-*O*-[3-(5-(3-Azidopropyl)-4,4-difluoro-4-bora-3a,4a-diaza-*s*-indacene-3-yl)propanoate]avermectin B_{1a}, 117.

A solution of 4”-*O*-[3-(5-(3-azidopropyl)-4,4-difluoro-4-bora-3a,4a-diaza-*s*-indacene-3-yl)propanoate]-5-*O*-(*tert*-butyldimethylsilyl)avermectin B_{1a} **116** (6 mg, 4 μmol) in MeOH (2.0 mL) was treated with a catalytic amount of *p*-toluensulfonic acid (3 mg). The reaction mixture was stirred at 18 ºC for 30 min. The reaction was then diluted with H_2O (15 mL) followed by EtOAc (20 mL). The organic layer was washed with H_2O (3x20 mL) and brine (20 mL). The organic phase was dried over Na_2SO_4 and concentrated under reduced pressure. Purification of the crude residue by flash column chromatography (0-40% EtOAc/PE) afforded the desired BODIPY-ivermectin B_{1a} complex **117** as a red oil (4 mg, 72%).

HRMS (ESI) calculated for $C_{65}H_{92}BF_2N_5O_{15}$ $[M-H]^+$: *m/z* 1230.6651, found *m/z* 1230.1914.

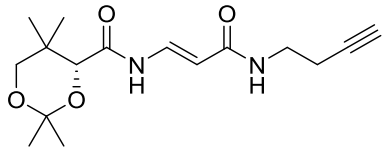

(*R,E*)-*N*-(3-(but-3-yn-1-ylamino)-3-oxoprop-1-en-1-yl)-2,2,5,5-tetramethyl-1,3-dioxane-4-carboxamide, 119.

A solution of (*R,E*)-3-(2,2,5,5-tetramethyl-1,3-dioxane-4-carboxamido)acrylic acid **28** (108 mg, 0.4 mmol) in CH_2Cl_2 (0.6 mL), was treated with BTFFH (188 mg, 0.6 mmol) followed by 1-amino-3-

butyne **118** (46 µL, 0.5 mmol) and *N,N*-diisopropylethylamine (100 µL, 0.5 mmol). The reaction mixture was heated to 80 °C for 2.5 h in the microwave oven. The reaction was then concentrated under reduced pressure. Purification of the crude residue by flash column chromatography (0-50% EtOAc/PE) afforded the desired alkyne **119** as a white solid (88 mg, 68%). The NMR data matches the literature data for this compound.[46]

^{1}H NMR ($CDCl_3$, 400 MHz) δ: 8.31 (1H, d, *J* = 10.4 Hz, CON*H*), 7.82 (1H, dd, *J* = 13.6, 10.8 Hz, NHC*H*), 5.87 (1H, d, *J* = 14.0 Hz, C*H*CO), 5.76 (1H, br s, N*H*CO), 4.21 (1H, s, OC*H*), 3.73 (1H, d, *J* = 11.8 Hz, CH_2Cq), 3.53-3.49 (2H, m, NHCH_2), 3.33 (1H, d, *J* = 11.8 Hz, CH_2Cq), 2.44 (2H, td, *J* = 6.4, 2.8 Hz, CH_2Cq), 2.03 (1H, appt, *J* = 2.4 Hz, CqC*H*), 1.51 (3H, s, Cq(CH_3)$_2$), 1.46 (3H, s, Cq(CH_3)$_2$), 1.06 (3H, s, Cq(CH_3)$_2$), 1.00 (3H, s, Cq(CH_3)$_2$). ^{13}C NMR ($CDCl_3$, 100 MHz) δ: 168.1 (*C*O), 166.1 (*C*O), 133.8 (NH*C*H), 105.9 (*C*HCO) 99.4 (*Cq*(CH$_3$)$_2$), 81.7 (*C*qCH), 77.4 (O*C*H), 71.2 (O*C*H$_2$), 70.0 (Cq*C*H), 37.9 (HN*C*H$_2$), 33.3 (*C*H$_2$Cq), 29.4 (Cq(*C*H$_3$)$_2$), 21.8 (Cq(*C*H$_3$)$_2$), 19.5 (*C*H$_2$Cq), 18.8 (Cq(*C*H$_3$)$_2$), 18.6 (Cq(*C*H$_3$)$_2$).

6. References

1. Davis, W. C., The History of Tuberculosis. *Eclectic Medical Journal*. **1932**, 12-15.

2. Vågene, Å. J.; Herbig, A.; Campana, M. G.; García, N. M. R.; Warinner, C.; Sabin, S.; Spyrou, M. A.; Valtueña, A. A.; Huson, D.; Tuross, N.; Bos, K. I.; Krause, J., Salmonella enterica genomes from victims of a major sixteenth-century epidemic in Mexico. *Nature Ecology & Evolution*. **2018**, 2 (3), 520-528.

3. Fleming, A., On the Antibacterial Action of Cultures of a Penicillium, with Special Reference to their Use in the Isolation of B. influenzæ. *Brit. J. Exp.Path*. **1929**, 10 (3), 226-236.

4. Alpert, P. T., Superbugs: Antibiotic Resistance Is Becoming a Major Public Health Concern. Home Health Care Management & Practice. **2017**, 29 (2), 130-133.

5. (a) WHO Global tuberculosis report 2017. http://www.who.int/tb/publications/global_report/en/ (accessed 19/02/2018); (b) WHO, World Malaria Report 2017. **2017**; p 196.

6. Neumann, E.; Schaefer-Ridder, M.; Wang, Y.; Hofschneider, P. H., Gene transfer into mouse lyoma cells by electroporation in high electric fields. *EMBO J*. **1982**, 1 (7), 841-845.

7. Gabriel, B.; Teissie, J., Direct Observation in the Millisecond Time Range of Fluorescent Molecule Asymmetrical Interaction with the Electropermeabilized Cell Membrane. *Biophys. J*. **1997**, 73, 2630-2637.

8. Gehl, J., Electroporation: Theory and methods, perspectives for drug delivery, gene therapy and research. *Acta Physiol. Scand*. **2003**, 177 (4), 437-447.

9. Belehradek, M.; Domenge, C.; Luboinski, B.; Orlowski, S.; Belehradek, J.; Mir, L. M., Electrochemotherapy, a new antitumor treatment. First clinical phase I-II trial. *Cancer*. **1993**, 72 (12), 3694-3700.

10. Edhemovic, I.; Brecelj, E.; Gasljevic, G.; Music, M. M.; Gorjup, V.; Mali, B.; Jarm, T.; Kos, B.; Pavliha, D.; Kuzmanov, B. G. In The First Clinical Experience with Electrochemotherapy of the Colorectal Liver Metastases. *MBEC* 2014. Springer. **2015**, 805-808.

11. Devarajan, P. V.; Jain, S., Targeted drug delivery: concepts and design. Springer. **2015**. [electronic book]

12. (a) Schiffelers, R. M.; Bakker-Woudenberg, I. A. J. M., Innovations in liposomal formulations for antimicrobial therapy. *Expert Opinion on Therapeutic Patents.* **2003,** *13* (8), 1127-1140. (b) Gursoy, A., Liposome-encapsulated antibiotics: Physicochemical and antibacterial properties, a review. *S.T.P. Pharma Sciences.* **2000,** *10* (4), 285-291.

13. (a) Gaspar, M. M.; Cruz, A.; Penha, A. F.; Reymão, J.; Sousa, A. C.; Eleutério, C. V.; Domingues, S. A.; Fraga, A. G.; Filho, A. L.; Cruz, M. E. M.; Pedrosa, J., Rifabutin encapsulated in liposomes exhibits increased therapeutic activity in a model of disseminated tuberculosis. *International Journal of Antimicrobial Agents*. **2008**, 31, 37-45; (b) Garnett, M. C., Targeted drug conjugates: principles and progress. *Advanced Drug Delivery Reviews*. **2001**, 53 (2), 171-216. (c) Couvreur, P.; Fattal, E.;

Andremont, A., Liposomes and Nanoparticles in the Treatment of Intracellular Bacterial Infections. *Pharmaceutical Research*. **1991**, 8 (9), 1079-1086.

14. Wilczewska, A. Z.; Niemirowicz, K.; Markiewicz, K. H.; Car, H., Nanoparticles as drug delivery systems. *Pharmacological Reports*. **2012**, 64 (5), 1020-1037.

15. Gabizon, A.; Horowitz, A. T.; Goren, D.; Tzemach, D.; Mandelbaum-Shavit, F.; Qazen, M. M.; Zalipsky, S., Targeting Folate Receptor with Folate Linked to Extremities of Poly(ethylene glycol)-Grafted Liposomes: In Vitro Studies. *Bioconjugate Chem*.**1999**, 10 (2), 289-298.

16. Bamrungsap, S.; Zhao, Z.; Chen, T.; Wang, L.; Li, C.; Fu, T.; Tan, W., Nanotechnology in therapeutics: a focus on nanoparticles as a drug delivery system. *Nanomedicine*. **2012**, 7 (8), 1253-1271.

17. Vlahov, I.; Leamon, C.; Parker, M.; Howard, S.J.; Santhapuram, H. K.; Reddy, J. A., Vitamin receptor binding drug delivery conjugates. US 7,601,332 B2. **2009**, 1-81.

18. Reddy, J. A.; Westrick, E.; Vlahov, I.; Howard, S. J.; Santhapuram, H. K.; Leamon, C. P., Folate receptor specific anti-tumor activity of folate–mitomycin conjugates. *Cancer Chemotherapy and Pharmacology*. **2006**, 58 (2), 229-236.

19. (a) Reddy, J. A.; Leamon, C. P., Folate Receptor Targeted Cancer Chemotherapy. *Springer*: New York. **2011**; p 135-150. (b) Arias, J. L.; Clares, B.; Morales, M. E.; Gallardo, V.; Ruiz, M. A., Lipid-Based Drug Delivery Systems for Cancer Treatment. *Current Drug Targets*. **2011**, 12 (8), 1151-1165. (c) Kularatne, S. A.; Low, P. S., Targeting of Nanoparticles: Folate Receptor. In Cancer Nanotechnology: Methods and Protocols, Grobmyer, S. R.; Moudgil, B. M., Eds. Humana Press Inc: Totowa, 2010; Vol. 624, pp 249-265.

20. Rebeille, F.; Ravanel, S.; Marquet, A.; Mendel, R.; Smith, A.; Warren, M., Roles of vitamins B5, B8, B9, B12 and molybdenum cofactor at cellular and organismal levels. *Nat. Prod. Rep.*, **2007**, 949-962.

21. Yokooji, Y.; Tomita, H.; Atomi, H.; Imanaka, T., Pantoate Kinase and Phosphopantothenate Synthetase, Two Novel Enzymes Necessary for CoA Biosynthesis in the Archaea. *J. Biol. Chem.* **2009**, 284 (41), 28137-28145.

22. Saliba, K. J.; Spry, C., Exploiting the coenzyme A biosynthesis pathway for the identification of new antimalarial agents: the case for pantothenamides. *Biochem. Soc. Trans.* **2014**, 42 (4), 1087-1093.

23. CDC Malaria Parasites. www.cdc.gov/malaria/about/biology/parasites.html (accessed 03/06/2016).

24. Ramachandran, S.; Hameed, P. S.; Srivastava, A.; Shanbhag, G.; Morayya, S.; Rautela, N.; Awasthy, D.; Kavanagh, S.; Bharath, S.; Reddy, J.; Panduga, V.; Prabhakar, K. R.; Saralaya, R.; Nanduri, R.; Raichurkar, A.; Menasinakai, S.; Achar, V.; Jimenez-Diaz, M. B.; Martinez, M. S.; Angulo-Barturen, I.; Ferrer, S.; Sanz, L. M.; Gamo, F. J.; Duffy, S.; Avery, V. M.; Waterson, D.; Lee, M. C. S.; Coburn-Flynn, O.; Fidock, D. A.; Iyer, P. S.; Narayanan, S.; Hosagrahara, V.;

Sambandamurthy, V. K., N-Aryl-2-aminobenzimidazoles: Novel, Efficacious, Antimalarial Lead Compounds. *J. Med. Chem*. **2014**, 57 (15), 6642-6652.
25. Tuteja, R., Malaria - an overview. *FEBS J.* **2007**, 274 (18), 4670-4679.
26. www.mcwhealthcare.com/malaria_drugs_medicines/life_cycle_of_plasmodium.htm. (accessed 25/03/2018).
27. Duffy, S.; Avery, V. M., Development and Optimization of a Novel 384-Well Anti-Malarial Imaging Assay Validated for High-Throughput Screening. *Am. J. Trop. Med. Hyg*. **2012**, 86 (1), 84-92.
28. Wirth, C. C.; Glushakova, S.; Scheuermayer, M.; Repnik, U.; Garg, S.; Schaack, D.; Kachman, M. M.; Weissbach, T.; Zimmerberg, J.; Dandekar, T.; Griffiths, G.; Chitnis, C. E.; Singh, S.; Fischer, R.; Pradel, G., Perforin-like protein PPLP2 permeabilizes the red blood cell membrane during egress of Plasmodium falciparum gametocytes. *Cell Microbiol.* **2014**, 16 (5), 709-733.
29. (a) Kamal El, B.; Rachel, Z.; William, H. W.; Nicola, S. C.; Buddy, U.; Choukri Ben, M., The Plasma Membrane Permease PfNT1 Is Essential for Purine Salvage in the Human Malaria Parasite *Plasmodium falciparum*. *Proc. Natl. Acad. Sci. U.S.A.* **2006**, (24), 9286; (b) Downie, M. J.; El Bissati, K.; Bobenchik, A. M.; Nic Lochlainn, L.; Amerik, A.; Zufferey, R.; Kirk, K.; Ben Mamoun, C., PfNT2, a Permease of the Equilibrative Nucleoside Transporter Family in the Endoplasmic Reticulum of Plasmodium falciparum. *J. Biol. Chem.* **2010**, 285 (27), 20827-20833; (c) Woodrow, C. J.; Penny, J. I.; Krishna, S., Intraerythrocytic *Plasmodium falciparum* Expresses a High Affinity Facilitative Hexose Transporter. *J. Biol. Chem.* **1999**, 274 (11), 7272-7277; (d) Charles J. Woodrow, a.; Richard J. Burchmore, a.; Sanjeev Krishna, a., Hexose Permeation Pathways in *Plasmodium falciparum*-Infected Erythrocytes. *Proc. Natl. Acad. Sci. U.S.A*. **2000**, (18), 9931; (e) Augagneur, Y.; Jaubert, L.; Schiavoni, M.; Pachikara, N.; Garg, A.; Usmani-Brown, S.; Wesolowski, D.; Zeller, S.; Ghosal, A.; Cornillot, E.; Said, H. M.; Kumar, P.; Altman, S.; Ben Mamoun, C., Identification and Functional Analysis of the Primary Pantothenate Transporter, PfPAT, of the Human Malaria Parasite *Plasmodium falciparum*. *J. Biol. Chem.* **2013**, 288 (28), 20558-20567.
30. de Villiers, M.; Macuamule, C.; Spry, C.; Hyun, Y.-M.; Strauss, E.; Saliba, K. J., Structural Modification of Pantothenamides Counteracts Degradation by Pantetheinase and Improves Antiplasmodial Activity. *ACS Med. Chem. Lett*. **2013**, 4 (8), 784-789.
31. Sugie, Y.; Dekker, K. A.; Hirai, H.; Ichiba, T.; Ishiguro, M.; Shiomi, Y.; Sugiura, A.; Brennan, L.; Duignan, J.; Huang, L. H.; Sutcliffe, J.; Kojima, Y., CJ-15,801, a novel antibiotic from a fungus, *Seimatosporium sp. Journal of Antibiotics*. **2001**, 54 (12), 1060-1065.
32. Geary, T. G.; Divo, A. A.; Bonanni, L. C.; Jensen, J. B., Nutritional requirements of *Plasmodium falciparum* in culture. III. Further observations on essential nutrients and antimetabolites. *J. Protozool.* **1985**, 32 (4), 608-13.
33. (a) Spry, C.; Saliba, K. J., The human malaria parasite Plasmodium falciparum is not dependent on host coenzyme A biosynthesis. J Biol Chem 2009, 284 (37), 24904-13. (b) Huber, S. M.; Lang, C.; Lang, F.; Duranton, C., Organic osmolyte channels in malaria-infected erythrocytes. *Biochem. Biophys. Res. Commun*. **2008**, 376 (3), 514-518; (c) Saliba, K. J.; Horner, H. A.; Kirk, K., Transport

and Metabolism of the Essential Vitamin Pantothenic Acid in Human Erythrocytes Infected with the Malaria Parasite *Plasmodium falciparum*. *J. Biol. Chem.* **1998**, 273 (17), 10190-10195; (d) Brohn, F. H.; Trager, W., Coenzyme A requirement of malaria parasites: enzymes of coenzyme A biosynthesis in normal duck erythrocytes and erythrocytes infected with *Plasmodium lophurae*. *Proc. Natl. Acad. Sci. U.S.A.* **1975**, 72 (6), 2456-8.

34. Saliba, K. J.; Kirk, K., CJ-15,801, a fungal natural product, inhibits the intraerythrocytic stage of *Plasmodium falciparum in vitro* via an effect on pantothenic acid utilisation. *Mol. Biochem. Parasitol.* **2005**, 141 (1), 129-131.

35. Van der Westhuyzen, R.; Hammons, Justin C.; Meier, Jordan L.; Dahesh, S.; Moolman, Wessel J. A.; Pelly, Stephen C.; Nizet, V.; Burkart, Michael D.; Strauss, E., The Antibiotic CJ-15,801 Is an Antimetabolite that Hijacks and Then Inhibits CoA Biosynthesis. *Chem. Biol.* **2012**, 19 (5), 559-571.

36. Han, C.; Shen, R.; Su, S.; Porco, J. A., Copper-Mediated Synthesis of N-Acyl Vinylogous Carbamic Acids and Derivatives: Synthesis of the Antibiotic CJ-15,801. *Organic Letters*. **2004**, 6 (1), 27-30.

37. Nicolaou, K. C.; Mathison, C. J. N., Synthesis of Imides, N-Acyl Vinylogous Carbamates and Ureas, and Nitriles by Oxidation of Amides and Amines with Dess–Martin Periodinane. *Angew. Chem. Int. Ed.* **2005**, 44 (37), 5992-5997.

38. Kashinath, K.; Swaroop, P. S.; Reddy, D. S., A green synthetic route to antimalarial and antibacterial agent CJ-15,801 and its isomer cis-CJ-15,801. RSC Advances. **2012**, 2 (9), 3596-3598.

39. (a) Sewell, A. L.; Villa, M. V. J.; Matheson, M.; Whittingham, W. G.; Marquez, R., Fast and Flexible Synthesis of Pantothenic Acid and CJ-15,801. *Organic Letters*. **2011**, 13 (4), 800-803. (b) Villa, M. V. J.; Targett, S. M.; Barnes, J. C.; Whittingham, W. G.; Marquez, R., An Efficient Approach to the Stereocontrolled Synthesis of Enamides. *Organic Letters*. **2007**, 9 (9), 1631-1633.

40. Paddock, S. W., Confocal microscopy methods and protocols. **1999**. Totowa, N.J. : Humana Press, [electronic book].

41. Johnson, M. E.; Blankschtein, D.; Langer, R. S.; Berk, D. A.; Jain, R. K.; Golan, D. E., Lateral diffusion of small compounds in human stratum corneum and model lipid bilayer systems. *Biophys. J.* **1996**, 71 (5), 2656-2668.

42. BODIPY, Molecular Probes, Invitrogen.

43. Rostovtsev, V. V.; Green, L. G.; Fokin, V. V.; Sharpless, K. B., A stepwise Huisgen cycloaddition process: Copper(I)-catalyzed regioselective "ligation" of azides and terminal alkynes. *Angew. Chem. Int. Ed.* **2002**, 41 (14), 2596-2599.

44. Zhao, Q.; Yin, C.; Kang, J.; Wen, Y.; Huo, F., A viscosity sensitive azide-pyridine BODIPY-based fluorescent dye for imaging of hydrogen sulfide in living cells. *Dyes and Pigments*. **2018**, 159, 166-172.

45. (a) Hansen, A. M.; Sewell, A. L.; Pedersen, R. H.; Long, D.-L.; Gadegaard, N.; Marquez, R., Tunable BODIPY derivatives amenable to ‘click’ and peptide chemistry. *Tetrahedron*. **2013**, 69 (39),

8527-8533. (b) Bañuelos, J.; Martín, V.; Gómez-Durán, C. F. A.; Córdoba, I. J. A.; Peña-Cabrera, E.; García-Moreno, I.; Costela, Á.; Pérez-Ojeda, M. E.; Arbeloa, T.; Arbeloa, Í. L., New 8-Amino-BODIPY Derivatives: Surpassing Laser Dyes at Blue-Edge Wavelengths. *Chemistry – A European Journal* **2011**, 17 (26), 7261-7270.

46. Sewell, A. L., Coenzyme A biosynthesis inhibitors as potential anti-parasitic agents. University of Glasgow: **2014**.

47. Gaudelli, N. M.; Townsend, C. A., Stereocontrolled Syntheses of Peptide Thioesters Containing Modified Seryl Residues as Probes of Antibiotic Biosynthesis (vol 7813, pg 6412, 2013). *J. Org. Chem.* **2013**, 78 (21), 11115-11115.

48. Caffrey, C. R.; Selzer, P. M., Parasitic Helminths : Targets, Screens, Drugs and Vaccines. John Wiley & Sons, Incorporated: Weinheim, GERMANY, **2012**, [electronic book].

49. (a) Miller, D. S., Daunomycin secretion by killfish renal proximal tubules. *Am. J. Physiol*. **1995**, 269 (2 Pt 2), R370-9; (b) Fricker, G.; Gutmann, H.; Droulle, A.; Drewe, J.; Miller, D. S., Epithelial transport of anthelmintic ivermectin in a novel model of isolated proximal kidney tubules. *Pharm Res.* **1999**, 16 (10), 1570-5.

50. (a) Balachandar, R.; Lu, N. C., Nutritional requirements for pantothenate, pantethine or coenzyme A in the free-living nematode *Caenorhabditis elegans*. *Nematology*. **2005**, 7 (5), 761-766; (b) Dougherty, E. C.; Hansen, E. L.; Nicholas, W. L.; Mollett, J. A.; Yarwood, E. A., Axenic cultivation of *Caenorhabditis briggsae* (nematoda: rhabditidae) with unsupplemented and supplemented chemically defined media*. *Ann. N. Y. Acad. Sci.* **1959**, 77 (2), 176-217; (c) Nicholas, W. L.; Hansen, E.; Dougherty, E. C., The B-Vitamins Required By *Caenorhabditis Briggsae* (Rhabditidae). *Nematologica*. **1962**, 8 (2), 129-135.

51. (a) Hunt, P. R., The *C. elegans* model in toxicity testing. *Journal of Applied Toxicology*. **2017**, 37 (1), 50-59. (b) O'Reilly, L. P.; Luke, C. J.; Perlmutter, D. H.; Silverman, G. A.; Pak, S. C., C. elegans in high-throughput drug discovery. *Advanced Drug Delivery Reviews.* **2014**, 69-70, 247-253. (c) Burns, A. R.; Wallace, I. M.; Wildenhain, J.; Tyers, M.; Giaever, G.; Bader, G. D.; Nislow, C.; Cutler, S. R.; Roy, P. J., A predictive model for drug bioaccumulation and bioactivity in Caenorhabditis elegans. *Nature Chemical Biology.* **2010**, 6, 549. (d) Gallo, M.; Mah, A. K.; Johnsen, R. C.; Rose, A. M.; Baillie, D. L., *Caenorhabditis elegans* dpy-14: an essential collagen gene with unique expression profile and physiological roles in early development. *Mol. Gen. Genet.* **2006**, 275 (6), 527-539. (e) Gravato-Nobre, M. J.; Nicholas, H. R.; Nijland, R.; O'Rourke, D.; Whittington, D. E.; Yook, K. J.; Hodgkin, J., Multiple genes affect sensitivity of *Caenorhabditis elegans* to the bacterial pathogen *Microbacterium nematophilum*. *Genetics.* **2005**, 171 (3), 1033-1045.

52. (a) Kocaoglu, O.; Carlson, E. E., Progress and prospects for small-molecule probes of bacterial imaging. *Nat. Chem. Biol.* **2016**, 12, 472; (b) Buckley, A. M.; Petersen, J.; Roe, A. J.; Douce, G. R.; Christie, J. M., LOV-based reporters for fluorescence imaging. *Curr. Opin. Chem. Biol*. **2015**, 27, 39-45.

53. Drepper, T.; Eggert, T.; Circolone, F.; Heck, A.; Krauss, U.; Guterl, J.-K.; Wendorff, M.; Losi, A.; Gärtner, W.; Jaeger, K.-E., Reporter proteins for in vivo fluorescence without oxygen. *Nature Biotechnol.* **2007**, 25 (4), 443-445.

54. (a) Chapman, S.; Faulkner, C.; Kaiserli, E.; Garcia-Mata, C.; Savenkov, E. I.; Roberts, A. G.; Oparka, K. J.; Christie, J. M., The photoreversible fluorescent protein iLOV outperforms GFP as a reporter of plant virus infection. *Proc. Natl. Acad. Sci. U.S.A.* **2008**, 105 (50), 20038-20043; (b) Wingen, M.; Potzkei, J.; Endres, S.; Casini, G.; Rupprecht, C.; Fahlke, C.; Krauss, U.; Jaeger, K.-E.; Drepper, T.; Gensch, T., The photophysics of LOV-based fluorescent proteins - new tools for cell biology. *Photochem. Photobiol.* **2014**, 13 (6), 875-883.

55. (a) Christie, J. M.; Hitomi, K.; Arvai, A. S.; Hartfield, K. A.; Mettlen, M.; Pratt, A. J.; Tainer, J. A.; Getzoff, E. D., Structural Tuning of the Fluorescent Protein iLOV for Improved Photostability. *J. Biol. Chem.* **2012**, 287 (26), 22295-22304; (b) Gadge, S.; Philip, J. K.; Volmostree, K., The molecular structure of green fluorescent protein. *Journal of Soils and Crops*. **2015**, 25 (1), 13-20.

56. Nanda, J. S.; Lorsch, J. R., Chapter Seven - Labeling of a Protein with Fluorophores Using Maleimide Derivitization. In Methods in Enzymology, Ed. Academic Press. **2014**, Vol. 536, pp 79-86.

57. Pasqua, A. E.; Matheson, M.; Sewell, A. L.; Marquez, R., Fast, Economic, and Green Synthesis of *N*-Formylated Benzotriazoles. *Org. Process Res. Dev.* **2011**, 15 (2), 467-470.

58. Robiette, R.; Richardson, J.; Aggarwal, V. K.; Harvey, J. N., Reactivity and Selectivity in the Wittig Reaction: A Computational Study. *J. Am. Chem. Soc*. **2006**, 128 (7), 2394-2409.

59. (a) Horstmann, B.; Korbus, M.; Friedmann, T.; Wolff, C.; Thiele, C. M.; Meyer-Almes, F.-J., Synthesis of azobenzenealkylmaleimide probes to photocontrol the enzyme activity of a bacterial histone deacetylase-like amidohydrolase. *Bioorganic Chemistry.* **2014**, 57, 155-161. (b) Gorostiza, P.; Volgraf, M.; Numano, R.; Szobota, S.; Trauner, D.; Isacoff, E. Y., Mechanisms of photoswitch conjugation and light activation of an ionotropic glutamate receptor. *PNAS*. **2007**, 104 (26), 10865-10870.

60. Cook, P. D.; An, H.; Haly, B.; Wang, T., Substituted cyclic compounds and mixtures comprising same. US-6,191,273B1. **1999**. 1-45.

61. Sen, S. E.; Roach, S. L., A Convenient Two-Step Procedure for the Synthesis of Substituted Allylic Amines from Allylic Alcohols. *Synthesis*. **1995**, (7), 756-758.

62. (a) Albericio, F.; Carpino, L. A., [7] Coupling reagents and activation. In Methods in Enzymology, Academic Press. **1997**; Vol. 289, 104-126; (b) Peng, L.; Jie-Cheng, X., Highly efficient synthesis of peptides by rational utilization of novel coupling reagents. *Chinese Journal of Chemistry*. **2000**, 18 (4), 456-466.

63. (a) Green, M.; Berman, J., Preparation of pentafluorophenyl esters of FMOC protected amino acids with pentafluorophenyl trifluoroacetate. *Tetrahedron Letters*. **1990**, 31 (41), 5851-5852; (b) Kisfaludy, L.; Mohacsi, T.; Low, M.; Drexler, F., Pentafluorophenyl Acetate: A New, Highly Selective Acetylating Agent1. *J. Org. Chem*. **1979**, 44 (4), 654-656.

64. (a) Kisfaludy, L.; Schön, I., Preparation and Applications of Pentafluorophenyl Esters of 9-Fluorenylmethyloxycarbonyl Amino Acids for Peptide Synthesis. *Synthesis*. **1983**, (4), 325; (b) Schmidt, U.; Weinbrenner, S., The synthesis of eurystatin A1. *J. Chem. Soc. Chem. Commun.* **1994**, (8), 1003-1004; (c) East, S. P.; Joullié, M. M., Synthetic studies of 14-membered cyclopeptide alkaloids. *Tetrahedron Letters*. **1998**, 39 (40), 7211-7214.

65. Kim, Y.; Ho, S. O.; Gassman, N. R.; Korlann, Y.; Weiss, S.; Landorf, E. V.; Collart, F. R., Efficient site-specific labeling of proteins via cysteines. *Bioconjugate Chem.* **2008**, 19 (3), 786-791.

66. Spry, C.; Sewell, A. L.; Hering, Y.; Villa, M. V. J.; Weber, J.; Hobson, S. J.; Harnor, S. J.; Gul, S.; Marquez, R.; Saliba, K. J., Structure-activity analysis of CJ-15,801 analogues that interact with *Plasmodium falciparum* pantothenate kinase and inhibit parasite proliferation. *European Journal of Medicinal Chemistry.* **2018**, 143, 1139-1147.

67. (a) Lewis, J. K.; Wei, J.; Siuzdak, G., Matrix-Assisted Laser Desorption/Ionization Mass Spectrometry in Peptide and Protein Analysis. In Encyclopedia of Analytical Chemistry, John Wiley & Sons, Ltd. **2006**; (b) Song, F., A study of noncovalent protein complexes by matrix-assisted laser desorption/ionization. *J. Am. Soc. Mass Spectrom*. **2007**, 18 (7), 1286-1290.

68. Keller, B. O.; Sui, J.; Young, A. B.; Whittal, R. M., Interferences and contaminants encountered in modern mass spectrometry. *Anal. Chim. Acta*. **2008**, 627 (1), 71-81.

69. Kaufman, J. M.; Jaber, A. J.; Stump, M. J.; Simonsick, W. J.; Wilkins, C. L., Interference from multiple cations in MALDI–MS spectra of copolymers. *Int. J. Mass Spectrom*. **2004**, 234 (1), 153-160.

70. (a) Wingen, M.; Potzkei, J.; Endres, S.; Casini, G.; Rupprecht, C.; Fahlke, C.; Krauss, U.; Jaeger, K.-E.; Drepper, T.; Gensch, T., The photophysics of LOV-based fluorescent proteins – new tools for cell biology. *Photochemical & Photobiological Sciences*. **2014**, 13 (6), 875-883. (b) Johnson, I. D.; Kang, H. C.; Haugland, R. P., Fluorescent membrane probes incorporating dipyrromethene boron difluoride fluorophores. *Analytical Biochemistry*. **1991**, 198 (2), 228-237.

71. (a) Shoop, W. L.; Mrozik, H.; Fisher, M. H., Structure and activity of avermectins and milbemycins in animal health. *Vet. Parasitol*. **1995**, 59 (2), 139-156; (b) Croft, S. L., The current status of antiparasite chemotherapy. *Parasitology*. **1997**, 114 Suppl, S3-S15.

72. (a) Geurden, T.; Chartier, C.; Fanke, J.; di Regalbono, A. F.; Traversa, D.; von Samson-Himmelstjerna, G.; Demeler, J.; Vanimisetti, H. B.; Bartram, D. J.; Denwood, M. J., Anthelmintic resistance to ivermectin and moxidectin in gastrointestinal nematodes of cattle in Europe. *Int. J. Parasitol*. **2015**, 5 (3), 163-171; (b) Edwards, G., Ivermectin: does P-glycoprotein play a role in neurotoxicity? *BioMed Central*. **2003**; (c) Jani, M.; Makai, I.; Kis, E.; Szabo, P.; Nagy, T.; Krajcsi, P.; Lespine, A., Ivermectin interacts with human ABCG2. *J. Pharm. Sci*. **2011**, 100 (1), 94-97.

73. Davies, H. G.; Green, R. H., Avermectins and milbemycins. *Natural Product Reports*. **1986**, 3 (0), 87-121.

74. Mrozik, H.; Chabala, J. C.; Eskola, P.; Matzuk, A.; Waksmunski, F.; Woods, M.; Fisher, M. H., Synthesis of milbemycins from avermectins. *Tetrahedron Letters*. **1983**, 24 (48), 5333-5336.

75. Neises, B.; Steglich, W., Simple Method for the Esterification of Carboxylic Acids. *Angew. Chem. Int. Ed.* **1978**, 17 (7), 522-524.

76. Mrozik, H.; Eskola, P.; Fisher, M. H.; Egerton, J. R.; Cifelli, S.; Ostlind, D. A., Avermectin acyl derivatives with anthelmintic activity. *J. Med. Chem*. **1982**, 25 (6), 658-63.

77. (a) Fuse, T.; Ikeda, I.; Kita, T.; Furutani, S.; Nakajima, H.; Matsuda, K.; Ozoe, F.; Ozoe, Y., Synthesis of photoreactive ivermectin B1a derivatives and their actions on *Haemonchus* and *Bombyx* glutamate-gated chloride channels. *Pesticide Biochemistry and Physiology*. **2015**, 120, 82-90; (b) Beasley, C. A.; Hwang, T.-L.; Fliszar, K.; Abend, A.; McCollum, D. G.; Reed, R. A., Identification of impurities in ivermectin bulk material by mass spectrometry and NMR. *Journal of Pharmaceutical and Biomedical Analysis.* **2006**, 41 (4), 1124-1134.

78. Gießler, K.; Griesser, H.; Göhringer, D.; Sabirov, T.; Richert, C., Synthesis of 3′-BODIPY-Labeled Active Esters of Nucleotides and a Chemical Primer Extension Assay on Beads. *Eur. J. Org. Chem*. **2010**, (19), 3611-3620.

79. Carter, K., Antiparasitic and Antibacterial Drug Discovery. Edited by Paul M. Selzer. Wiley-VCH. **2009**, [electronic book].

80. (a) Schwarz, R. S.; Bauchan, G. R.; Murphy, C. A.; Ravoet, J.; de Graaf, D. C.; Evans, J. D., Characterization of Two Species of Trypanosomatidae from the Honey Bee *Apis mellifera*: *Crithidia mellificae* Langridge and McGhee, and *Lotmaria passim* n. gen., n. sp. *Journal of Eukaryotic Microbiology*. **2015**, 62 (5), 567-583; (b) Paxton, R. J., Does infection by Nosema ceranae cause "Colony Collapse Disorder" in honey bees (Apis mellifera)? *Journal of Apicultural Research*. **2010**, 49 (1), 80-84.

81. Moreno, S. N. J.; Docampo, R., The role of acidocalcisomes in parasitic protists. *Journal Of Eukaryotic Microbiology*. **2009**, 56 (3), 208-213.

82. Yamagishi, J.; Wakaguri, H.; Yokoyama, N.; Yamashita, R.; Suzuki, Y.; Xuan, X.; Igarashi, I., The *Babesia bovis* gene and promoter model: an update from full-length EST analysis. *BMC Genom*. **2014**, 15 (1), 678.

83. Schuster, F. L., Cultivation of *Babesia* and *Babesia*-Like Blood Parasites: Agents of an Emerging Zoonotic Disease. *Clin. Microbiol. Rev.* **2002**, 15 (3), 365-373.

84. Spry, C.; Saliba, K. J., The human malaria parasite *Plasmodium falciparum* is not dependent on host coenzyme A biosynthesis. *J Biol Chem*. **2009**, 284 (37), 24904-13.

85. "Tuberculosis". <http://www.nobelprize.org/educational/medicine/tuberculosis/readmore.html> (accessed 18 Feb 2018).

86. Pollock, J. M.; Neill, S. D., *Mycobacterium bovis* Infection and Tuberculosis in Cattle. *The Veterinary Journal*. **2002**, 163 (2), 115-127.

87. WHO Leprosy. http://www.who.int/mediacentre/factsheets/fs101/en/ (accessed 19/02/2018).

88. Shiloh, M. U.; DiGiuseppe Champion, P. A., To catch a killer. What can mycobacterial models teach us about Mycobacterium tuberculosis pathogenesis? *Current Opinion in Microbiology*. **2010**, 13 (1), 86-92.

89. Sambandamurthy, V. K.; Wang, X. J.; Chen, B.; Russell, R. G.; Derrick, S.; Collins, F. M.; Morris, S. L.; Jacobs, W. R., A pantothenate auxotroph of *Mycobacterium tuberculosis* is highly attenuated and protects mice against tuberculosis. *Nat. Med*. **2002**, 8 (10), 1171-1174.
90. Cole, S. T.; Brosch, R.; Parkhill, J.; Garnier, T.; Churcher, C.; Harris, D.; Gordon, S. V.; Eiglmeier, K.; Gas, S.; Barry Iii, C. E.; Tekaia, F.; Badcock, K.; Basham, D.; Brown, D.; Chillingworth, T.; Connor, R.; Davies, R.; Devlin, K.; Feltwell, T.; Gentles, S.; Hamlin, N.; Holroyd, S.; Hornsby, T.; Jagels, K.; Krogh, A.; McLean, J.; Moule, S.; Murphy, L.; Oliver, K.; Osborne, J.; Quail, M. A.; Rajandream, M. A.; Rogers, J.; Rutter, S.; Seeger, K.; Skelton, J.; Squares, R.; Squares, S.; Sulston, J. E.; Taylor, K.; Whitehead, S.; Barrell, B. G., Deciphering the biology of *Mycobacterium tuberculosis* from the complete genome sequence. *Nature*. **1998**, 393, 537.
91. Daffe, M.; Reyrat, J.-M., The Mycobacterial Cell Envelope. ASM Press: Washington, US. **2008**, 153-165.
92. Sarathy, J. P.; Dartois, V.; Lee, E. J. D., The Role of Transport Mechanisms in *Mycobacterium Tuberculosis* Drug Resistance and Tolerance. *Pharmaceuticals.* **2012**, Vol 5, Iss 11, 1210-1235.
93. Jarlier, V.; Nikaido, H., Mycobacterial cell wall: structure and role in natural resistance to antibiotics. *FEMS Microbiol. Lett.* **1994**, 123 (1-2), 11-18.
94. Mailaender, C.; Reiling, N.; Engelhardt, H.; Bossmann, S.; Ehlers, S.; Niederweis, M., The MspA porin promotes growth and increases antibiotic susceptibility of both *Mycobacterium bovis* BCG and *Mycobacterium tuberculosis*. *Microbiology*. **2004**, 150 (4), 853-864.
95. Senaratne, R. H.; Mobasheri, H.; Papavinasasundaram, K. G.; Jenner, P.; Lea, E. J. A.; Draper, P., Expression of a Gene for a Porin-Like Protein of the OmpA Family from *Mycobacterium tuberculosis* H37Rv. *J. Bacteriol*. **1998**, 3541-47.
96. Chanput, W.; Mes, J. J.; Wichers, H. J., THP-1 cell line: An in vitro cell model for immune modulation approach. *Int. J. Immunopharmacol.* **2014**, 23 (1), 37-45.
97. Tsuchiya, S.; Yamabe, M.; Yamaguchi, Y.; Kobayashi, Y.; Konno, T.; Tada, K., Establishment and characterization of a human acute monocytic leukemia cell line (THP-1). *Int. J. Cancer.* **1980**, 26 (2), 171-176.
98. Stokes, R. W.; Doxsee, D., The Receptor-Mediated Uptake, Survival, Replication, and Drug Sensitivity of *Mycobacterium tuberculosis* within the Macrophage-like Cell Line THP-1: A Comparison with Human Monocyte-Derived Macrophages. *Cell. Immunol.* **1999**, 197, 1-9.
99. (a) Bohsali, A.; Abdalla, H.; Velmurugan, K.; Briken, V., The non-pathogenic mycobacteria *M. smegmatis* and *M. fortuitum* induce rapid host cell apoptosis via a caspase-3 and TNF dependent pathway. *BMC Microbiology*. **2010**, 10, 237-237; (b) Qin, Z., The use of THP-1 cells as a model for mimicking the function and regulation of monocytes and macrophages in the vasculature. *Atherosclerosis*. **2012**, 221 (1), 2-11.
100. Stiernagle, T., Maintenance of *C. elegans*. WormBook. **2006**, 1-11.
101. Bork, S.; Okamura, M.; Matsuo, T.; Kumar, S.; Yokoyama, N.; Igarashi, I., Host serum modifies the drug susceptibility of Babesia bovis in vitro. *Parasitology*. **2005**, 130 (5), 489.

102. Tognazzo, M.; Schmid-Hempel, R.; Schmid-Hempel, P., Probing Mixed-Genotype Infections II: High Multiplicity in Natural Infections of the Trypanosomatid, *Crithidia bombi*, in its Host, *Bombus spp. PLoS ONE*. **2012**, 7(11): e49137.
103. Horstmann, B.; Korbus, M.; Friedmann, T.; Wolff, C.; Thiele, C. M.; Meyer-Almes, F.-J., Synthesis of azobenzenealkylmaleimide probes to photocontrol the enzyme activity of a bacterial histone deacetylase-like amidohydrolase. *Bioorganic Chemistry*. **2014**, 57, 155-161.
104. Wakisaka, K.; Arano, Y.; Uezono, T.; Akizawa, H.; Ono, M.; Saji, H.; Nakayama, M.; Ohomomo, Y.; Kawai, K., A novel radioiodination reagent for protein radiopharmaceuticals with L-lysine as a plasma-stable metabolizable linkage to liberate m-iodohippuric acid after lysosomal proteolysis. *J. Med. Chem.* **1997**, 40 (16), 2643-2652.

7. Appendix

7.1 MALDI spectra of pantothenic acid and CJ-15,801 analogues coupled to phiLOV(R475G,K476C).

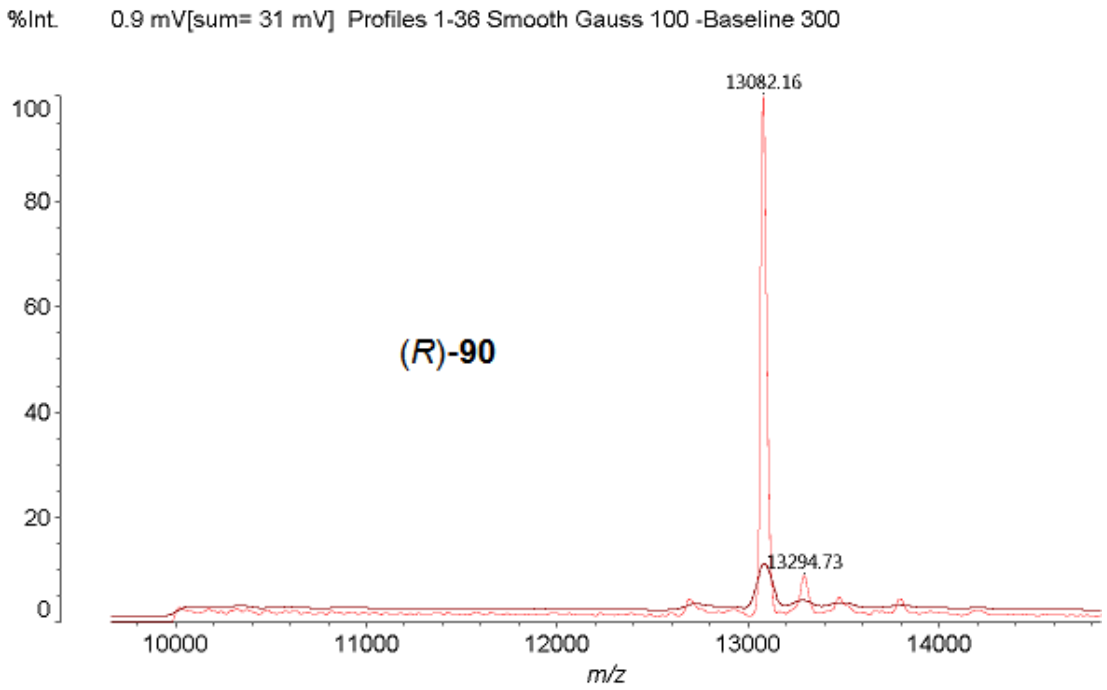

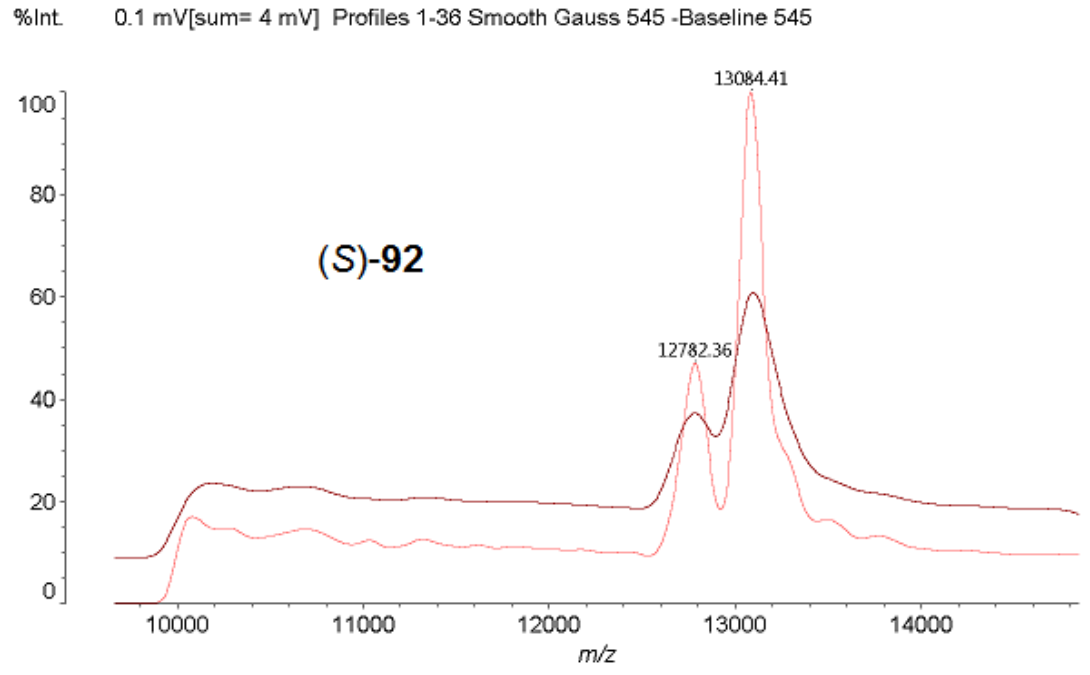

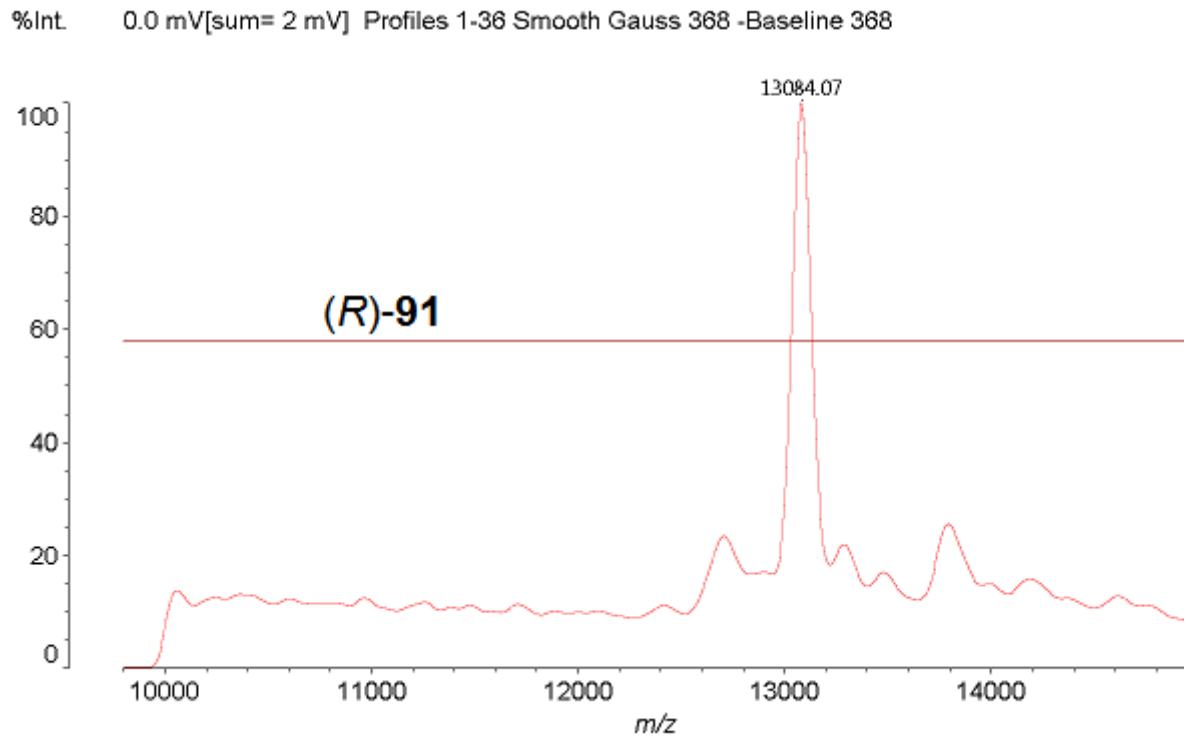
%Int.
0.0 mV[sum= 2 mV] Profiles 1-36 Smooth Gauss 368 -Baseline 368
13084.07
100
80
60
40
20
0
(R)-91
10000
11000
12000
13000
14000
m/z

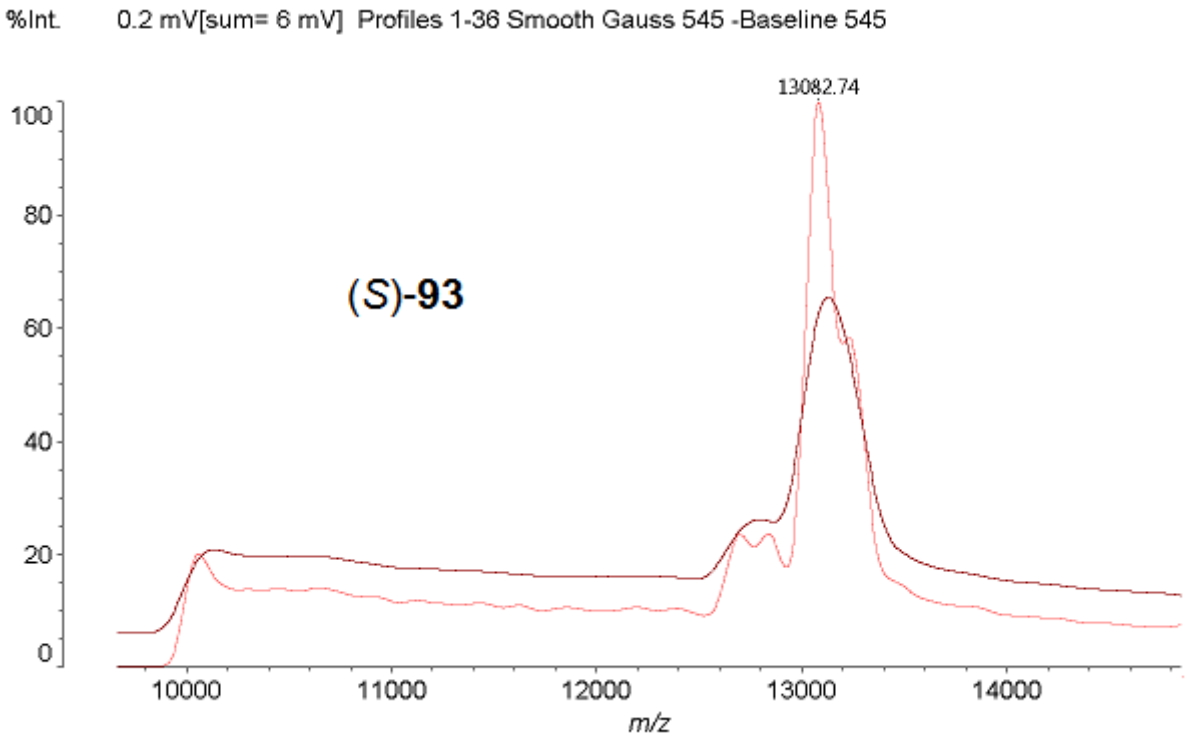
%Int.
0.2 mV[sum= 6 mV] Profiles 1-36 Smooth Gauss 545 -Baseline 545
13082.74
100
80
60
40
20
0
(S)-93
10000
11000
12000
13000
14000
m/z

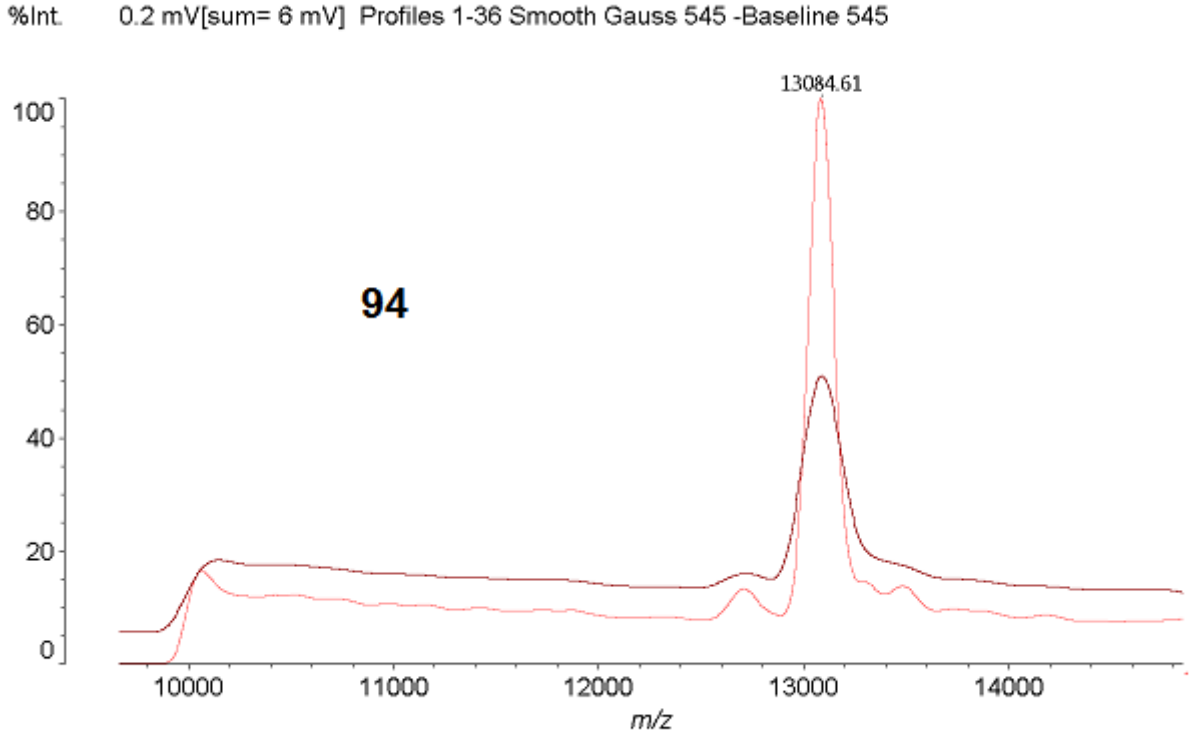
%Int.
0.2 mV[sum= 6 mV] Profiles 1-36 Smooth Gauss 545 -Baseline 545
13084.61
100
80
60
40
20
0
94
10000
11000
12000
13000
14000
m/z

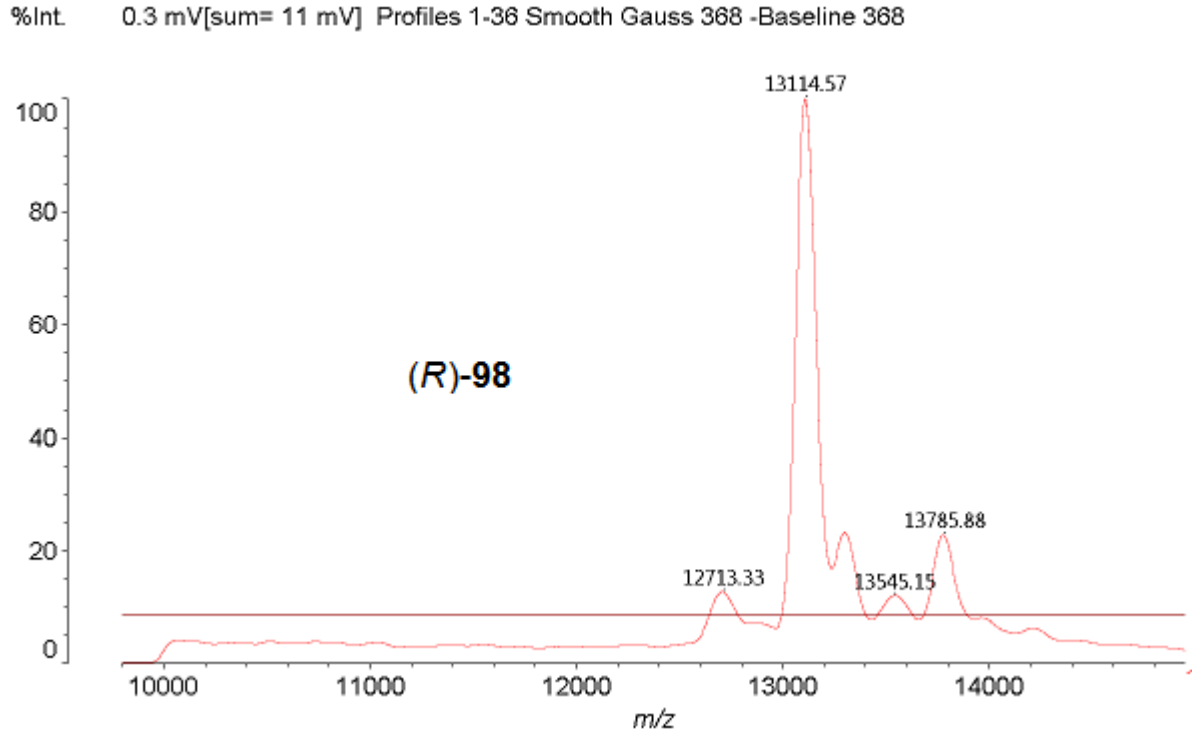
%Int.
0.3 mV[sum= 11 mV] Profiles 1-36 Smooth Gauss 368 -Baseline 368
13114.57
100
80
60
40
20
0
(R)-98
13785.88
12713.33
13545.15
10000
11000
12000
13000
14000
m/z

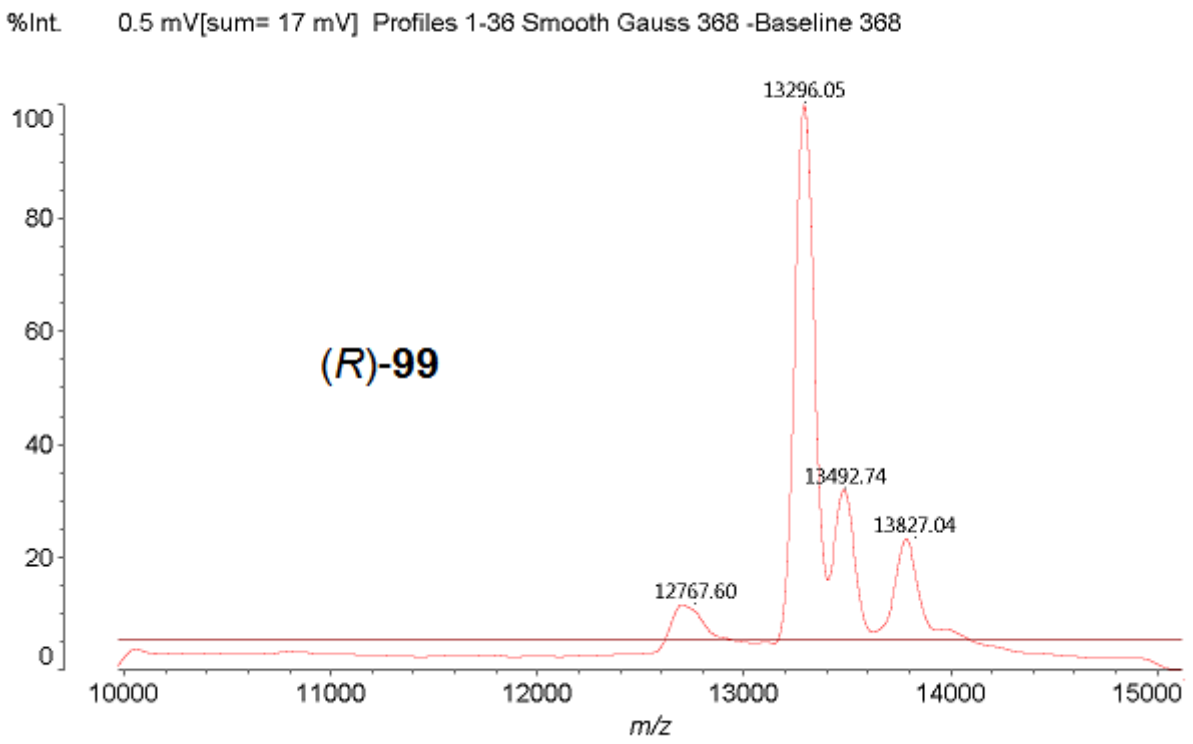
%Int.
0.5 mV[sum= 17 mV] Profiles 1-36 Smooth Gauss 368 -Baseline 368
(R)-99
13296.05
13492.74
13827.04
12767.60
100
80
60
40
20
0
10000
11000
12000
13000
14000
15000
m/z

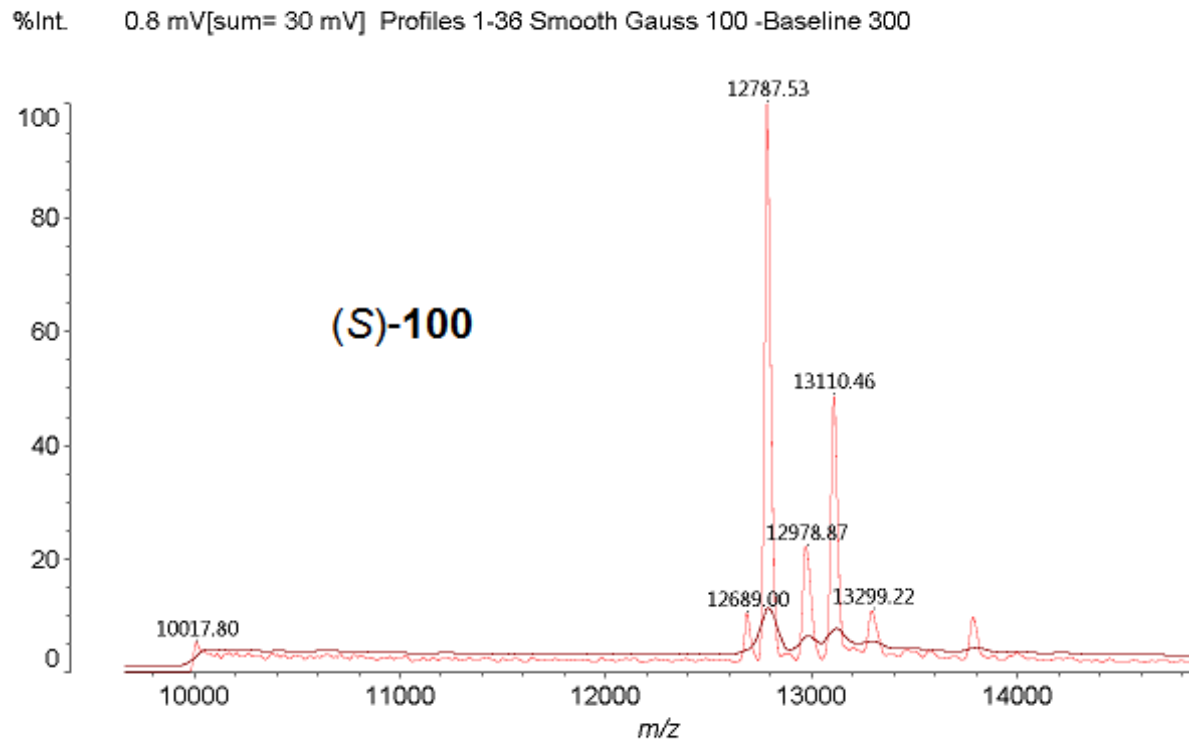
%Int.
0.8 mV[sum= 30 mV] Profiles 1-36 Smooth Gauss 100 -Baseline 300
(S)-100
12787.53
13110.46
12978.87
12689.00
13299.22
10017.80
100
80
60
40
20
0
10000
11000
12000
13000
14000
m/z

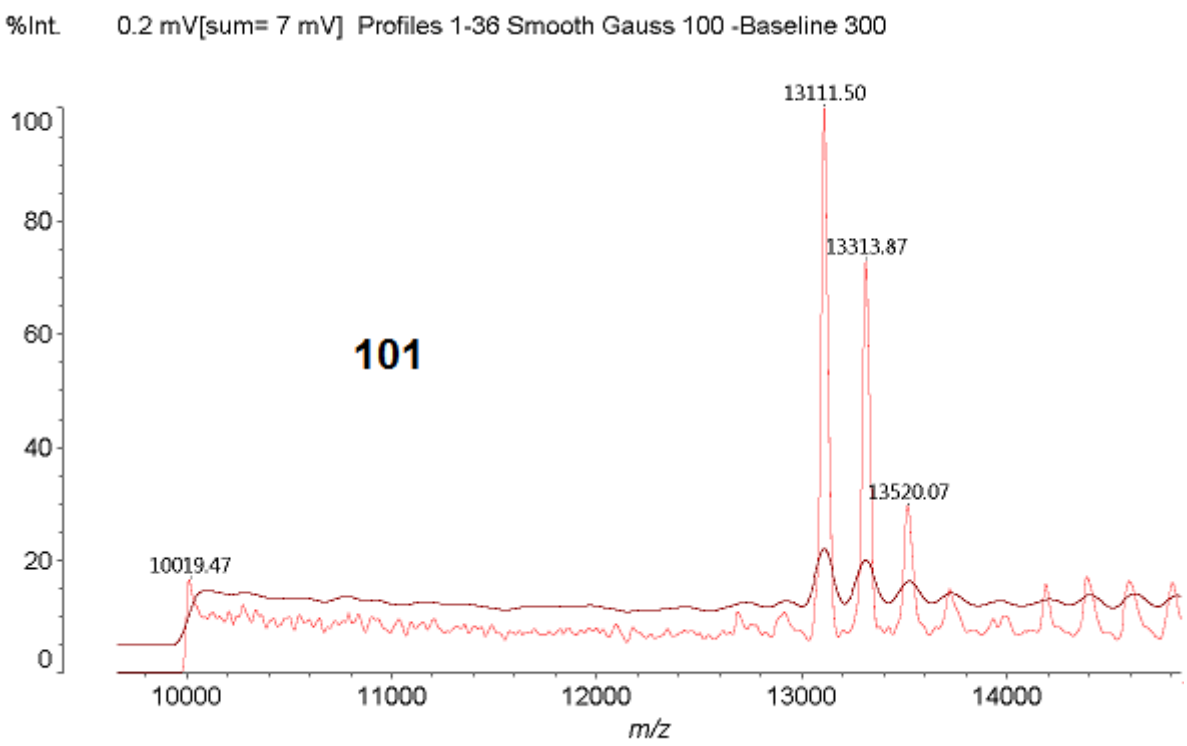
%Int.
0.2 mV[sum= 7 mV] Profiles 1-36 Smooth Gauss 100 -Baseline 300
101
13111.50
13313.87
13520.07
10019.47
100
80
60
40
20
0
10000
11000
12000
13000
14000
m/z

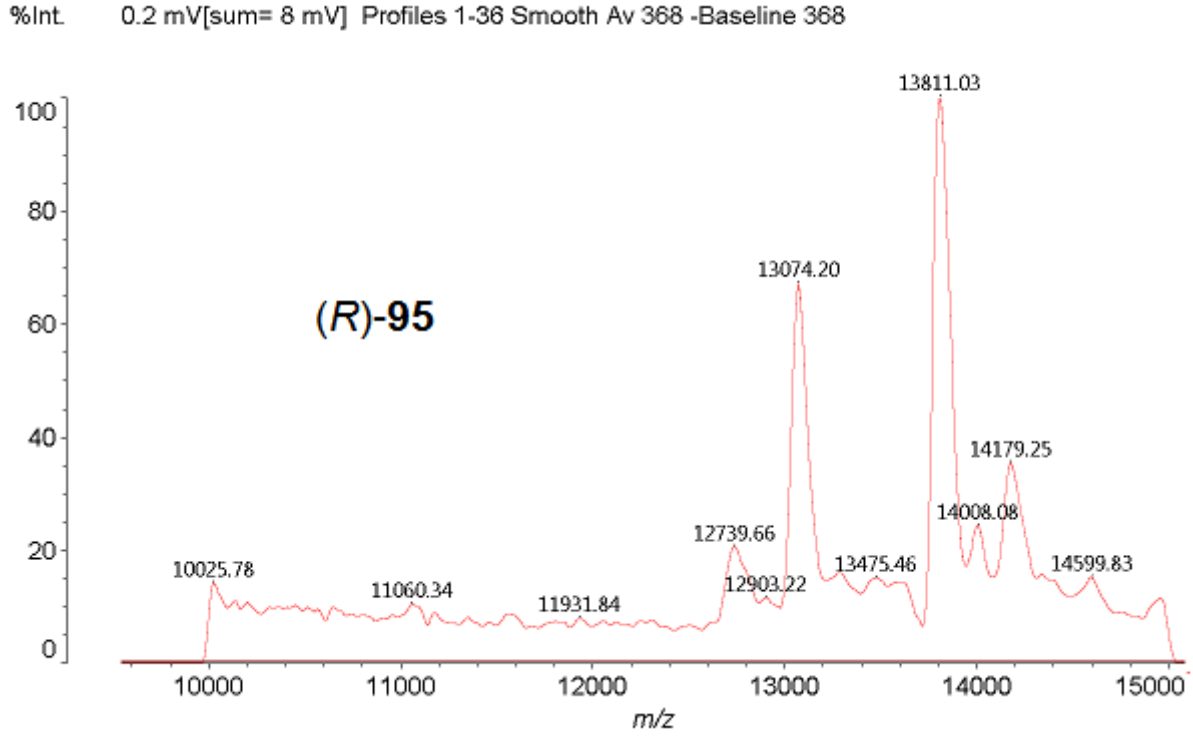
%Int.
0.2 mV[sum= 8 mV] Profiles 1-36 Smooth Av 368 -Baseline 368
(R)-95
13811.03
13074.20
14179.25
14008.08
12739.66
10025.78
13475.46
14599.83
11060.34
12903.22
11931.84
100
80
60
40
20
0
10000
11000
12000
13000
14000
15000
m/z

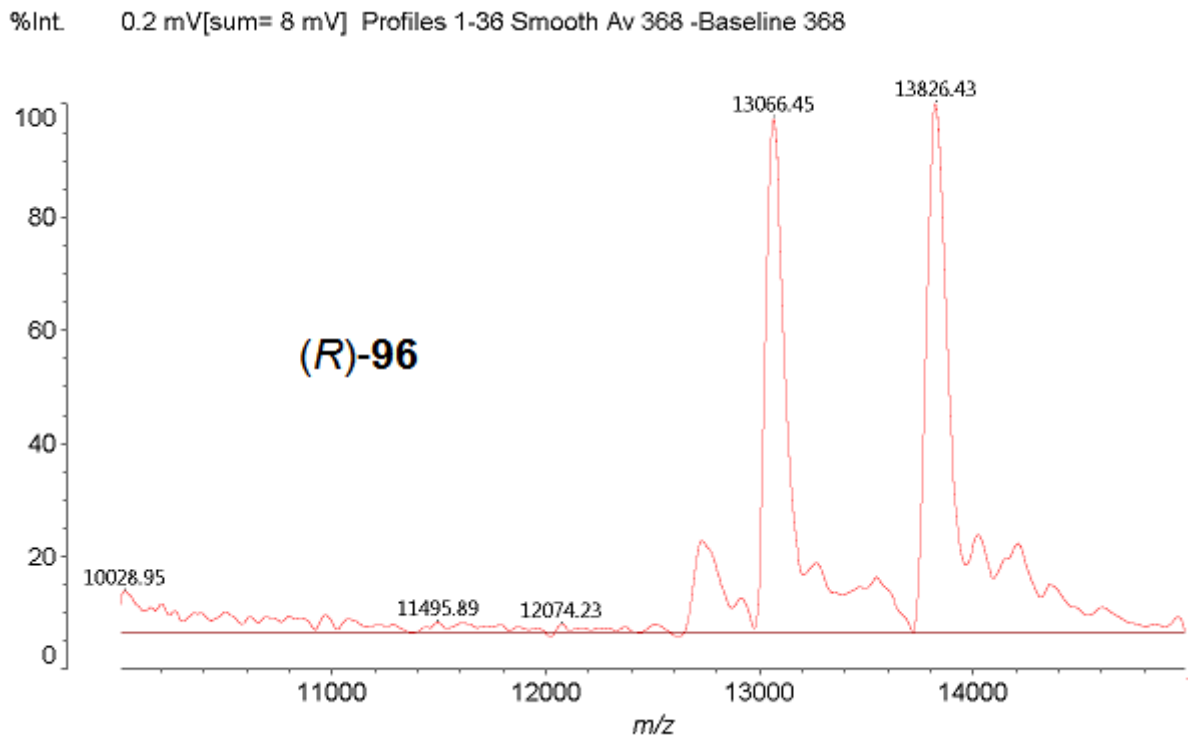
%Int.
0.2 mV[sum= 8 mV] Profiles 1-36 Smooth Av 368 -Baseline 368
100
80
60
40
20
0
13066.45
13826.43
(R)-96
10028.95
11495.89
12074.23
11000
12000
13000
14000
m/z

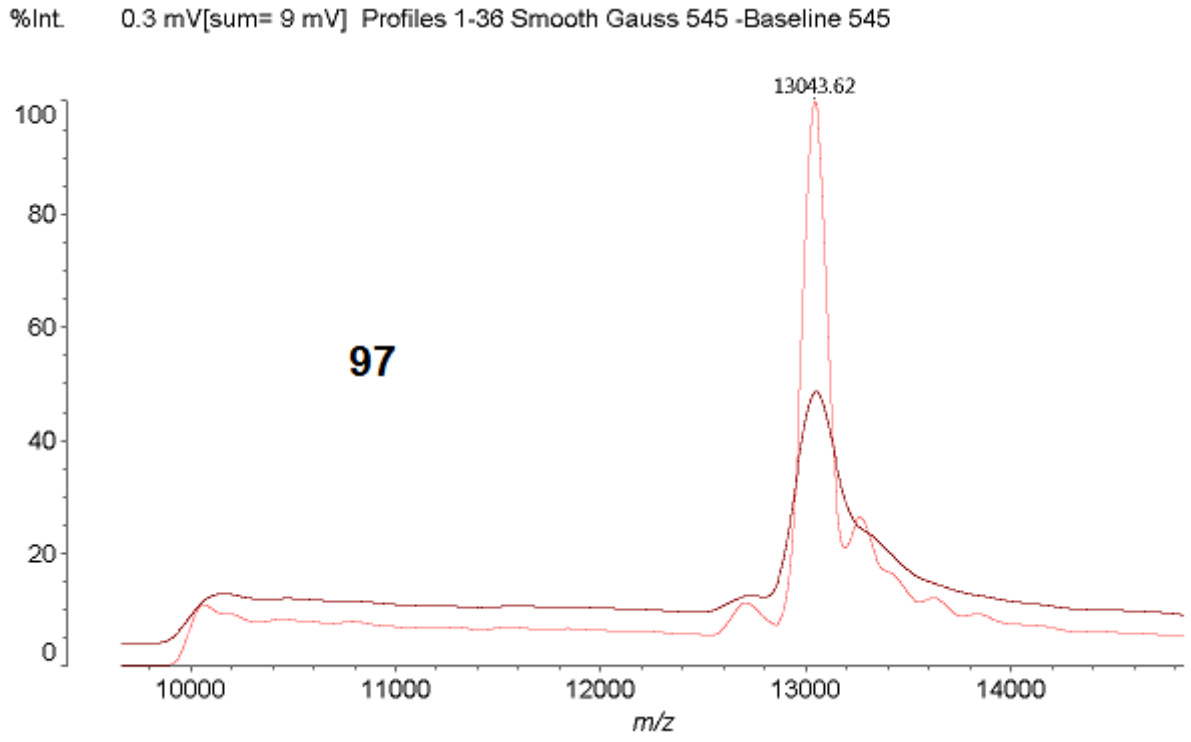
%Int.
0.3 mV[sum= 9 mV] Profiles 1-36 Smooth Gauss 545 -Baseline 545
100
80
60
40
20
0
13043.62
97
10000
11000
12000
13000
14000
m/z

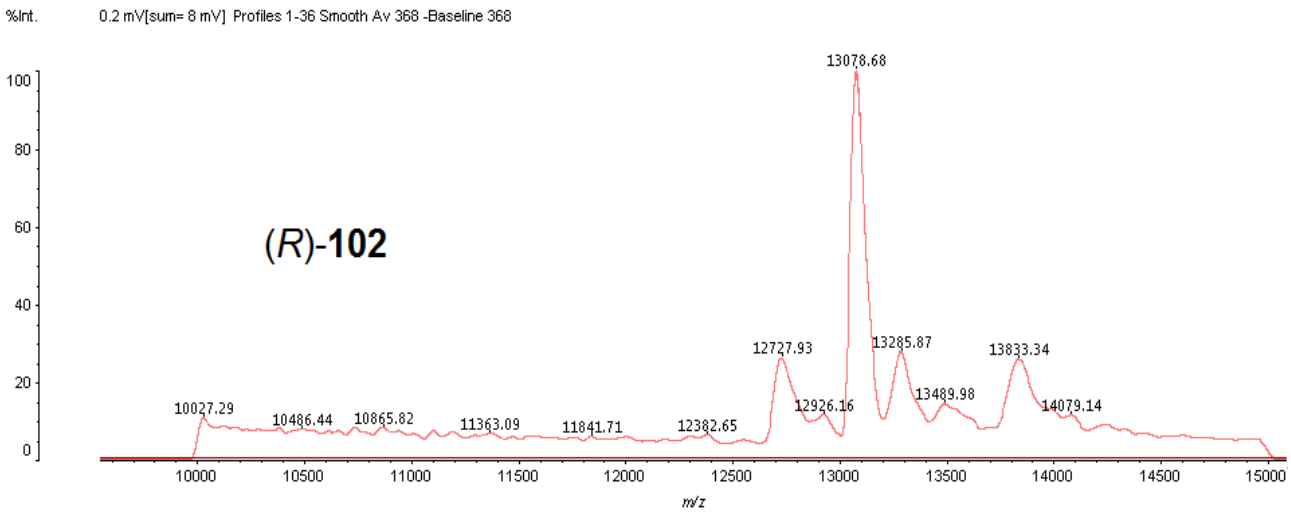
%Int.
0.2 mV[sum= 8 mV] Profiles 1-36 Smooth Av 368 -Baseline 368
(R)-102
13078.68
12727.93
13285.87
13833.34
10027.29
10486.44
10865.82
11363.09
11841.71
12382.65
12926.16
13489.98
14079.14
m/z

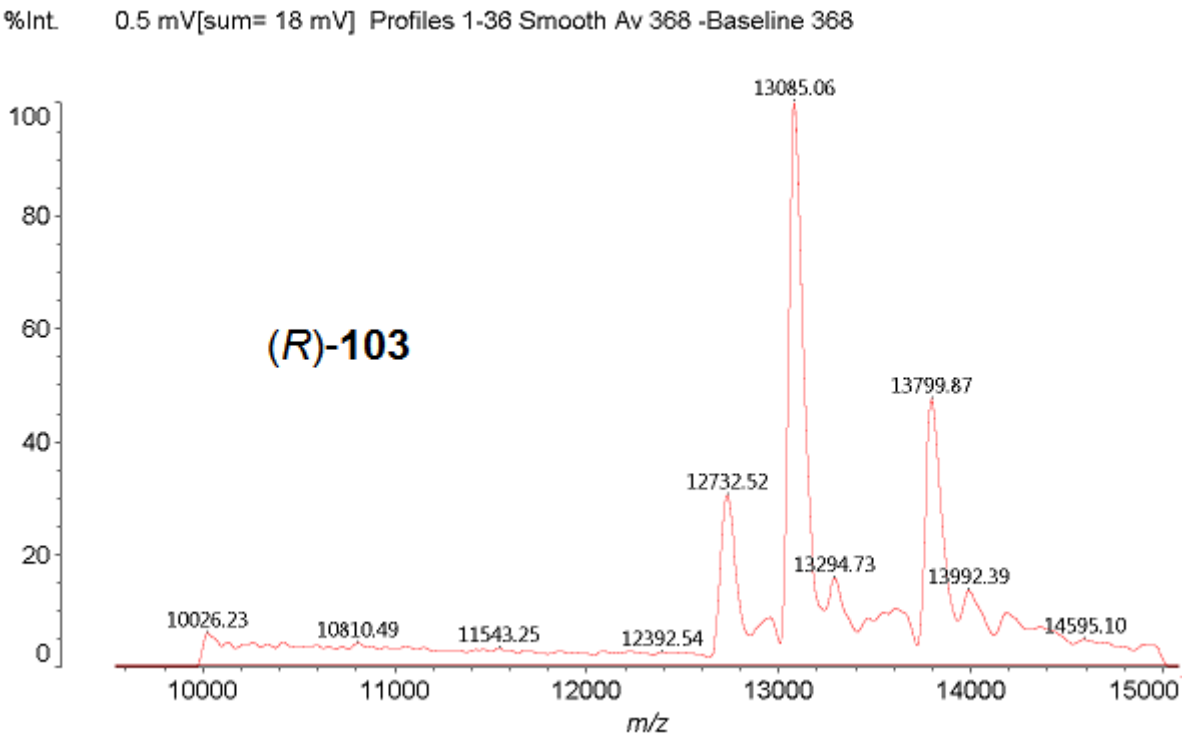
%Int.
0.5 mV[sum= 18 mV] Profiles 1-36 Smooth Av 368 -Baseline 368
(R)-103
13085.06
13799.87
12732.52
13294.73
13992.39
10026.23
10810.49
11543.25
12392.54
14595.10
m/z

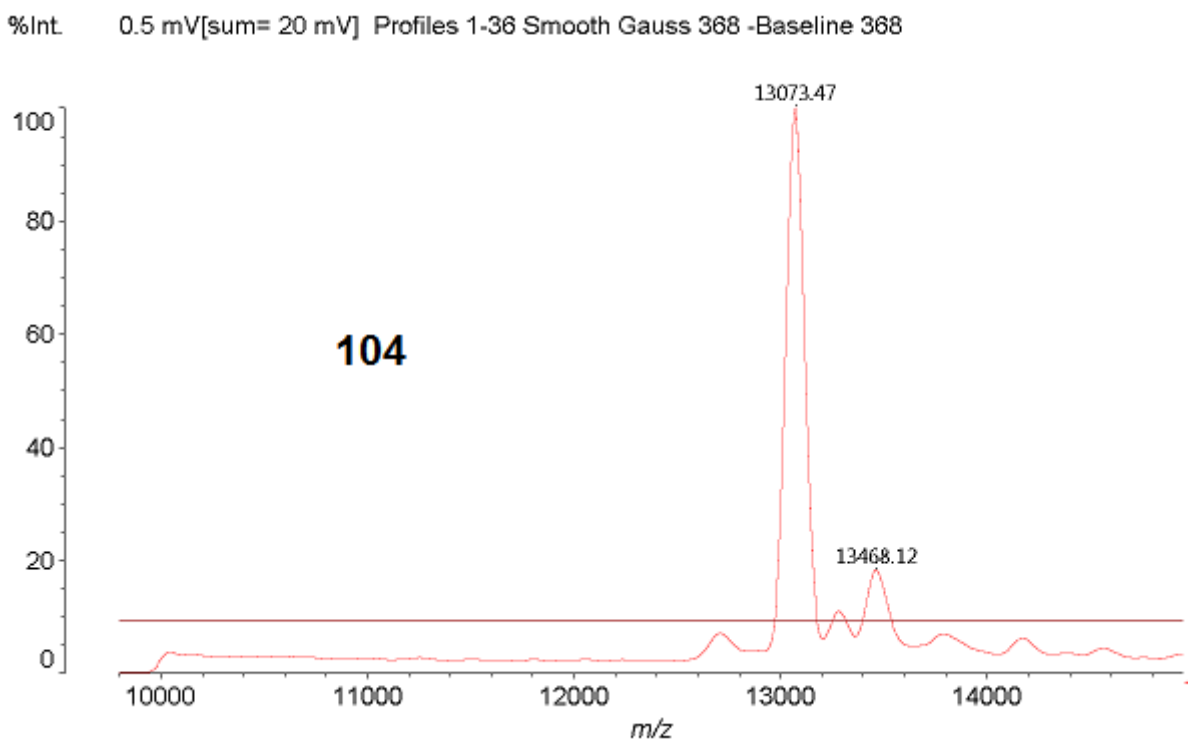
%Int.
0.5 mV[sum= 20 mV] Profiles 1-36 Smooth Gauss 368 -Baseline 368
13073.47
13468.12
104
100
80
60
40
20
0
10000
11000
12000
13000
14000
m/z